AD NUMBER

AD825354

NEW LIMITATION CHANGE

TO

Approved for public release, distribution unlimited

FROM

Distribution authorized to U.S. Gov't. agencies and their contractors; Administrative/Operational Use; 31 Oct 1967. Other requests shall be referred to Army Missile Command, Redstone Arsenal, AL.

AUTHORITY

OASD ltr, 14 Mar 1969

AD825354

STATEMENT #2 UNCLASSIFIED

This document is subject to special export controls and each transmittal to foreign governments or foreign nationals may be made only with prior approval of Army Missile Command attn: AMSMI-PEKL - Redstone Arsenal, Alabama

CONTRACT DA-AH01-67-C1609

FINAL REPORT TO THE
UNITED STATES ARMY MISSILE COMMAND
REDSTONE ARSENAL, ALABAMA

REPORT NO. AMC-3
OCTOBER 31, 1967

TURBINE FLOWMETER PERFORMANCE MODEL

Prepared by Richard E Thompson
Richard E. Thompson
Research Engineer

and Jerry Grey
Jerry Grey, President

Approved by Jerry Grey
Jerry Grey, President

GREYRAD CORPORATION
SIXTY-ONE ADAMS DRIVE
PRINCETON, N. J. 08540

609 921-2939

PAGES ______

ARE

MISSING

IN

ORIGINAL

DOCUMENT

TABLE OF CONTENTS

Table of Contents--continued

Table of Contents--continued

LIST OF ILLUSTRATIONS

List of Illustrations--continued

List of Illustrations--continued

I. SUMMARY

A complete analytical model and computer program describing the performance of flowmeters in the high Reynolds number regime has been formulated. One of the primary innovations of this model is its capability for describing arbitrary axisymmetric inlet flow fields, in contrast to the flat velocity profiles used in all prior analyses. Other key features of the model are the consideration of finite flow deflection angles by the rotor blades, and the utilization of actual empirical bearing-torque data in the retarding torque formulation.

Other well-known effects included in the model are those of manufacturing tolerances; meter temperature; fluid temperature, density, and viscosity; number of blades; blade shape (e.g., flat or helical); preswirler configuration; fluid-drag retarding torque; readout-device retarding torque; type of bearing (ball or journal); etc. The model was intended for use with storable propellants, but would be suitable for cryogenic propellants with little or no modification, providing the pertinent input data were available.

Capability of the model to predict meter performance, as well as to determine output sensitivity to all the above parameters, was demonstrated by numerical examples with two different fluids, utilizing input data from commercial meters in the 2" size range. The results of these calculations clearly demonstrated, for the first time, that the inlet velocity profile dominates flowmeter performance. Effects of all retarding torques were relatively small, becoming important only at the lower Reynolds numbers, with blade-tip and hub fluid drag far outweighing all other retarding torques.

On the basis of the results of these calculations, a recommended test program was formulated to (a) evaluate the analytical model, (b) evaluate the few empirical effects which could not be included in the model due to lack of appropriate test data, and (c) determine the effect of piping configuration and upstream conditions on meter inlet velocity profile. It was also recommended that an analytical study be performed to determine the effects of asymmetric profiles, not included in the present study.

Because of the overwhelming importance of the velocity profile in determining meter variations, it was strongly recommended that the test program be designed around Item (c), which requires little in the way of standard turbine flowmeter test capability. Evaluation of the analytical model [Item (a)] and, in particular, of the effects of asymmetric velocity profiles, can be performed with a combination of standard flowmeter test facilities and the specialized inlet-profile evaluation capability needed for Item (c).

II. INTRODUCTION

A. Purpose

The purpose of the program, as stated in the original Proposal Request, was as follows:

> "The objective of this study is to develop or adapt an existing model that describes flowmeter performance. To be included in the model will be the effects of design, manufacture, installation, off-line calibration with different fluids, and fluid dynamic properties of the fluid being metered. An experimental program to verify and evaluate the effects of the various parameters in the model will be outlined but not performed. ...
>
> "The contractor shall provide all that is necessary to accomplish the study outlined in the following phases:
>
> "a. Phase I - Literature Survey.
>
> The contractor shall conduct a literature survey to determine the applicability of existing turbine flowmeter performance models.
>
> "b. Phase II - Model Development.
>
> The contractor shall adapt an existing model or develop a model considering but not limited to those of the following items which are felt to be currently within the state-of-the-art:
>
> (1) Design Effects:
>
> (a) Meter and blade material
> (b) Bearing material
> (c) Meter size
> (d) Cavitation

(2) Manufacturing Effects:

(a) Quality control on dimensions
(b) Surface finish
(c) Lubricity of surfaces

(3) Installation Effects:

(a) Upstream valves and elbows
(b) Inlet fluid swirl velocity
(c) Meter position - horizontal or vertical
(d) Inlet internal surface finish
(e) Asymmetric velocity profile

(4) Off-site calibration with substitute fluid:

(a) Calibration shifts between fluids
(b) Breaking in running and/or working time

(5) Fluid dynamic effects of metered fluid:

(a) Chemical reactivity
(b) Entrained particles
(c) Fluid temperature, viscosity and density

All items within state-of-the-art will be included in the model and reasons given for not including the remaining items.

"c. Phase III - Outlining of Experimental Program:

The contractor shall outline an experimental program that will meaningfully verify the theoretical model and evaluate the magnitude of influence of the factors included in the model as they affect turbine flowmeter performance accuracy. This outline shall include the materials, equipment, and manpower estimates required to conduct the program. The program experiments are not to be performed. ..."

B. History

Shortly after the advent of turbine flowmeters as measurement devices for propellant flow rates in rocket engines, it was found that flowmeter registration in propulsion test-stand and flight applications often varied somewhat from the meter calibration data. Since the accuracy level of the calibration facilities was generally far better than the measured discrepancies, it was clear that variations in test parameters must be responsible for the observed differences in meter output.

A number of analytical and experimental studies were conducted, as will be described in detail in Section III of this report, in order to determine those parameters which affected flowmeter registration, and to establish the quantitative dependence of meter performance on the various factors. Although a great deal was accomplished by these studies, there were several serious omissions as well as some conflicting results. In order to resolve these shortcomings, it was decided that the ICRPG (Inter-agency Chemical Rocket Propulsion Group) would initiate an analytical program to develop a complete turbine flowmeter performance model, taking into account all possible parameters which might affect meter performance. This analysis was to be followed by a test program, to be formulated on the basis of the results obtained from the analytical study.

The present report describes the development and results of the analytical program, which was funded on April 26, 1967 by the U. S. Army Missile Command, Redstone Arsenal, Alabama, under Contract DA-AH01-67-C1609 with Greyrad Corporation of Princeton, New Jersey. This report also includes detailed recommendations for the follow-on test program.

C. Acknowledgments

The preparation of a comprehensive and useful performance model was dependent in a large part upon the assistance of the turbine flowmeter and bearing industry.

Mr. John Yard of Fischer & Porter Company provided details of their meter designs required for computer test cases. Mr. Milton November of Potter Aeronautical Corporation provided several comprehensive test reports concerning the effects of vibration, acceleration, and upstream piping on meter registration. Responses to the flowmeter performance questionnaire were also received from Mr. Kenneth Abramson of

Cox Instruments and Mr. Edward Miller of Foxboro Company. The essential bearing drag data were provided by Mr. Norman Dean of Miniature Precision Bearing Corporation.

Members of the ICRPG Experimental Measurements Committee who directed the study effort assisted with responses to the industry flowmeter user and facility questionnaire. Mr. Ben Wilson, the Project Engineer at USAMC, Redstone Arsenal, also assisted in the literature survey by obtaining many technical reports.

III. SURVEY OF TURBINE FLOWMETER LITERATURE

Phase I of the contract consisted of a survey of prior turbine flowmeter literature and the formulation of an approach to some of the analytical problems in the model. The results of this survey were given in the Second Monthly Progress Report of the subject contract, which had limited distribution. A summary of the literature survey and pertinent references is presented here for convenience, since it formed the basis for the definition of the model.

A search of recent literature was made through the use of nine abstracts and indexes. A card file of more than 200 references was prepared with a brief abstract of each item. Based on the abstracts given, reports that were considered pertinent to the contract were documented in the form of a second-draft bibliography of approximately 80 references. These references were reviewed to determine the applicability of existing models to the proposed flowmeter performance model. The literature survey was divided into theoretical papers about turbine flowmeters or turbomachinery effects and experimental papers dealing with effects that can best be represented empirically. The following sections summarize some of the important points made in the key references listed at the end of the report.

A. Review of Previous Theoretical Models

Theoretical models of turbine meters are generally based on either the momentum approach or the airfoil approach. Proper application of the momentum approach requires complete fluid guidance; i.e., all fluid particles crossing the plane of the leading edges of the blades are given the same change in angular momentum (at a given radius) as those particles adjacent to the blade. The driving torque is then expressed as a function of the change in angular momentum of the fluid.

In the airfoil approach, the forces exerted by the fluid on a differential-area element of the blade are integrated over the blade length to obtain the driving torque.

The application of momentum and airfoil theory can vary with the investigator, depending upon the effect he is trying to demonstrate. The paper by Lee and Evans[1] and the paper of Rubin, Miller and Fox[2] are typical examples of the different techniques that are employed to describe the same basic device. Reference 1 considers first an ideal fluid at a given flow rate which defines an ideal nonslip rotor speed ω_i. When considering a real meter with retarding torques, the rotor will turn at a speed ω_L which differs from the ideal speed by an amount $\Delta\omega$ called the rotor slip. The dimensionless ratio $\frac{\Delta\omega}{\omega_i}$ is formed, which is called the fractional rotor slip. The influences of fluid-retarding torques and nonmagnetic drag are then illustrated in terms of the fractional rotor slip. This treatment has been referred to as the "coefficient approach," in that each effect can be demonstrated in terms of the same parameter; i.e., as some type of coefficient to the ideal speed.

In considering this approach, it became apparent that it is not possible to examine a given effect independent of all others, because of the complex interrelationship of terms. For example, in considering meter dimensional effects due to temperature, the resultant geometry change leads to a change in the fluid velocity profile which combines with the change in fluid properties to affect the rotor torque.

Reference 2 considers both the momentum and airfoil approach, but chooses to deal directly with the torque equations which are non-dimensionalized by a normalizing torque. Presentation of the data is made in terms of a slip parameter which is the ratio of the tangent of the effective angle of attack to the tangent of the blade stagger angle. Unfortunately, the two slip parameters of References 1 and 2 cannot be directly compared, since Reference 2 assumes that the direction of the leaving velocity is parallel to the blade. The paper was restricted to a theoretical model of driving torques and did not consider bearing drag and other retarding torques. Also, a constant lift coefficient was assumed, independent of the number of blades and the rotor space/chord ratio variation with radius. A more detailed discussion of the important analytical problem areas examined in the literature survey is given in the following paragraphs:

1. <u>Blade Interference Effects</u>

Application of the momentum or airfoil theory depends upon the type of meter design. For turbine meters with a small number of blades, full guidance of the fluid is not insured, and a theoretical model based on the airfoil approach is considered more suitable. However, if the airfoil approach is applied to rotor designs with an increasing number of blades, the point must be reached where the airfoil and momentum approaches merge to give the same results. Reference 2 compares these approaches and attempts to show the importance of the solidity parameter and its relationship to slip, in order to indicate the operating regimes in which the momentum and airfoil analyses give similar results and where they differ.

Although the approach of Reference 1 is satisfactory for the assumptions stated, it cannot be directly applied in the present analysis because of the restrictive assumptions of uniform velocity profile and no consideration of blade interference effects.

If isolated airfoil blade theory is applied to a multiple-bladed rotor, the analysis suggests that doubling the number of blades or blade area would give twice as much torque without limit. Obviously, there .st be an upper limit at which blade interference starts affecting the lift coefficient used in the calculation.

Because previous analyses have not treated this problem in any detail, very little is available in the flowmeter literature to contribute to its analysis. The problem can be approached in either of two ways:

(a) The first is based on the use of experimental data generated as part of wind tunnel experiments on cascades. This approach is used by Jepson,[3] who modifies the isolated airfoil and drag co-efficients to account for the "cascade effect."

Reference 3 suggests that C_L/C_{Li} and C_d/C_{di} depend only on the space/chord ratio and are independent of the angle of incidence over the range 0° to 20° and within "reasonable accuracies" up to incidences of 45°. Therefore, knowing the space/chord ratio from the rotor dimensions, and the isolated airfoil lift and drag coefficients, the curves of C_L/C_{Li} and C_d/C_{di} can be used to obtain the actual lift and drag coefficients.

The major limitation in using experimental data of this type is that the data were obtained using a particular blade shape and aspect ratio, and the meter blades should be of a similar design to correctly use the curves. The test conditions for the curves in Reference 3 are not specified, and the importance of matching geometries is not discussed.

(b) An alternate approach to the problem, which was used in the present analytical model, is the application of potential theory to incompressible inviscid two-dimensional cascade flow. Straight cascade theory can be applied properly to study blade interference effects in an actual rotor where the blades diverge because the lift coefficient C_L and the space-to-chord ratio s/c are calculated at a given radius and vary continuously with r, and are in this fashion integrated into the driving torque expressions. Since most turbine theoretical models use straight-line blade profiles, a potential flow analysis requiring straight blades is not a severe restriction. An analysis similar to the type used is given in Reference 4.

Treatment of the problem requires the conformal mapping of the exterior of a cascade of straight line profiles into the exterior of a circle. A more detailed description of the use of cascade theory in the present model is found in Section IV of this report, which gives a technical description of the model.

2. Boundary Layer and Wake Effects

Our discussion in the previous paragraphs concerned incompressible inviscid two-dimensional flow and therefore did not deal with the effects of boundary layers and wakes. For a single profile having a relatively small lift, the influence of the boundary layer on the pressure distribution is generally disregarded. However, for flow through cascades of high solidity, the boundary layer becomes important because in some cases, its displacement of the external flow cannot be neglected. The problem is complicated by the fact that some knowledge of the pressure distribution over the profile surface must be known to properly apply boundary layer theory.

Boundary layers are also responsible for generating secondary flows when blades of finite length are considered. Boundary layers at the blade ends near the hub and tip, combined with pressure gradients caused by turning the stream, generate secondary flows toward the blade ends on the lower blade surface and away from the ends on the upper surface. In addition, immediately downstream of the surface of the blade, there is a surface of discontinuity of velocity, equivalent to a vortex sheet. From finite wing theory, this vortex sheet is unstable and rolls up into two trailing vortices which interact with the wall boundary layers.

It must be remembered that most of the literature dealing with boundary layer and secondary flow effects in cascades is concerned with axial flow compressor and turbine design, where the flow is turned through large angles and the pressure difference across the blade row is high. Also, boundary layers from previous stages contribute significantly to the secondary flow problem. If, however, the pressure gradient across the blade is small, the boundary layer analysis can be simplified by assuming zero pressure gradient. Commonly, the boundary layer thickness on turbine blading remains very small over the whole length, owing to the fact that a decrease in pressure predominates. Again, this remark applies more to turbomachinery with large pressure differences, but the fact remains that a favorable pressure gradient will tend to minimize boundary layer spreading.

Preliminary calculations of blade boundary layer thicknesses for a typical turbine flowmeter are described in Section IV. These calculations indicate that the trailing edge boundary layer thickness is very small in proportion to the blade spacing, and the pressure gradient along the blade will be small, which is known to be the case experimentally.

Any attempt at an analytical description of secondary flows and three-dimensional effects was considered completely beyond the scope of this study. Very little exists in the literature describing these effects. Meter manufacturers have not conducted flow visualization tests, and they did not have any data to indicate that these effects were worth pursuing.

3. Blade Shape Effects

In addition to the space/chord ratio, angle of attack, and trailing edge thickness, other meter geometry parameters must be discussed in terms of the analytical model. Previous theoretical treatments assumed a helical blade shape, because it simplified the geometry of the problem. Since the power requirements to drive the rotor are small, however, the fluid is deflected very little in passing the blade, and the flat plate represents a satisfactory geometry. Because of the similarity of the velocity triangle and the geometric triangle for a helix, a helical blade will theoretically present to the fluid a flat plate geometry at a constant angle over the total blade height. Actually this is only true for the average velocity, since the lower velocities at the meter walls do not satisfy this condition. Helical blades are used in the performance model with the option of specifying a flat blade geometry.

4. Meter Dimensional Effects

The discussions in the previous sections have been concerned primarily with the geometry of the rotor blading and its effect on meter performance. Other meter dimensional effects include changes in the meter body because of temperature effects, unmetered volume flow through the annular blade tip clearance area because of manufacturing tolerances, and boundary layer displacement thickness effects caused by boundary layer formation on the meter walls.

Calibration of turbine flowmeters for cryogenic operation has been examined by Grey[5,6]. From this analysis, small changes in rotor speed at constant volumetric flow rate become:

$$\frac{\Delta \omega}{\omega} = - \frac{\Delta (A_h - A_r)}{(A_h - A_r)} + \frac{\Delta (\tan \alpha)}{\tan \alpha} - \frac{\Delta R}{R}$$

It can be shown[5] that for isotropic materials, this becomes $\frac{\Delta \omega}{\omega} = -3 \beta_1 \Delta T$ where ΔT is the temperature difference between the operating temperature and the calibration temperature. These expressions were derived for zero blade clearance. Staniszlo and Krause (Reference 7, Appendix B) have expanded the analysis of Grey to include the unmetered volume flow that passes through the annular blade-tip clearance area. The expression for $\frac{\Delta\omega}{\omega}$ thus contains additional terms that are functions of the velocity of the fluid through the blade tip clearance area. Calculated results are given in Reference 7, but the importance of the additional terms is not discussed. Although this analysis is more generalized, it still has limitations in that it assumes that rotor retarding torques do not exist and that blade blockage is zero.

Minkin, Hobart and Warshawsky (Reference 8) have theoretically predicted meter calibration factors based on thermal expansion alone and with the blade tip clearance and boundary layer effects included in the analysis of Reference 7 above. Reference 8 implies that a difference of 0.3% exists due to the added terms for liquid hydrogen. A portion of this correction is due to the different coefficients of thermal expansion of the rotor hub and meter body, and the remainder is due to the inclusion of blade leakage in the analysis. A discussion of the magnitude of these terms is found in Section IV of this report.

5. Meter Dynamic Effects

The bearing design and description is one of the major aspects of a model of the meter dynamic effects. In a Rocketdyne report by R. L. Smith (Reference 9), an attempt is made to expand on the work of Rubin, Miller and Fox to include the bearing drag and friction terms to complete the model. The driving torque model was taken directly from Reference 2. The resulting equation for bearing drag is very complex and difficult to evaluate analytically. The expression was so cumbersome that Smith was forced to resort to determining the proper proportionalities with undetermined constants that hopefully could be obtained experimentally.

The analysis of Reference 9 is an indication of how rapidly the model becomes complicated when the bearing drag terms are included. Reference 9 does consider fluid and magnetic drag in an approximate manner. A complete model should include fluid drag on the hub and fluid drag between the blade tip and the housing. The importance of these effects is discussed in the model description section of this report.

B. Discussion of Empirically Represented Effects

A portion of the literature search concerned meter characteristics that could only be described with empirical expressions. It was hoped that a thorough search of the literature would produce information on empirical factors used by commercial turbine meter manufacturers or sufficient test data to deduce these factors. Unfortunately, very little information is available, and even that is generally restricted to qualitative remarks or limited test data that cannot be correlated with any degree of success.

1. Meter Installation Effects

The effects of upstream geometry and swirl on meter operation is generally removed in the test installation with flow straighteners or sufficiently long approaches. Zanker, in Reference 10, describes in considerable detail the development of a flow straightener for use with an orifice-plate flowmeter in disturbed flows. Although sensitivity of turbine meters to flow disturbances may be completely different than orifice plates, the paper does contain an interesting discussion of factors involved in designing an effective flow straightener.

Inlet disturbances were produced by partially blocking the flow, by a rotating perforated plate, and a rotating impeller. Velocity distributions were measured and the effect of gauze, honeycomb, and combination straighteners on settling length were recorded. Although this report is quite detailed in its treatment of artificially generated disturbances, very little is devoted to the velocity profiles of naturally generated disturbances. Also, the effectiveness of the straightener is evaluated in terms of the error in the discharge coefficient for an orifice plate which bears no known relationship to error in turbine meter registration.

In Reference 11 by West, the effects of "non-standard" installations are discussed in a similar fashion. West considers the flow around a bend and the observed bend loss coefficients. He emphasizes the fact that the velocity distribution before the bend and the appropriate Reynolds number range must be considered carefully because tests on a particular bend and pipe arrangement are only applicable to that arrangement, since the parameters listed above have a direct influence on the results. Velocity profiles at different diameters downstream of the bend are given for different radius bends and a given inlet velocity condition. It would be nearly impossible to catalog a complete flow range, since the profiles are quite asymmetric and adequate empirical expressions do not exist.

2. Meter Vibration and Transient Effects

The literature was consulted briefly to determine if any meter vibration and transient effects could be simulated simply with empirical expressions. Vibration due to rotor unbalance is a very involved subject and the complexity of expressions describing this phenomenon makes their use in the model impractical. This effect is a function of the particular meter design and cannot be generally described. Meter manufacturers statically and dynamically balance turbine rotors and carefully control bearing clearances to avoid internally generated vibration.

The effect of external vibration on turbine flowmeter performance is discussed in a very limited fashion in most references. An exception is a Potter Aeronautical qualification test report on their Model 1-5851, 1.5 to 25 gpm turbine flowmeter which was mounted on a vibration machine and tested at NASA-MSFC (Reference 12). Details of the test sequence and discussion of the test data are presented in Section V.

3. <u>Orientation and Acceleration Effects</u>

In addition to the influence of upstream geometry previously mentioned, the installation of a flowmeter is also important in terms of orientation and gravity loading. Very little could be found on meter orientation except in References 13, 8 and 12. Smith (Reference 13) discusses the effect of acceleration on the accuracy of both high and low frequency one-inch Potter flowmeters. The high frequency model is unaffected up to 20 g, but the low frequency model gives 10% or more error at 20 g for the low flow rates where it is most sensitive. The data in Reference 13 are limited, and no comparisons are made with other meters, so no conclusions can be drawn.

Similar acceleration tests on Potter meters are described in Reference 12. A Potter Model 1-5851 was placed on a centrifuge and accelerated to 10 g's while maintaining a constant flow of 1.68 gpm. Post-acceleration calibrations indicated a "K" factor shift of no more than 0.08%.

4. <u>Pulsating Flow Effects</u>

Errors in attempting to measure pulsating flow are described in References 14 and 15. Reference 14 uses a control system approach to determine the response of the meter to a step disturbance λV_o. This analysis indicates that a pulsation intensity of 0.25 can lead to a meter error of 3%. However, this is a rather severe pulsation intensity. (The analysis is based on a fixed blade angle of 45° to simplify expressions, so the effect on other blade angles is not illustrated.) Reference 15 recommends a practical pulsation intensity threshold of 0.1, below which the performance of all types of flowmeters will differ negligibly from the mathematical ideal of steady flow. A majority of the meter manufacturers consulted believed that pulsating flow was not that commonly encountered and that errors were usually small.

5. <u>Test Procedures and Calibration Facilities</u>

The remainder of the literature survey was devoted to a review of papers dealing with test procedures and calibration facilities in Government and private industry.

References 7 and 8 are two very recent and enlightening reports on the calibration and use of turbine type flowmeters for liquid hydrogen service. Reference 7 is concerned with the simulation of liquid hydrogen turbine flowmeter calibrations by using high pressure nitrogen gas. It emphasizes that for proper simulation the kinematic viscosities should be the same to insure that the Reynolds numbers of the flow through the meter will be equal for a given flow velocity, and that the densities of the fluids should be the same so that the torque-retarding force balance on the meter is the same for both fluids at a given fluid velocity. (Naturally, it is difficult or nearly impossible to find simulation fluids that satisfy both requirements, but ambient temperature nitrogen at approximately 60 atmospheres comes close to liquid hydrogen.)

Reference 7 also suggests that for complete simulation the fluids should have the same temperature, to ensure that dimensional changes are the same and that bearing surface conditions should be the same in both fluids. These two factors were not simulated, and it is probably quite idealistic to hope that a simulation fluid could meet these requirements as well as the first two. The tests did demonstrate, however, that the liquid hydrogen calibration factor at full-scale can be simulated with nitrogen to 0.4%.

Reference 8 contains an easily-read description of a typical calibration test program, data reduction, and data presentation. The report summarizes calibration terminology, testing procedure, criteria for defective meters, calibration system reproducibility, and the effect of use, upstream conditions, and meter orientation on calibration factors. The last two items were of particular interest, since it was desirable to include these as empirical effects in the analysis. Unfortunately, the results were very closely related to meter type (and manufacturer), being negligible for one design and significant for another. Since the testing was conducted by NASA, the meters were not identified as to model type or manufacturer, and therefore the data are of little general value. NASA representatives were contacted about releasing the names of the meter manufacturers, but they regret that this is not possible.

Accumulated experience during the NASA test program revealed that a defective meter implied defective bearings which could be detected quite easily with the following crude test: blow dry air gently into the meter and then observe how the rotor decelerates smoothly, finally oscillating with decreasing amplitude about the rest point because of the magnetic coupling between the blade and the pickup coil. Failure to oscillate is generally indicative of a defective bearing.

References 16 to 20 are typical of the papers concerned with the current application of turbine type meters, particularly in the aerospace industry. Reference 16 is a very good discussion of calibration techniques for non-cryogenic liquid flowmeters, concerning the selection and calibration of instrumentation, types of weighing procedures, and evaluation of equipment. This paper documents some of the pitfalls in calibrating liquid flowmeters for those not too familiar with the procedure.

In the last ten years, a considerable effort has been expended in private industry to establish the much more complex cryogenic flow calibration facilities. Because of the nature of the fluid, the approach to the storage and measurement of the fluid is quite different than for ambient temperature hydrocarbons. Temperature compensation becomes important, and the often nonlinear operation of the meter requires accurate calibration. The facilities at Pratt and Whitney, West Palm Beach, Florida; NASA's Lewis Research Center, Cleveland, Ohio; Aerojet-General, Sacramento, California; and NBS, Boulder, Colorado, are described in References 17, 18, 19, and 20 respectively.

IV. ANALYSIS OF TURBINE FLOWMETER PERFORMANCE MODEL

The primary purpose of the study was to develop a throretical model of turbine flowmeter performance that would allow the study of various geometry and fluid effects without the limiting restrictions of other models. Analysis of the rotor driving torque is based on the airfoil approach, which is valid for rotors with a few number of blades or wide spacing. For increased blade numbers and narrower spacing, blade interference effects are accounted for in a reduced blade lift coefficient, which is described generally in terms of the variation of the blade stagger angle and space/chord ratio with rotor radius.

The rotor driving torque is derived for an element of blade area with thickness dr at a radius r. The total driving torque is obtained by numerically integrating from the blade root to the tip. This eliminates the need to define a mean effective radius through which the blade forces act. The geometry, velocity, density, and lift and drag coefficients are expressed generally as functions of r and included in the integration. Blade interference effects and the general expression of all rotor driving torque parameters as functions of radius have not been included in previous models. Also, the model is valid for both helical and flat-bladed rotors of constant rotor width and blade thickness.

Since the rotor driving torque is directly dependent upon the fluid velocity, it is important to have a completely general and well defined expression for the velocity profile, as opposed to the effective average velocity used in previous models. This is accomplished through the use of a velocity subroutine that predicts the velocity profile for turbulent flow through an annulus. The analysis is based upon Reichardt's expression for eddy diffusivity of momentum and parallels the analysis of turbulent flow in a circular pipe. To study the importance of velocity profile, provision was also made to specify the velocity profile, forcing the program to use this contour in the torque integration. In this way one can specify a uniform or flat velocity profile, the fully developed pipe velocity profile, or an actual velocity profile obtained experimentally.

The approach velocity is used with the rotor geometry and speed to define the inlet velocity vector diagram. The departure velocity and angle are related through the blade geometry to the inlet conditions. Following the practice accepted in turbomachinery analysis, the lift and drag coefficients are defined in terms of the velocity at an angle which is the average of the inlet and outlet angles. Some previous models assumed that the flow departure angle was the same as the blade angle.

Counteracting the fluid driving torque will be several fluid drags as well as mechanical and electrical retarding torques. Fluid drag past the rotor blades has a component which opposes the driving torque. As was the case with the driving torque expression, the geometry, velocity and drag coefficient are radius dependent. (Capability for radius-dependent fluid property variations is available, but it is not likely that this effect will need to be included.) A similar fluid drag has been included at the rotor hub. The program also accounts for blade tip clearance drag at the meter housing. The analysis is similar to that used to determine retarding torques for lightly loaded journal bearings.

Because of the flexibility of the program, meter dimensional effects can be readily determined. The appropriate meter geometry is expressed as a function of temperature through the definition of a reference state and the coefficient of thermal expansion for the material. In this way, the use of different materials for the rotor and meter body can be accounted for. By directly entering all of the geometry into the numerical integration routine, all meter dimensional effects, including manufacturing tolerances, can be accounted for with several test cases. In this way, expressing the rotor speed change directly in coefficient form as in previous analyses can be avoided and the reflection of the geometry change in small changes in velocity profile, limits of integration, etc., can be directly included.

Most of the analysis of retarding torques was focused on the determination of bearing drag. Provisions are made in the program for the use of either ball bearing designs or journal bearings. Recent ball bearing literature was reviewed, but no running torque calculation routine was found that would give accurate predictions while avoiding the complex computer solution of Jones [21] or Scibbe and Anderson[22]. Although these computation routines could be incorporated in the torque analysis as a subroutine, this approach was not followed because it would require the performance model user to have a very detailed knowledge of the bearing design, including the pitch diameter, race curvatures, initial contact angle, etc. It was concluded that this information would probably not be readily available to the user, who might also be unfamiliar with the terminology. For these reasons, it was more practical to obtain the running torque from curves of torque vs speed and load entered directly into the program for the particular bearing and fluid combination associated with the meter being tested. These curves or tables are obtained by direct measurement or from analytical predictions made by bearing manufacturers familiar with design details. In this fashion, lubricity effects will be incorporated as directly measured for a bearing design, and uncertain analytical predictions can be avoided.

The bearing thrust load, which determines bearing drag, is composed partially of the axial components of the driving force and the fluid drag on the rotor blades and hub. Blade flow blockage and acceleration loadings also contribute to the bearing thrust load. The bearing thrust load is integrated over the blade length in the same manner as the driving torque. The total thrust load is then used to specify the bearing torque at the given speed.

Because some meter designs employ journal bearings, a retarding torque analysis was made of a simple journal bearing. These bearings are lightly loaded, so the effect of radial loading on drag was not included. The analysis was included primarily to account for the Potter designs, which have a "floating" hub, and therefore thrust loadings were also not included.

Finally, as part of the study of turbine rotor retarding torques, the drag contributions due to typical magnetic and RF pickups were determined. The primary objective was to determine generally the order of magnitude of these retarding torques in comparison with the bearing drag and other fluid drags. The RF pickup had virtually no effect on the turbine rotor; however, the magnetic pickup exerts a retarding torque, which was included in the overall rotor torque balance equation.

The previous paragraphs have described briefly the features of the program and the various components of the rotor torque balance equation. The actual rotor speed is determined by assuming a given rotor speed, calculating the magnitude of the driving and retarding torques for that speed, and then iterating on the rotor speed until the sum of the torques equals zero. Thus, the actual rotor speed will correspond to the condition:

> Driving torques - blade fluid drag torques - rotor hub fluid drag torque - blade tip clearance drag torque - bearing drag - bearing retarding torques - magnetic pickup retarding torque = 0.

A more detailed description of these terms and the development of the theoretical model to include these effects is given in the following paragraphs.

A. Blade Interference Effects

A portion of the literature surveyed and the discussion of the previous section dealt with blade interference effects and the importance of space-to-chord ratio or other solidity parameters on lift and driving torque. The general conclusion to be drawn from these remarks was that a variable lift coefficient must be included in a driving torque analysis. This analysis should also accommodate a departing flow angle different from the blade angle. The analysis outlined in this section is based on the application of potential theory to incompressible inviscid two-dimensional cascade flow to include these effects. The cascade or rotor geometry defining the nomenclature used is shown in Figure 1. Straight cascade theory can be applied properly to study blade interference effects in an actual rotor where the blades diverge, because the lift coefficient C_L and the space-to-chord ratio s/c are calculated at a given radius and vary continuously with r, and are in this fashion integrated into the driving torque expressions. Since most turbine theoretical models use straight-line blade profiles, a potential flow analysis requiring straight blades is not a severe restriction. The analysis is similar to that given in Reference 4.

Treatment of the problem requires the conformal mapping of the exterior of a cascade of straight-line profiles into the exterior of a circle. Any strip of the cascade located in the z plane can be mapped conformally into the inside or the outside of a circle in the ζ plane. The origin and goal of the cascade flow are transformed into a vortex source and sink in the ζ plane at the points -R and +R respectively on the real axis. Since our main interest is the effect of spacing on the lift coefficient for flow through the cascade with an angle of attack, the complex potential may be considered as the superposition of a flow parallel to the straight line profile as mentioned above plus a free flow velocity normal to the profiles, which gives additional vortices at $\pm R$ and $\pm 1/R$ as functions of the circulation.

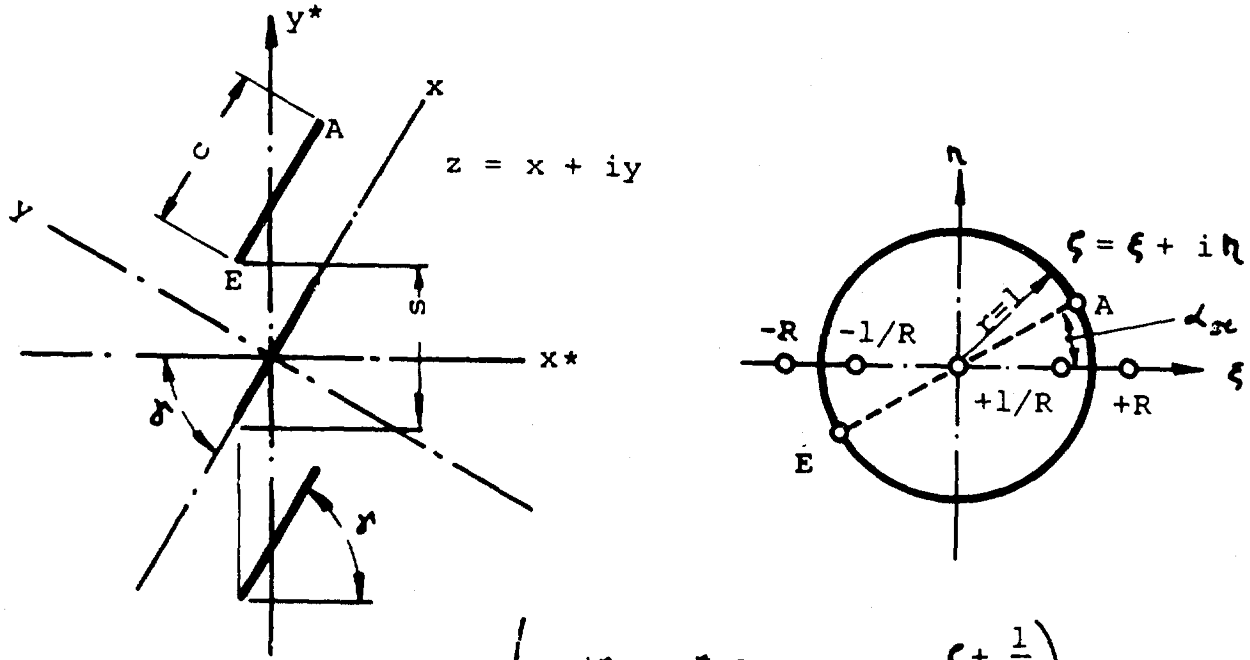

$$z^* = \frac{s}{2\pi}\left(e^{-i\gamma} \ln \frac{\zeta+R}{\zeta-R} + e^{i\gamma} \ln \frac{\zeta+\frac{1}{R}}{\zeta-\frac{1}{R}} \right)$$

Fig. 1. Conformal mapping of a straight-line profile cascade on the unit circle with symmetrically located singularities.

The key parameters in the solution are the blade angle γ' relative to the hub axis, the space-to-chord ratio s/c, an angle α_{st} that defines the branch points of the circle, the position R of the sources and sinks, and the ratio C_L/C_{Li} of lift with blade interference to single profile lift. Three distinct equations involving these parameters can be solved to obtain $C_L/C_{Li} = f\,(s/c, \gamma)$.

The three equations that result from the transformation are:

(1) $\tan \alpha_{st} = (\tan \gamma)\ \frac{R^2-1}{R^2+1}$

(2) $$\frac{c}{s} = \frac{1}{\pi}\left\{\cos\gamma \ln\left(\frac{R^2 + 2R\cos\alpha_{st} + 1}{R^2 - 2R\cos\alpha_{st} + 1}\right) + 2\sin\gamma\left(\tan^{-1}\frac{2R\sin\alpha_{st}}{R^2-1}\right)\right\}$$

(3) $$\frac{C_L}{C_{Li}} = K_o = \frac{4}{\pi}\ \frac{s}{c}\ \frac{R}{R^2+1}\ \frac{\cos\alpha_{st}}{\cos\gamma}$$

where $C_L = 2\pi K_o \sin\delta$ (actual) $\quad \delta$ = effective angle of attack

The parameters of Equations 1, 2 and 3 above are related as shown in Figures 2, 3 and 4 respectively. This modification of the lift coefficient with space-to-chord ratio (s/c) and stagger angle (γ) must be incorporated in the driving torque analysis.

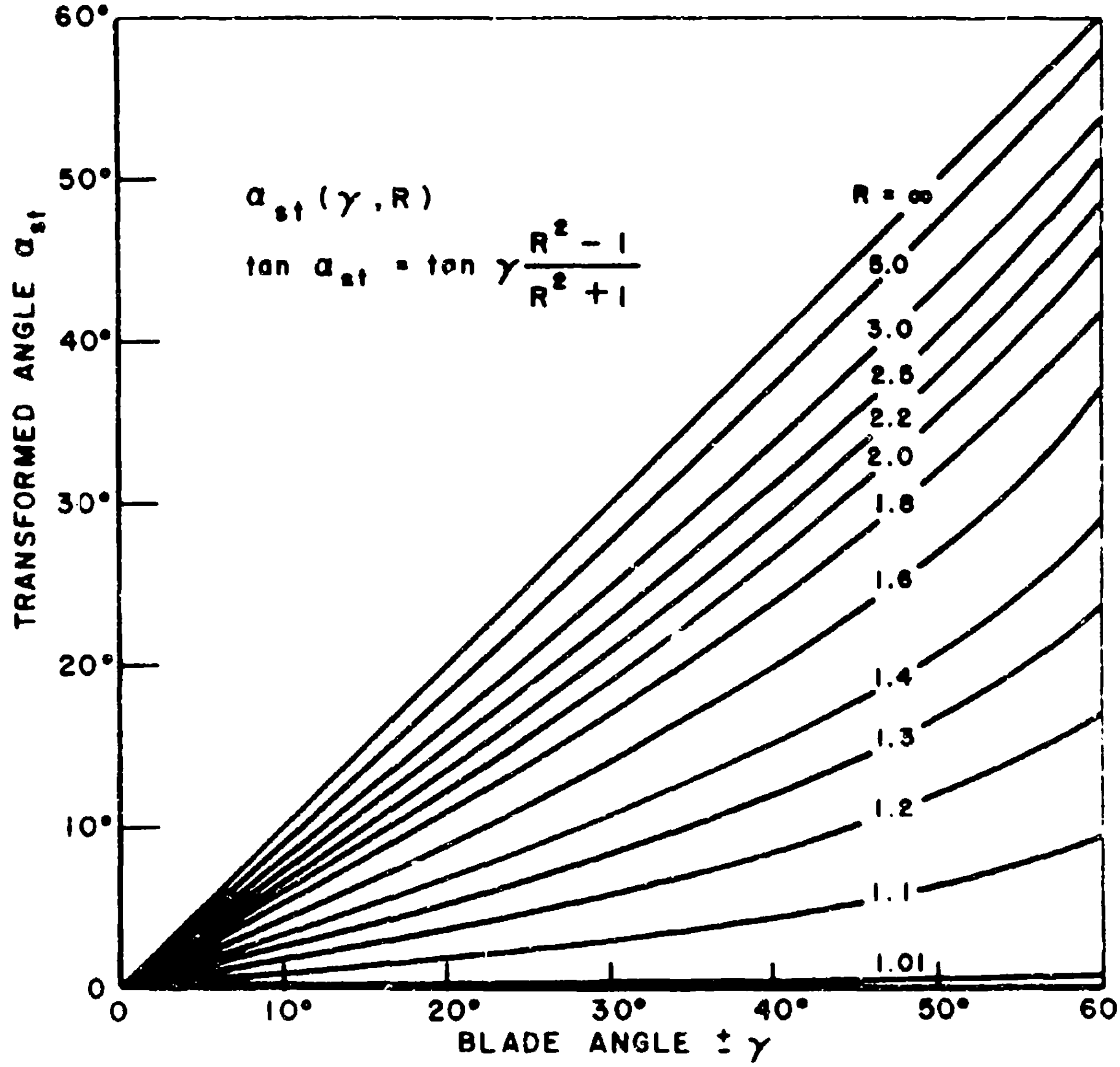

FIGURE 2

RELATIONS BETWEEN α_{st}, R AND γ

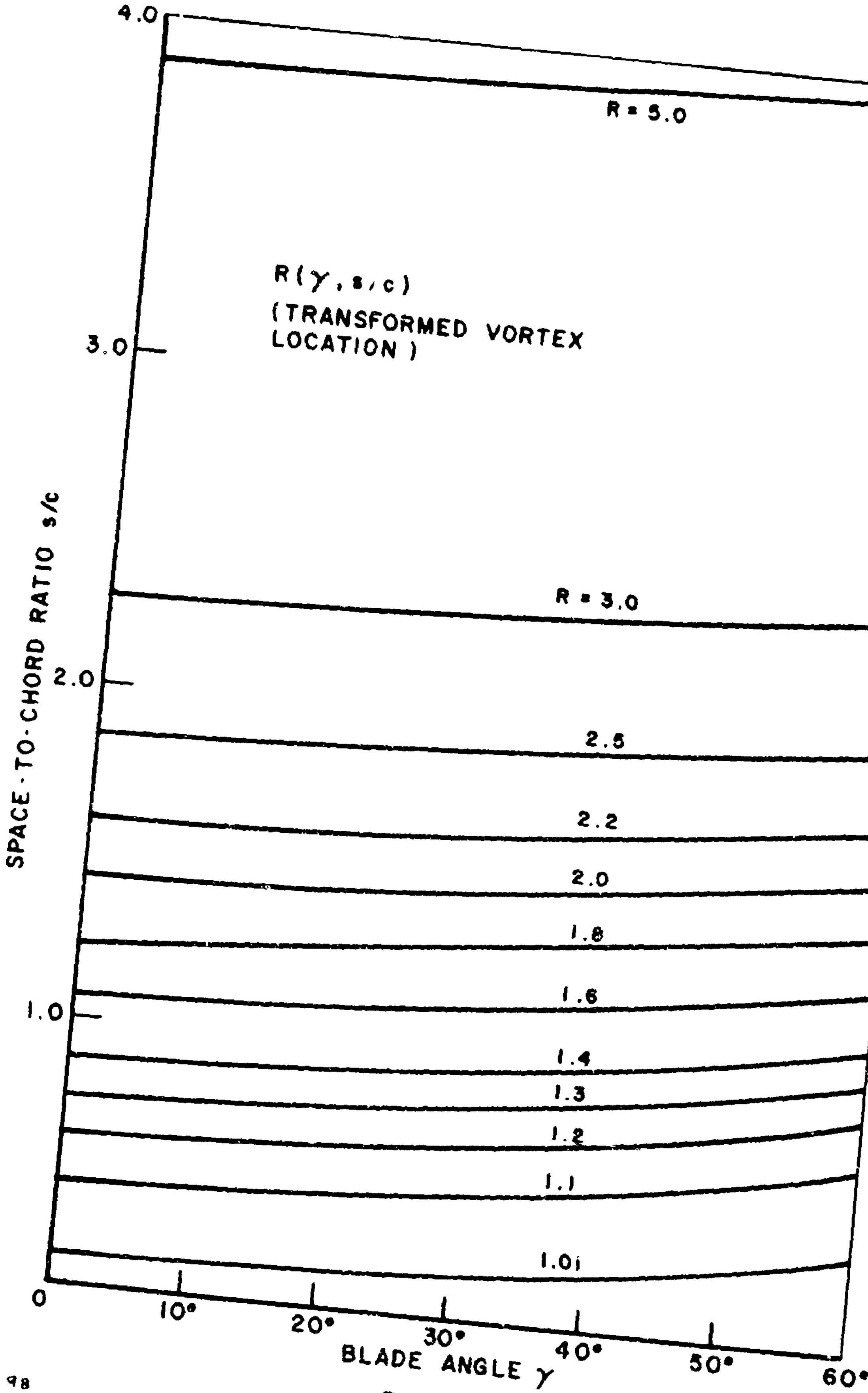

98

FIGURE 3

RELATIONS BETWEEN R, γ AND s/c

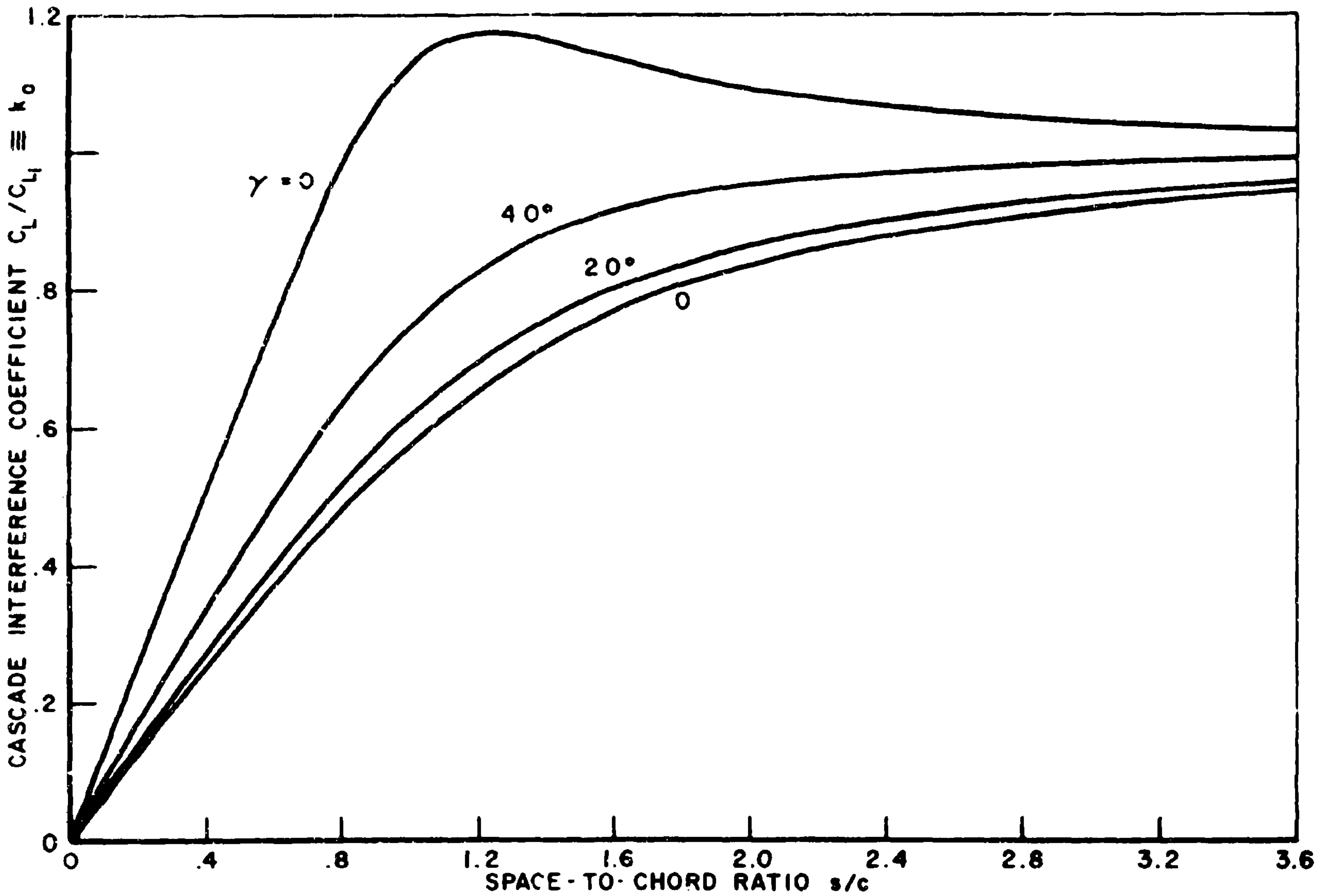

FIGURE 4

CASCADE INTERFERENCE COEFFICIENT k_o FOR COMPARISON WITH SINGLE-PROFILE THEORY

B. Rotor Driving Torque Analysis

As mentioned in the introduction to this section, the torque expression is derived for an element of blade area cdr at a radius r. The total torque is then obtained by integrating this expression from the hub radius R_h to the tip radius R_T. The fluid inlet velocity is assumed to be axial, and varies with radius as calculated in the velocity subroutine. For meters with a pre-swirler, the approach velocity is calculated in a different manner.

Figure 5 shows the velocity vector diagram for a turbine meter blade with absolute inlet velocity V_1 and tangential blade velocity $r\,\omega_a$. The axial component of all absolute velocities is V_z and must be constant for a given flow area to satisfy the continuity equation. The inlet velocity relative to the blade U_1 and the relative exit velocity U_2 are not assumed equal as in previous studies. The inlet velocity makes an angle β_1 with the meter axis. The exit velocity makes an angle β_2 with the meter axis which may be different from the blade angle. (Some earlier studies have assumed that the exit angle is independent of the approach angle β_1, and that the exit velocity is always parallel to the blade. Potential theory indicates that this is true only for small spacings of $s/c < 0.7$, which is generally not the case in turbine meters.)

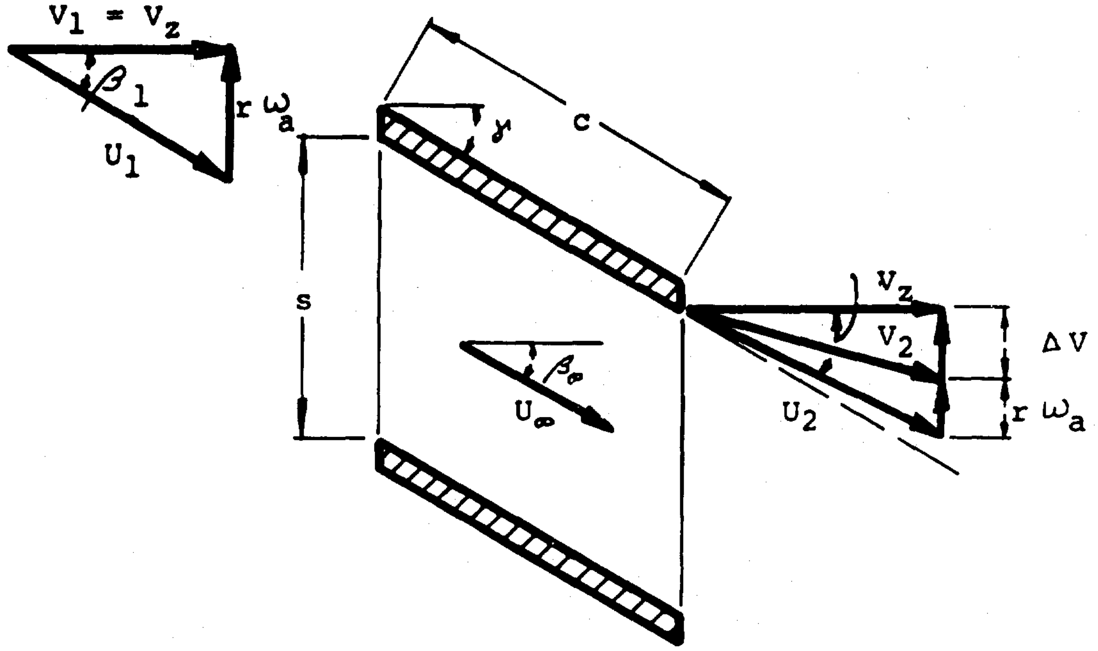

Fig. 5. Velocity Vector Diagram for Turbine Meter Blade

Following the practice in turbomachinery analyses and cascade theory, it can be shown that the vector average of the velocities upstream and downstream of the cascade plays the role of the velocity at infinity for an isolated airfoil, since the blade force is normal to this velocity for an inviscid fluid. Therefore, the lift and drag coefficients are defined perpendicular to the direction of the mean flow velocity

$$\vec{U}_\infty = \frac{\vec{U}_1 + \vec{U}_2}{2}$$

The mean flow velocity direction and the normal to the cascade axis have an included angle β_∞ defined by:

$$\tan \beta_\infty = \frac{1}{2} (\tan \beta_1 + \tan \beta_2)$$

The effective angle of attack is defined by

$$\delta = \gamma - \beta_\infty$$

rather than by the difference between γ and the inlet velocity angle β_1. The exit velocity angle β_2 must be known before the effective angle of attack can be defined. Since the exit velocity angle is a function of the space-to-chord ratio s/c and the stagger angle γ , blade spacing and interference effects are incorporated in this way also in the determination of the lift coefficient.

The lift and drag forces must be resolved into components perpendicular and parallel to the rotor axis. The driving torque comes from the lift component less the induced drag component:

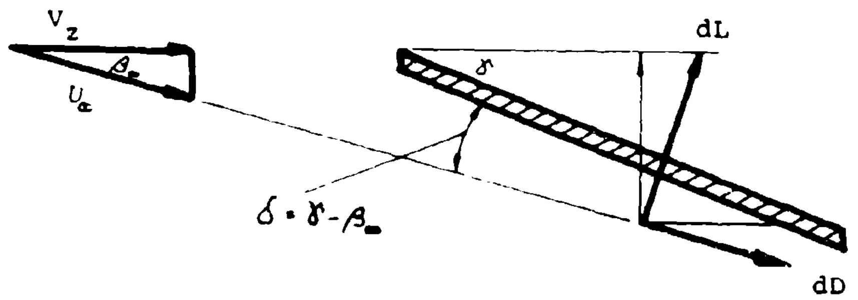

$$dT = Nr\,(dL \cos \beta_\infty - dD \sin \beta_\infty)$$

where $dL = (1/2\, \rho\, U_\infty^2)\; C_L\; (c\; dr)$

$$C_L = 2\,\pi\, K_c\, \sin \delta$$

$$\delta = \gamma - \beta_\infty$$

$$K_c = \frac{C_L}{C_{Li}} = f\left(\frac{s}{c}, \gamma\right)$$ from the potential flow analysis of cascades

$$dD = (1/2\, \rho\, U_\infty^2)\; C_D\; (c\; dr)$$

For smooth flat plates in turbulent flow and zero angle of attack:

$$C_D = 0.074\; (Re_c)^{-1/5}$$

From the mean flow velocity vector diagram:

$$U_\infty = \frac{V_z}{\cos\beta_\infty}$$

where V_z = absolute approach velocity = f(r);

and $$dL = \left(\tfrac{1}{2}\rho \frac{V_z^2}{\cos^2\beta_\infty}\right) 2\pi K_o \sin\delta \ c \ dr$$

$$dD = \left(\tfrac{1}{2}\rho \frac{V_z^2}{\cos^2\beta_\infty}\right) C_D \ c \ dr$$

Thus, $$dT = \tfrac{1}{2} V_z^2 \ c \ N\left[\frac{2\pi K_o \sin\delta}{\cos\beta_\infty} - C_d \frac{\sin\beta_\infty}{\cos^2\beta_\infty}\right] r \ dr$$

At this point, it is desirable to introduce some expressions relating β_1, β_2, δ, and β_∞ through the lift coefficient. Usually the lift coefficient is defined by:

$$C_L = \frac{2\Gamma}{U_\infty c}$$

where $$\Gamma = s V_z (\tan\beta_2 - \tan\beta_1)$$

and $$U_\infty = \frac{V_z}{\cos\beta_\infty}$$

Therefore, $$C_L = 2\frac{s}{c}\cos\beta_\infty(\tan\beta_2 - \tan\beta_1)$$

but $$C_L = 2\pi K_o \sin\delta \quad \text{also.}$$

Equating,

$$2\frac{s}{c}\cos\beta_\infty(\tan\beta_2 - \tan\beta_1) = 2\pi K_o \sin\delta$$

or $$\frac{s}{c}\frac{1}{\pi K_o}(\tan\beta_2 - \tan\beta_1) = \frac{\sin\delta}{\cos\beta_\infty}$$

This substitution can be made directly into the torque expression on the previous page. Other useful relationships can be obtained from trigonometric expansion of the term on the right:

$$\frac{\sin \delta}{\cos \beta_\infty} = \frac{\sin(\gamma - \beta_\infty)}{\cos \beta_\infty}$$

$$= \frac{\sin \gamma \cos \beta_\infty - \cos \gamma \sin \beta_\infty}{\cos \beta_\infty}$$

$$= \sin \gamma - \cos \gamma \tan \beta_\infty$$

$$= \sin \gamma - \frac{\cos \gamma}{2} (\tan \beta_1 + \tan \beta_2)$$

Thus,

$$\frac{s}{c} \frac{1}{\pi K_o} (\tan \beta_2 - \tan \beta_1)$$

$$= \cos \gamma \left[\tan \gamma - \frac{(\tan \beta_1 + \tan \beta_2)}{2} \right]$$

Let the deflection coefficient q be defined by:

$$q = \frac{K_o}{\frac{2}{\pi} \frac{s}{c} \frac{1}{\cos \gamma}} = \frac{\pi c K_o \cos \gamma}{2s}$$

$$= \frac{2R}{R^2 + 1} \cos \alpha_{st}$$

The deflection coefficient q is a function of the space-to-chord ratio s/c and the blade stagger γ, and can be computed by making use of previously calculated terms. This dependence is shown in Figure 6.

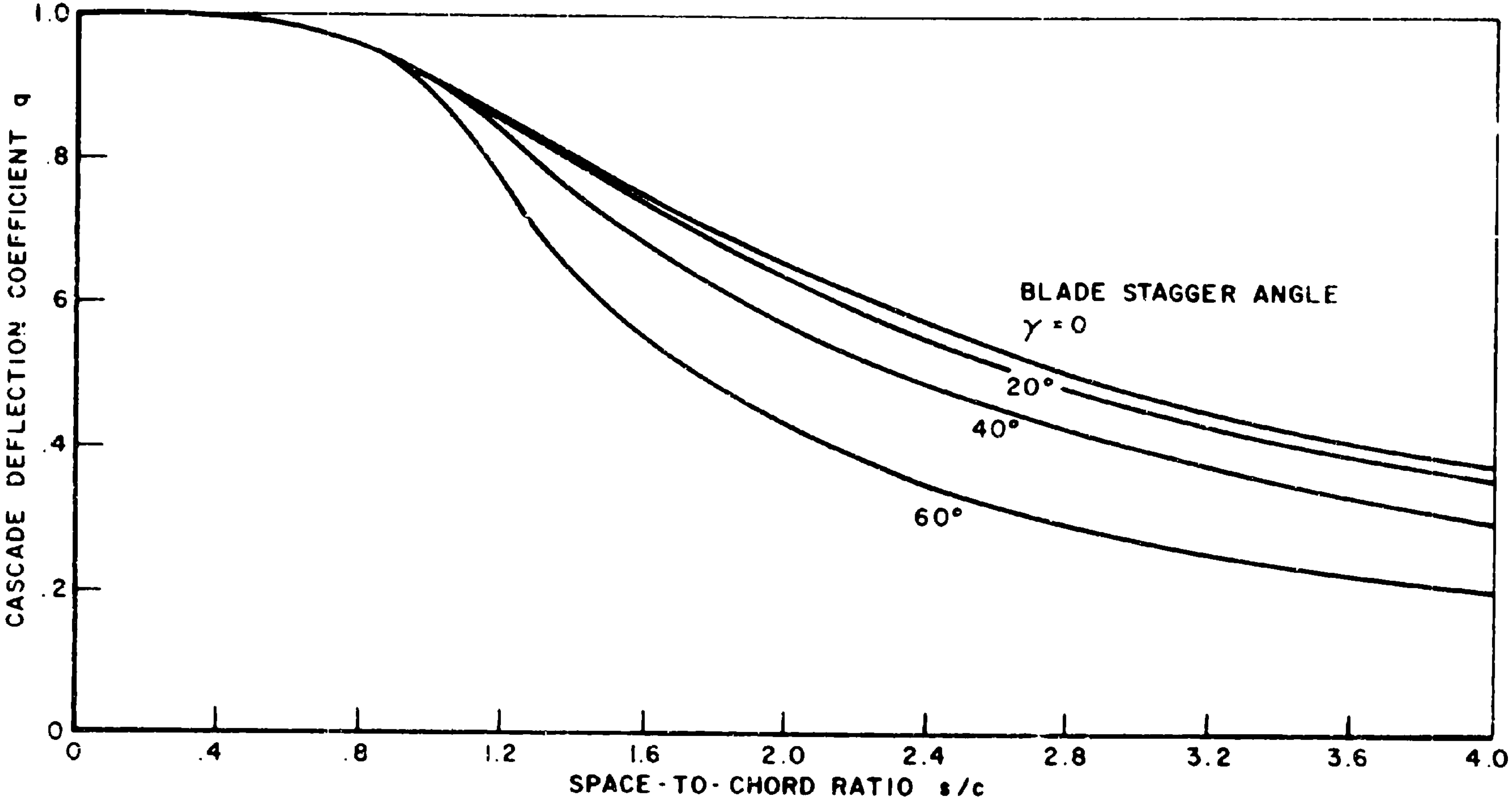

FIGURE 6

CASCADE DEFLECTION COEFFICIENT q VS s/c

Then $\dfrac{(\tan \beta_2 - \tan \beta_1)}{2q} = \tan \gamma - \dfrac{(\tan \beta_1 + \tan \beta_2)}{2}$

or, after some algebra,

$$\frac{\tan \beta_2 - \tan \beta_1}{\tan \gamma - \tan \beta_1} = \frac{2q}{1 + q}$$

Since $K_o = f(\gamma, s/c)$ and $q = f(K_o, s/c, \gamma)$, then β_2 can be determined as a function of β_1 and the geometry. Having related β_2 to β_1 through q, we can return to the substitution in the driving torque expression:

$$dT = \tfrac{1}{2} \rho V^2(r)\, cN \left[2 \frac{s}{c} (\tan \beta_2 - \tan \beta_1) - C_D \frac{\tan \beta_\infty}{\cos \beta_\infty} \right] r\, dr$$

From the velocity vector diagram below:

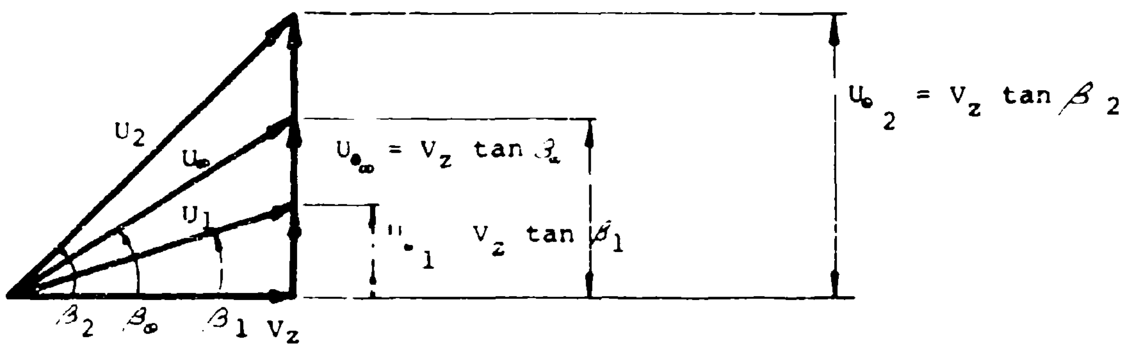

$$U_{\theta_\infty} = \frac{U_{\theta_1} + U_{\theta_2}}{2} = \frac{V_z}{2} (\tan \beta_1 + \tan \beta_2)$$

$$U_\infty = \left[V_z^2 + U_{\theta_\infty}^2 \right]^{1/2}$$

$$\text{or} \quad U_{\infty} = V_z \left[1 + \tfrac{1}{4}(\tan\beta_1 + \tan\beta_2)^2 \right]^{\frac{1}{2}}$$

$$\cos\beta_{\infty} = \frac{V_z}{U_{\infty}} = \left[1 + \tfrac{1}{4}(\tan\beta_1 + \tan\beta_2)^2 \right]^{-\frac{1}{2}}$$

$$\tan\beta_{\infty} = \frac{U_{\theta_{\infty}}}{V_z} = \frac{\tan\beta_1 + \tan\beta_2}{2}$$

$$\frac{\tan\beta_{\infty}}{\cos\beta_{\infty}} = \frac{(\tan\beta_1 + \tan\beta_2)}{2} \left[1 + \tfrac{1}{4}(\tan\beta_1 + \tan\beta_2)^2 \right]^{\frac{1}{2}}$$

Thus,
$$dT = \tfrac{1}{2}\rho V^2(r) cN \left\{ 2\,\frac{s}{c}(\tan\beta_2 - \tan\beta_1) - C_D\,\frac{(\tan\beta_1 + \tan\beta_2)}{2} \left[1 + \tfrac{1}{4}(\tan\beta_1 + \tan\beta_2)^2 \right]^{\frac{1}{2}} \right\} r\,dr$$

Using the previously derived expression relating β_2 to the blade geometry and inlet angle:

$$\tan\beta_2 - \tan\beta_1 = \frac{2q}{1+q}\,(\tan\gamma - \tan\beta_1)$$

But from the velocity vector diagram and definition of the lead of a helical blade:

$$\tan\beta_1 = \frac{r\,\omega_a}{V(r)}$$

$$\tan\gamma = \frac{2\pi r}{L}$$

so that

$$\tan\beta_2 - \tan\beta_1 = \frac{2q}{1+q}\left(\frac{2\pi r}{L} - \frac{r\,\omega_a}{V(r)} \right)$$

$$\text{or} \quad \frac{\tan\beta_2 + \tan\beta_1}{2} = \frac{q}{1+q}\left(\frac{2\pi r}{L} \right) + \frac{1}{1+q}\left(\frac{r\,\omega_a}{V(r)} \right)$$

Finally, therefore, the driving torque becomes:

$$T_d = \int_{R_h}^{R_T} \rho\, V^2(r)\, Ns \,\frac{2q}{1+q}\left(\frac{2\pi r}{L} - \frac{r\,\omega_a}{V(r)}\right) r\,dr$$

$$- C_D \int_{R_h}^{R_T} \rho\, V^2(r) \quad cN \left[\frac{q}{1+q}\left(\frac{2\pi r}{L}\right) + \frac{1}{1+q}\left(\frac{r\,\omega_a}{V(r)}\right)\right]$$

$$\left\{1 + \left[\frac{q}{1+q}\left(\frac{2\pi r}{L}\right) + \frac{1}{1+q}\left(\frac{r\,\omega_a}{V(r)}\right)^2\right]^{\frac{1}{2}}\right\} r\,dr$$

The driving torque expression given above includes modification of the theoretical lift coefficient for blade interference effects, but the single profile lift coefficient used is that of an ideal infinite wing without accounting for a finite aspect ratio or blade "airfoil" efficiency.

For a blade of finite length:

$$C_{L_{act}} = \left(\frac{\lambda}{1 + \frac{2\lambda}{AR}}\right) 2\pi K_o \sin\delta$$

where λ = blade "airfoil" efficiency $(0.9 < \lambda < 1.0)$

AR = blade aspect ratio $\dfrac{(R_T - R_h)^2}{\text{blade area}}$

Defining an effective lift experimental factor ϵ :

$$\epsilon = \frac{\lambda}{1 + \frac{2\lambda}{AR}}$$

the first term in a driving torque equation becomes:

$$\int_{R_h}^{R_T} \epsilon \rho V^2(r) \, Ns \left(\frac{2}{1 + q} \right) \left(\frac{2 \pi r}{L} - \frac{r \omega_a}{V(r)} \right) r \, dr$$

It is apparent that integration to obtain a closed form expression for driving torque is not possible, partly because of the desired dependence of density and velocity on radius. Therefore, numerical integration on the computer was chosen as the method for obtaining a solution. For a given radius, the rotor configuration specifies s, c, and δ, which give K_c and q. The velocity and density at r are specified from the flow conditions and the integrated driving torque can be obtained. For the case of flat blades, the term $\frac{2 \pi r}{L}$ can be replaced by tan δ in the torque expression and the blade stagger angle substituted directly.

C. Rotor Hub Fluid Drag

The fluid friction drag on the rotor hub has a component which contributes to the fluid retarding torque. The fluid drag on the rotor hub is:

$$F_h = (\tfrac{1}{2} \rho U_\infty^2)_h \; C_D \, A \cos \beta_e$$

The retarding torque becomes:

$$T_h = \tfrac{1}{2}N(\rho\, U_\infty^2)_h \; C_D(Cs \cos \gamma)_h \; \sin \beta_\infty \; R_h$$

$$= \tfrac{1}{2}N(\rho\, V^2)_h \; C_D(Cs \cos \gamma)_h \; \frac{\tan \beta_\infty}{\cos \beta_\infty} \; R_h$$

$$= \tfrac{1}{2}N(\rho\, V^2)_h \; C_D(Cs \cos \gamma)_h \left(\frac{\tan \beta_1 + \tan \beta_2}{2} \right) \left[1 + \tfrac{1}{4}(\tan \beta_1 + \tan \beta_2)^2 \right]^{\frac{1}{2}} \; R_h$$

$$= \tfrac{1}{2}N(\rho\, V^2)_h \; C_D(Cs \cos \gamma)_h \left[\left(\frac{q}{1+q} \right) \tan \gamma + \left(\frac{1}{1+q} \right) \tan \beta_1 \right] \left\{ 1 + \left[\left(\frac{q}{1+q} \right) \tan \gamma + \left(\frac{1}{1+q} \right) \tan \beta_i \right]^2 \right\}^{\frac{1}{2}} R_h$$

V_h must be an effective free-stream velocity in the vicinity of the hub, since V_h is actually zero for viscous flow. The value used in the numerical case was taken as the mean flow velocity $\bar{V}$.)

D. Blade Tip Clearance Drag

As the meter blades rotate in close proximity to the meter body, a blade tip clearance drag imposes a retarding torque on the rotor which is dependent upon the clearance. The retarding torque is very similar to that in a journal bearing, and the analysis is based on this analogy. The drag is proportional to the friction factor which is a function of the Reynolds number based on the rotor clearance. The retarding torque is:

$$T_{BT} = \left(f \rho \frac{U^2}{2} \right) (ct) \; R_T \; N$$

where $\omega_a = \dfrac{U}{R_T}$

$$f = \frac{0.078}{Re^{0.43}}$$

Thus, $T_{BT} = \dfrac{0.078}{2 \; Re^{0.43}} \rho \, \omega_a^{2} \, R_T^{3} \; ct \; N$

where the Reynolds number is defined as $Re = \rho \dfrac{\omega_a R_T (R_B - R_T)}{\mu}$

This friction factor, based upon the bearing analogy, may be somewhat higher than actual. A similar calculation was made expressing the blade tip clearance drag as a function of the drag coefficient based on the blade thickness; however, this calculation was not considered valid, since the controlling dimension should be the clearance. Hence the bearing analogy is preferred.

E. Velocity Profiles

This study is restricted to fully developed turbulent flow with the meter located a distance downstream of the inlet that will guarantee fully formed velocity profiles (~ 25 to 40 diameters). The discussion in this section is also restricted to smooth pipes. Empirical correction factors will be necessary for other pipe conditions.

Several options exist in the program to specify the velocity profile. A subroutine permits the calculation of the velocity profile for turbulent flow through the annular rotor area. The option also exists to specify the velocity profile based on a curve-fit of experimental data, or predicted analytically to study other effects. The only restriction is that the velocity profile be axisymmetric. This limitation is necessary, because without it the integration routine would become very complicated, requiring weighting of portions of the annular flow to get equivalent average velocities, etc.

To study the importance of velocity profiles, a calculation routine is also provided to determine the fully developed pipe profile. However, the application of this routine is not recommended, because flow through the straightener and rotor hub areas is better described by the annular flow subroutine.

1. Annular Flow Velocity Profile

One of the most thorough studies of flow in annuli is that of Levy, Reference 23. The analytical predictions of the velocity profile, plane of zero shear, mixing length, eddy diffusivity, and friction factor provide very good agreement with test data. The analysis is based upon Reichardt's expression for eddy diffusivity of momentum. The theory parallels that of flow in a circular pipe and requires only the assumption of the form of the eddy diffusivity of momentum and a mixing length constant near the outer tube wall.

It is interesting to note that the point of maximum velocity for turbulent profiles in annuli does not correspond to the midpoint of the annulus, and therefore the inner and outer portions of the velocity profile curve will be different. The velocity profiles starting from the rotor support hub and the outer meter wall have the same velocity and eddy diffusivity at the plane of zero shear.

The following equations are necessary to obtain the desired solution. Details of the analysis are found in Reference 23. (Several mistakes found in this reference have been corrected below):

$$u^+ = \frac{1}{K} \ln \left[1.5y^+ \frac{1 + \eta}{1 + 2\eta^2}\right] + \frac{2s(1 - s)}{K(1 + s)(2s - 1)} \ln \left(\frac{1 + \eta}{2}\right)$$

$$+ \tfrac{1}{2} \frac{s(1 - s)(1 - 3s)}{K(1 + s)\left[s^2 + \tfrac{1}{2}(1 - s)^2\right]} \ln \left(\frac{1 + 2\eta^2}{3}\right)$$

$$+ \frac{6}{K(1 + s)} \frac{\ln \left[\eta(1 - s) + s\right]}{\left[\left(\frac{1 - s}{s}\right)^2 - 1\right]\left[\left(\frac{s}{1 - s}\right)^2 + 2\right]}$$

$$+ \frac{\sqrt{2}}{K} \frac{(1 - s)s}{1 + s} \frac{\tan^{-1}\sqrt{2} - \tan^{-1}\eta\sqrt{2}}{s^2 + \tfrac{1}{2}(1 - s)^2}$$

$$+ 14.84 - \frac{1}{K} \ln 42 \qquad (1)$$

where

$$u^+ = \frac{V_z}{\sqrt{\tau_R/\rho}}$$

$$y_i^+ = \frac{(r - R_h)\sqrt{\tau_{R_h}/\rho}}{} \quad \text{for } r < r_m$$

$$y_o^+ = \frac{(R_b - r)\sqrt{\tau_{R_b}/\rho}}{} \quad \text{for } r > r_m$$

$$\eta = \frac{r - r_m}{R - r_m}$$

$$s = \frac{r_m}{R}$$

Equation 1 is valid on both sides of the annulus. For the region near the meter body wall, subscripts b should be used with the terms K, $\tilde{\tau}_R$, s and R. Subscripts h apply to the region near the rotor hub.

$$\frac{\tilde{\tau}_{R_h}}{\tilde{\tau}_{R_b}} = \frac{R_b}{R_h} \frac{(r_m^2 - R_h^2)}{(R_b^2 - r_m^2)} \tag{2}$$

$$\frac{K_o}{K_i} = \left(\frac{r_m - R_h}{R_b - r_m}\right)^{3/2} \left(\frac{R_b}{R_h}\right)^{\frac{1}{2}} \left(\frac{r_m + R_h}{R_b + r_m}\right)^{\frac{1}{2}} \tag{3}$$

$$\frac{K_o}{K_i} = \sqrt{\frac{\tilde{\tau}_{R_b}}{\tilde{\tau}_{R_h}}} \quad \frac{A}{B} \tag{4}$$

where

$$A = \ln 1.5 + \ln\left[\frac{|R_b - r_m|}{\nu} \sqrt{\tilde{\tau}_{R_b}/\rho}\right] - \frac{2s_o(1 - s_o)}{(1 + s_o)(2s_o - 1)} \ln 2 - \frac{1}{2} \frac{s_o(1 - s_o)(1 - 3s_o)}{(1 + s_o)\left[s_o^2 + \frac{1}{2}(1 - s_o)^2\right]} \ln 3$$
$$+ \frac{6 \ln s_o}{(1 + s_o)\left[\left(\frac{1 - s_o}{s_o}\right)^2 - 1\right]\left[\left(\frac{s_o}{1 - s_o}\right)^2 + 2\right]} + \frac{s_o(1 - s_o)\sqrt{2}\tan^{-1}\sqrt{2}}{(1 + s_o)\left[s_o^2 + \frac{1}{2}(1 - s_o)^2\right]} + 14.84\,K_o - \ln 42 \tag{5}$$

The term B is given by the above expression except for substituting R_h, τ_{R_h}, s_i and K_i for R_b, τ_{R_b}, s_o and K_o.

$$\frac{(R_b - r_m)\sqrt{\tau_{R_b}/\rho}}{\nu} = \tfrac{1}{2}\,\mathrm{Re}\sqrt{\frac{f}{2}}\left(\frac{1-\frac{r_m}{R_b}}{1-\frac{R_h}{R_b}}\right)^{3/2}\left(1+\frac{r_m}{R_b}\right)^{\frac{1}{2}} \qquad \text{(a)}$$

(6)

$$\frac{(r_m - R_h)\sqrt{\tau_{R_b}/\rho}}{\nu} = (R_b - r_m)\frac{\sqrt{\tau_{R_b}/\rho}}{\nu}\;\frac{K_o}{K_i} \qquad \text{(b)}$$

where Re is the Reynolds number expressed in terms of the hydraulic diameter of the channel:

$$\mathrm{Re} = \frac{2\,\bar{v}\,R_b\left(1-\frac{R_h}{R_b}\right)}{\nu}$$

The calculation procedure is as follows:

(1) From the design volumetric flow rate q, determine the average velocity $\bar{v}$ from:

$$\bar{v} = \frac{q}{\pi(R_b^2 - R_h^2)}$$

For application in the swirler region, the average velocity $\bar{v}_s$ is:

$$\bar{v}_s = \frac{q}{\pi(R_{os}^2 - R_{is}^2) - Nt_s\,(R_{os} - R_{is})}$$

(2) Calculate the Reynolds number based on the hydraulic diameter from:

$$Re = 2\bar{v}\,\frac{R_b\left(1 - \frac{R_h}{R_b}\right)}{\nu} \quad \text{or} \quad \frac{\rho\,\bar{v}\,2(R_b - R_h)}{\mu}$$

(3) For the first approximation, the use of the hydraulic diameter to predict friction factor based on smooth pipe friction factor relations is satisfactory:

$$f = \frac{0.046}{(Re)^{0.2}}$$

Other friction factor expressions (as a function of pipe roughness) can be substituted if desired.

(4) K_o is taken equal to 0.4 and a value of r_m is assumed. Calculate $\dfrac{(R_b - r_m)\sqrt{\tau_{R_b}/\rho}}{\nu}$ from Equation 6(a).

(5) Calculate K_o/K_i from Equation 3.

(6) Calculate $\dfrac{(r_m - R_h)\sqrt{\tau_{R_h}/\rho}}{\nu}$ from Equation 6(b).

(7) Calculate $\dfrac{\tau_{R_b}}{\tau_{R_h}}$ from Equation 2.

(8) Calculate s_o, s_i and η_o, η_i from Equation 1.

(9) Calculate A and B terms from Equation 5.

(10) Repeat Calculations 1 through 9 until Equation 4 is satisfied.

(11) The velocity distributions are finally calculated for Equation 1 giving $V_z = f(r)$ for substitution in the driving torque equations.

Because of the logarithmic relationship between u^+ and y^+, some difficulties are encountered in evaluating the velocity profile extremely close to the walls. In this region, the velocity profile can be considered to be relatively independent of the annular configuration, and will follow the profile that would exist in a full pipe profile. In this region, the expression $u^+ = y^+$ is commonly used for values of y^+ less than 5.0. This assumption is also made for the annular velocity profile calculations.

2. Fully Developed Pipe Velocity Profile

Turbulent flow through pipes has received considerable attention in the past because of its obvious importance in many fields. A large part of this work was experimental, with the most significant work in the area of velocity profile determination performed by J. Nikuradse. A discussion of his work is found in Schlichting, Reference 24.

Nikuradse carried out a very thorough experimental investigation into velocity profiles in smooth pipes over a very wide range of Reynolds numbers ($4 \times 10^3 < Re < 3.2 \times 10^6$), where Reynolds number is based on the mean flow velocity $\bar{v}$ and the pipe diameter D: $Re = \frac{\bar{v}D}{\nu}$. Nikuradse found that it is possible to represent the velocity profile by the empirical expression:

$$\frac{V(r)}{V_{max}} = \left(\frac{y}{R}\right)^{\frac{1}{n}}$$

where the exponent n varies slightly with Reynolds number and V_{max} is the maximum velocity in the cross section. Using the expression above, the ratio of the mean to maximum velocity $\bar{v}/V_{max}$ is found to be:

$$\frac{\bar{v}}{V_{max}} = \frac{2n^2}{(n+1)(2n+1)}$$

The values of n increase slightly with Reynolds number, as shown in the table below and Figure 7.

Re	n
4×10^3	6.0
2.3×10^4	6.6
1.1×10^5	7.0
1.1×10^6	8.8
2.0×10^6	10.0

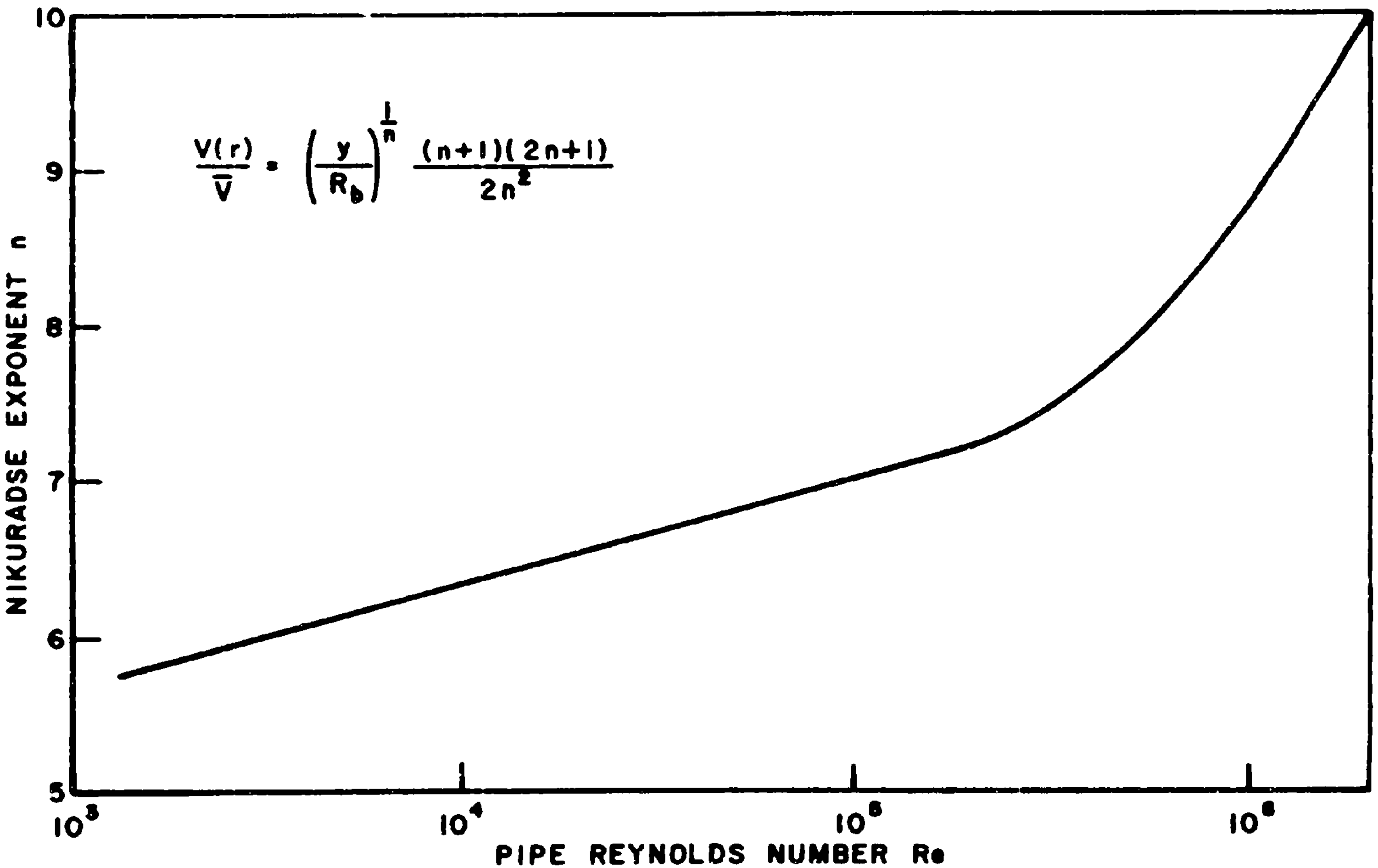

FIGURE 7

TURBULENT FLOW VELOCITY PROFILE DETERMINATION

For a given flow rate and pipe diameter, the Reynolds number can be obtained and the velocity profile determined from:

$$\frac{V(r)}{\bar{V}} = \left(\frac{y}{R_b}\right)^{\frac{1}{n}} \frac{(n + 1)(2n + 1)}{2n^2}$$

The velocity profile given above is for turbulent flow in an unobstructed pipe, and represents the flow upstream of the metering section. It should not be confused with the velocity profile at the blade inlet section, since the flow straightener, rotor hub and housing obstruct a portion of the flow, resulting in a different profile. The actual profile may be a transition flow approaching the annular profiles. The presence of the flow straighteners suggests that the annular profile is a better representation of the actual fluid behavior than the fully developed pipe profile just described. One reason for this is that zero velocity will exist at the hub support, which will not be true for pipe flow profiles. Therefore, the fully developed pipe profiles are not recommended for actual use, and were included in the program only as a tool to study the importance of velocity profile on meter performance.

The final velocity profile option is the provision for specifying the profile by means of constants obtained from the curve fit of experimentally measured profiles or a theoretically specified profile for parametrically exploring the effects on meter registration.

1. Meter Dimensional Effects

Although the study is concerned primarily with storable propellants, the importance of meter dimensional effects can best be illustrated for cryogenics. The problem of temperature compensation in calibration factors for cryogenic operation was first treated by Grey in References 5 and 6. More recently, Staniszlo and Krause[7] in NASA TND-3773 published a derivation of a thermal correction factor for liquid hydrogen that included allowances for blade tip clearance and boundary layer effects. Reference 8, a companion report, presented data indicating that a difference of 0.3% could exist due to the added terms for blade tip clearance. The expression is given below:

$$\frac{\Delta \omega}{\omega} = -\beta_R \, \Delta T \left[3 + \frac{\left(2 \frac{\beta_h}{\beta_R} D_H^2 - D_{BR}^2\right)}{D_H^2 - D_R^2} \left(\frac{V_n}{\bar{V}_s} - \frac{D_H^2 - D_{BR}^2}{D_H^2 - D_R^2} \right)^{-1} \right]$$

The first factor, $-3\beta\Delta T$, was originally derived by Grey and the remainder represents the correction for blade-tip clearance effects. The predicted 0.3% change seemed quite large, and for this reason a sample calculation was made using the conditions outlined in the analysis:

$$\beta_H = 6.1 \times 10^{-6} \text{ in/in} \qquad \text{303 Stainless}$$

$$\beta_R = 3.9 \times 10^{-6} \text{ in/in} \qquad \text{17-4 PH Stainless}$$

$$\Delta T = -447^\circ F$$

Of the 0.3% change due to blade tip clearance effects, a portion of this correction is due to the clearance change caused by the housing and rotor having different thermal coefficients of expansion, and the remainder is the true correction term for including clearance leakage in the analysis. The calculation indicated that 0.11%, or approximately one-third of the correction, is due to the inclusion of clearance leakage in the analysis.

Both References 6 and 7 have based their analysis on geometrical relationships which are true only if there are no retarding torques. Since the purpose of this study is to develop a general model, with retarding torques and variable velocity profile, the approach used in the above references does not apply. Dimensional effects are therefore included by making the appropriate geometry temperature-dependent by defining a reference geometry and the appropriate coefficients of thermal expansion. In this way, different coefficients of expansion for the rotor and meter body can be included.

Assuming isotropic materials:

$$R_b = R_{b_o} (1 + \beta_b \Delta T)$$

$$R_h = R_{h_o} (1 + \beta_r \Delta T)$$

$$R_T = R_{T_o} (1 + \beta_r \Delta T)$$

where β_b = coefficient of thermal expansion for the meter body

β_r = coefficient of thermal expansion for the rotor hub and blades

With these expressions, a change in operating temperature, and hence meter geometry, results in a change in the mean flow velocity and velocity profile for a constant flow rate. Changes in these parameters appear directly in the torque equation and limits of integration.

G. Model Flow Rate and Fluid Property Requirements

The turbine flowmeter performance model is restricted to fully developed turbulent flow of a single-phase incompressible Newtonian liquid. This implies restrictions on the flow rate, line pressure, and approach length upstream of the meter. The transition from laminar to turbulent flow occurs somewhere in the Reynolds number range of 2300 to 4000. To insure fully turbulent flow for less than meter design flow rates, the model is restricted to flows with a minimum Reynolds number of 10,000 at the actual flow rate.

Since the performance model is restricted to single-phase fluids, the pressure downstream of the meter should always exceed the fluid vapor pressure by at least 25%.

The inlet length required for fully developed turbulent flow is considerably shorter than for laminar flow. Experimental measurements of inlet length by various investigators reported in Schlichting (page 502) vary from 25 to 40 diameters in one case to 50 to 100 diameters in another. As a general rule, a minimum of 40 pipe diameters should exist between the supply tank and the meter.

Most turbine flowmeters contain flow straighteners upstream of the rotor to remove any swirl the fluid may have acquired in passing through upstream elbows and other piping. Where straightening vanes are not employed, a straight run of pipe upstream and downstream of the meter is required. Since these requirements are experimentally determined, there is some variation in the length of pipe recommended. The American Petroleum Institute, Reference 25, recommends 10 pipe diameters upstream and $2\frac{1}{2}$ diameters downstream as a minimum. The American Gas Association, Reference 26, has prepared similar data for orifices, and recommends from sixteen pipe diameters (for the case of a simple el) to 40 diameters (for els in different planes) upstream. A minimum of five pipe diameters downstream is recommended.

H. Blade Boundary Layer Growth Calculations

The driving torque and blade interference analysis assumes incompressible inviscid flow. As mentioned in earlier sections, a viscous flow analysis of the blade boundary layer region and trailing edge wake appeared to be beyond the scope of the study, because these effects were of primary importance in turbomachinery with large turning angles and pressure differences, and would be less important in turbine flowmeters. To conduct this analysis, it would be necessary to determine the ideal potential pressure distribution around the contour of the blades; the boundary layer on the blade; and the losses due to mixing in the wake behind the cascade. Therefore, a rough boundary layer growth calculation was made for a typical 2", 225 gpm turbine flowmeter to determine if the boundary layer was small enough to be neglected.

The meter had a rotor hub and body diameter of 0.834" and 1.781" respectively. Calculations were made for maximum design flow rates in water, N_2O_4, and 50/50 hydrazine blend. The boundary layer thicknesses at the trailing edge were:

Fluid	δ
H_2O	0.014"
N_2O_4	0.011"
50/50 Blend	0.014"

These boundary layers represent from 4% to 9.5% of the spacing (on a 14-bladed rotor) at the tip and hub, respectively. Therefore, there is little possibility of boundary layer interaction in the blade row.

Note that the numbers given above are for the boundary layer thickness, which is approximately eight times the displacement thickness, and therefore the portion of the flow influenced by the boundary layer is very small in proportion to the total flow.

I. Modification of Velocity Vector Diagram for Preswirler

Several meter designs employ deflection blades at the end of the straightening vanes to impart to the fluid an intentional swirl as it approaches the rotor blades. These deflection blades are integral with the flow straightener and are commonly formed by inclining the trailing edge of the straightener blade to the desired angle. Generally, the number of preswirl blades is less than the number of rotor blades, and space-to-chord ratios are larger.

The use of intentional preswirl upstream of the rotor blades came about through empirical studies with previous meter designs. Meter manufacturers found that blade length had a direct bearing on the Reynolds number region in which "viscosity hump" occurred. This problem was solved by shortening the blades, but the meter characteristic was no longer flat in the high Reynolds number regime. Through experimentation, it was found that the use of preswirlers lifted the high Reynolds number end of the curve to give a flat characteristic.

An analysis of the preswirler is necessary since it modifies considerably the approach velocity vector diagram for rotor. Since the space-to-chord ratio may be large with a few number of blades, complete fluid guidance cannot be assumed and the actual departure velocity and departure angle must be calculated. The analysis is virtually identical to that employed in the analysis of the rotor, since the preswirler is just a fixed cascade. The previous expressions are somewhat simplified, because the angular velocity terms are not present. Therefore, the same equations can be used to calculate a deflection coefficient as a function of the preswirler space-to-chord ratio and blade stagger angle. The deflection coefficient and velocity vector diagram allow the calculation of the departure velocity and angle.

The flow is deflected in the direction of the rotor rotation as shown in velocity vector diagram below:

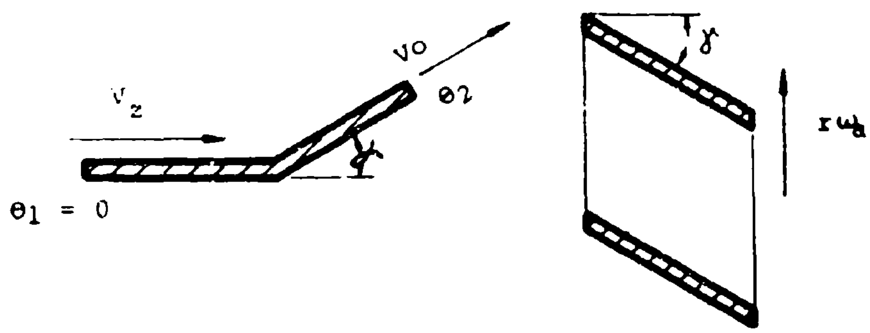

Blade interference effects and a deflection coefficient can be calculated for the straightener using the same expressions as for the rotor:

$$\frac{\tan \theta_2 - \tan \theta_1}{\tan \alpha - \tan \theta_1} = \left(\frac{2q}{1 + q}\right)_{\text{straightener}}$$

where $\quad q = f(s/c, \alpha\ , \text{etc.})$ and $\tan \theta_1 = 0.$

Thus, $\quad \tan \theta_2 = \left(\frac{2q}{1 + q}\right)_s \tan \alpha$

In some meter designs, the flow straightener hub and rotor hub have slightly different radii. However, the continuity equation must be satisfied, and therefore the straightener axial velocity will be modified slightly.

$$V_{z_s} \pi (R_{os}^2 - R_{is}^2) = V_{z_R} \pi (R_b^2 - R_h^2)$$

$$V_{z_R} = \left(\frac{R_{os}^2 - R_{is}^2}{R_b^2 - R_h^2}\right) V_{z_s}$$

The velocity vector diagram at the rotor becomes:

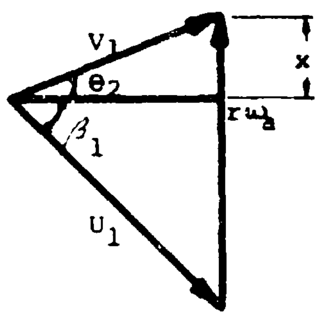

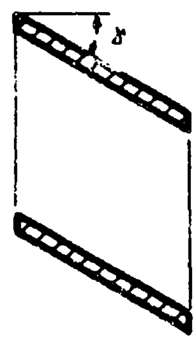

$$x = \tan \theta_2 V_{z_R} = \left(\frac{2q}{1 + q}\right)_s \tan \alpha \left(\frac{R_{os}^2 - R_{is}^2}{R_b^2 - R_h^2}\right) V_{z_s}$$

$$\tan \beta_1 = \frac{r\omega_a - x}{V_z}$$

$$\tan \beta_1 = \frac{r\omega_a - \left(\frac{2q}{1 + q}\right) \tan\alpha \left(\frac{R_{os}^2 - R_{is}^2}{R_b^2 - R_h^2}\right) V_{z_s}}{V_z}$$

The rotor torque equation can be evaluated for the case of preswirler designs by making the same substitution for

$\tan \beta_1$. In the above equation, V_z is the axial velocity for the rotor annulus at radius r, and V_{z_s} is the axial velocity for the flow straightener annulus.

J. Pressure Drop Calculation

An accurate analysis of the pressure drop through a turbine flowmeter requires a study of the effect of blade thickness, spacing, and departure angle on friction losses and downstream energy dissipation in the fluid wake. As mentioned in earlier sections, a detailed analysis of wake dissipation effects is beyond the scope of the program without an accompanying pressure distribution and boundary layer analysis. Therefore, a wake analysis will not be performed, although those interested in further reading on this subject should consult Reference 4, pages 75-79.

A simplified way of describing the energy loss which occurs in the viscous flow through a rotor or cascade is through the introduction of a dimensionless loss coefficient:

$$\zeta_v = \frac{\Delta h}{\frac{1}{2}\rho V_z^2} = \frac{\text{loss in total head}}{\text{dynamic pressure of axial component}}$$

A discussion of the calculation of loss coefficients of a two-dimensional cascade is found in a paper by Schlichting (Reference 27). Application of boundary layer theory to a cascade in at least an approximate manner is necessary to obtain the relation between the loss coefficient, the deflection coefficient, the angle of inflow, and all the geometric parameters of the cascade. The deflection coefficient has been obtained from potential theory, but the loss coefficient can only be obtained from viscous-flow theory. As summarized by Schlichting, the losses associated with a cascade consist of losses in the nonseparated boundary layer; of additional losses due to separation if it occurs; and of losses due to turbulent mixing in the wake. Because of the small angles of attack, separation is not a problem. The losses due to wake mixing will be omitted as previously discussed to simplify the computation, so in this regard the pressure drop calculation is approximate.

The loss coefficient obtained from Schlichting (Reference 27) is:

$$\zeta_v = \frac{2\,\Theta}{\cos^2 \beta_{2\,corr}}$$

where Θ denotes a dimensionless momentum thickness obtained from the momentum thickness at the trailing edge of the blade by the following formula:

$$\Theta = \frac{\vartheta_{t_S} + \vartheta_{t_P}}{s \cos \beta_{2\,corr}}$$

where θ_{t_S} and θ_{t_P} denote the momentum thickness at the trailing edge for the suction side S and the pressure side P of the blade. The expressions also contain $\beta_{2\,corr}$, which is the angle of outflow in potential flow corrected to take into account the influence of the boundary layer on the potential flow. Since the blade turning angles and pressure drops are small compared to those of conventional turbines, the influence on the angle of outflow should be small. For this reason, β_2 from the potential flow analysis will be used in computations given above. Because the blades are flat with no camber and run at very small angles of attack, the trailing edge momentum thicknesses should be comparable. Combining the previous expressions based on these approximations:

$$\Delta h = (\tfrac{1}{2} \rho V_z^2) \frac{4 \theta_t N}{S \cos^3 \beta_2}$$

$$\theta_t = 0.036 \;c\; (Re_c)^{-1/5}$$

In addition to the viscous losses due to the blades, there is the additional friction loss on the meter walls, as in any pipe:

$$\Delta P = (\tfrac{1}{2} \rho V_{pipe}^2) \left(\frac{4fL}{D}\right)$$

where L = meter length and $f = \dfrac{0.046}{(Re_D)^{0.20}}$

The expression given above cannot be properly applied for flow through an annulus, however. The pressure drop through an annular space of inner diameter D_1 and outer diameter D_2, taken from McAdams (Reference 28) is given by:

$$\frac{\Delta P}{\Delta L} = \frac{32 \mu V}{\left(D_2^2 + D_1^2 - \dfrac{D_2^2 - D_1^2}{2.3 \log_{10} (D_2/D_1)} \right)}$$

This expression is preferred in the annular region between the hub and the housing approaching the rotor. It is also applied in the annular region between the flow straightener support and the meter body.

K. Bearing Retarding Torques

The complexity of bearing drag or retarding torque expressions was mentioned briefly in the initial literature survey. A majority of the recent references in this field are based on the paper of Scibbe and Anderson, Reference 22. This analysis is based on the assumption that ball spin torque is the major contributor to total bearing torque. To properly use this analysis, one must have a detailed knowledge of the bearing design, since the major parameters include inner and outer race contact angle, pitch diameter, race curvature, ball diameter, outer race ball load, coefficient of sliding friction, etc.

Generally, it would be expected that a user of turbine flowmeters, interested in turbine meter performance, would not be familiar with the design details of a particular bearing used in a meter. In addition to the complexity of the torque expressions and the many unknowns, these parameters can vary widely with axial and radial clearances, which in turn vary with temperature. This has been pointed out by Smith in Reference 9, where the direct use of the ball bearing torque expressions in a turbine flowmeter analysis was not practical for these reasons. The most convenient way of introducing bearing retarding torques into the turbine meter analysis is through retarding torque speed and load curves or tables obtained by direct measurement or from analytical predictions made by bearing manufacturers familiar with design details.

For those interested in the design of a turbine meter and important factors in obtaining low bearing torque designs, References 29 to 31 should be consulted. Of these, Reference 31 is more directly concerned with design parameters affecting bearing torque, and gives certain general rules for bearing geometry design that will give an optimum bearing (minimum torque and maximum life):

1. The contact angle should be as large as the practical design of the bearing dictates, since a change in the contact angle has a more pronounced effect on life than on torque. The life will be increased significantly while the torque will be only slightly affected.

2. The pitch diameter should be made as small as possible, since this simultaneously reduces torque and increases life.

3. IRC* should be utilized for bearings with bore sizes near or less than 50 millimeters. IRC is advantageous for two reasons:

   (a) It generally results in less torque than ORC curvatures.

   (b) It enables the use of an arbitrarily small value of the inner race curvature factor f_i, which is the more critical race curvature in determining fatigue life at typical operating speeds.

---

* IRC is inner race control, with pure rolling at the inner race and a combination of rolling and spinning at the outer race.

These remarks generally hold true except that a larger inner race curvature factor may be desirable to obtain low torque, sacrificing bearing life to some extent.

Generally, the parameter changes to increase bearing life or minimize torque are in direct oppostion to each other, as shown in the tabulation below:

Criteria for-	Number of balls, n	Ball diameter, d	Pitch diameter, E	Initial contact angle (unloaded), β'	Race curvature combination, f_o/f_i
Low ball-spin torque	Small (for IRC)	Small	Small	Small (for IRC)	Large f at spinning contact
High fatigue life	Large	Large	Small	Large	Both f's small

A general summary of the importance of these parameters, also taken from Reference 31, is given below:

1. Race curvature seemed to be the most important single variable. A change in curvature factor over the range examined (0.52 to 0.58) changed torque by a factor of three, or life by a factor of four in some cases.
2. The examined change in contact angle (15° to 20°) produced negligible changes in torque (less than 5%), except during inner-race control near the transition speed. The effect on life was significant. Increasing the angle from 15° to 20° doubled the life in one case.
3. For the change in ball number examined (25% to 35%), the effects on life were much greater than the effects on torque. The torque changes were in the range of 5% to 20%. On the other hand, life increased by over 100% at typical loads and speeds.
4. For a 25% to 40% increase in ball diameter, torque increased by as much as 100% for one case. Life increased markedly with ball diameter for all conditions. At typical loads and speeds, the increase was from 400% to 700%.

5. A decrease in the pitch diameter caused a decrease in torque and an increase in life for all conditions examined.

To determine the availability of bearing drag data, the Product Development Group at Miniature Precision Bearing, Keene, New Hampshire, was contacted. Miniature Precision uses a desk-top computer model of bearing performance which has the capability of projecting running torque measurements to other speeds. In 18 years of bearing work, the Chief Engineer at Miniature Precision Bearing has not found any simplified analytical bearing models that would be suitable for inclusion in our turbine meter performance model. Instead, Miniature Precision Bearing uses their program to predict bearing torque variation with shaft speed and load.

One factor which has not been mentioned in this discussion, but which was emphasized by Fischer and Porter, is the importance of lubricity. The bearing torque vs. rotor speed and thrust load curves mentioned previously are dependent upon the fluid being used for bearing lubrication, as one would expect. When changing fluids, or when calibrating in one fluid and running in another, it is desirable to have actual bearing torque data for each fluid. However, when this is not possible and analytical predictions must be utilized, the dependence on fluid properties must be known. Therefore, it should be pointed out that the analysis of Scibbe and Anderson (Reference 22), derived from the papers of Jones (Reference 21), is based on an expression in which ball and spin torques are directly proportional to the coefficient of sliding friction μ, which is assumed to be independent of normal pressure. But, quoting from Jones:

> "Actually, the coefficient of friction is a complex function of a number of variables. Among these are: the unit pressure and sliding velocities at different points within the pressure area, the nature of the contacting surfaces, the temperature, and the type of lubricant. The functional relationship between all factors is not known at this time..."

The ball spin torque is only a portion of the total bearing torque, which must include retainer drag, etc. Therefore, bearing retarding torques obtained by direct measurement in the operating fluid are preferred to analytical predictions.

Miniature Precision Bearing has a running torque tester which conforms to the requirements of Military Standard 206. Measurements made with this instrument at one given speed compare favorably with analytical predictions. However, the test speed is quite slow and not typical of meter operating speeds. Some bearing torque testers produce noisy signals with excursions of the same magnitude as the quantity being measured. For this reason, Rocketdyne and others have built their own dynamic integrating torque measuring instruments.

A typical example of a turbine flowmeter bearing is a Miniature Precision Bearing S518C with a 1/8" bore and 5/16" O.D., used in a 2" Fischer and Porter turbine flowmeter. The running torque vs. speed and thrust load is shown in Figure 8 for operation in water. This information was entered in the program in tabular form for machine interpolation.

1. Bearing Thrust Load

The proper determination of the running torque requires a knowledge of the thrust load used to enter the figures previously mentioned. Calculation of the bearing thrust load is very similar to the driving torque calculation in that the thrust load is the sum of the axial components of the previously calculated lift and drag forces.

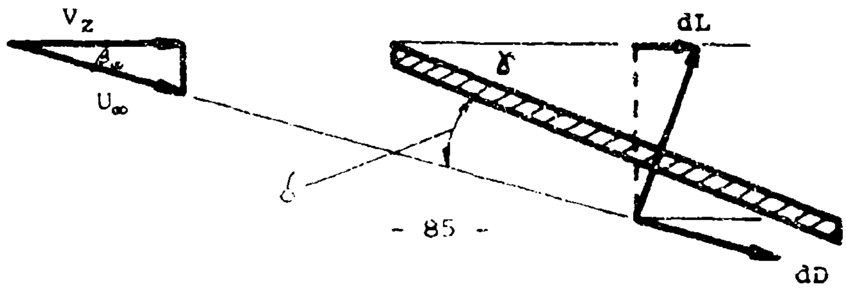

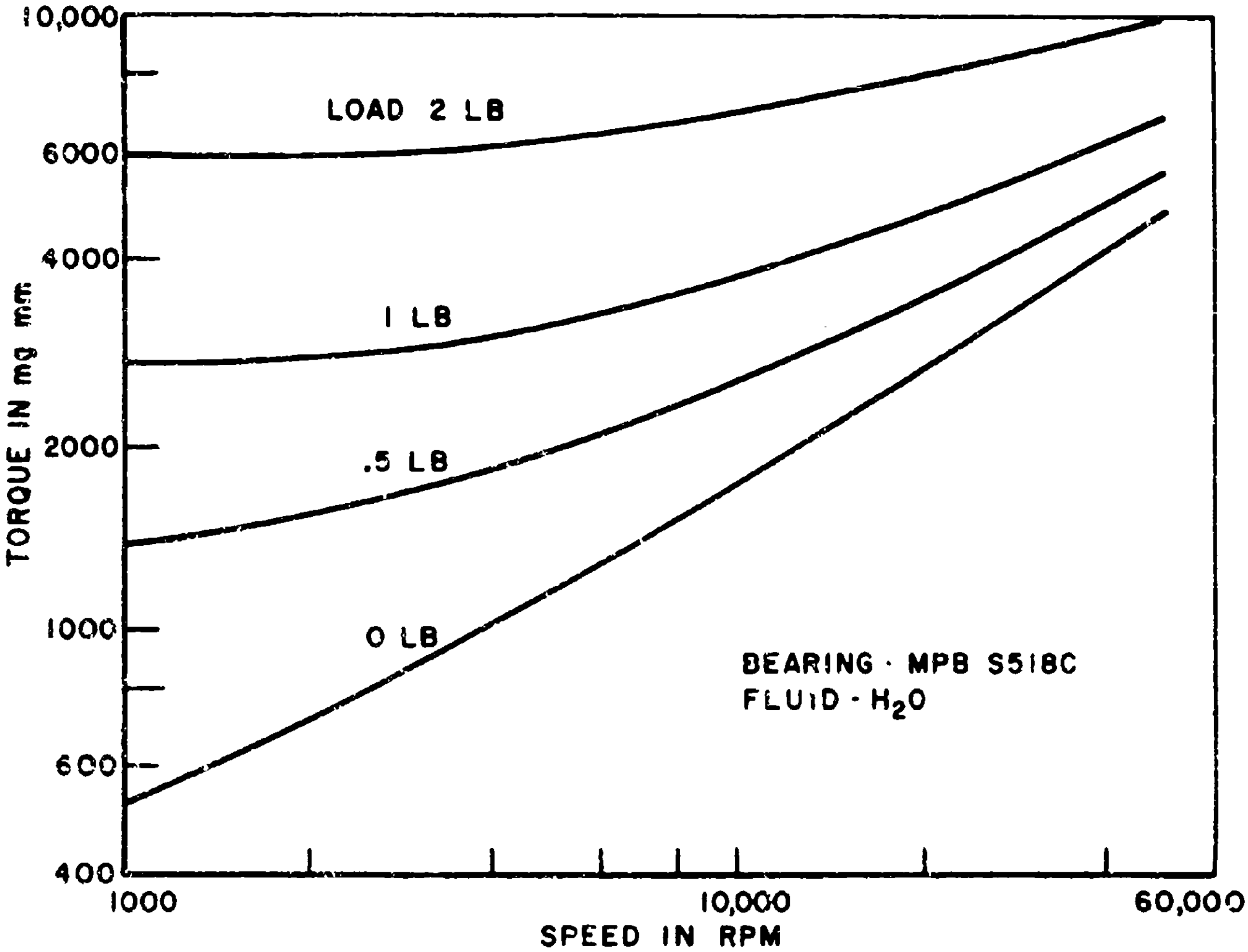

FIGURE 8

BEARING RUNNING TORQUE VS SPEED AND LOAD

From the velocity vector diagram on page 85:

$$dL = (\tfrac{1}{2}\rho U_\infty^2)\ C_L\ (c\ dr)$$

where $C_L = 2\pi K_c \sin\delta$ from potential flow analysis

$$\delta = \gamma - \beta_\infty$$

$$U_\infty = \frac{V_z}{\cos\beta_\infty}$$

$$dD = (\tfrac{1}{2}\rho U_\infty^2)\ C_D\ (c\ dr)$$

Substituting in the blade thrust load equation:

$$dF = N(dL \sin\beta_\infty + dD\cos\beta_\infty)$$

$$= \tfrac{1}{2}\frac{\rho V_z^2}{\cos^2\beta_\infty} N\left(C_L\ c\ \sin\beta_\infty + C_D\ c\cos\beta_\infty\right) dr$$

$$= \tfrac{1}{2}\rho V_z^2\ cN\left(2\pi K_c \frac{\sin\delta}{\cos\beta_\infty}\tan\beta_\infty + C_D\frac{1}{\cos\beta_\infty}\right) dr$$

which, after some algebra and the inclusion of finite blade effects, becomes:

$$F = \int_{R_h}^{R_T} \tfrac{1}{2}\epsilon\,\rho(r)V^2(r)\,N s\left[\left(\frac{2q}{1+q}\right)^2\left(\frac{2\pi r}{L}\right)^2 + \frac{4q(1-q)}{(1+q)^2}\left(\frac{2\pi r}{L}\right)\left(\frac{r\omega_a}{V}\right) - \frac{4q}{(1+q)^2}\left(\frac{r\omega_a}{V}\right)^2\right] dr$$

$$+ \tfrac{1}{2}C_D\int_{R_h}^{R_T}\rho V^2 cN\left\{1+\left[\left(\frac{q}{1+q}\right)\left(\frac{2\pi r}{L}\right)+\left(\frac{1}{1+q}\right)\left(\frac{r\omega_a}{V}\right)\right]^2\right\}^{\frac{1}{2}} dr$$

The thrust load computed above is not the total bearing thrust load, since the axial component of fluid drag on the rotor hub also contributes:

$$F_h = (\tfrac{1}{2}\rho_h U_{\infty h}^2)\, C_D\, (cs \cos \gamma)_h \cos\beta_\infty N$$

$$= \frac{\tfrac{1}{2}\rho_h V_h^2}{\cos \beta_\infty}\, C_D\, (cs \cos\gamma)_h N$$

$$= N \tfrac{1}{2}\rho_h V_h^2\, C_D\, (cs \cos\gamma)_h \left[1 + \tfrac{1}{4}(\tan\beta_1 + \tan\beta_2)^2\right]^{\frac{1}{2}}$$

$$= N \tfrac{1}{2}\rho_h V_h^2\, C_D\, (cs \cos\gamma)_h \left\{1 + \left[\left(\frac{q}{1+q}\right)(\tan\gamma) + \left(\frac{1}{1+q}\right)(\tan\beta_1)\right]^2\right\}^{\frac{1}{2}}$$

as is shown in the following sketch:

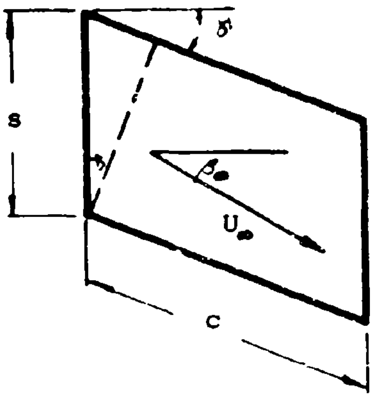

V_h must be an effective free stream velocity in the vicinity of the hub, since V_h is actually zero for viscous flow. The value used in the numerical case was taken as the mean flow velocity $\bar{v}$.

Additional bearing thrust loads will be encountered for a meter experiencing acceleration plus the blade pressure load:

$$F_r = M_r (a + g \cos \phi) + \Delta P_{rotor} (R_t - R_h) tN$$

where M_r = rotor mass

ϕ = angle between meter axis and vertical

For cases where the acceleration is inclined to the meter axis, the expression above can be modified to include proper components.

2. Journal Bearing Option

Because some small turbine meters and industrial meters employ journal bearings, an option was included in the computer program to substitute the frictional characteristics of a journal bearing at zero load.

The analysis of a simple journal bearing is based primarily on the paper by Taylor (Reference 32), who studied the fluid motion in the annular film between rotating concretric cylinders. The frictional characteristics of the unloaded bearing were used as the criterion to determine the mode of flow in the lubricant film. The shear stress may be defined by:

$$\tau = f \frac{\rho u^2}{2}$$

where f = coefficient of friction

u = journal velocity

The coefficient of friction is a function of the Reynolds number based on the bearing radial clearance c_{JB}. For a laminar bearing:

$$f = \frac{2}{Re}$$

For turbulent flow, test data from bearings with no load gives a coefficient of friction:

$$f = \frac{0.078}{Re^{0.43}}$$

Transition occurs at a critical Reynolds number based on Taylor's theory of stability of fluid films. For laminar operation:

$$\omega_a < \frac{41.1 \ \nu}{c_{JB}^{3/2} \ r_s^{1/2}}$$

where c_{JB} = radial clearance. Since $\omega_a = \frac{u}{r_s}$, then:

$$Re_{crit} = \frac{uc_{JB}}{\nu} = 41.1 \sqrt{\frac{r_s}{c_{JB}}}$$

This critical Reynolds number has been observed by test. Using the appropriate coefficient of friction, the retarding torque is:

$$T_{JB} = (f \frac{\rho u^2}{2})(2\pi r_s L_{JB})\ r_s$$
$$= f \rho \pi L_{JB} \omega_a^2 r_s^4$$

where L_{JB} = bearing length

r_s = shaft radius

L. Retarding Torque Due to Readout Device

As part of the study of turbine rotor retarding torques, the drags due to a typical magnetic and RF pickup were determined. The primary objective was to determine generally the order of magnitude of these retarding torques in comparison with the bearing drag and other fluid drags.

Because of variations in pickup design with meter manufacturers, the magnitude of the drags computed cannot be applied to other designs, but their proportional relationship to the total drag can be considered typical of these units.

The Fischer and Porter Company very generously provided detailed drawings of the magnetic pickup for their Model 10C1505 turbine flowmeter and the RF pickup and

and amplifier circuit for their Model 10C1510 turbine flowmeter. For both examples, a 2" meter with a maximum flow of 200-225 gpm was chosen

Several simplifying assumptions and approximations were necessary to obtain an estimate of the losses in the rotor and the magnet. A more detailed estimate of these losses is not practical analytically, and can be more easily determined experimentally with a few tests on an actual meter.

1. Magnetic Pickup

The total rotor retarding torque resulting from the use of a magnetic pickup can be attributed to three types of power losses. A generated power loss exists through the pickup coil and external load. Eddy current losses exist in the coil components, meter body and rotor. Hysteresis losses are experienced by the core pin, rotor and magnet.

(a) Generated Electrical Power

Electrical power is generated in the pickup coil due to the flux linkage change resulting from the turbine blade passing the core pin. This loss results from the loading effects of the preamplifier on the coil. The power lost in the pickup coil winding must be included.

A "worst case" analysis of the Fischer and Porter Model 10C1505 (2" 200 gpm) turbine flowmeter and Model 556E2271AA preamplifier was based on the following assumptions:

(1) The input capacitance of the preamp is only a few picofarads and is negligible compared to the load resistance at the low frequencies under consideration (30-600 hz).

(2) The inductive reactance of the coil is low compared to the circuit resistance. An approximate calculation of the coil inductance based on construction details proved this assumption to be valid.

(3) Skin effects in the coil wire are negligible, and the AC resistance equals its DC resistance.

(4) The induced EMF in the coil is a pure sine wave.

(5) The preamp is located at the pickup coil and its input resistance is low.

With these assumptions, an equivalent electrical circuit was analyzed to determine the coil current and power based on the open circuit voltage and calculated coil resistance from the meter instruction bulletin. The power generated was determined at the minimum flow of 30 hz and at the maximum flow corresponding to 600 hz. The losses due to generated power are 0.028 microwatts and 11.2 microwatts respectively.

The generated power loss can be reduced by at least two orders of magnitude by redesign of the pickup coil or interposing a field effect transistor source follower between the pickup coil and the differential amplifier. The latter would also permit remote location of the differential amplifier.

(b) Eddy Current Losses

As the turbine rotor blades pass the pickup coil core pin, a change in flux linkages causes induced currents in all conductors in the region. This includes the turbine rotor, core pin, end spacer, body, and coil housing. The eddy current losses in these components are calculated in the following paragraphs. The magnet, being ferritic, is non-conducting.

(1) Core Pin

Calculation of the eddy current losses requires a knowledge of the skin depth and the time rate of change of the flux. The skin depth is the distance from the surface at which the current is $1/e$ the surface current density. The skin depth is calculated from:

$$\delta = \frac{1}{(2.54)(2\pi)\sqrt{(\mu_r \sigma f) \times 10^{-9}}} \quad \text{in.}$$

where μ_r = relative magnetic permeability

σ = conductivity, in mhos per cm^3

f = frequency (30 and 600 hz)

The time rate of change of flux is related to the induced EMF in the pickup coil through a coupling coefficient:

$$E_i = -k_c N \frac{d\Phi}{dt}$$

where E_i = induced EMF in the pickup coil

k_c = coefficient of coupling

N = number of pickup coil turns

$\frac{d\Phi}{dt}$ = time rate of change of flux (webers/sec)

The total eddy current loss in the core pin is then calculated from:

$$P_c = \frac{\delta^2 L \left(\frac{d\Phi}{dt}\right)^2}{2\pi D^2 \rho} \left[\left(\frac{D}{\delta} - 1\right) + e^{-\frac{D}{\delta}}\right]$$

where L = pin length

ρ = resistivity

D = diameter

The core pin eddy current losses at minimum (30 hz) and maximum (600 hz) flow are 0.04 microwatts and 3.16 microwatts respectively. These eddy current losses could be virtually eliminated by using a ferrite material instead of iron or steel.

(2) Coil Housing

In a similar fashion, the eddy current losses were calculated for the coil housing, making certain approximations for the geometry of the housing. The current density was assumed constant throughout the shell. The coil housing eddy current losses at minimum and maximum flow are 0.108 microwatts and 43.1 microwatts respectively.

These losses can be greatly reduced (by a factor of 10^6) if the pickup coil housing is magnetically shielded from the pickup coil and magnet by a ferrite shell, or by using a ferrite core and cup assembly instead of a separate core pin and magnet assembly.

(3) Rotor

Eddy current losses in the rotor are large compared to other components and were calculated after making the following assumptions to simplify the geometry:

(3.1) Rotor blades are flat.

(3.2) Blade has a rectangular cross section.

(3.3) All of the flux causing an induced EMF in the pickup coil passes through the rotor blades and outer hub. Thus the flux varies as a sine wave through the following values:

$$o, -\frac{\phi_m}{2}, o, +\phi_m, o, -\frac{\phi_m}{2}, o$$

as the blade makes a half revolution past the pickup coil. The condition ϕ_m occurs with the blades directly under the core pin.

(3.4) Because of the I-beam type of construction of the hub, all of the flux and losses will exist ir the outer hub only.

(3.5) At minimum flow, the skin depth is more than fourteen times the blade half-thickness, and the eddy current density will be assumed constant throughout at the surface value. At maximum flow, skin depth calculations indicate that a uniform density equal to 90% of the surface density can be used.

Based on these assumptions, the total rotor eddy current losses are 12.45 microwatts at minimum flow and 5,000 microwatts at maximum flow. This is the best analytical estimate of these losses, but the assumptions and simplification of the geometry could possibly result in an estimate that is high by a factor of 5 to 10. A more detailed analytical estimate is not practical; experimental measurements on an actual meter are required.

(4) <u>Coil Spool, End Rings, End Spacer and Body</u>

In a similar fashion, the eddy current losses were calculated for the coil spool, end rings, end spacer and body. For the coil spool, the eddy current loss at minimum flow is 0.289 microwatts and at maximum flow

105.9 microwatts. This loss can be eliminated by using a non-conducting material for the coil spool.

The total body eddy current losses at minimum flow are 0.12 microwatts and at maximum flow 49.4 microwatts. Body eddy current losses may be reduced by minimizing the volume of material penetrated by the alternating flux, and by using the highest resistivity material consistent with environmental and fabrication requirements. To achieve the former, redesign and miniaturization of the pickup assembly is required.

(c) Hysteresis Losses

The hysteresis power losses can be estimated from:

$$P_h = k_h f B_m^{1.6} V \quad \text{watts}$$

where B_m = the peak alternating flux density in kilolines/in^2.

f = frequency, hz

V = volume, in^3

k_h = the hysteresis constant for the material

(1) Core Pin

Using the above formula, the hysteresis losses in the core pin are 0.067 microwatts at minimum flow and 1.34 microwatts at maximum flow.

(2) Rotor

The hysteresis power loss is proportional to the area of the B-H curve of the material, the volume of the material traversing the loop, and the number of times the loop is traversed per second. For the rotor blades, a non-symmetrical loop is traversed at a varying rate. However, only a small error will be made by assuming a symmetrical loop (to $\pm B_m$) is traversed at a rate equivalent to once per revolution per blade. The actual power loss will be about 75%-85% of that calculated.

The hysteresis loop traversed by each rotor hub section is symmetrical between $+\frac{\phi_m}{2}$ and $-\frac{\phi_m}{2}$ and is traversed once per revolution. The rotor total hysteresis loss is 0.132 microwatts at minimum flow and 2.64 microwatts at maximum flow.

(3) Magnet

The calculation of magnet hysteresis losses is based on the following assumptions:

(3.1) The magnet volume traversing a minor hysteresis loop is that volume directly behind the core pin.

(3.2) The Steinmetz coefficient (k_n) for Indox is 5×10^{-3} joules/cycle-kiloline-inch.

Based on these assumptions, the hysteresis losses in the magnet are 171 microwatts at minimum flow and 3420 microwatts at maximum flow. These losses seem high, and raise the theoretical question of whether the internal flux of a permanent magnet can be varied by merely varying the reluctance of the external path.

In addition, the Steinmetz coefficient of 5×10^{-3} assumed for Indox I could be as small as 10^{-3} at the flux levels in question. Therefore, the estimated magnet hysteresis losses may be high by a factor of 5.

(d) <u>Calculation of Rotor Retarding Torque</u>

A tabulation of the various losses calculated in the previous sections is given in Table I. These values in watts must be converted to torque with the use of the expression:

$$T = 0.1175 \ \frac{NP}{f} \ \text{ft-lb}$$

where N = number of turbine blades

P = power losses in watts

f = output frequency, hz

Based on the assumptions used, a worst case and a most optimistic case total retarding torque can be calculated. For the worst case, the retarding torque is 1.1×10^{-3} in-oz at minimum flow and 2.59×10^{-3} in-oz at maximum flow. For the most optimistic case at minimum flow, the retarding torque is 0.72×10^{-4} in-oz and 0.512×10^{-3} in-oz at maximum flow. These values are then entered in the overall rotor torque balance equation to determine the actual rotor speed.

In conducting this analysis, several suggestions were made for lowering the retarding torque. By redesign of the pickup, these torques could probably be lowered by at least one order of magnitude and possibly two.

TABLE I

LOSSES FOR MAGNETIC PICKUP FLOWMETER

Loss and Type	Min. Flow (in μW)	Max. Flow (in μW)
A. Generated Power		
Pickup Coil and Load	0.028	11.20
B. Eddy Current Losses		
Core Pin	0.040	3.16
Coil Housing	0.108	43.10
End Spacer and Body	0.123	49.35
Rotor	12.450	5000.00
Coil Spool	0.289	105.90
C. Hysteresis Losses		
Core Pin	0.067	1.34
Rotor	0.132	2.64
Magnet	171.000	3420.00
TOTALS	184.24	8636.69

2. RF Pickup

An analysis of the RF pickup and preamplifier circuit was conducted for the Fischer and Porter Model 10C1510 turbine flowmeter (2" 225 gpm). An RF pickup is desirable for some applications, since the modulation method of signal generation eliminates magnetic drag on the rotor assembly, thereby appreciably extending the lower nominal flow rate range of the meter. Combined with minimum-torque bearings in the rotor assembly, the meter is able to operate over extended linear flow ranges (up to 75:1).

The RF pickup differs from the magnetic pickup in that an externally powered oscillator/preamplifier applies a high frequency carrier signal to the pickup coil. As the rotor blades cut the field of the coil, the amplitude of the carrier signal is modulated at a rate corresponding to the rotor speed, and hence, proportional to flow rate. This modulated signal is in turn detected, amplified, and shaped by the oscillator/preamplifier for transmission. The turbine rotor assembly and meter operation are similar in some ways to an induction motor rotor, although there is no intention to purposely "drive" the rotor. As will be shown below, this possibility does exist and was examined to define the magnitude of driving torques.

(a) General Conclusions

Based on the analysis of an induction motor "model," it was concluded that an accelerating (positive) torque will be supplied to the rotor by the pickup. Some of the logic and factors that led to this conclusion are outlined below:

(1) The pickup coil is supplied with single phase excitation; therefore, there is no directional preference inherent in the construction.

(2) The synchronous speed of the pickup coil excitation is very greatly in excess of the rotor speed; therefore, only motor action can result and all "motor losses" must be supplied by the instrumentation. These motor losses include all eddy current losses in the conducting materials within the field of the pickup coil and all hysteresis losses in all magnetic materials within the field of the pickup coil.

(3) The "motor losses" not included are fluid friction and bearing losses, since it is assumed that these losses are chargeable to the fluid being metered.

(4) A retarding torque cannot be supplied to the rotor because for the single phase induction motor type construction, braking is impossible. Also, rotor speeds in excess of the pickup coil exciting current are impossible by design, and induction generator action is precluded.

(b) Induction Motor "Model"

Because of the possibility that the RF pickup circuit would "motor" the rotor, it was desirable to determine the magnitude of this torque and the maximum influence on the rotor torque balance. This maximum driving torque was calculated from an induction motor model based on the following assumptions:

(1) The induction motor is two-pole single phase with a squirrel-cage single-turn rotor.

(2) The skew of the blades due to the helical lead is neglected.

(3) The rotor speed is so slow compared to synchronous speed that essentially the starting torque is being calculated.

(4) The maximum flux developed in the pickup coil core is not attenuated by passage through the stainless steel body. Actually, at 35 to 40 khz, the flux might be reduced by a factor of 5 or 10. For purposes of computation, the 30 maxwells estimated will be reduced to 10 maxwells.

With these assumptions, the rotor constants were calculated and the rotor power determined. The induced EMF in the rotor is 15.6 millivolts with a current of 1.32 amps. For the given geometry and rotor speeds, this corresponds to a driving torque of 1.4×10^{-5} in-oz. This torque does not vary from maximum flow to minimum flow, because at maximum flow the induction motor slip

$$S = \frac{s_O - s}{s} = 0.995$$

indicating that it is essentially starting torque that is supplied.

The driving torque estimated is the maximum influence that can be expected, and the actual torque may be considerably less. The estimated RF pickup torque is used in the overall rotor torque balance. However, it is very small in magnitude compared to the other terms, and one can essentially assume that the RF pickup has little influence on the rotor speed in comparison with the magnetic pickups.

V. INSTALLATION EFFECTS ON TURBINE FLOWMETERS

A literature search aimed at producing information on empirical factors used by commercial turbine meter manufacturers to account for the effects of upstream geometry and installation effects yielded very little useful information. Unfortunately, coverage of the subject in most references is restricted to general qualitative remarks or to limited test data for a specific flowmeter in a specific test installation which cannot be generalized.

Because of an apparent lack of data in the published literature, several turbine flowmeter manufacturers were questioned on this and other points, and a questionnaire was prepared and distributed to organizations represented on the ICRPG Experimental Measurements Committee. Responses to these questionnaires (detailed in Appendix D) yielded very little organized data, although several organizations have bits and pieces of unreduced data dealing with these effects.

A. Upstream Pipeline Configuration

Of the literature reviewed, the most useful report dealing specifically with the influence of upstream piping on the turbine flowmeter registration was supplied by Potter Aeronautical Corp., Reference 33. The objective of the report was to determine the effect of flow straighteners on performance of the standard series Pottermeter Model 7/8-27 installed in various velocity profile distortion and swirl-inducing piping configurations. Since these tests were conducted specifically to study piping effects, the data could be more conveniently analyzed than data from other references where piping effects were of secondary importance and other parameters changed from test to test.

To obtain a qualitative estimate of piping effects from the Potter data, plastic overlays of the test data were prepared to visualize the introduction of an elbow, straightener, etc., as it appeared in the calibration curves.

The first test consisted of a control or standard "straight run" primary calibration with approximately 85" of straight section piping upstream of the 7/8" meter and approximately 24" of straight section downstream. In addition, a flow straightener was installed 13" upstream of the meter. This reference calibration will be referred to as Test A.

In Test B the flow straightener was moved to a position immediately upstream of the meter. The calibration was virtually identical to Test A, except that registration was lower at all flow rates by approximately 0.05%.

Tests C and D were conducted with a straightener immediately upstream of the meter and a piping configuration which included a mitered elbow 1-1/2" upstream of the straightener. An AN 821-16 elbow was, in turn, approximately 6" upstream of the mitered elbow.

Without the flow straightener, the meter registered lower flows (than Test A) over a large portion of the flow range. However, with the overlays, it is possible to shift the data so that the points virtually coincide with Test A by increasing the low flow rates by as much as 0.13% and reducing the high flow rates by 0.02%. Introduction of the flow straightener does not eliminate the error, but rather it causes the reverse to happen, the meter reads low at the high flow rates and coincides with Test A at low flows. In this case the data are 0.17% low at high flow rates.

Tests E and F reversed the relative positions of the mitered elbow and the AN 821-16 elbow. Without the straightener, the meter registration was significantly lower for all flow rates than of the previous cases. However, the shape of the curve was similar to Test A, and the data could be made essentially equal by shifting it upward by 0.71% at low flow and 0.51% at high flow. The introduction of a flow straightener did result in a significant improvement in meter registration, although all flows read less than Test A by about 0.20%.

It should be mentioned that the plane of the elbows relative to each other and the meter was not specified for these tests. These relationships have a direct bearing on meter registration and must be kept tne same in switching line components for comparison tests. There is no quantitative way to predict how the mitrered elbow - AN 821-16 elbow combination gives significantly lower meter readings than the reverse. Qualitatively, it appears that a mitered elbow downstream of a smooth radius elbow tends to disorganize the swirl produced by it, where in the reverse case the swirl generated by the smooth elbow is passed directly into the meter. Unfortunately, neither of these elbows was tested separately upstream of the meter to determine the relative changes in meter registration.

Tests G and H were conducted with a single 1-1/2" radius, 90° copper elbow (different from the previous tests) 6" upstream of the meter, followed by a 3" straight section, an AN 821-16 elbow, a hose with a 90° bend, a second AN 821-16 elbow and a straight discharge pipe. Without the straightener, the meter registration was low at all flow rates by 0.89%. By raising each data point by these values, the curve could be made coincident with Test A. The introduction of the flow straightener resulted in a considerable improvement in registration, with the meter reading low by only 0.38%.

Tests I and J were conducted to determine the importance of downstream piping, using a 90° copper elbow and other plumbing of Test G downstream of the meter, with a 72" straight section upstream. For these tests the flow straightener was installed on the downstream side of the meter. Without the straightener the meter registered low by 0.33% at low flow rates and low by 0.07% at high flow rates. With the straightener the test data were closer to Test A, being 0.18% low at low flows.

As would be expected, Tests I and J illustrate qualitatively that upstream piping is much more important than downstream piping, although a straightener does help to a limited degree where complicated plumbing is very close to the meter exit on the downstream side.

Tests K and L were conducted with a 1" hose upstream of the meter, secured in a bent "S" condition with reverse curves of 3" radius through 90°. Approximately 12" downstream of the meter was an AN 821-16 elbow, followed by 6" of straight section, followed by a mitered elbow. Without the straighteners, the meter registered lower than any of the previous tests (low by 0.93%). Introduction of the straightener improved the readings, which were then low by only 0.10%.

From the tests with the "S" bend hose and the 1-1/2" radius, 90° elbow, it is apparent that long moderate radius bends have a more significant influence on meter error than a sharp mitered elbow. However, the reader should be cautioned that data shifts mentioned for the Potter tests cannot and should not be used in any way to correct meter factors for similar installations the reader may encounter. Generally, the velocity profile downstream of a series of disturbances is a function of the Reynolds Number, pipe diameter, flow rate, friction factor, spacing between components and radius of curvature. Test conditions would have to be virtually identical to the Potter tests to be able to use the meter correction factors mentioned above if a flow straightener was not used.

The Potter tests do point out the importance of the use of a flow straightener upstream of the meter, but since the design of the straightener was not available, little can be said about its merits relative to other designs. There is no guarantee that flow straighteners of another manufacturer or of a different size will behave with the same characteristics.

Although the Potter test report was the most useful reference available dealing specifically with piping effects, the test configurations deserve constructive criticism on the following points:

1. Combinations of several types of elbows were introduced both upstream and downstream of the meter without determining the effect of each of these components individually.
2. The planes of the elbow were not specified in relationship to each other and the meter, and the straightener design was not available.

3. The degree of damping is a function of line length, but the length of line between components in the same configuration was not a parameter in the study.
4. Test data were presented as a plot of total cycles per 100 lbs. of water, without defining a reference temperature or correcting for specific gravity variations with temperature from test to test.
5. The standard "straight run" primary calibration (Test A) against which all subsequent tests were compared, is based on the use of a flow straightener 13" upstream of the meter, yet in subsequent tests with various piping configurations the straightener was placed immediately upstream of the meter inlet.

These remarks are not intended to be critical of Potter, since they have made a significant contribution in the form of test data which others have not obtained. The major point to be made is that meter manufacturers or users in general have not had the funds and/or the time to explore in a <u>controlled</u> fashion all the parameters involved in the influence of upstream piping on meter registration, and it is quite unlikely that these data will be obtained without the funding of tests for this specific purpose.

Fischer & Porter conducted some tests with a 1-1/2" flowmeter downstream of various elbows, reducers, and a flow straightener. Unfortunately, the spacing, elbow radius of curvature, etc., are not specified. Fischer & Porter also conducted comparative tests of their meters with those of Cox, Potter and Waugh to determine their sensitivity to a flow swirler upstream of the meter; unfortunately, the degree of swirl for these tests was not defined.

Data obtained on piping effects as a secondary effort in a large program tend to have so many qualifications that restrict the data to a given configuration that the information cannot be generalized. In a study of Jupiter missile flowmeters, Reference 34, flowmeter alignment and orientation were investigated. Distinct calibration shifts were produced by rotating the flowmeter on its axis to the next set of bolt holes on the mating flange. After some investigation it was determined that the relative orientation of the LOX tank exit anti-vortex assembly and the meter had a direct bearing on the calibration. The noted effect was peculiar to that particular installation.

In a similar fashion, an in-place flowmeter calibration system was established for the Apollo Service Module Propulsion System, Reference 35. Flowmeters were calibrated with water in four configurations: a straight pipe, the F-3 propellant feed lines with an in-place calibration "tee," the feed lines with the engine interface, and the feed lines with the engine interface plus a "jumper" extension. Although the calibrations show the influence of these piping configurations on the flowmeter constant, the calibration shifts are peculiar to that given installation, since component spacings, fluids, etc., were not changed for a given configuration.

An indication of the complexity of the problem can be found in reviewing References 10 and 11. Zanker[10] discusses the development of a flow straightener for use upstream of an orifice-plate, although some of the philosophy applies to turbine flowmeters where the objective is to reduce swirl. The most important parameter in piping effects is the meter approach velocity distribution as influenced by Reynolds Number, pipe diameter, flow rate, friction factor, settling lengths, pipe bend radius of curvature, etc., some of which are dependent variables. Zanker studied the swirl damping properties of straighteners and found that certain straightener designs for certain flow situations can actually retard the process of achieving a normal pipe velocity distribution. There are several types of swirl, the most easily simulated being the solid body rotation type swirls generated with an impeller or rotating perforated plate and the free vortex or constant energy type swirl produced by guide vanes. Very strong swirls can be produced in this fashion that persist much longer than those due to axial velocity disturbances and are recommended as part of a test program to study the influence of swirl on meter registration.

West in Reference 11 discusses the importance of velocity distribution in pipes downstream of a bend, and observed bend loss coefficients. He emphasizes the fact that the velocity distribution before the bend and the appropriate Reynolds Number range must be considered carefully because tests on a particular bend and pipe arrangement are only applicable to that arrangement, since these parameters (as previously mentioned) have a direct influence on the results. Velocity profiles at different diameters downstream of a bend are given for different radius bends and a given inlet velocity condition.

The technical approach of West is well organized and defined. For example, flow through a bend is considered by defining the two radii and the angle of deflection. In addition, the inner wall roughness of the bend and/or the roughness height relative to the pipe bore must be known and must be related to the relative roughness of the pipes before and after the bend. The velocity distribution before the bend and the appropriate Reynolds Number range are specified. Velocity profiles at various distances downstream of the bend are obtained with pitot traverses. The measure of bend influence is categorized by two ratios, V_{mean}/V_{centre} and V_{mean}/V_{max} where:

V_{mean} = the mean velocity in pipe

V_{centre} = the central velocity in the pipe

V_{max} = the maximum velocity at the peak in the velocity profile curve

These ratios also allow for the description of symmetric profiles. West found that turbulent flow through a typical bend required 40 diameters for the velocity profile to recover.

By carefully organizing a detailed test program that accurately defines and records the test parameters previously mentioned, a significant advance can be made in determining the importance of upstream piping on turbine flowmeter calibration constants, but this type of organized approach in any detail has not been conducted to date.

B. Vibration

The effect of vibration on turbine flowmeter performance has been discussed in very few references. However, Potter Aeronautical provided a qualification test report on their Model 1-5851 1.5-to-25 gpm turbine flowmeter which was mounted on a vibration machine and tested at NASA-MSFC. The test sequence consisted of a resonance search, random vibration, and a post-vibration calibration for comparison with earlier calibrations. Details of the test sequence and results from Reference 12 are outlined below:

1. Resonance Search

A constant flow of approximately one-half full scale was maintained through the meter during resonance search testing. Along each of its three mutually perpendicular axes, the flowmeter was subjected to sine wave vibration sweeps at a maximum of 5 g's peak input level to the vibration equipment. The duration of each sweep was no more than 5 minutes. Two sweeps, one increasing frequency (20 cps - 2000 cps) and one decreasing frequency (2000 cps - 20 cps), were applied. Output of the flowmeter was recorded on an oscillograph. Axes are defined in Figure 9.

No internal resonances were noted during sinusoidal vibration in the 20 cps to 2000 cps frequency range. No change in output frequency occurred during vibration.

2. Random Vibration

A constant flow of approximately one-half full scale was maintained through the meter during random vibration testing. Random vibration was applied to the flowmeter along each of its three mutually perpendicular axes according to the following schedule. Axes are defined in Figure 9.

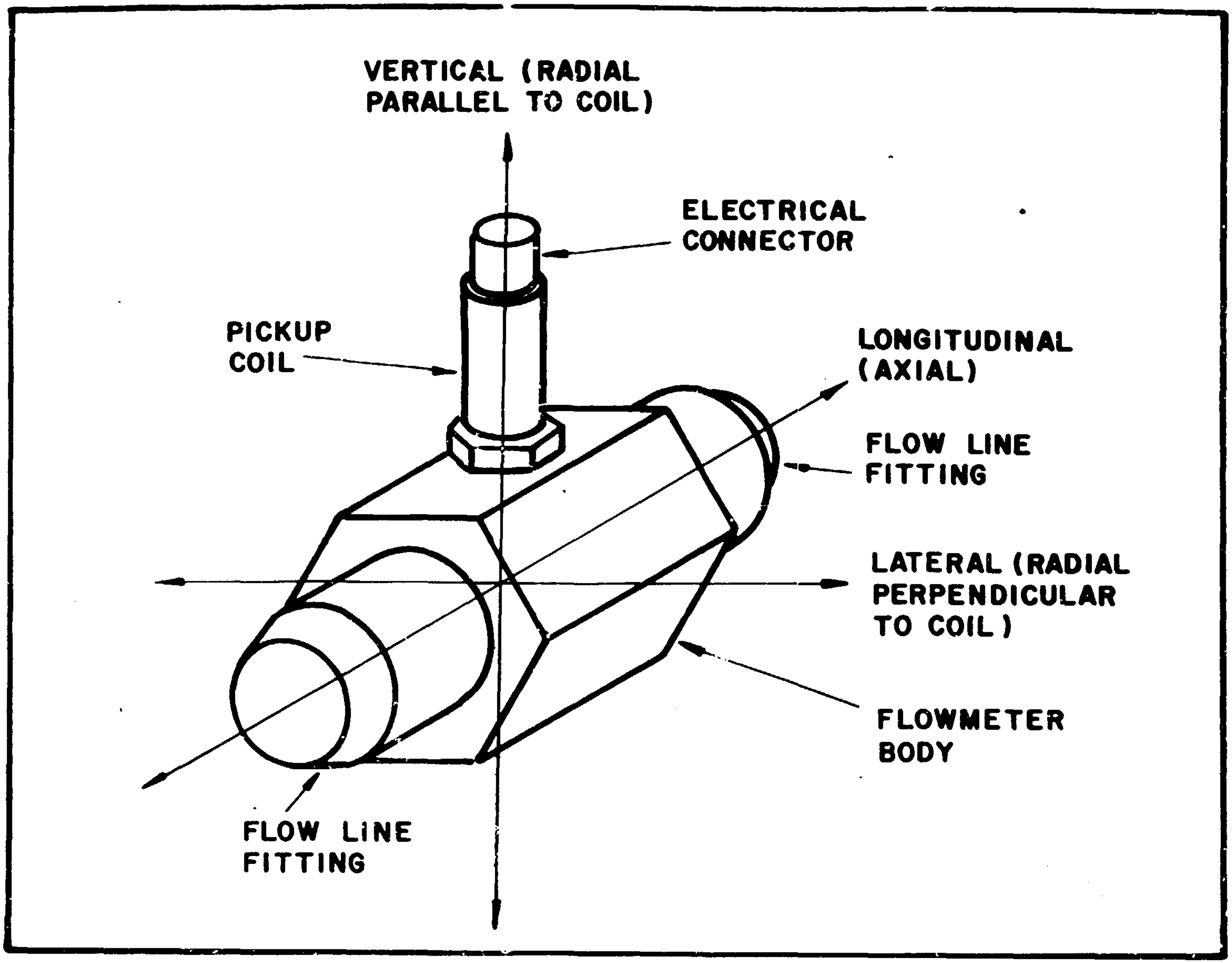

FIGURE 9

AXIS IDENTIFICATION FOR VIBRATION TESTS

103

20 to 200 cps - 2db/octave

201 to 700 cps - 0.64 g^2/cps

701 to 900 cps - 17.5 db/octave

901 to 2000 cps - 0.15 g^2/cps

Permanent oscillograph recordings were taken of the meter output before, during, and after vibration. Meter output was recorded directly, then fed through the converter input filter circuit and recorded, unless vibration produced no noticeable noise in the output.

Very little output noise was detected during vibration in the axial direction and in the radial direction parallel to the pickup coil; no input filter was used between the flowmeter and the oscillograph. Noise appeared during random vibration in the radial direction perpendicular to the pickup coil; therefore an input filter was used. Oscillograph recordings were obtained during random vibration which indicated that the flowmeter performed satisfactorily during random vibration, and no change in output frequency occurred.

3. Post-Vibration Calibration

After all vibration tests were completed, the flowmeter was calibrated to determine whether vibration had affected calibration.

Results of the post-vibration calibration are given in Table II. Deviation or non-repeatibility of the median "K" factor of the post-vibration calibration from the average of median "K" factors of the pre-environmental test calibration verification was -0.037%; a maximum of ±0.5% was allowable. No physical damage was noted.

Data from these tests indicate that the meter was susceptible to random vibration along only one axis, and the noise that appeared on the output was not critical, since no change in output frequency occurred.

Based on the results of the vibration testing of the Pottermeter, vibration does not have a significant effect on meter registration up to 5 g's peak input level.

Similar test data on meters of other manufacture were not available. Fischer & Porter did provide a communication concerning the vibration results on a 3/4" turbine meter. In this case, only the axial component was significant, with no effects when the vibration was purely transverse. The axial vibration of 8 g's peak level was examined by Fischer & Porter as a type of pulsation error similar to the axial vibration of a long column of flowing water in a long length of pipe. The worst

TABLE II

POST-VIBRATION CALIBRATION

% Full-Scale Output	Output Frequency (cps)	Output Voltage Into 3 k ohms (mV peak-to-peak)	Pressure Drop Across Meter (psi)	Actual Flowrate (GPM)	"K" Factor (cps/gps)	Linearity (% Deviation from Median "K" 1011.15)
10	43.845	190	0.07	2.592	1014.93	+0.374
20	83.627	350		4.975	1008.65	-0.247
40	160.857	620	0.28	9.581	1007.37	-0.374
60	242.063	790		14.408	1008.22	-0.290
80	322.335	960	0.97	19.173	1008.72	-0.240
100	406.598	1200	1.52	24.166	1010.76	-0.240

case is a combination of low frequency at high g levels at the low end of the flow range. Even in this case, errors of 0.1 to 0.2% at low flow would be present only for a meter mounted in a 3 or 4 ft. length of pipe vibrated at frequencies below 200 cps.

Based on the test reports available, meter vibration does not lead to significant meter errors for the types tested up to 8 g's. Fischer & Porter has had no complaints in the field about error from external vibration, except that caused by increased wear. Internally generated vibration is avoided by most meter manufacturers by statically and dynamically balancing the rotors and carefully controlling bearing clearances. For the reasons given above, vibration effects were not included in the turbine meter performance model.

C. Acceleration

Because very few turbine flowmeter users or manufacturers have access to a centrifuge, there are very few references available on the effects of acceleration. Two references were obtained, both dealing with Potter units, that included a rather detailed description of acceleration effects. Potter Aeronautical provided a qualification test report on their Model 1-5851, 1.5 to 25 gpm turbine flowmeter which was mounted on a centrifuge (Reference 12).

A constant flow of 1.68 gpm was maintained during acceleration. The least fluctuation occurred when the flowmeter was mounted with acceleration applied along the axial axis. The largest fluctuation occurred when the flowmeter was accelerated along the radial axis perpendicular to the coil, but the fluctuation did not exceed allowable limits. Shifts in output frequency for 10 g's acceleration are given in Table III from Reference 12. Deviation, or non-repeatibility of the median "K" factor of the post-acceleration calibrations from the average of median "K" factors of the pre-environmental test calibration verification was no more than -0.08%, well within the specified ±0.5%.

The small acceleration error observed is presumably due to increased bearing drag. There is no apparent explanation for the increased error with the radial load as opposed to the axial load.

Acceleration tests on a 1" Potter flowmeter are described in Reference 13 for both high frequency and

TABLE III

EFFECTS OF ACCELERATION ON OUTPUT FREQUENCY

10 G Acceleration Vector	Output Frequency (cps)			% Full-Scale Change During 1 Minute Acceleration	% Full-Scale Acceleration Error
	Average Before and After Acceleration Flowmeter Stationary	During Acceleration			
		1 Minute	4 Minute		
Radial, perpendicular to coil					
Test	28.5	24.		-1.13	-0.88
Comparison	15.5	14.5		-0.25	
Radial, parallel to coil - outboard					
Test	27.5	24.5	21	-0.75	-0.75
Comparison	12.5	12.5	11	0	
Radial, parallel to coil - inboard					
Test) 4.15 gpm	64.5	62		-0.63	-0.63
Comparison) 4.15 gpm	32.5	32.5		0	
Test	26	24	24.5	-0.50	-0.50
Comparison	12	12	12.5	0	
Axial, opposite flow					
Test	29.5	28.5		-0.25	-0.25
Comparison	16	16		0	
Axial, with flow					
Test	29.5	29.5		0	-0.13
Comparison	16	16.5		+0.13	

low frequency models. The results of these tests are shown in Figures 10 and 11 for accelerations up to 25 g's. The high frequency units appear to be relatively insensitive to acceleration, whereas the low frequency units are susceptible at lower flow rates for accelerations exceeding 10 g's.

The error due to acceleration is non-linear with acceleration, with distinct breaks in the curve making it difficult to use the data for empirical correlations. Also, the meters were not identified as to bearing type, which is essential to an adequate description of bearing drag.

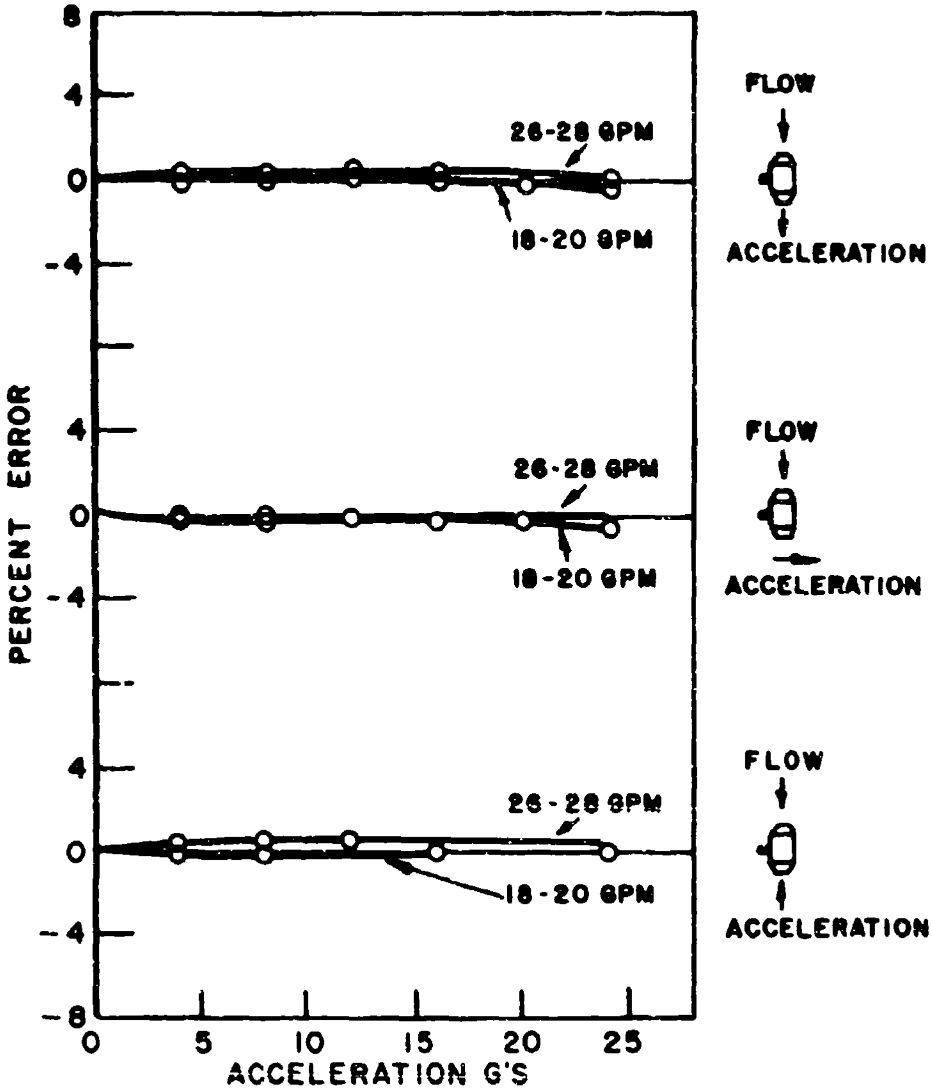

FIGURE 10

EFFECT OF ACCELERATION ON HIGH FREQUENCY, ONE INCH, MISSILE TYPE FLOWMETER (POTTER)

/0 4

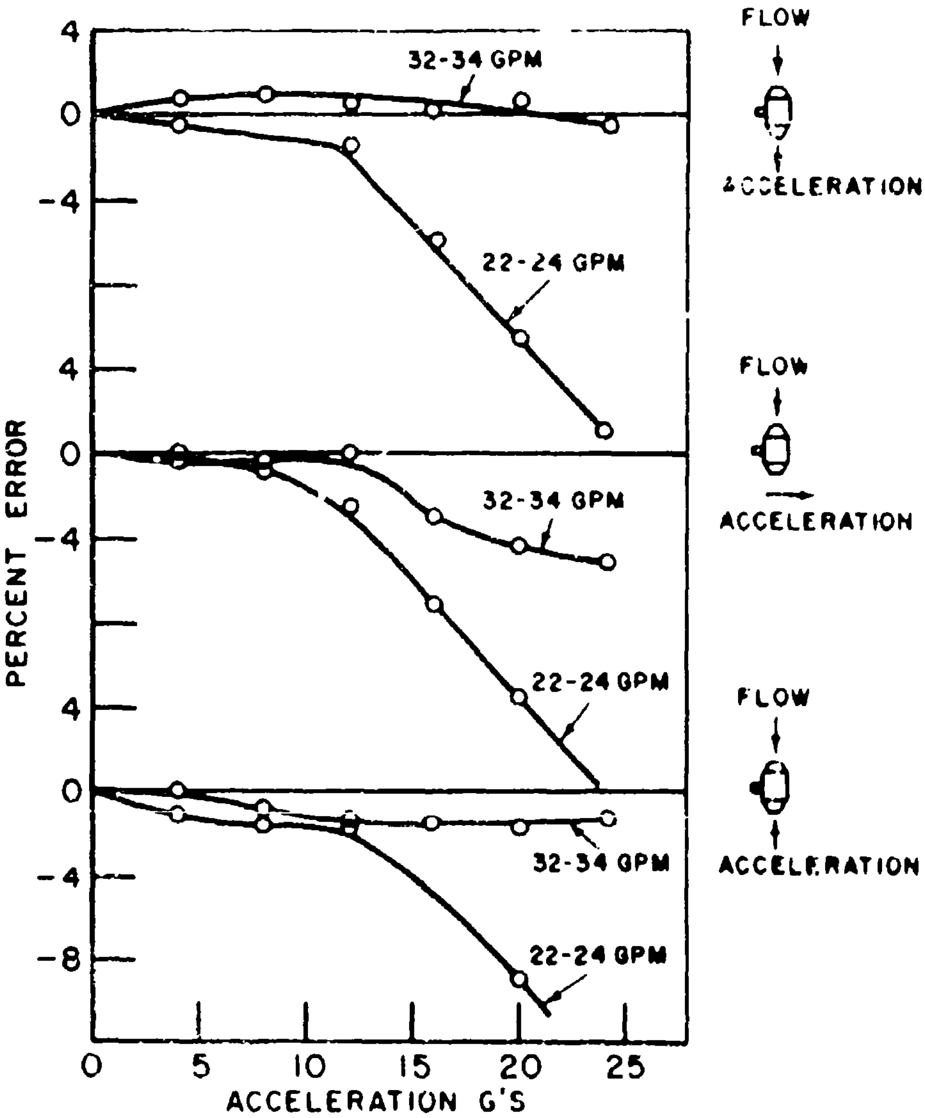

FIGURE II

EFFECT OF ACCELERATION ON LOW FREQUENCY, ONE INCH, MISSILE TYPE FLOWMETER (POTTER)

VI. NUMERICAL METHOD AND EXAMPLES

A. Summary of Equations

Derivation of the pertinent equations used in the performance model were given in Section IV. These equations must be assembled into an iteration scheme which keeps assuming a rotor speed until a balance is achieved between the driving torques and the retarding torques; i.e., until the net torque is effectively zero. A summary of these equations from the previous sections is given below:

Driving Torque

$$T_d = \int_{R_h}^{R_T} \epsilon \rho V_z^2 N s \left(\frac{2q}{1+q} \right)_{rotor} (\tan \gamma - \tan \beta_1) \, r \, dr$$
$$- \tfrac{1}{2} \int_{R_h}^{R_T} C_D \rho V_z^2 N c \left[\left(\frac{q}{1+q} \right) \tan \gamma + \left(\frac{1}{1+q} \right) \tan \beta_1 \right]$$
$$\left\{ 1 + \left[\left(\frac{q}{1+q} \right)_{rotor} \tan \gamma \right. \right.$$
$$\left. \left. + \left(\frac{1}{1+q} \right)_{rotor} \tan \beta_1 \right]^2 \right\}^{\frac{1}{2}} r \, dr \qquad (1)$$

where $\tan \gamma = \frac{2\pi r}{L}$ for helical rotor

$\tan \gamma$ = constant for flat blade

$$\tan \beta_1 = \frac{r\,\omega_a - \left(\frac{2q}{1+q}\right)_{\text{straightener}} \tan \alpha \left(\frac{R_{os}^2 - R_{is}^2}{R_b^2 - R_h^2}\right) V_{z_s}^2}{V_z}$$

for meters with a preswirler

$$\tan \beta_1 = \frac{r\,\omega_a}{V_z}$$ for meters with conventional flow straightener

Rotor Hub Fluid Drag

$$T_h = \tfrac{1}{2} N \rho \bar{v}^2 C_D (cs \cos \gamma)_h \left[\left(\frac{q}{1+q}\right)\tan \gamma + \left(\frac{1}{1+q}\right) \tan \beta_1\right]_{\bar{r}} \left\{1 + \left[\left(\frac{q}{1+q}\right) \tan \gamma + \left(\frac{1}{1+q}\right) \tan \beta_1\right]_{\bar{r}}^2\right\}^{\frac{1}{2}} R_h \qquad (2)$$

where the same expressions for $\tan \gamma$ and $\tan \beta_1$ apply.

Blade Tip Clearance Drag

$$T_{BT} = \frac{0.078}{2(Re)^{0.43}} \rho \, \omega_a^2 \, R_T^3 \, ctN \qquad (3)$$

where $Re = \dfrac{\rho \, \omega_a R_T (R_B - R_T)}{\mu}$

c = blade chord at the tip

t = blade thickness

Pickup Drag

$$\text{Pickup Drag} = T_p \qquad (4)$$

where T_p = constant for an RF pickup from Section IV(L)

$T_p = a + b\,\omega_a^2$ for a magnetic pickup based on the analysis in Section IV(L)

Bearing Drag

$$\text{Bearing Drag} = T_{BRL} \qquad (5)$$

where the bearing drag is obtained as a function of speed and load from experimental data such as shown in Figure 8, Section IV(K).

To obtain the bearing drag, the bearing thrust load is calculated from the expression:

$$F_B = \frac{1}{2}\int_{R_h}^{R_T} \epsilon \rho V_z^2 N_s \left[\left(\frac{2q}{1+q}\right)^2 \tan^2 \gamma\right.$$

$$+ \frac{4q(1-q)}{(1+q^2)} \tan \gamma \tan \beta_1 - \frac{4q}{(1+q)^2} \tan^2 \beta_1$$

$$+ \frac{1}{2}\int_{R_h}^{R_T} C_D \rho V_z^2 \; cN \left\{1 + \left[\left(\frac{q}{1+q}\right) \tan \gamma\right.\right.$$

$$\left.\left. + \left(\frac{1}{1+q}\right) \tan \beta_1\right]^2\right\}^{\frac{1}{2}} dr$$

$$+ \frac{1}{2} N \rho \bar{V}^2 \; C_D (cs \cos \gamma)_h \left\{1 + \left[\left(\frac{q}{1+q}\right) \tan \gamma\right.\right.$$

$$\left.\left. + \left(\frac{1}{1+q}\right) \tan \beta_1\right]^2\right\}^{\frac{1}{2}} + M_r (a + g \cos \phi)$$

$$+ \Delta P_{rotor} (R_T - R_h) Nt$$

where M_r = rotor mass

ϕ = angle between meter axis and vertical (i.e., 90° if horizontal)

ΔP = pressure drop across the rotor

The option exists in the program to substitute a journal bearing for the ball bearing unit. In this case, Equation 5 is replaced by:

$$T_{JB} = f \rho \pi L_{JB} \omega_a^2 r_s^4 \qquad (5a)$$

where L_{JB} = bearing length

r_s = shaft radius

$$f = \frac{2}{Re} \quad \text{if} \quad Re < 41.1 \sqrt{\frac{r_s}{c_{JB}}}$$

$$f = \frac{0.078}{Re^{0.43}} \quad \text{if } Re > 41.1 \sqrt{\frac{r_s}{c_{JB}}}$$

c_{JB} = radial clearance and $Re = \dfrac{r_s \omega_a c_{JB}}{\nu}$

Several secondary calculations and subroutines are essential to use of the equations given above. The velocity profile is calculated in a completely self-contained subroutine based on the equations given in Section IV(E). At each given radius, this subroutine is entered and the velocity at that radius calculated. A subroutine is also used to calculate the blade deflection coefficient based on the given geometry used in conjunction with the equations in Section IV(A).

In addition to the actual rotor speed, the program also computes the ideal rotor speed. The "ideal" rotor speed is that speed at which the rotor would operate for zero angle of attack in a flat velocity profile without blade interference effects and with no retarding torques. It can be shown that:

$$\omega_i = \left[\frac{2\pi}{L} + \frac{3}{2} \left(\frac{R_T^2 - R_h^2}{R_T^3 - R_h^3} \right) \tan \alpha \right] \bar{v}$$

for a meter with a preswirler and a helical bladed rotor;

$$\omega_i = \frac{2\pi}{L} \bar{v}$$

for a meter without a preswirler and with helical rotor blades;

and $$\omega_i = \frac{3}{2} \left(\frac{R_T^2 - R_h^2}{R_T^3 - R_h^3} \right) \tan \gamma$$

for a meter with flat blades and no preswirler.

B. Description of Computer Program

The major iteration loop in the computer program involves the rotor speed ω_a, which must satisfy the torque balance:

$$T_d - T_h - T_{BT} - T_p - T_{BRL} = 0 \qquad (6)$$

based on the expressions for these terms given in the preceding summary. The rotor speed either appears explicitly in these equations or implicitly through tan β, and various Reynolds number expressions. For the test cases to be described in the following section, 200 points were evaluated across the rotor blade to determine T_d and the bearing thrust load by numerical integration. Values for turbine inlet velocity, angle of attack, interference coefficient, deflection coefficient, straightener velocity, blade lift torque, blade drag torque, and net driving torque are evaluated at each radius and printed as shown in the sample output in Appendix C.

Based on the assumed speed ω_a, the net driving torque is obtained from Equation (1) and the bearing thrust load and retarding torque determined from Equation (5). The hub and blade tip drag are calculated and, with the pickup drag, are included in the torque balance, Equation (6). This procedure is followed for two rotor speeds to determine the behavior of the driving torque function and to predict a new speed. The new estimate for rotor speed is usually quite accurate, and the calculation will converge in three or four iterations regardless of the nature of the first guess. With practice or experience for a given meter, it is possible to guess the actual speed very closely. However, for the convergence technique being used, it is actually better to guess a speed approximately 1% removed from the actual speed, since it allows the machine to work with larger differences in preparing its new estimate. Details of the program operation and preparation of input are given in Appendix B.

C. Numerical Results

To determine the relative importance of various retarding torques and effects included in the performance model, a grid of test cases was prepared. A "nominal" or reference case was chosen, and then various parameters such as flow rate, temperature, fluid, bearing type, velocity profile, etc. were varied independently for comparison of the magnitude of each effect. For the purposes of the study, the reference case was:

Fluid: Water

Temperature: 70°F

Flow Rate: Rated capacity

Velocity Profile: Annular (based on turbine area)

Bearing Type: Ball bearings

Pickup Type: RF

Geometry: Nominal geometry and tolerances

The geometry of a typical meter in the 2" size range, Fischer and Porter Model 10C1510 2" 225 gpm was used to evaluate the performance model. Although the performance model is readily adaptable to many meter designs, this model was chosen because of its straightforward conventional design and the availability of detailed design information and prints provided by Fischer and Porter Company, Warminster, Pennsylvania. A cross section of this meter, illustrating typical interior geometry used in the program, is shown in Figure 12. The rotor has fourteen helical blades.

The first test case was that for the nominal design, to determine if the program was predicting a rotor speed and meter factor within normal manufacturing tolerances of what was known to be the actual rotor speed. The computed rotor speed was 897.02 radians/sec with a meter factor of 532.99 cycles/gallon, which compared extremely well with the manufacturers nominal meter-to-meter mean rotor speed of 897.60 radians/sec and meter factor of 533.33 cycles/gallon in water at 70°F. The manufacturer supplied calibration curves selected at random for this meter model with meter factors of 534.2 and 541.0, so the predicted rotor speed is well within the manufacturing tolerances. Other calculated data indicated that at this speed, the rotor hub drag and blade tip drag are the predominant retarding torques, of nearly equal magnitude, providing

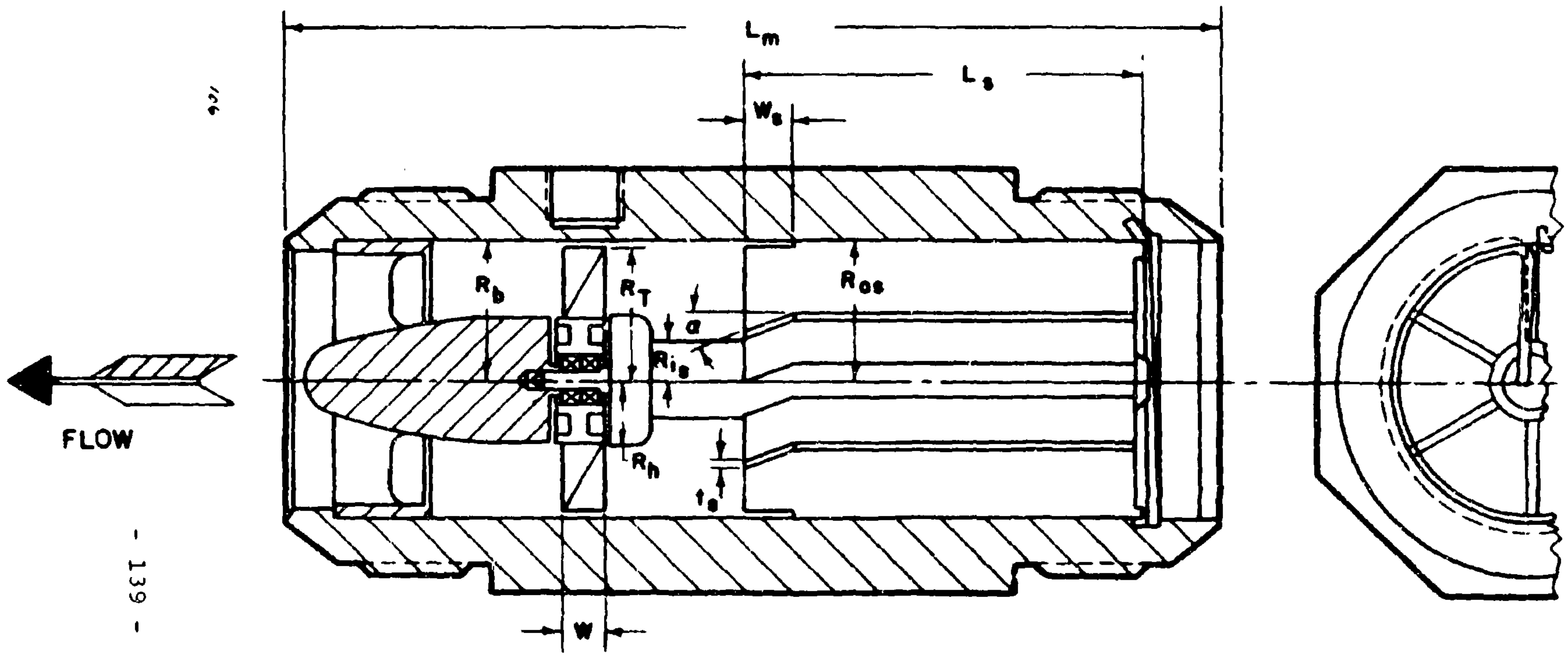

FISHER & PORTER MODEL 10C1510

FIGURE 12

TURBINE METER GEOMETRY

the balance with the rotor driving torque. The bearing torque is very small in comparison (less than 10%) and will become an important factor only at minimum flow rates. The predicted pressure drop is 8.3 psi, compared to 8.6 psi obtained by the manufacturer. The driving torque required to overcome the retarding torques is very small, approximately 0.0019 ft-lb. To provide this driving torque, the blades are required to operate at an integrated or "effective" angle of attack of only 0.076 degees, although portions of the blade operate at angles of attack varying from +6.5 degrees to -8.8 degrees.

The first parameter to be varied was the volumetric flow rate q. Test cases were run for 50% q, 75% q, and nominal q, which was 225 gpm. The rotor speed,meter factor, and other parameters for these cases were:

	$\bar{V}$ ft/sec	Net Angle of Attack, Deg.	ΔP, psi	Meter Factor cycles/gal	ω_i rad/sec	ω_a rad/sec
100% q	37.12	0.0764	8.3	532.99	922.3	897.0
75% q	27.84	0.0776	4.9	533.39	691.7	673.3
50% q	18.56	0.0790	2.4	533.39	461.1	448.8

The first column is the average turbine inlet velocity for the given flow rate, followed by the blade "net" angle of attack and meter pressure drop. The meter factor is the equivalent cycles/gallon output for the actual rotor speed. Its "flat" characteristic indicates that at these speeds the retarding torques are small, and the rotor speed is therefore linear. The next two columns are the "ideal" rotor speed and actual rotor speed. The "ideal" rotor speed is that speed at which the rotor would operate for zero angle of attack in a flat velocity profile without blade interference effects and with no retarding torques. The actual rotor speed is that predicted by the program with all retarding torques, interference effects, and the abovementioned losses included. As would be expected, the actual speed is less than the ideal speed, in this case about 3%, most of which is due to profile and interference effects rather than to retarding torques.

In computing the net driving torque, a series of 200 points were evaluated from the blade root to tip. The turbine inlet velocity profiles obtained for the different flow rates is shown in Figure 13. The rotor hub radius was 0.417", where the velocity effectively becomes zero. The profile is shown only to the blade tip (0.875" radius), which is the reason the velocity profile does not go to zero at the outside radius. The velocity profiles shown

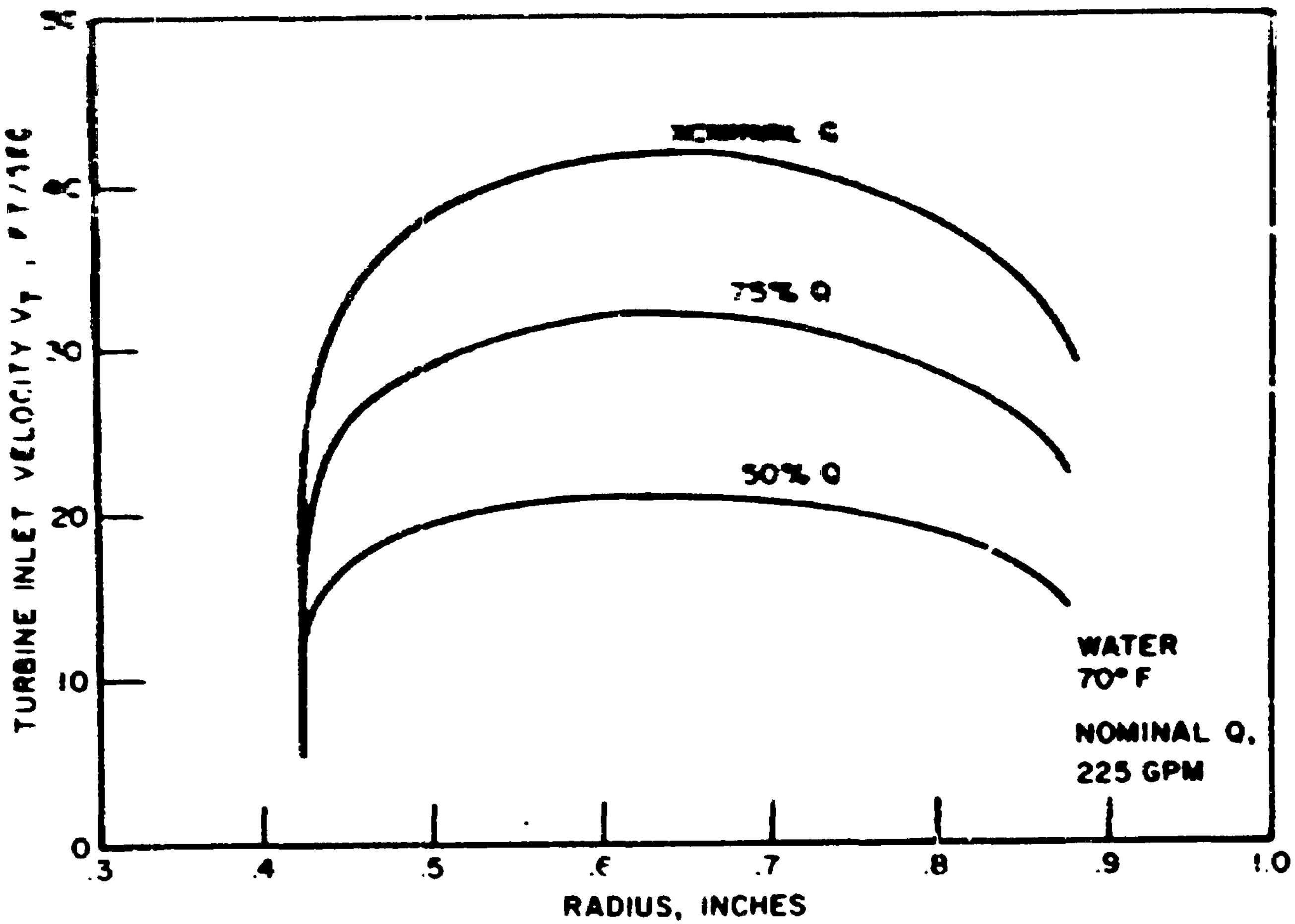

FIGURE 13

TURBINE INLET VELOCITY PROFILE
DEPENDENCE ON FLOW RATE

are based on the analysis of Levy (Reference 23) and some local departures from actual profile shapes may exist.

The blade angle of attack variation with radius is shown in Figure 14. This curve illustrates very well the fact that although the "net" or integrated blade angle of attack is effectively zero, portions of the blade do operate at significant angles of attack, up to 8 degrees. With a helical blade of specified lead, the tangent of the blade stagger angle is linearly proportional to radius, as is the tangent of the inlet velocity angle for a flat velocity profile at any one given rotor speed. Therefore, it is theoretically possible for all of the blade to operate at essentially zero zngle of attack. This, however, is not the case when one considers an actual velocity profile, as Figure 14 illustrates. Since the net driving torque required at "null" speed varies only slightly with flow rate, the slight variations in angle of attack do not appear on the plot, and the angle of attack is essentially constant with flow rate.

Figure 15 illustrates the variation of the turbine blade interference coefficient K_0 with radius. The interference coefficient is the ratio of theoretical blade lift,

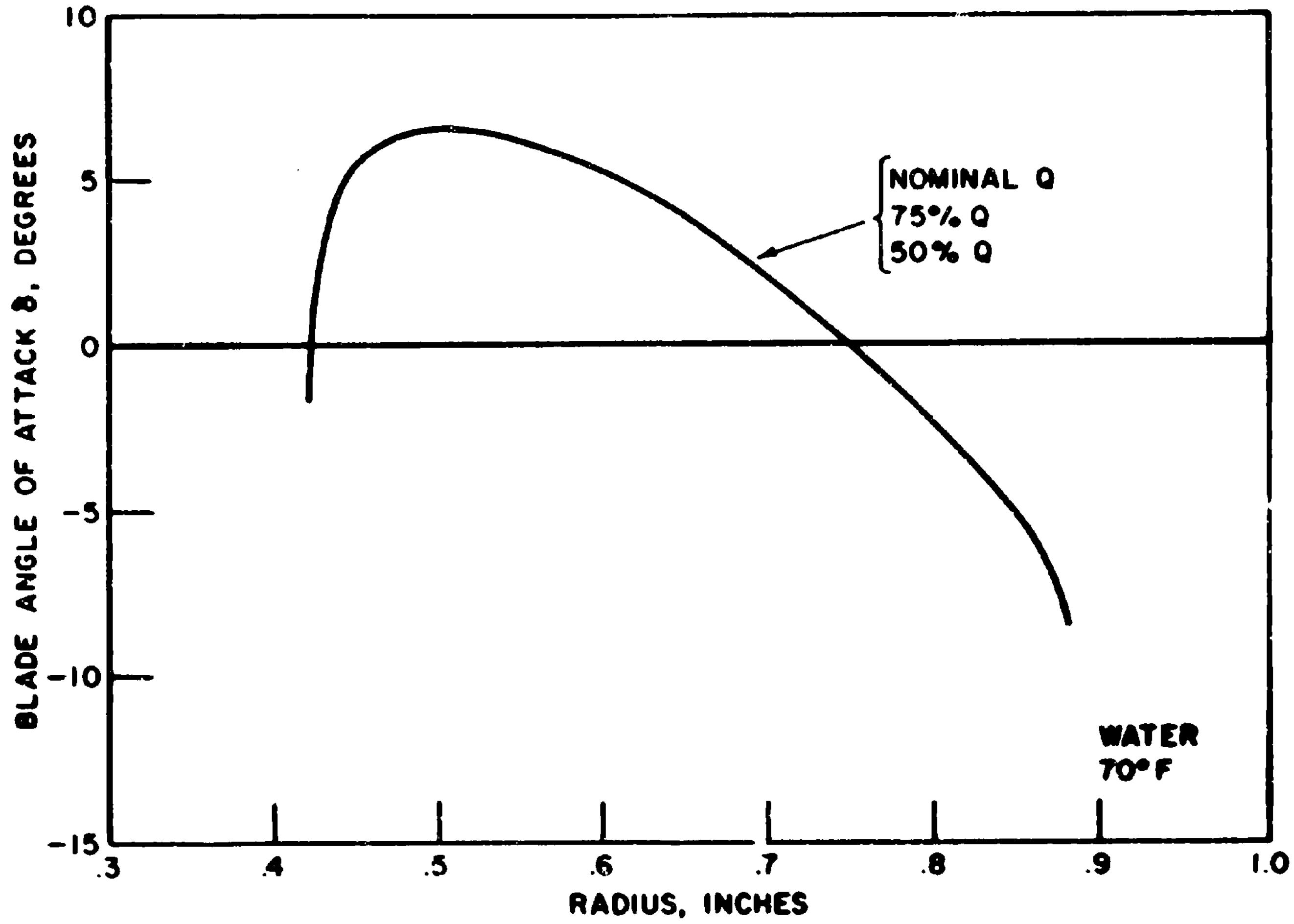

FIGURE 14

BLADE ANGLE OF ATTACK FOR THREE TEST FLOW RATES

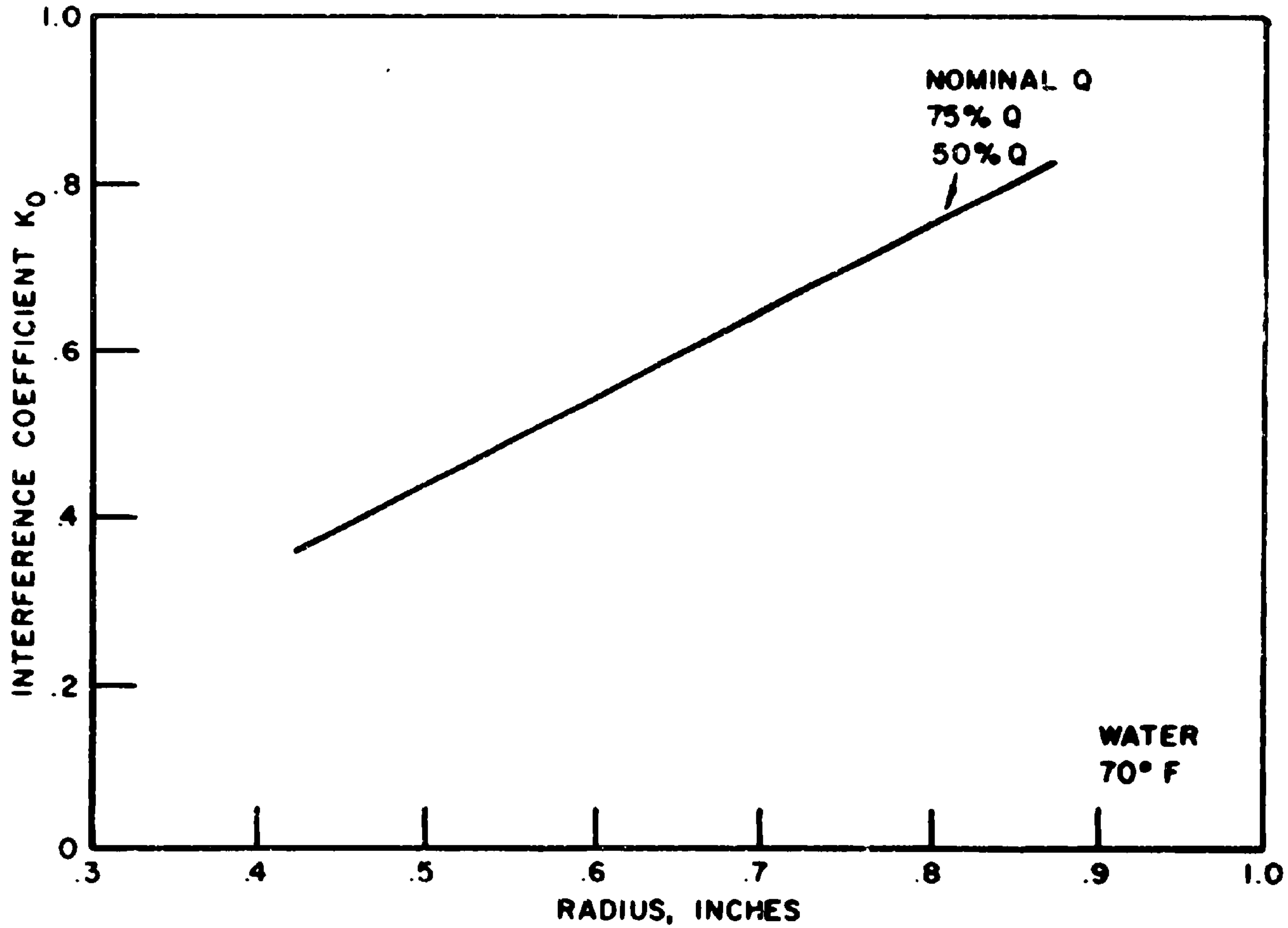

FIGURE 15

TURBINE BLADE INTERFERENCE COEFFICIENT
FOR TEST FLOW RATES

109

accounting for interference effects from adjacent blades, to the theoretical single-airfoil lift. This ratio is a function of the blade stagger angle and the space-to-chord ratio, which accounts for the variation with radius. When $K_o = 1$, interference does not take place, and the lift of the blade is the same as that of a single blade in the same flow field. The importance of including blade interference effects is clearly illustrated in Figure 15, where K_o reaches values as low as 0.4 near the rotor hub and is considerably less than 1.0 over most of the blade length.

The driving torque per unit blade length variation with radius is shown in Figure 16. This "torque" is actually the force per unit blade length multiplied by the moment arm to that blade element, and indicates the relative contribution of elements along the blades to the total rotor driving torque. The variation of this parameter with flow rate depends considerably on the velocity profile, since the velocity enters the torque expression as a squared term. The large negative values at larger radii correspond to the negative angle of attack caused by the decrease in velocity near the outer meter wall. Again these curves point out the value

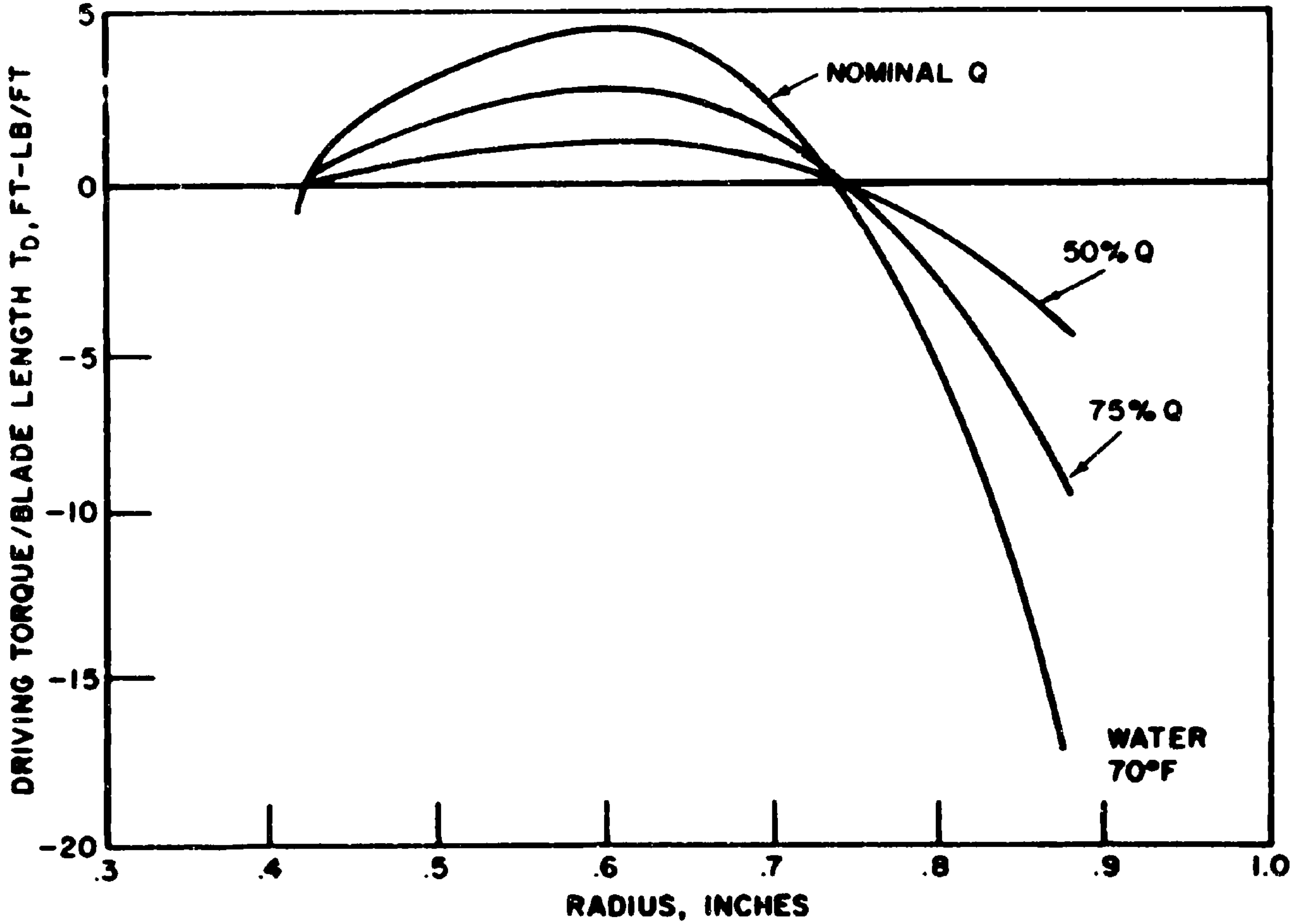

FIGURE 16

DRIVING TORQUE PER UNIT BLADE LENGTH

of using an actual velocity profile and numerical integration over the blade length, as opposed to assuming a flat velocity profile.

The second major parameter to be varied was the fluid and meter temperature (assumed equal to each other at all times). The fluid properties were varied for each case, and the changes in meter geometry were calculated within the program, based on coefficients of thermal expansion provided for the rotor and the meter body. In this way, variations in all major meter dimensions can be included. As mentioned previously, the reference case was water at a flow rate of 225 gpm. Other parameters for these cases were:

	$\bar{V}$ ft/sec	Net Angle of Attack, Deg.	ΔP, psi	Meter Factor cycles/gal	ω_i rad/sec	ω_a rad/sec
40°F	37.137	0.0765	9.1	534.81	922.89	900.09
70°F	37.115	0.0764	8.3	532.99	922.28	897.02
100°F	37.093	0.0766	7.6	530.57	921.68	892.94
150°F	37.057	0.0767	6.6	525.39	920.67	884.24

The major effects being illustrated here are due primarily to changes in meter geometry with temperature, and changes in fluid viscosity. The turbine inlet velocity profile variations with temperature are shown in Figure 17. The slightly higher velocities at the lower temperatures are due to the smaller meter geometry for the same flow rate, as shown also in the previous tabulation of average velocities. The increased fluid viscosity at the lower temperatures is reflected in a slightly larger curvature in the velocity profile and an increased pressure drop.

The blade angle of attack and interference coefficient variations with radius are shown in Figures 18 and 19. Changes in these parameters with temperature are very small, so the different curves appear as a single line in the plots. The dependence of driving torque per unit blade length on temperature is shown in Figure 20. Again, the variations are due primarily to velocity profile effects, with the slightly lower velocities at 150°F producing slightly lower torques. Although Figure 20 tends to suggest that the 40°, 70°, and 100°F cases are identical and the 150°F case is different, this is not the case. Actually, the torque values are different in each case, but it is only at 150°F that the difference is large enough to be distinguished in the plots.

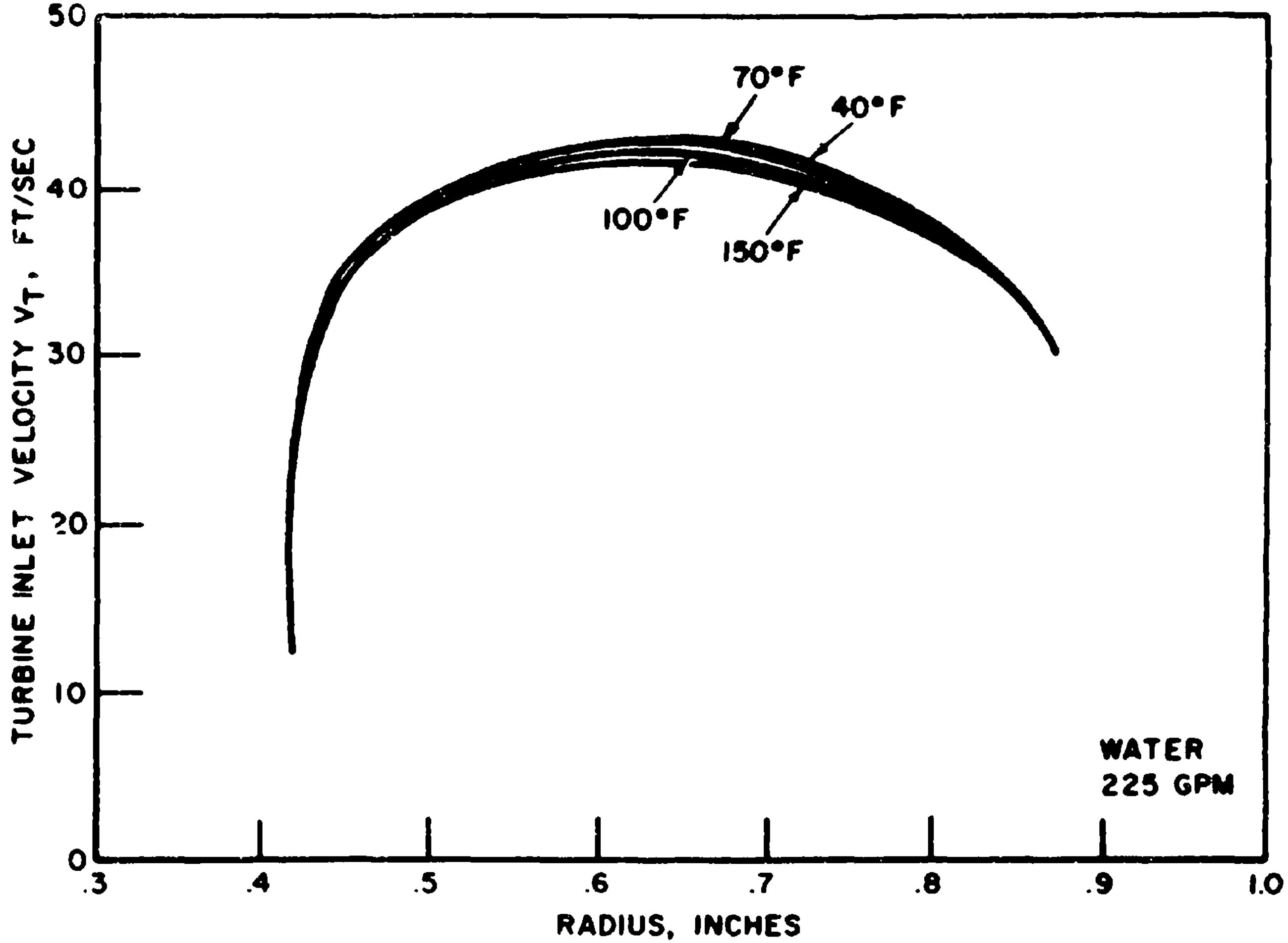

FIGURE 17

TURBINE INLET VELOCITY PROFILE
VS TEMPERATURE

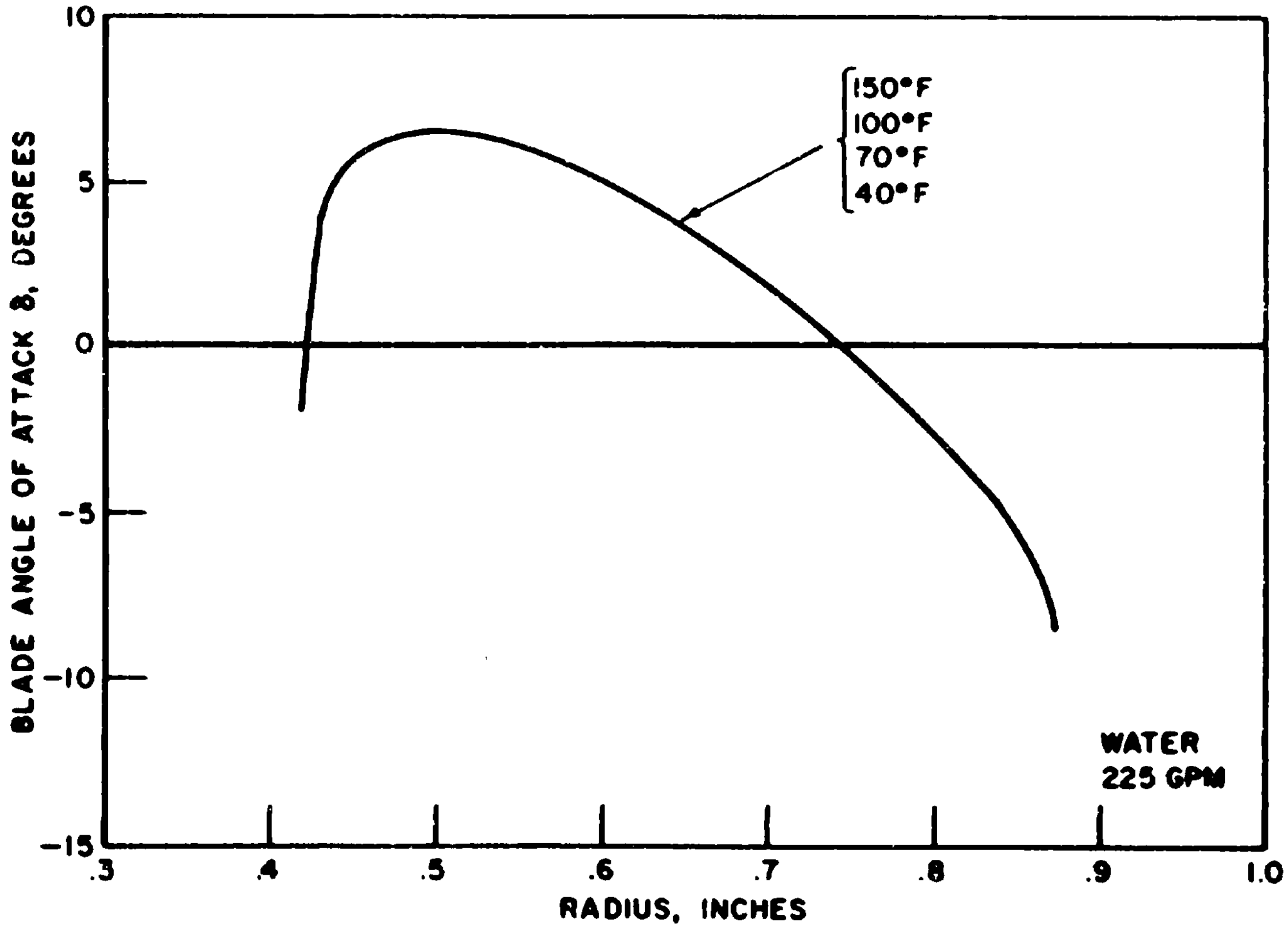

FIGURE 18

BLADE ANGLE OF ATTACK FOR FOUR TEMPERATURE CASES

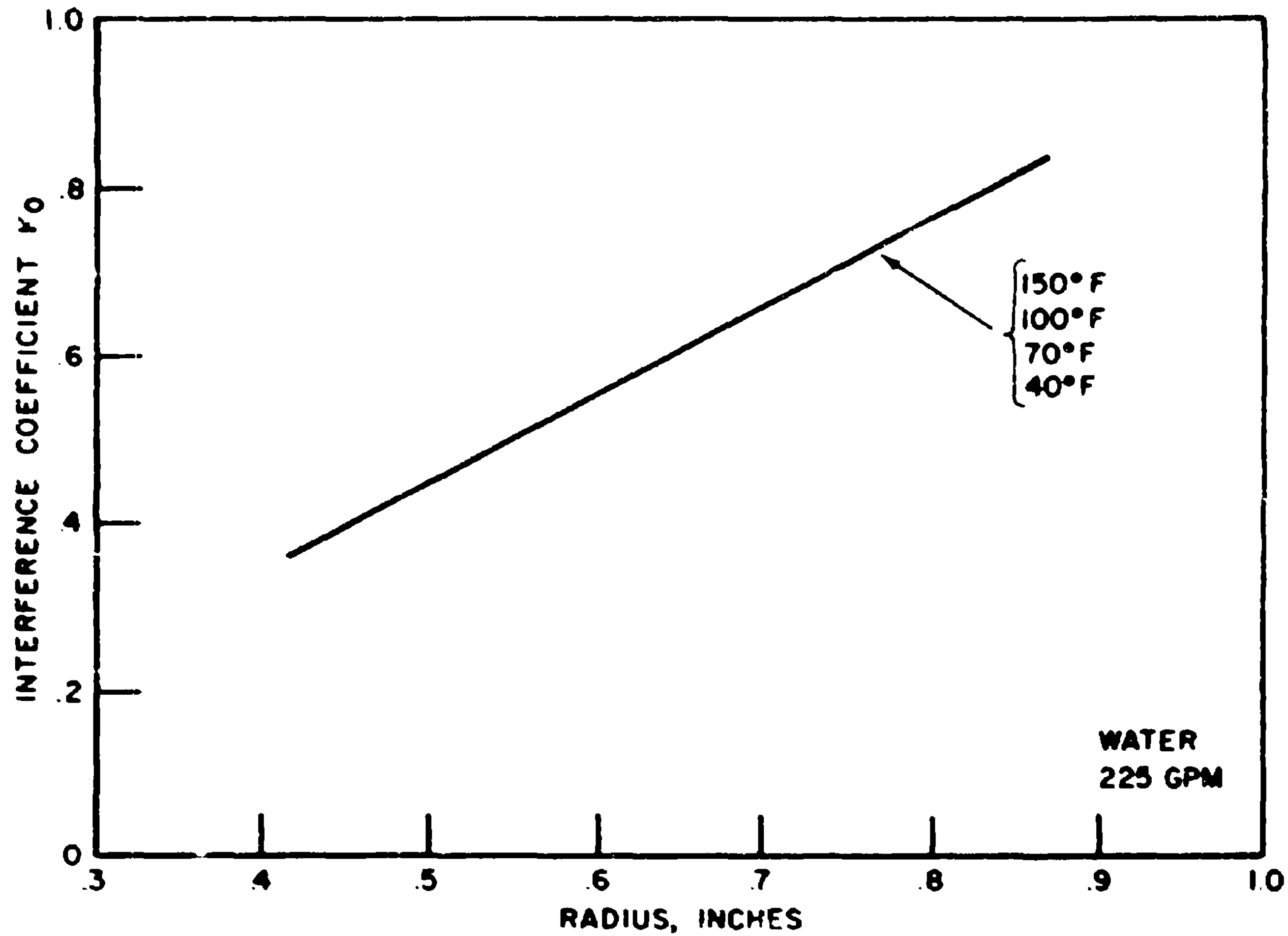

FIGURE 19

TURBINE BLADE INTERFERENCE COEFFICIENT
FOR TEMPERATURE CASES

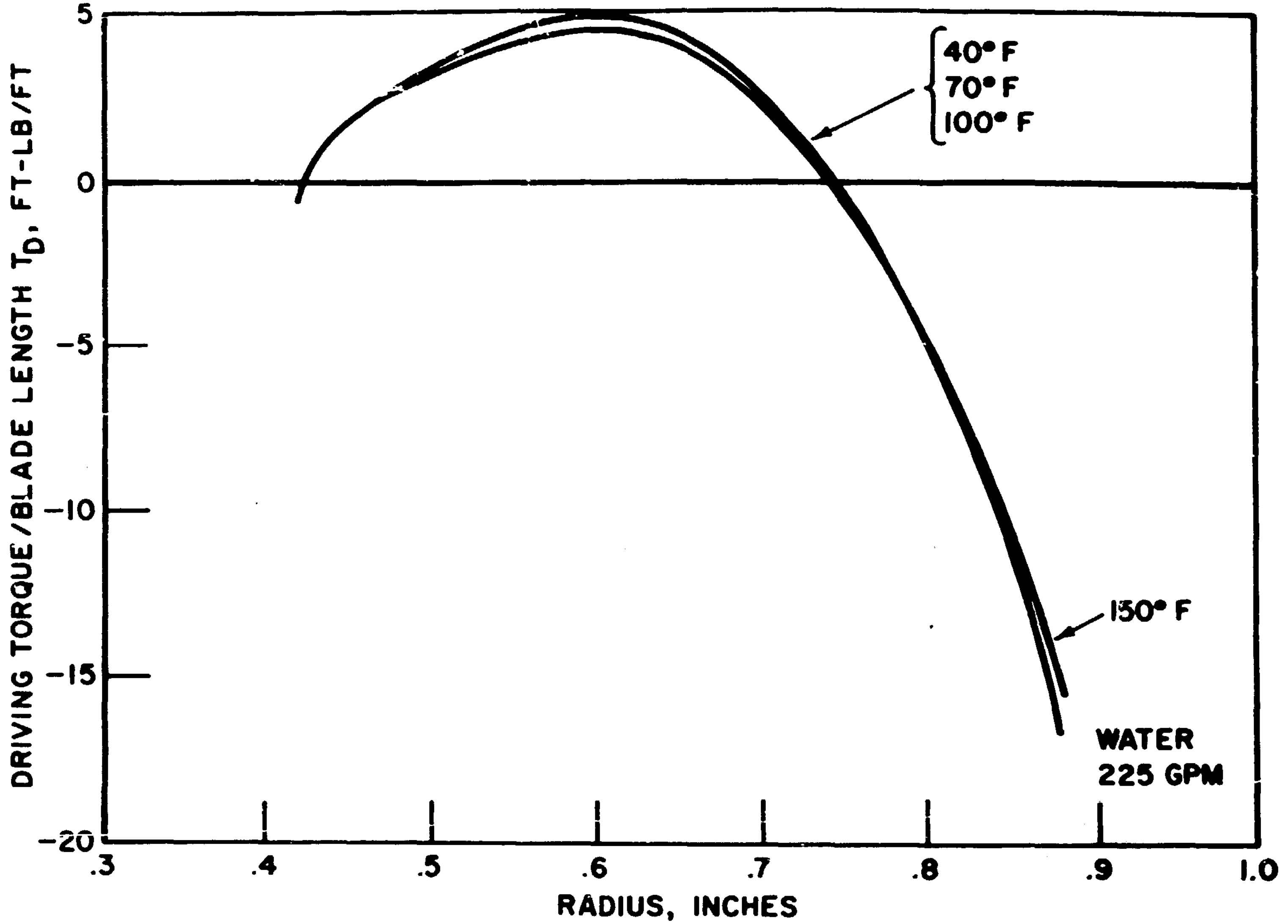

FIGURE 20

DRIVING TORQUE PER UNIT BLADE LENGTH
DEPENDENCE ON TEMPERATURE

The next area of study was the effect of manufacturing tolerances on meter performance and registration. Based on the test cases previously discussed, the most important non-fluid effect appears to be the geometry-velocity profile relationship. For this reason, the parameters selected for the tolerance study were the hub radius, blade tip radius and meter body radius. The rotor hub drag and blade tip drag are the predominant retarding torques, and therefore variations in the three dimensions selected should affect these parameters. The particular meter being modeled had a rotor hub diameter tolerance of ± 0.002, a blade tip diameter tolerance of ± 0.003, and a meter bore tolerance of ± 0.001. These tolerances were stacked so as to give the minimum flow area and blade tip clearance for the first case and the maximum flow area and blade tip clearance for the second case. The comparison with the nominal case is shown below:

Geometry	$\bar{v}$ ft/sec	Net Angle of Attack, Deg.	ΔP, psi	Meter Factor cycles/gal	ω_i rad/sec	ω_a rad/sec
Minimum	37.165	0.0765	8.28	532.62	922.82	896.40
Nominal	37.115	0.0764	8.27	532.99	922.28	897.02
Maximum	37.012	0.0763	8.23	532.77	920.44	896.65

From the minimum to the maximum geometry case, the blade tip drag decreased by 10%, but the hub drag is still the dominant term, so that significant changes in the rotor speed did not occur. There are two compensating effects taking place in the geometry changes. One would expect the rotor speed to primarily follow the fluid average velocity as indicated by the ideal speed. However, the high velocity of the minimum geometry is offset by the higher blade tip drag, causing the rotor to operate at a slower speed. From the minimum to the nominal geometry case, the average velocity has decreased, but the percentage decrease in the retarding torque is ten times as great, and the rotor speed actually increases. In the maximum-geometry case, the decrease in velocity overrides the decrease in retarding torques.

The differences in the velocity profiles, blade angle of attack, interference coefficient, and driving torque for the three cases are so small that they cannot be detected on the plots, and therefore these figures are not shown. The maximum change in meter factor with these manufacturing tolerances was only 0.07%. Therefore, manufacturing effects were not explored in any further detail although the capability to do so exists in the present program.

The next set of test cases was prepared to explore the characteristics of the same meter model in oil. Based on the availability of bearing drag data, MIL-L-6085 oil, which has a viscosity of 20 centistokes at 70°F, was selected. The results of these test cases at different flow rates are given below:

	$\bar{v}$ ft/sec	Net Angle of Attack, Deg.	ΔP, psi	Meter Factor cycles/gal	ω_i rad/sec	ω_a rad/sec
100% q	37.115	0.0727	14.2	523.27	922.28	880.66
75% q	27.836	0.0718	8.5	519.19	691.71	655.35
50% q	18.558	0.0523	4.1	512.23	461.14	431.04

The meter factors are approximately 2.0% to 2.5% lower than those for water at the same flow rate, which is not unusual for this amount of change in the fluid viscosity. As would be expected, also, the pressure drops are larger. The velocity profiles for these cases, shown in Figure 21, are similar to those for water, except for the increased curvature due to the increased viscosity. The blade angle of attack and interference coefficient (Figures 22 and 23) are effectively independent of flow rate, as was observed in water. The driving torque profile, Figure 24, reflects

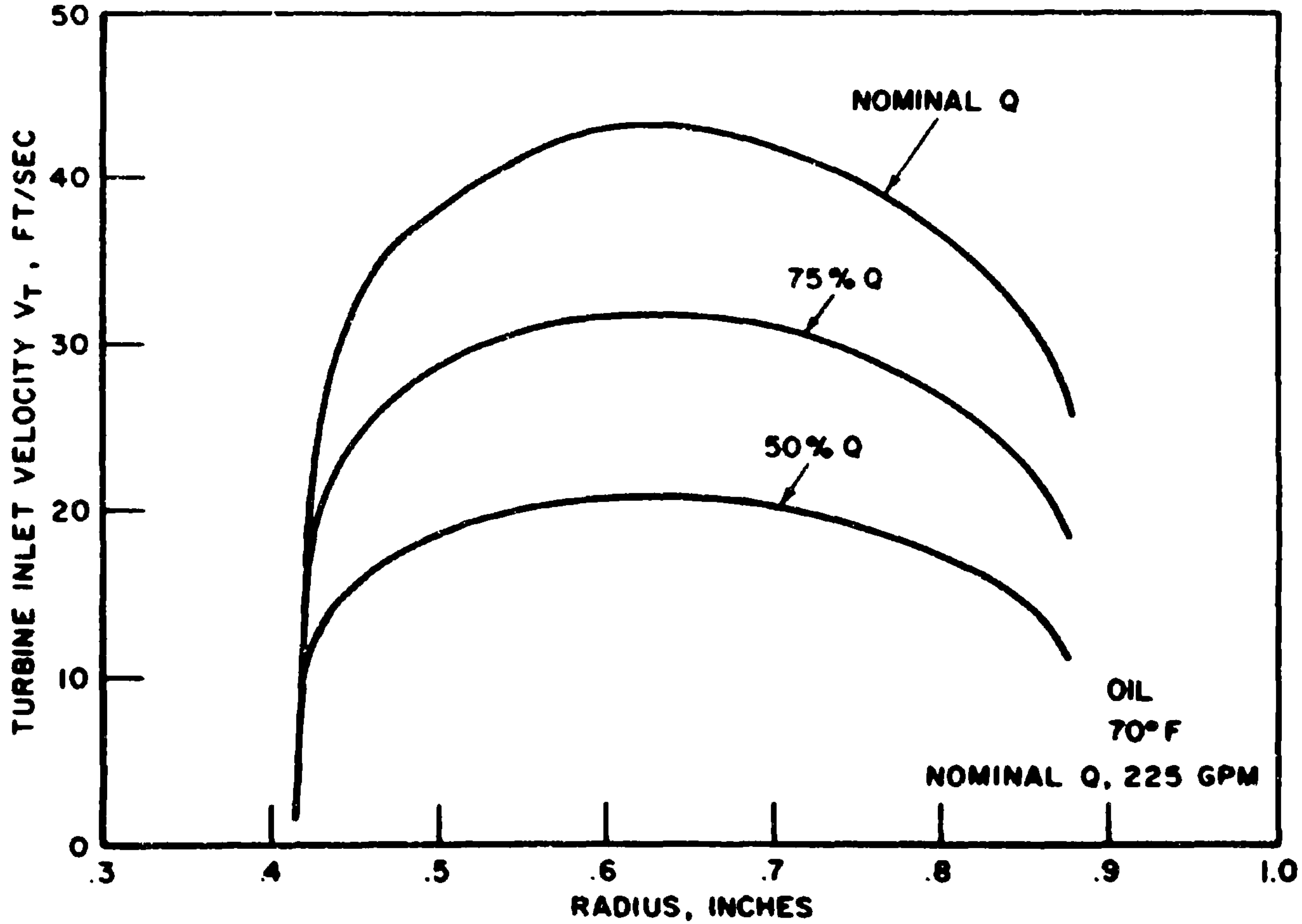

FIGURE 21

TURBINE INLET VELOCITY DEPENDENCE ON FLOW RATE

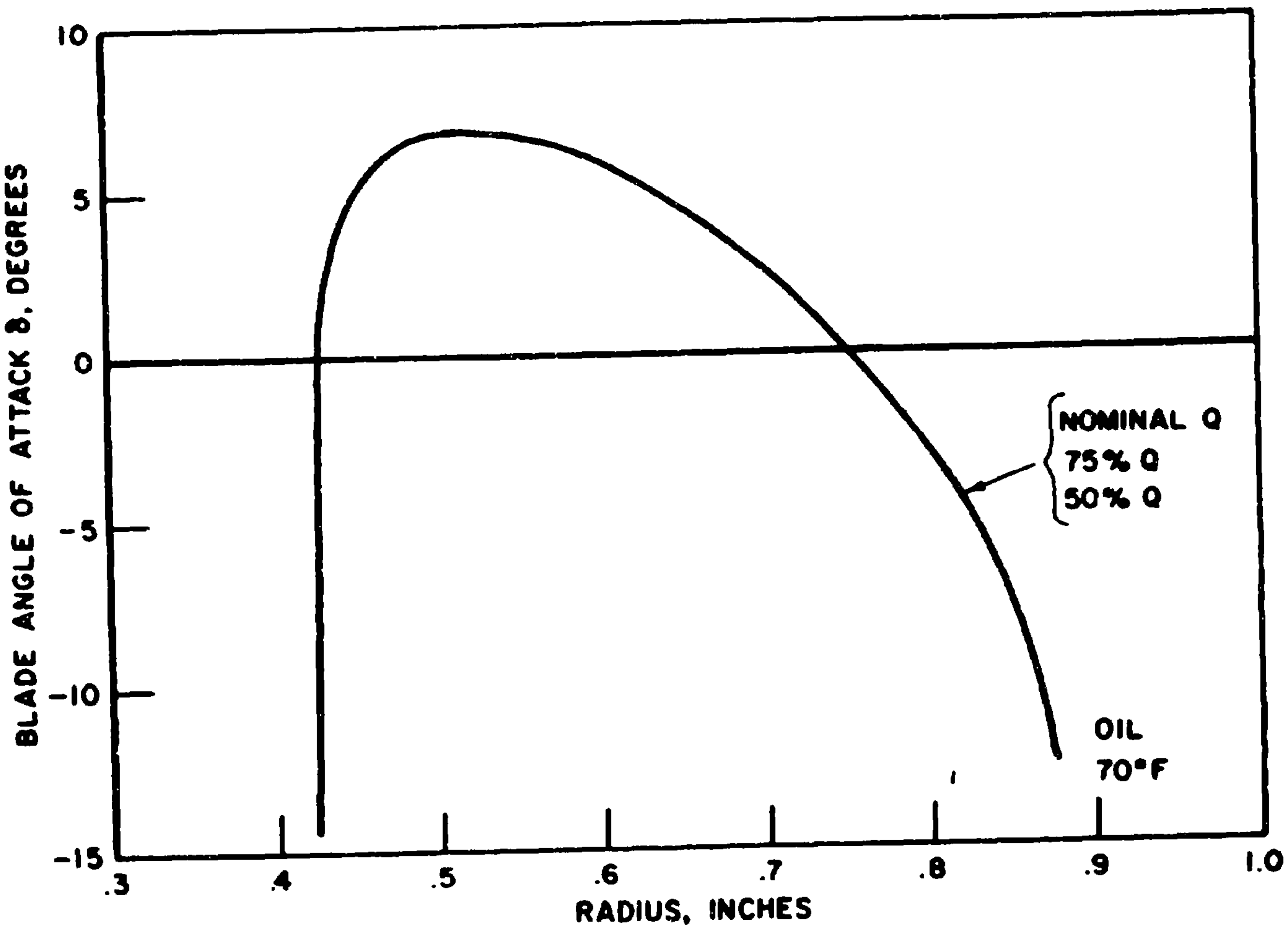

FIGURE 22

BLADE ANGLE OF ATTACK FOR THREE TEST FLOW RATES

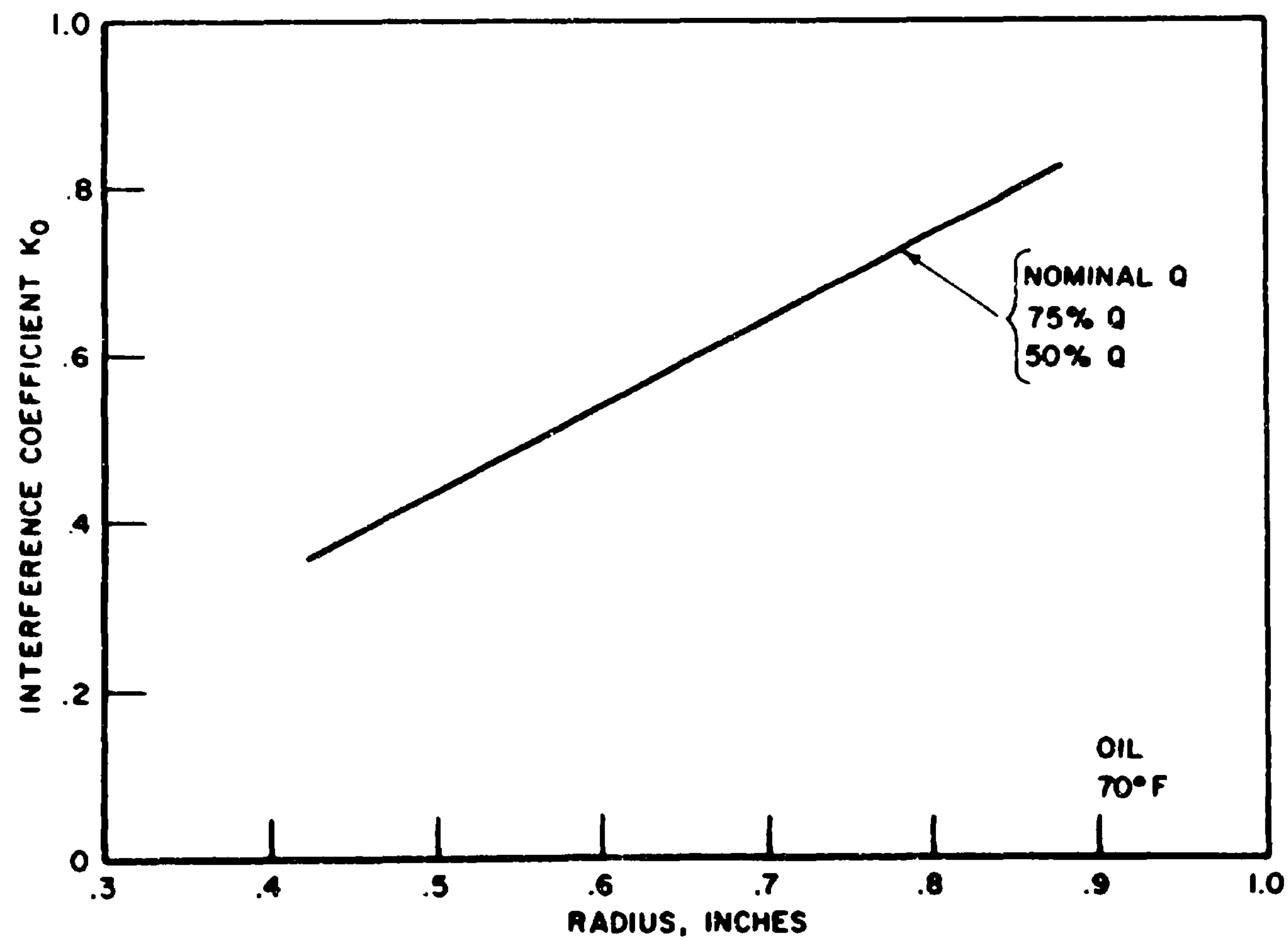

FIGURE 23

TURBINE BLADE INTERFERENCE COEFFICIENT
FOR TEST FLOW RATES

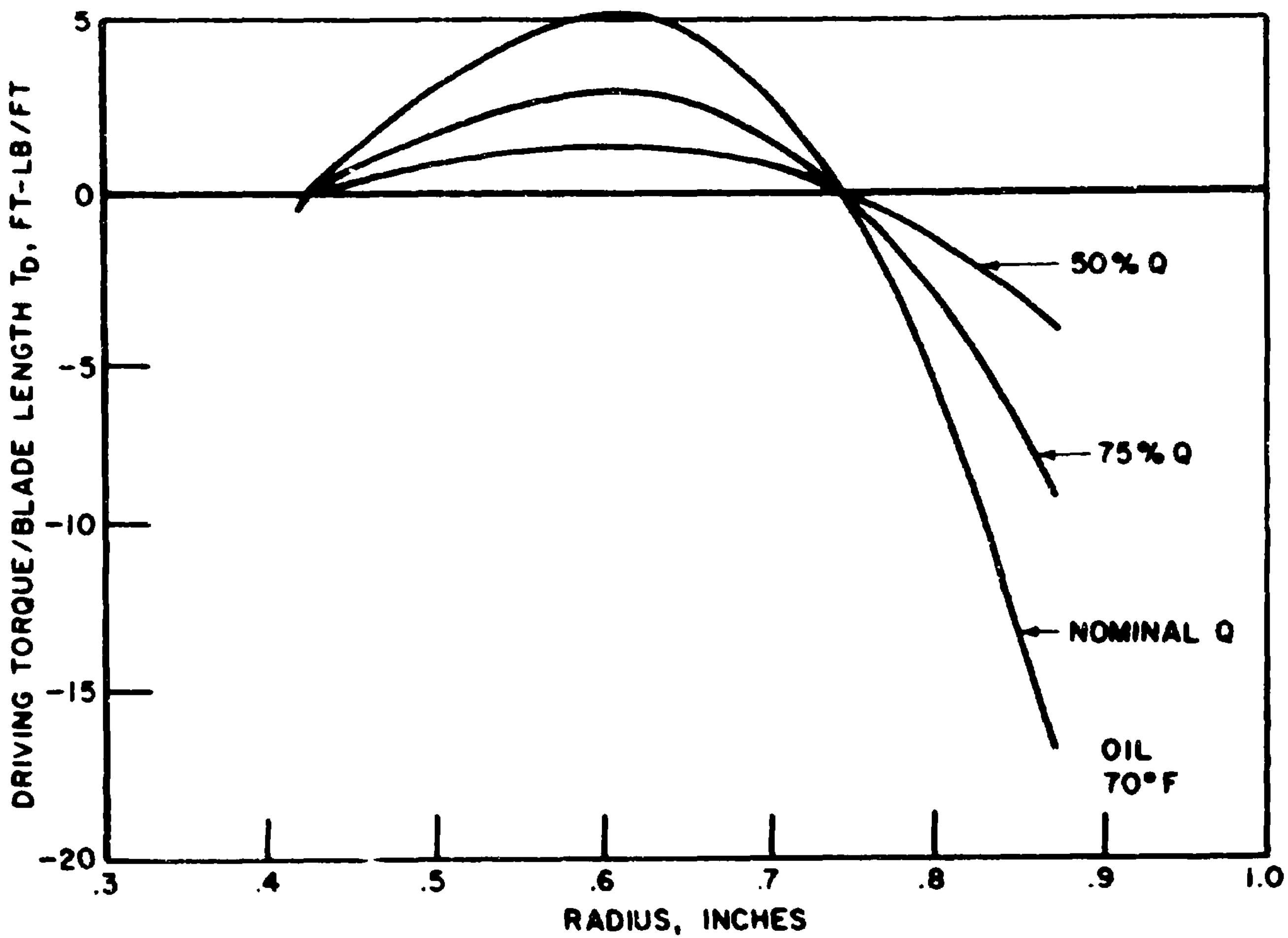

FIGURE 24

DRIVING TORQUE PER UNIT BLADE LENGTH
DEPENDENCE ON FLOW RATE

the shape of the velocity profiles with flow rate and the blade angle of attack.

Because of the difference in fluid properties between water and oil, it is informative to make a direct comparison of these two cases on the same graph for the nominal flow rate, as shown in Figures 25, 26 and 27. The increased curvature of the oil velocity profile in Figure 25 is carried over into the blade angle of attack and driving torque curves.

To better understand the importance of blade interference effects as related to blade number, several fictitious cases were prepared with rotors having eight and four blades each but with the same geometry and lead as the fourteen-bladed rotor. Results of the eight-bladed case are given below; computation of the four-bladed case was not accomplished due to nonconvergence resulting from the excessively large interpolation interval in space/chord ratio dependence of R (see Figure 3). Since this would have required extensive program additions, as well as additional computer checkout and operation time, this case was not run. The effect of blade number, however, is clearly indicated by the comparison between the fourteen-bladed and eight-bladed cases:

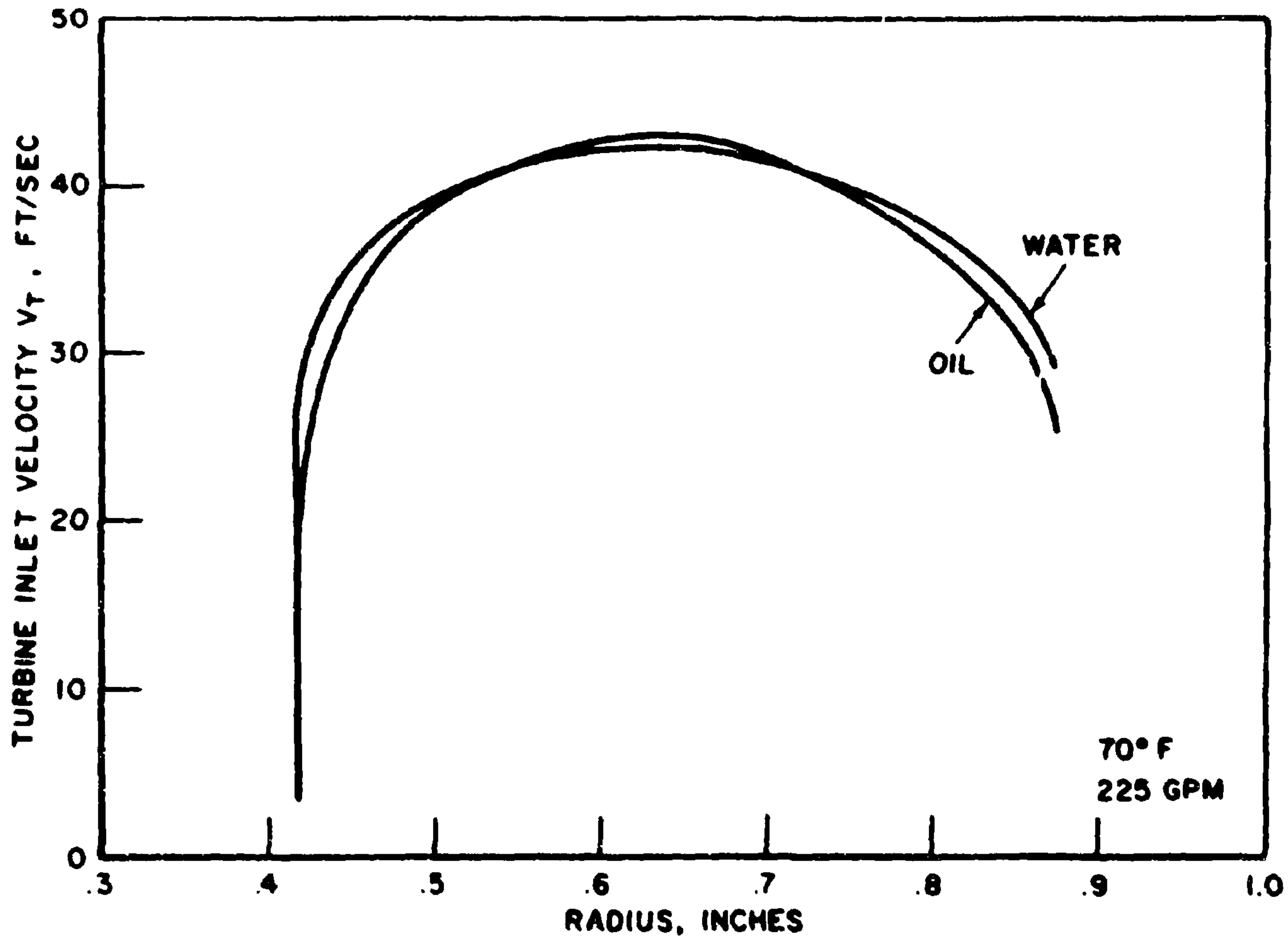

FIGURE 25

TURBINE INLET VELOCITY PROFILES FOR WATER AND OIL

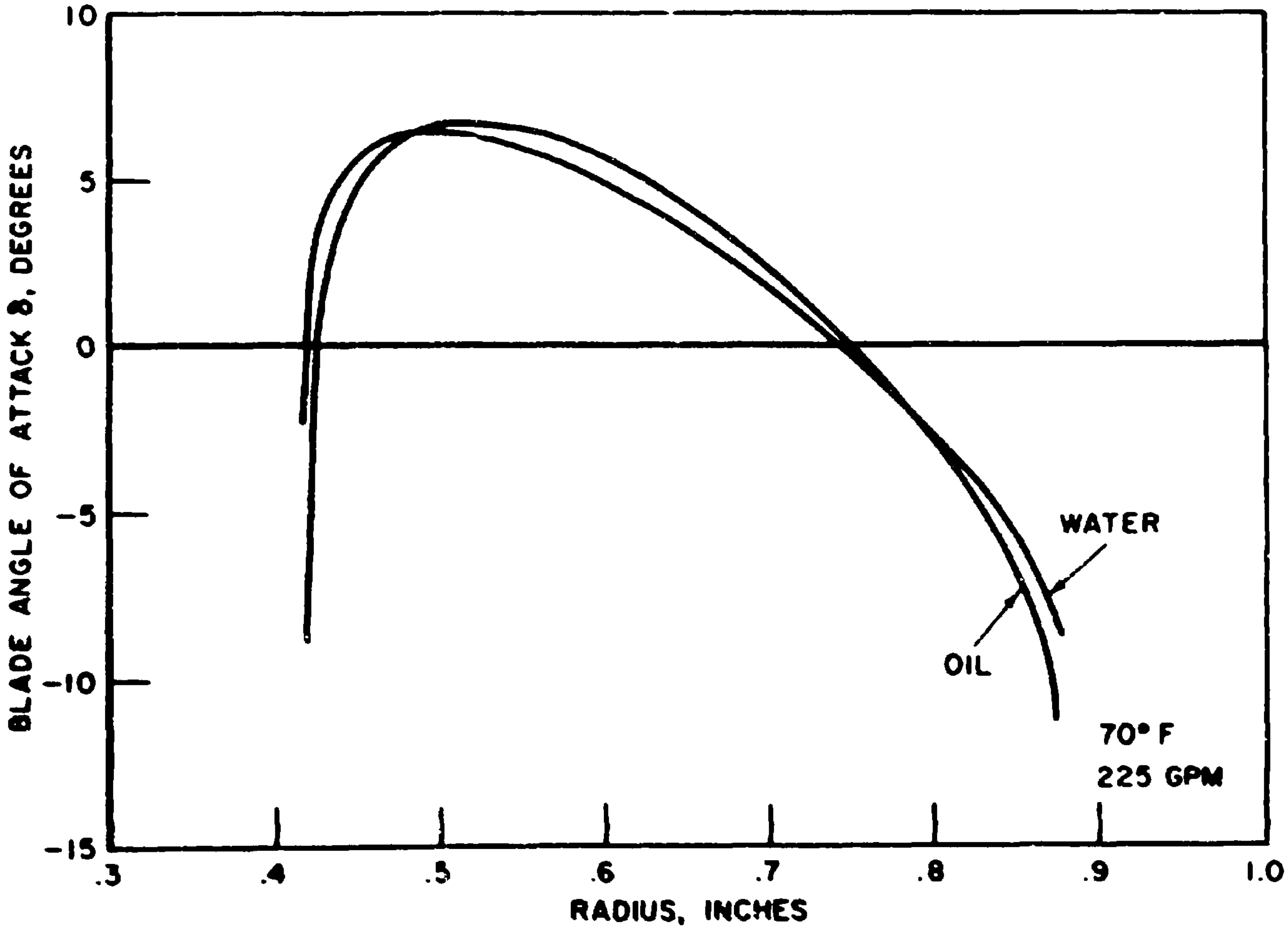

FIGURE 26

BLADE ANGLE OF ATTACK FOR WATER AND OIL

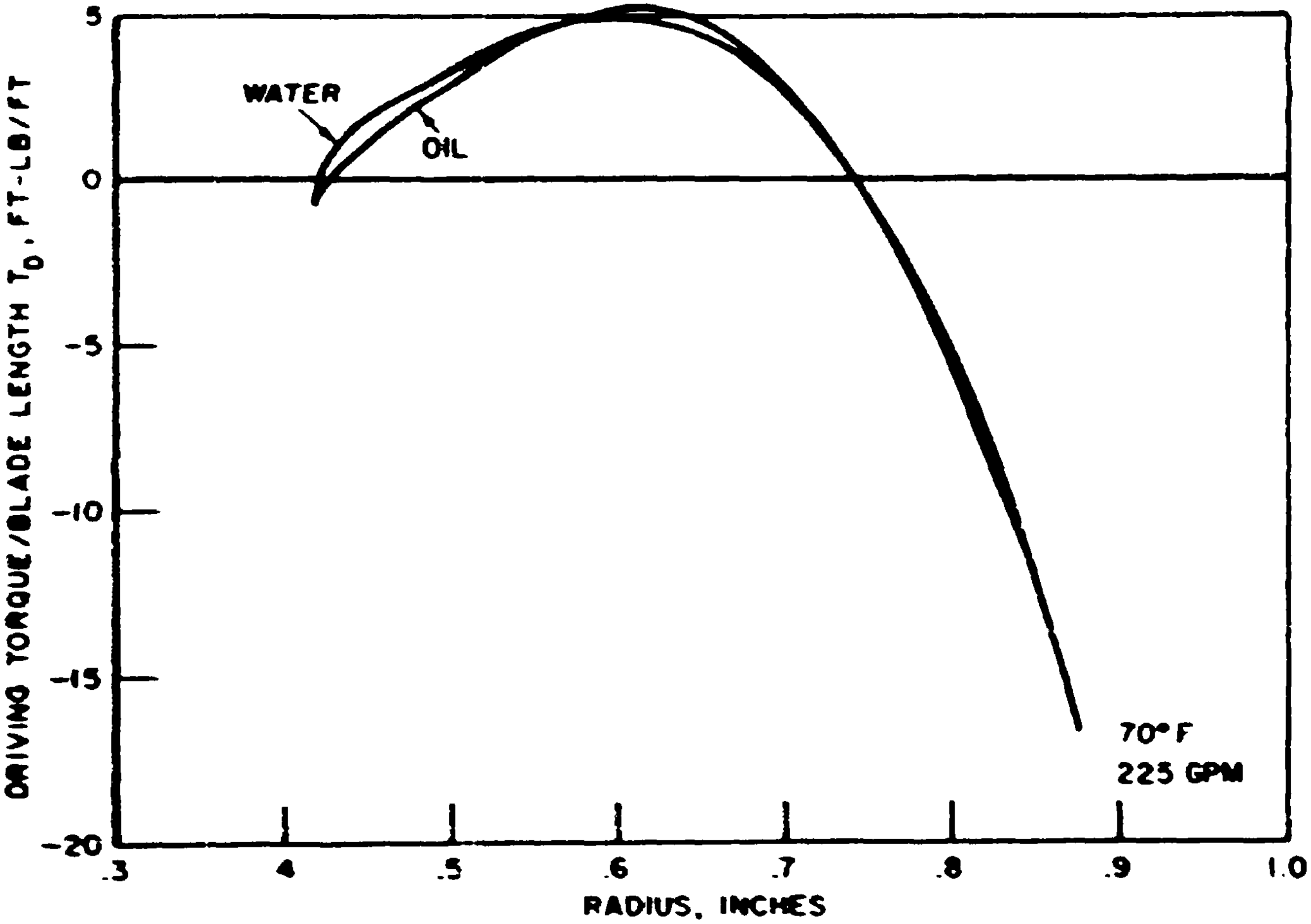

FIGURE 27

DRIVING TORQUE PER UNIT BLADE LENGTH
FOR WATER AND OIL

No. of Blades	$\bar{V}$ ft/sec	Net Angle of Attack, Deg.	ΔP, psi	Meter Factor cycles/gal	ω_i rad/sec	ω_a rad/sec
14	37.115	0.0764	8.3	532.99	922.28	897.02
8	37.115	0.0592	4.9	309.84	922.28	912.56

The velocity profiles are identical and are not shown. Variations in the angle of attack occur near the rotor tip where the angles of attack become large and interference from adjacent blades is more important (see Figure 28). The most significant change occurs in the interference coefficient shown in Figure 29. The driving torque is actually less for the lower blade numbers as shown in Figure 30, but the rotor speed is much higher due to the significant decrease in blade tip drag as well as the reduction in interference effects. As would be expected, the rotor is approaching the ideal speed, since at low blade numbers the blade operates as an isolated airfoil.

The capability to analyze a flat bladed rotor was desired to have as flexible a program as possible. A significant percentage of the meters used, Potter's in particular, have flat blades and these can be accommodated with the proper input format. Because details of the Potter designs were not available, a fictitious case was used to verify that

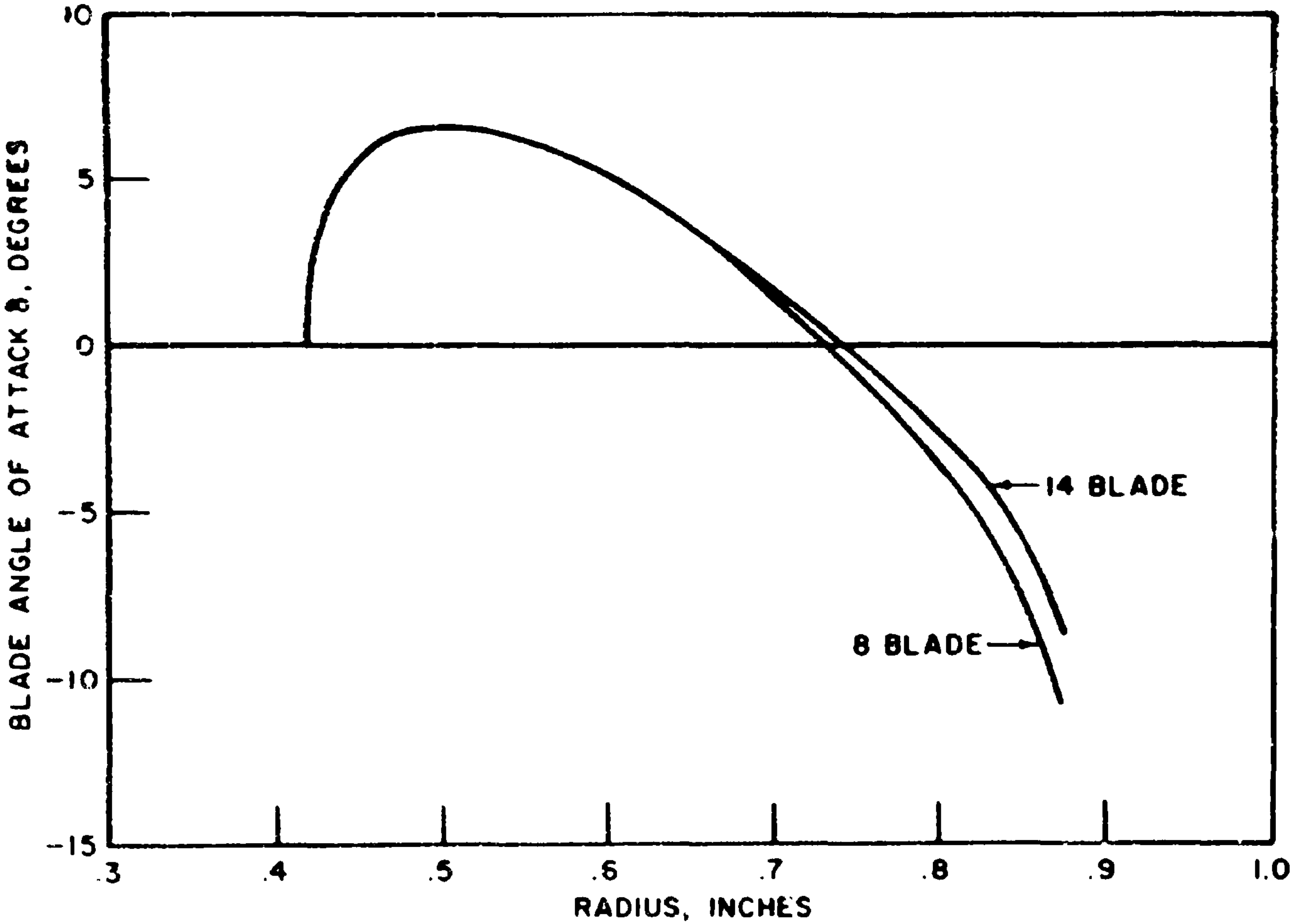

FIGURE 28

EFFECT OF NUMBER OF BLADES
ON LOCAL BLADE ANGLE OF ATTACK

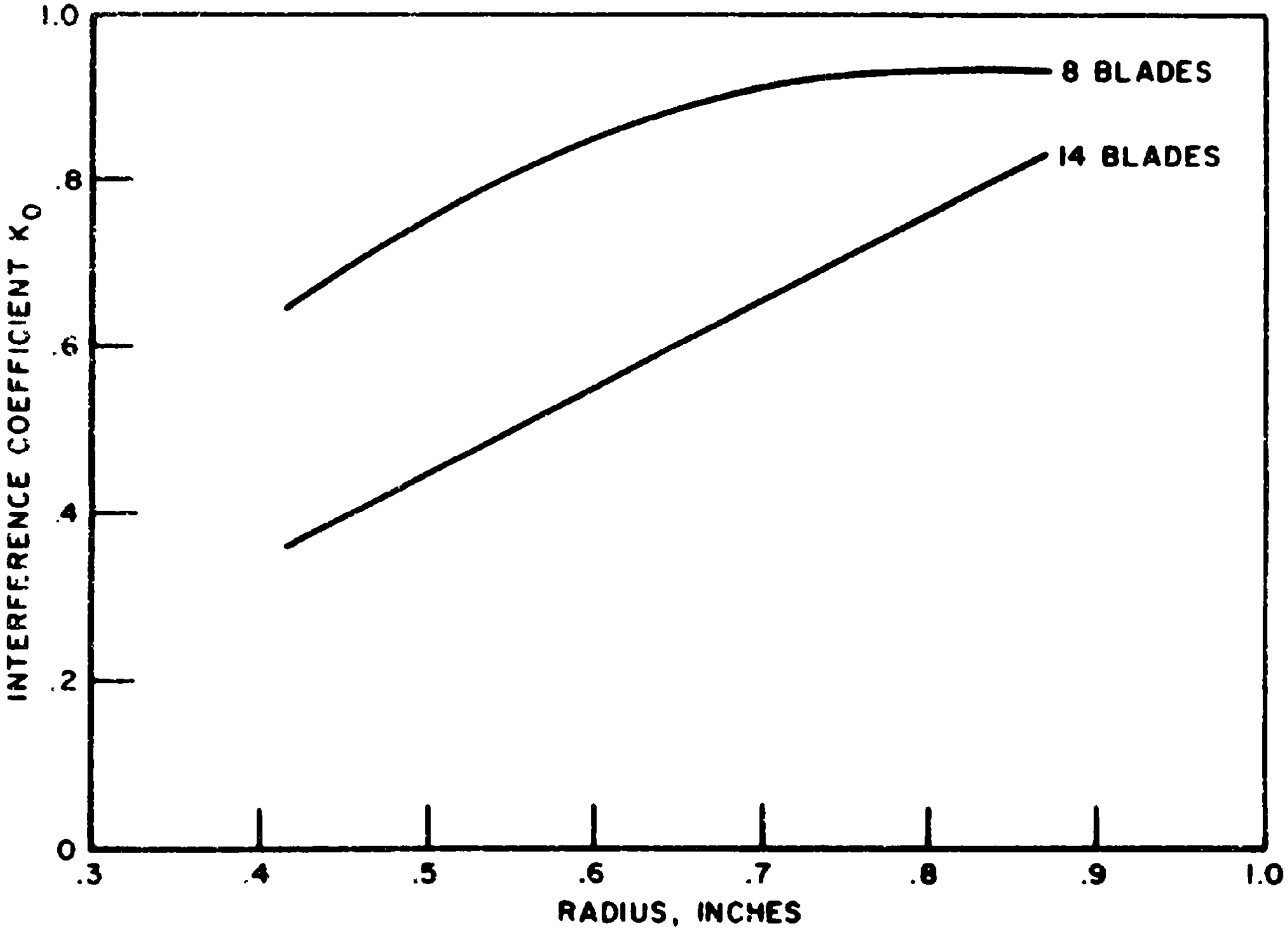

FIGURE 29

EFFECT OF NUMBER OF BLADES
ON INTERFERENCE COEFFICIENT K_0

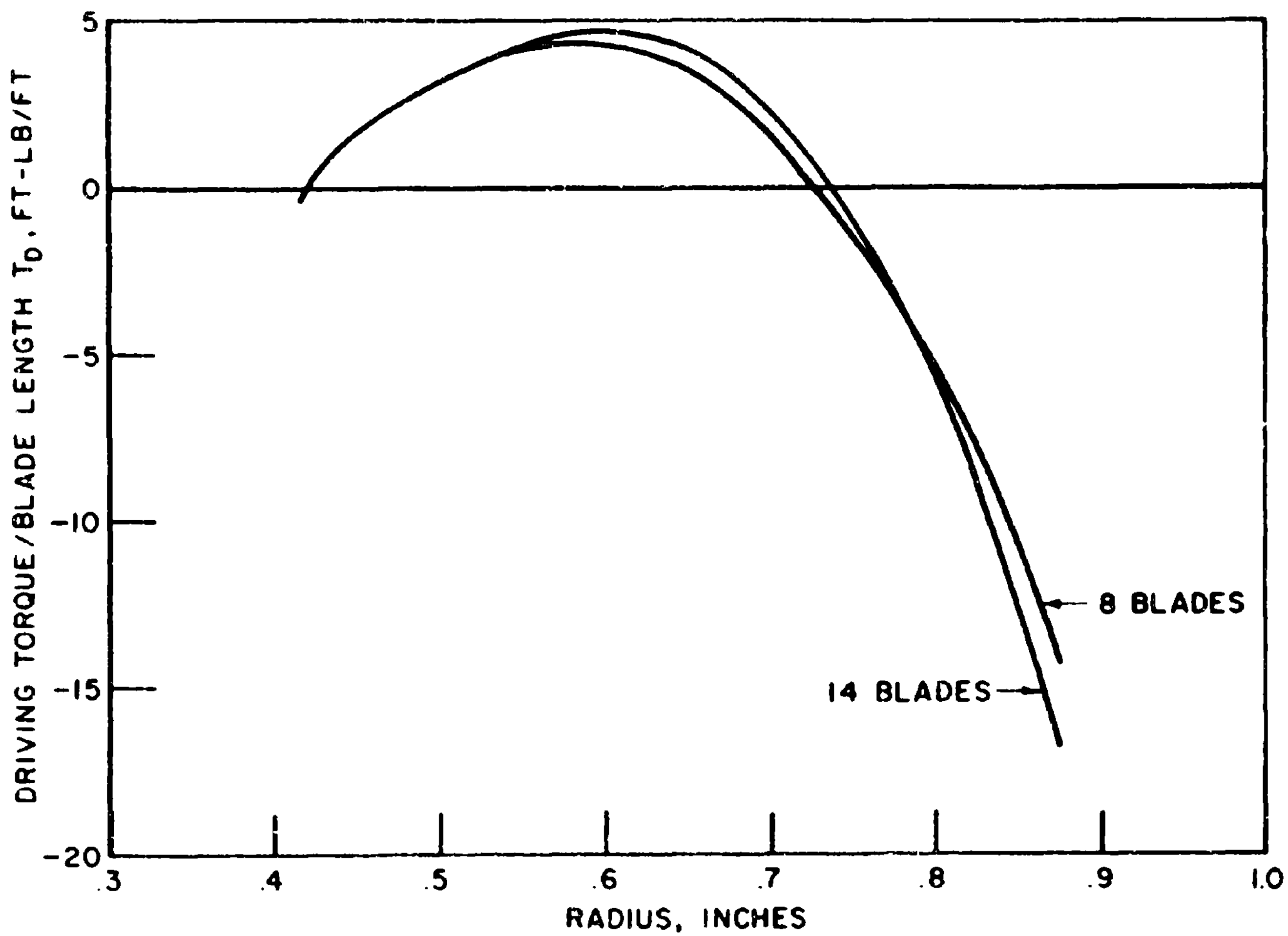

FIGURE 30

EFFECT OF NUMBER OF BLADES ON DRIVING TORQUE the program would function properly for these cases. The blade angle selected was the mean blade angle of the previous helical rotor.* Comparison with the helical rotor having the same blade number is shown below:

Blade Type	$\bar{V}$ ft/sec	Net Angle of Attack, Deg.	ΔP, psi	Meter Factor cycles/gal	ω_i rad/sec	ω_a rad/sec
Helical	37.115	0.0764	8.3	532.99	922.28	897.02
Flat	37.115	0.0991	8.0	511.41	899.05	860.70

The most significant change, as would be expected, is in the blade angles of attack (Figure 31). Because the blade is flat, these angles are larger at the hub and at the blade tip. The blade interference coefficients shown in Figure 32 are virtually identical, as they should be, since the helical rotor is assumed to have a flat profile at any radius. The larger variation in angle of attack is reflected in the driving torque curves as shown in Figure 33.

Test cases were run on nominal-geometry meters to establish the changes resulting from the substitution of journal bearings for the nominal-case, ball bearings. Because the bearing drag

---

* Note that this arbitrary selection of blade angle for the flat blade implies that the computed rotor speed has no significance. The flat-blade effects therefore appear in the shapes of the torque, angle of attack, and K_o curves (see Figures 31, 32 and 33).

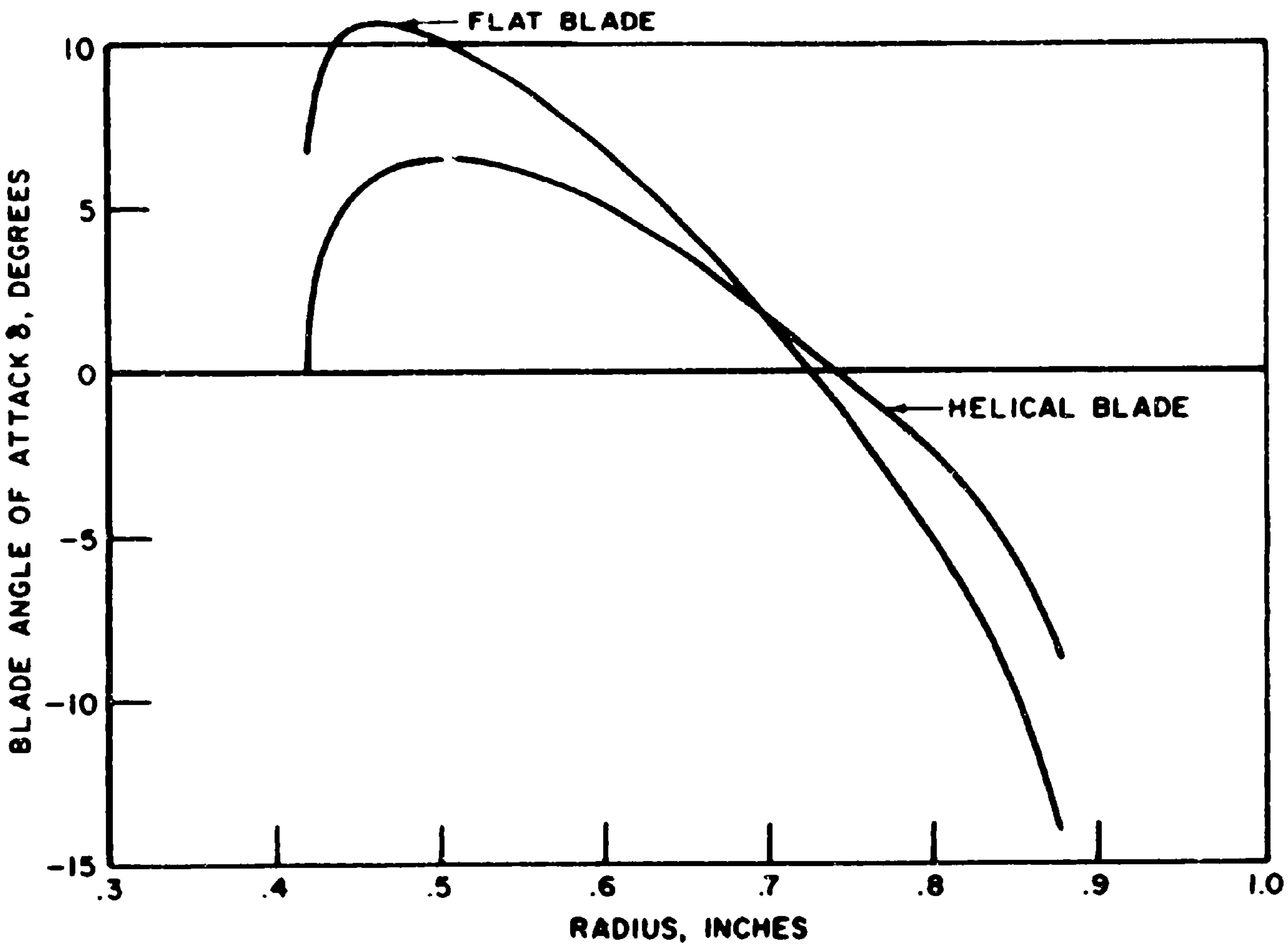

FIGURE 31

EFFECT OF BLADE SHAPE
ON LOCAL BLADE ANGLE OF ATTACK

125

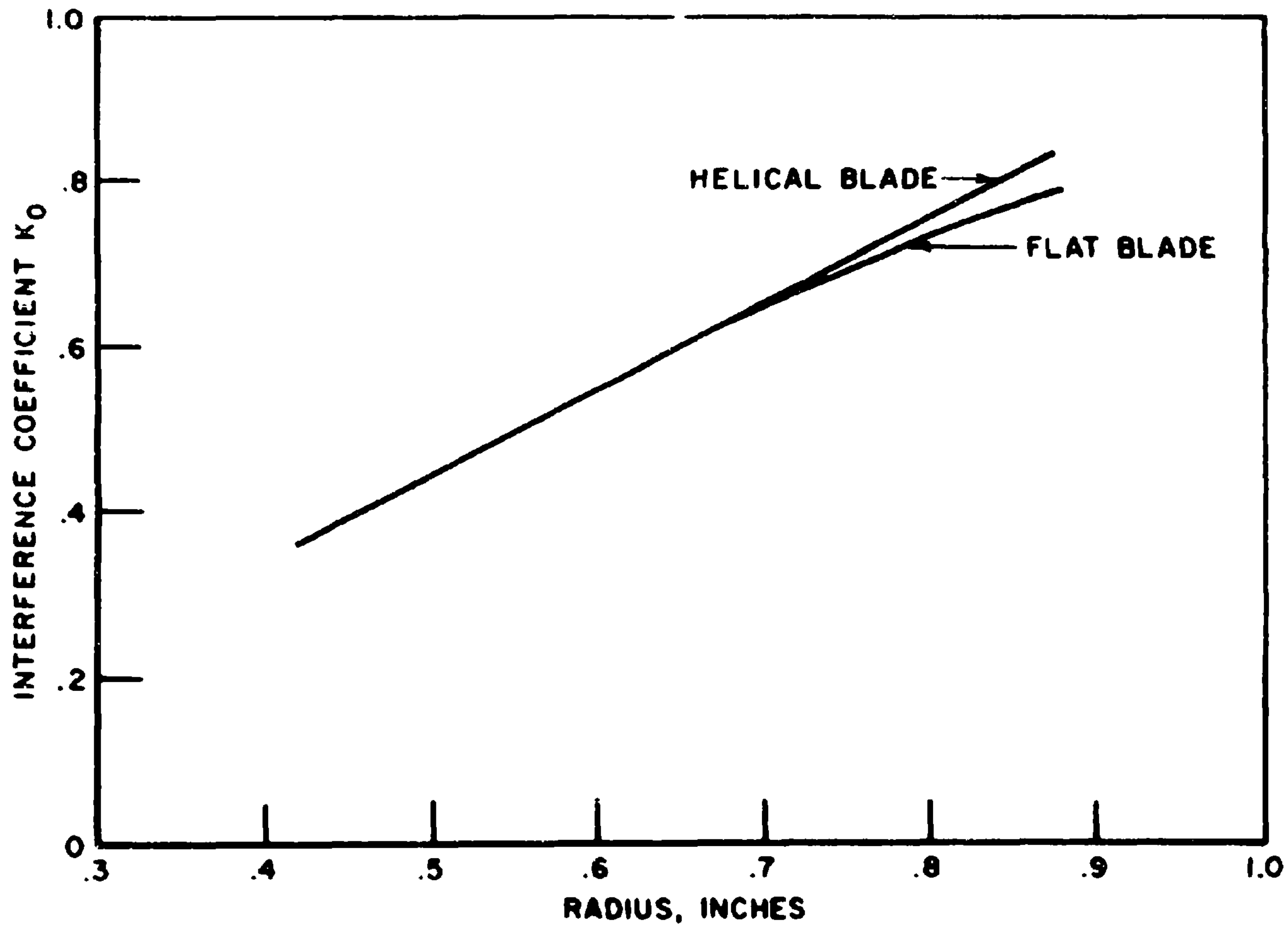

FIGURE 32

EFFECT OF BLADE SHAPE
ON INTERFERENCE COEFFICIENT K_o

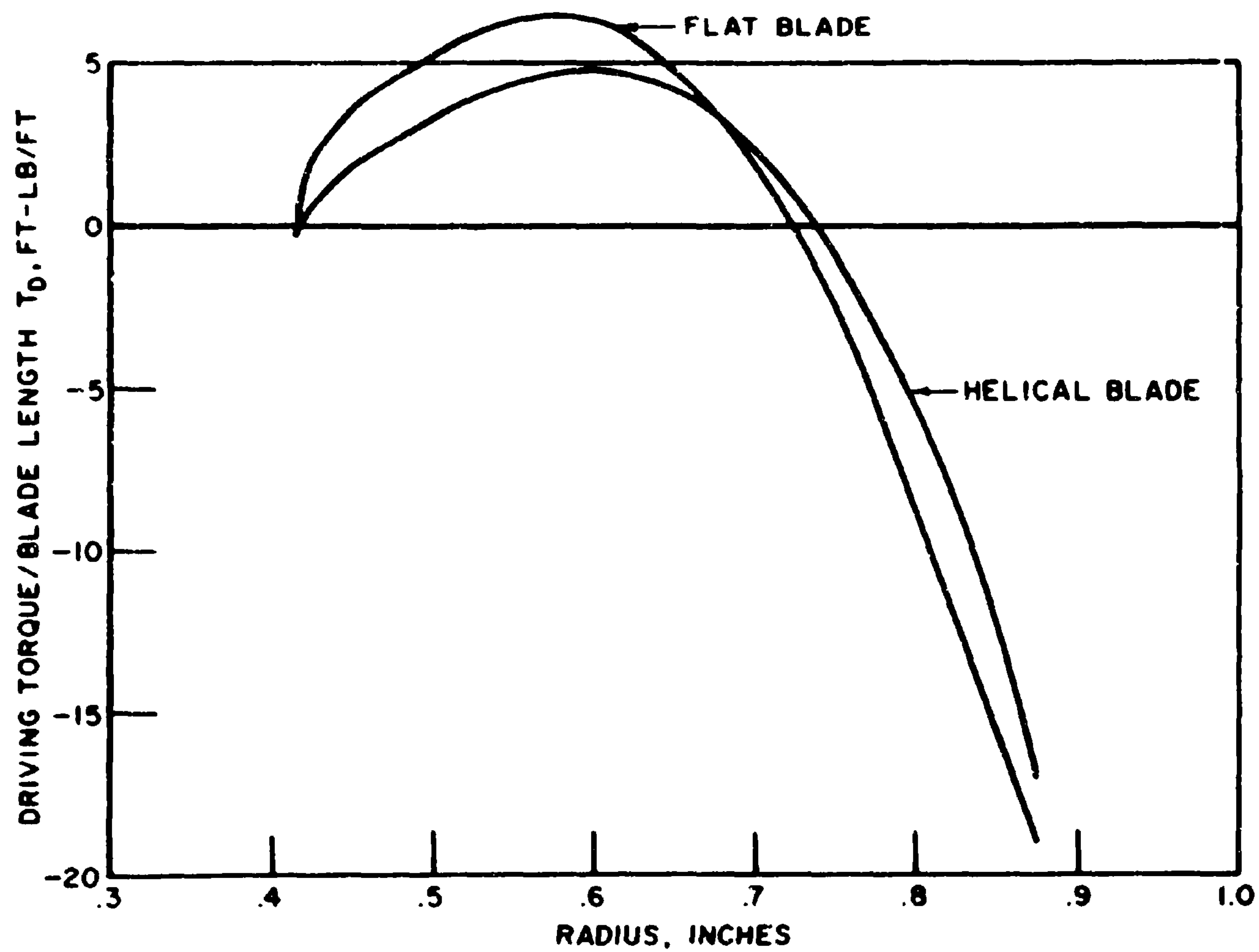

FIGURE 33

EFFECT OF BLADE SHAPE ON DRIVING TORQUE

was so small for the high Reynolds-number ranges evaluated in this study, there was no detectable effect on meter performance, and these data are therefore not included here.

A final meter-configuration evaluation was made to determine the effect of readout drag; i.e., nominal cases were run with RF and magnetic pickups. As might be expected, the drag effect of the readout device was so small as to be indistinguishable, and thus these data are also not presented in this report.

Based on the results of the test cases with water and oil, it is clear that one of the most significant parameters in the program is the velocity profile, Velocity enters many expressions as a squared term, and the shape of the profile is directly reflected in the driving torque curves. To further illustrate the importance of the velocity profile on the final rotor speed, several test cases imposing various profiles on the blades were prepared.

In the first case, a flat velocity profile with V everywhere equal to the average velocity $\bar{V}$ was used. This simulates the assumption common to virtually all prior analyses. For the second case, the velocity profile in the flow straightener was imposed on the rotor. The flow-st aightener region commonly has a larger flow area, and a transition occurs to a smaller annular area as the fluid passes over the hub assembly. Because of this transition, some questions were raised about whether the turbine meter inlet velocity profile or flow straightener velocity profile should be used. Both of these cases were included to determine which gave rotor speeds more closely related to the actual speed. A final fictitious case consisted of forcing the Nikuradse full-pipe velocity profile on the turbine, a limiting case that would exist only if no flow straighteners were used and the hub obstruction was negligible. The results of these cases are shown below:

Profile	$\bar{v}$ ft/sec	Net Angle of Attack, Deg.	ΔP, psi	Meter Factor cycles/gal	ω_i rad/sec	ω_a rad/sec
Standard	37.115	0.0764	8.3	532.99	922.28	897.019
Average Velocity $\bar{v}$	37.115	0.0785	8.2	506.95	922.28	853.197
Straightener Velocity V_s	37.115	0.0827	8.3	509.72	922.28	857.86
Full Pipe	37.115	0.1048	8.3	402.93	922.28	678.14

The velocity profiles for these test cases are shown in Figure 34. The flatter profile of Nikuradse is based on the

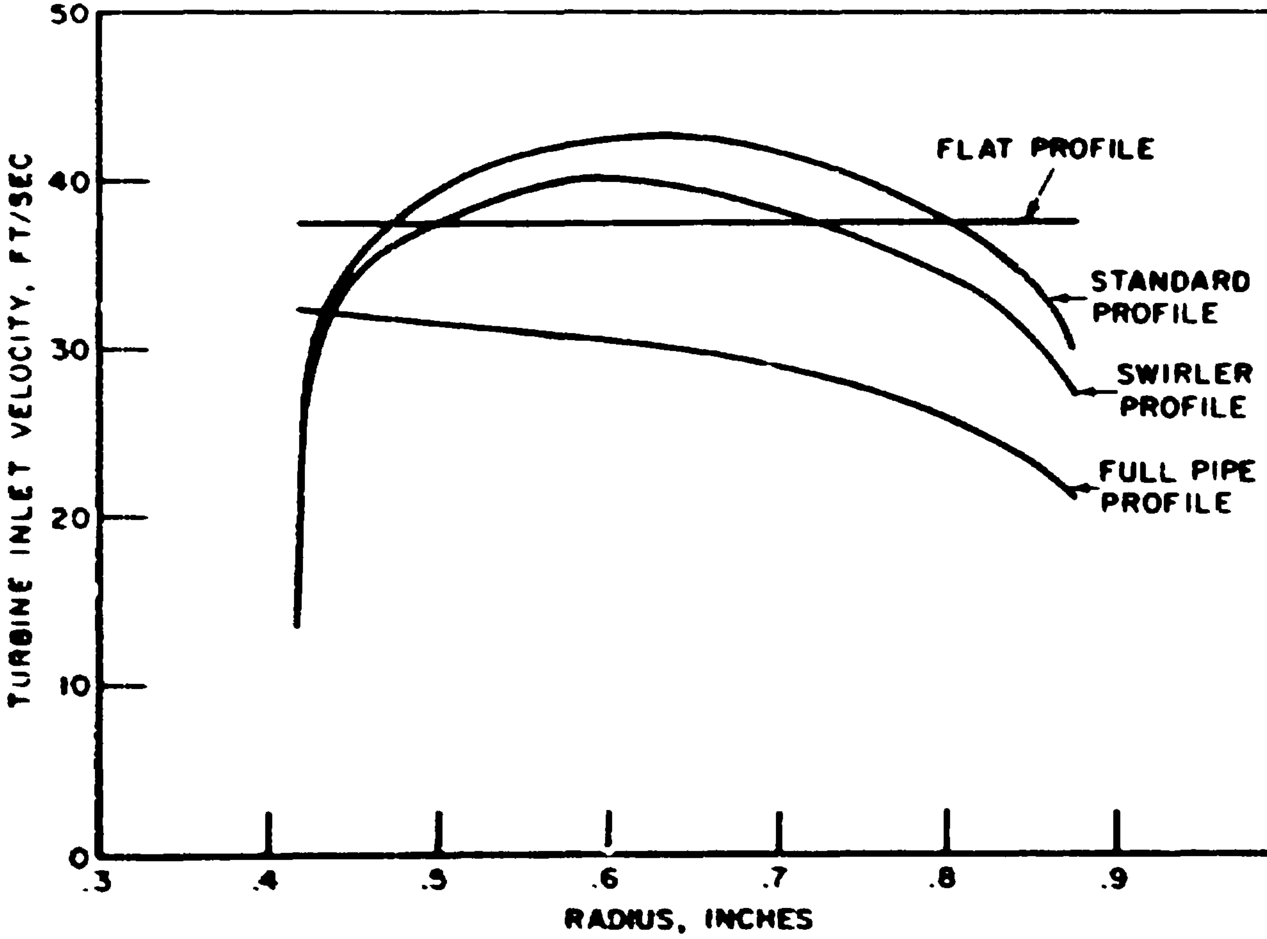

FIGURE 34

SELECTED T[illegible] INLET VELOCITY PROFILES full pipe diameter. The blade angle of attack variations shown in Figure 35 for the standard and swirler profiles are similar, except at the larger radius where the velocity profiles have slightly different curvatures. Since the full pipe profile does not go to zero at the rotor hub, the angles of attack in this region are large. It must be remembered that this is a fictitious case used only to demonstrate the importance of velocity profile effects. However, the previously assumed flat profile at the average velocity is equally fictitious, since it also does not satisfy the requirement of zero velocity at the rotor hub and meter wall and, therefore, misrepresents the blade angle of attack and driving torque variations when compared with the standard velocity profile as shown in Figures 35 and 37.

Since there are no changes in blade geometry when the velocity profiles are changed, the blade interference coefficient remains the same, as shown in Figure 36.

The driving torque curves (Figure 37) reflect the combined effects of the blade angle of attack variations and the shape of the velocity profile. The flat and full pipe curves show large departures from the standard and swirler torque curves. The torque crossover points from

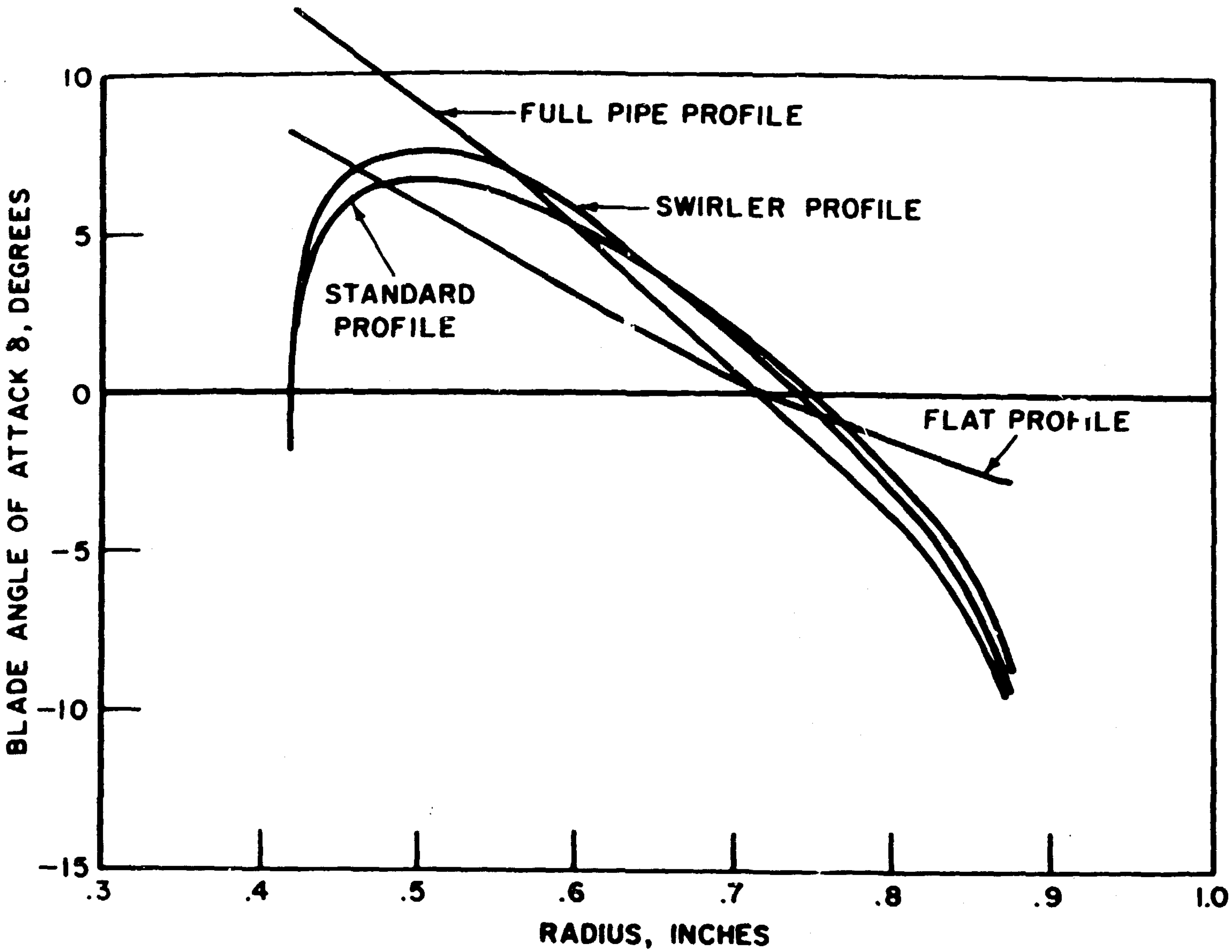

FIGURE 35

BLADE ANGLE OF ATTACK
FOR SELECTED VELOCITY PROFILES

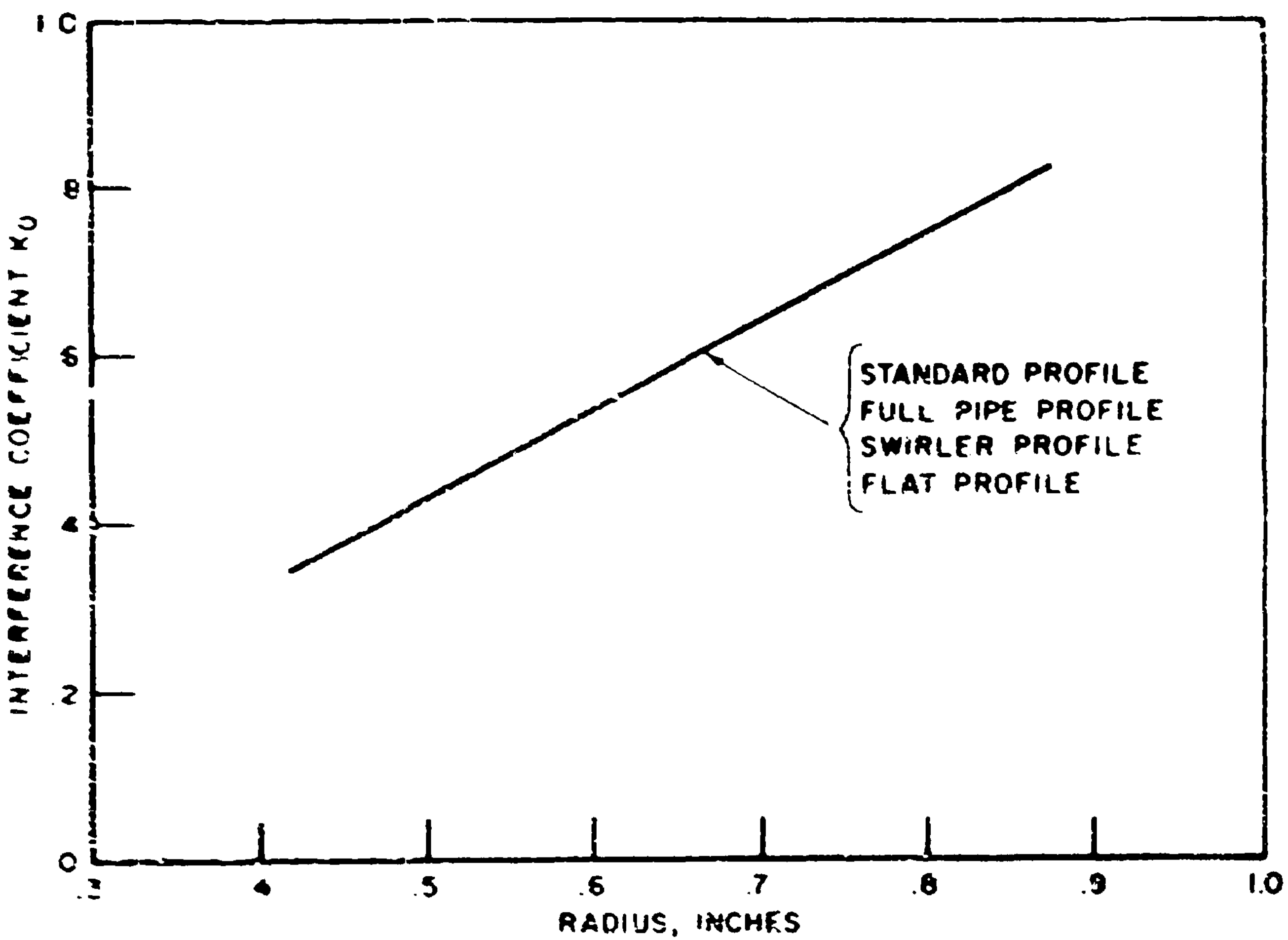

FIGURE 36

BLADE INTERFERENCE COEFFICIENT
FOR SELECTED VELOCITY PROFILES

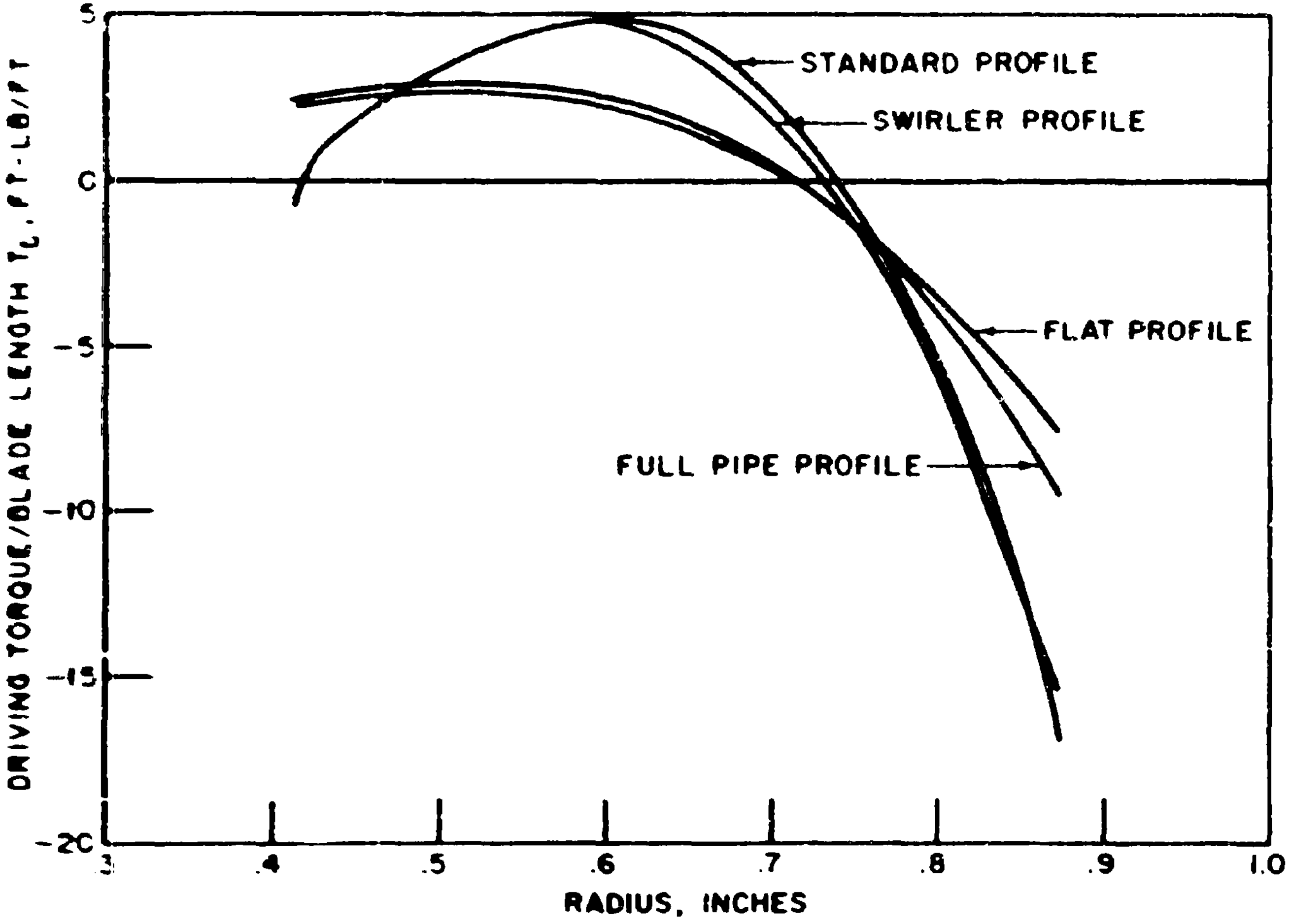

FIGURE 37

BLADE DRIVING TORQUE FOR SELECTED VELOCITY PROFILES positive to negative are not the same in this case, since the blade angle of attack crossing points are different also. An important point, however, is that the past assumption of a flat velocity profile gives a driving torque curve that departs significantly from that of the standard velocity profile. Even more important is the fact that only the standard velocity profile based on the annular area at the turbine inlet gives the correct rotor speed and meter factor. Although the driving torque curves for the swirler velocity are similar to those for the standard profile, only the latter gives the correct rotor speed, as shown in the previous tabulation.

VII. CONCLUSIONS

A complete analytical model of the turbine flowmeter has been formulated, including, for the first time, the capability for examining arbitrary (non-flat) inlet velocity profiles. The developed performance model includes an analysis of the dominant retarding torques and factors influencing the net driving torque. Although some secondary effects have not been included, the model is complete in terms of being able to quantitatively predict turbine meter performance. This has been demonstrated with the example of a meter where the fluid passes from a preswirler with flat blades to a helical bladed rotor. The predicted rotor speed was well within normal meter-to-meter tolerances. Several factors outlined in the original Work Statement have not been accounted for in the present study. These are asymmetric velocity profile (see Recommendations, Section VIII), breaking-in running, chemical reactivity of the fluid, and the presence of entrained particles or cavitation (other than their effect on velocity distribution, which <u>is</u> included in the model). These effects, as well as acceleration and vibration, were considered in the course of the study, and were placed in the category of operational factors rather than performance factors. There are also other factors which account for meter-to-meter variations, but which obviously cannot be included in an analytical model. One of these is the hand tailoring sometimes used by the meter manufacturers to bring meters within tolerance, including the occasional bending of several blade tips and filing of blade edges.

As part of the flowmeter performance model study, numerical test cases were prepared to explore the model's capability to predict the dependence of meter registration on flow rate, temperature, fluid, meter geometry (including manufacturing tolerances), bearing type, blade number, blade geometry, and velocity profile. Of all these parameters, the velocity profile was found to have the largest effect on the rotor speed and meter factor. Meter geometry effects due to temperature did result in distinct changes in meter registration; however, variations with normal manufacturing tolerances could not be detected. Effects of changing fluid properties (i.e., viscosity, temperature, etc.) were observed, as predicted, but were important principally through their effect on velocity profile.

The present analysis obtained the bearing retarding torque from data supplied by the bearing manufacturer, as being typical of the given bearing design. Based on these data, the bearing drag does not appear as a significant retarding torque. However, meter manufacturers generally do not have a running torque tolerance on bearings, and individual bearings they purchase are not tested nor are they purchased in matched pairs. Customarily, bearings with high drag are eliminated during calibration based on the overall meter acceptance tolerance. This would suggest large bearing-to-bearing variations in drag could be tolerated before the bearing drag appears as a dominant term during calibration to the degree that the meter is rejected. Production information on these variations were not available from the bearing manufacturer, since the bearings are only occasionally spot checked. However, they claim that these variations are "small." These factors cannot be included in a general analytical model since they are peculiar to a specific flowmeter and bearing design. They also underscore the importance of using actual bearing drag data, since these effects would not appear in a typical analytical bearing model. However, the capability to study these effects in terms of total meter performance exists with the present model once the meter and bearing design is selected and the specific data obtained. In any case, for the flow rates simulated (in both water and oil), the bearing drag was found not to be the dominant retarding torque, often comprising less than 20% of the blade tip drag and rotor hub drag. The use of journal or ball bearings also made no difference in the high-Reynolds-number range explored in this study.

The most important single conclusion to be drawn from the present program is that the primary factors influencing rotor speed in the high-Reynolds-number regime covered by this study are the velocity profile and the associated aerodynamic balance of the rotor. The magnitudes of all the retarding torques are small in this flow regime, and the slope of the driving torque vs. speed curve is so large that small changes in the retarding torques will not produce significant changes in actual rotor speed. Since the velocity profile has such a marked effect on flowmeter performance, its accurate description is essential to a useful and accurate turbine flowmeter performance model. For this reason, experimental verification of the computed profile and other velocity effects is essential to the establishment of the performance model as a useful tool for understanding meter performance, operating and installation effects, and key parameters in meter design.

VIII. RECOMMENDATIONS

A. Analytical

The analytical performance model developed during this program is far more comprehensive than prior studies, and appears to characterize actual meter operating performance quite accurately, as indicated by the sample numerical cases described earlier. However, this study is no different than any other analytical formulation, in that areas always exist where recommendations can be made for further refinements.

The most desirable feature to be added to the present program would be the capability to accommodate nonsymmetric velocity profiles, one of the topics suggested in the original Work Statement of the subject contract, but far too difficult and ill-defined to have been included in the scope of the present study. This effect could possibly be treated by some type of analytical transformation technique which would convert the nonsymmetric profile to an equivalent symmetric profile at the turbine inlet. The complicating factor in this transformation is the transition from an asymmetric velocity profile in a full pipe diameter to annular flow at the turbine inlet. At the present time, little is known about this transition in turbulent flow for a non-swirling symmetric velocity profile. This, then, should be the starting point for investigation in this area, proceeding to experimental correlations between asymmetric full pipe profiles and measured turbine inlet velocity profiles. Because of the sensitivity of meter registration to the velocity profile, these effects can only be modeled with the assistance of detailed experimental testing.

A significant potential area for follow-up programs, therefore, would be development of an analytical representation relating upstream or installation factors quantitatively to the turbine meter inlet velocity profile. This, of course, can only be done <u>after</u> completion of the test program described in the next paragraph, but such a representation would effectively tie together the present analysis, which essentially starts with a velocity profile, and the actual meter installation. The above mentioned asymmetric profile transformation would also be a key link in providing a complete picture of the turbine flowmeter performance, since it is virtually certain that at least some pipeline elements (e.g., elbows) will produce asymmetric velocity profiles and asymmetric swirl.

Another possible area for refinement is the blade tip clearance drag, since it appears from the numerical case examined that this constitutes a significant retarding torque. The present analysis is based on an analogy with bearing fluid drag. Although the geometries are different, this approach should be conservative, but a more refined analysis possibly should be considered.

B. Experimental Test Program

There are three major goals in the recommended experimental program:

1. Evaluate the applicability of the analytical model developed under the present program.
2. Estimate, if possible, the magnitudes of the few parameters which could not be quantified analytically.
3. Establish quantitatively the effects of installation and upstream piping configuration factors.

Of these three goals, it is clear from the above-stated conclusions of the present high-Reynolds-number study that No. 3 is by far the most critical, since the upstream effects determine the velocity profile, which, in turn, dominates flowmeter performance predictability. It is therefore recommended that, should the experimental program be limited because of funding restrictions, this area be emphasized to the exclusion, if necessary, of the other two above-stated goals.

Following Item 3 in importance is Item 1, whereas Item 2, although certainly of interest, probably does not entail any significant performance variations. Thus, the test program recommendations detailed in Appendix E are broken down into the three classes of tests indicated.

Note, also, that the instrumentation necessary for Goal No. 3 is not, in general, the type of instrumentation needed for turbine flowmeter evaluation, and that the requisite test facilities for this area of the experimental program do not include flowmeter provers or calibration installations of the conventional type. This special facility requirement, therefore, must be kept in mind when the test program is being implemented. Appendix E also includes, therefore, a brief description of the necessary facilities and instrumentation, as well as an outline of the evaluation program.

REFERENCES

(1) Lee, W. F. Z. and Evans, H. J.,"Density Effect and Reynolds Number Effect on Gas Turbine Flowmeters" ASME Paper 64-WA/FM-1, 1964

(2) Rubin, M.; Miller, R. W.; Fox, W. G. "Driving Torques in a Theoretical Model of a Turbine Meter" Transactions of ASME, J. of Basic Eng. June 1965 pg 413

(3) Jepson, P. "Transient Response of a Helical Flowmeter" Journal Mechanical Engineering Science Vol 6, No. 4, 1964, pg 337

(4) "Aerodynamics of Turbines and Compressors," W. R. Hawthorne, Editor, Princeton University Press, 1964

(5) Grey, J. "The Turbine Flowmeter for Cryogenic Liquids" ISA Preprint 111-59, Sept, 1959

(6) Grey, J. "Calibration of Turbine Flowmeters for Cryogenic Operation" American Rocket Society Journal, Feb. 1960

(7) Staniszlo, A. J. and Krause, L. N. "Simulation of Liquid Hydrogen Turbine-Type Flowmeter Calibrations Using High-Pressure Gas" NASA TND-3773, Dec. 1966

(8) Minkin, H. L.; Hobart, H. F.; and Warshawsky, I. "Performance of Turbine-Type Flowmeters in Liquid Hydrogen" NASA TND-3770, Dec. 1966

(9) Smith, R. L. "Analysis of the Sensitivity of an Uncompensated Helical Bladed Turbine Flowmeter" Rocketdyne Technical Report 65-13, Nov. 1965

(10) Zanker, K. J. "The Development of a Flow Straightener for Use with Orifice-Plate Flowmeters in Disturbed Flows" Flow Measurement in Closed Conduits, Vol. II, Symposium at National Engineering Labs, Sept. 27-30, 1960, East Kilbride, Scotland

(11) West, R. G. "The Problems of Non-Standard Installations and some General Conclusions" Instrument Practice August 1961 pg 973

(12) NASA-MSFC Astrionics Laboratory Report R-ASTR-IM-65-1, Mar 4, 1965 "Qualification Testing of the Potter Aeronautical Co. Turbine Flowmeter Model 1-5851, R-ASTR-IM Type III"

(13) Smith, O. L. "Accuracies and Calibration Techniques of Turbine-Type Flowmeters" ISA 6th National Flight Test Instrumentation Symposium Proc. May 2-5, 1960

(14) Haalman, A. "Pulsation Errors on Turbine Flowmeters" Control Engineering, Vol. 12, #5, May 1965, pg 89

(15) Head, V. P. "A Practical Pulsation Threshold for Flowmeters" Transactions of the ASME, Oct. 1956, pg 1471

(16) Shafer, M. R. and Ruegg, F. W. "Liquid-Flowmeter Calibration Techniques" Transactions of the ASME, Oct. 1958, pg. 1369

(17) Bucknell, R. L. "Calibration Systems and Turbine-Type Flow Transducers for Cryogenic Flow Measurements" Advances in Cryogenic Engineering, Vol. 8, pp 360-370

(18) Minkin, H. L.; Hobart, H. F.; and Warshawsky, I. "Liquid-Hydrogen Flowmeter Calibration Facility" Advances in Cryogenic Engineering Vol. 7, pg 189

(19) Deppe, G. R. and Dow, R. H. "The Design, Construction and Operation of A Cryogenic Flow Calibration Facility" Advances in Cryogenic Engineering, Vol. 8 pp. 371-377

(20) Alspach, W. J. and Flynn, T. M. "Considerations When Using Turbine-Type Flowmeters in Cryogenic Service" Advances in Cryogenic Engineering, Vol. 10, pg 246

(21) Jones, A. B. "Ball Motion and Sliding Friction in Ball Bearings" ASME Transactions Ser. D Vol 81 1959 pg 1-12

(22) Scibbe, H. W. and Anderson, W. J. "Evaluation of Ball Bearing Performance in Liquid Hydrogen at DN Values to 1.6 Million" ASLE Transactions Vol 5, No. 1 April 1962 pp 220-232

(23) Levy, S. "Turbulent Flow in an Annulus" General Electric Atomic Power Equipment Department Report GEAP 4976 Oct 1965

(24) Schlichting, H. "Boundary Layer Theory," 4th Edition McGraw Hill, 1960

(25) American Petroleum Institute Report API RP 550 2nd Edition Mar 1965 "Manual on Installation of Refinery Instruments and Control Systems"

(26) American Gas Association, Gas Measurement Committee Report #3 "Orifice Metering of Natural Gas" Dec 1966

(27) Schlichting, H. "Application of Boundary-Layer Theory in Turbomachinery". Trans. of ASME, J. of Basic Engineering, Dec. 1959 pg 543

(28) McAdams, W. H. "Heat Transmission" 3rd Edition McGraw Hill, 1954

(29) Miller, S. T.; Parker, R. J.; and Zoetsky, E. V. "Apparatus for Studying Ball Spinning Friction" NASA TND-2796 May 1965

(30) Cunningham, R. E. and Anderson, W. J. "Evaluation of 40-Millimeter-Bore Ball Bearings Operating in Liquid Oxygen at DN Values to 1.2 Million" NASA TND-2637, Jan 1965

(31) Mayer, J. T. and Litzler, T. C. "An Approximate Determination of the Effects of Geometry on Ball-Bearing Torque and Fatigue Life" NASA TND-2792, May 1965

(32) Taylor, G. I. "Fluid Friction Betweeen Rotating Cylinders" Proc. of Royal Soc. of London, England Series A Vol 157 1936 pp 546-560

(33) Moore, E. D.; Bullard, C. P.; and Misenhimer, J. T., "Evaluation of Fluid Flow Straightener" Potter Pacific Corp. Report PP-2 July 18, 1959

(34) McElroy, C. L. "Measuring Accuracies of the JUPITER Missile Flowmeters" Army Ballistic Missile Agency Report DT-TR-1-60, May 1960

(35) Schulz, G. H., and Deford, J. F. "Simulated Altitude Testing of the Apollo Service Module Propulsion System" Report AEDC TR-65-233

Additional References of General Interest:

(a) Grey, J. "Transient Response of the Turbine Flowmeter" Jet Propulsion, Feb. 1956

(b) Lee, W. F. Z. and Karlby, H. "A Study of Viscosity Effects and its Compensation on Turbine Type Flowmeters" Trans. of ASME Journal of Basic Engineering, Sept. 1960 pg 717

(c) Schlichting, H. "Problems and Results of Investigations on Cascade Flow" Journal of Aeronautical Sciences, Vol. 21, #3, Mar. 1954, pg 163

(d) Lieblein, S., and Roudebush, W. H. "Low-Speed Wake Characteristics of Two-Dimensional Cascade and Isolated Airfoil Sections" NACA Technical Note 3771, Oct. 1956

(e) Carter, A. D. S. and Cohen, E. M. "Preliminary Investigation into the Three-dimensional Flow through a Cascade of Aerofoils" Brit. Aeronaut Research Council Repts. and Mem. 2339, 1949

(f) Carter, A. D. S. and Hughes, H. P. "A Theoretical Investigation into the Effect of Profile Shape on the Performance of Aerofoils in Cascade" Brit. Aeronaut Research Council Repts. and Mem. 2384, 1950

(g) Howell, A. R. "The Present Basis of Axial Flow Compressor Design; Part I - Cascade Theory and Performance" Brit. Aeronaut Research Council Repts. and Mem. 2095, 1942

APPENDIX A

LIST OF SYMBOLS

APPENDIX A

LIST OF SYMBOLS

AR	=	blade aspect ratio
a	=	acceleration of meter
c	=	chord of blade
c_{JB}	=	journal bearing radial clearance
C_D	=	local drag coefficient
C_L	=	theoretical lift coefficient of a blade with interference effects
C_{Li}	=	theoretical life coefficient of a single isolated blade
f	=	friction factor
F	=	blade aerodynamic bearing thrust load
F_h	=	bearing thrust load due to rotor hub fluid drag
F_r	=	bearing thrust load due to pressure drop and acceleration
K_i	=	mixing length constant for inner portion of velocity profile
K_O	=	mixing length constant for outer portion of velocity profile
$K_\circ$	=	cascade interference coefficient
L_{JB}	=	journal bearing length
L_m	=	overall meter length
L	=	lead of helical blade
L_s	=	length of flow straightener

M_r	=	rotor mass
N	=	number of rotor blades
N_b	=	number of bearings
N_s	=	number of straightener blades
ΔP	=	pressure drop due to friction losses
Q, q	=	design volumetric flow rate
r	=	radius to differential blade element
r_m	=	radius to plane of zero shear
r_s	=	journal bearing shaft radius
R	=	transformed vortex location in potential flow solution
R_b	=	meter body radius
R_h	=	turbine rotor hub radius
R_T	=	turbine rotor tip radius
R_{b_o}	=	meter body radius at reference temperature of 70°F
R_{is}	=	inner radius of flow straightener
R_{os}	=	outer radius of flow straightener
R_{T_o}	=	rotor tip radius at reference temperature of 70°F
Re	=	Reynolds number
s	=	rotor blade spacing
s_i	=	zero shear plane radius/inner radius of annulus
s_o	=	zero shear plane radius/outer radius of annulus

$\frac{s}{c}$ = rotor or straightener space-to-chord ratio

t = rotor blade thickness

t_s = straightener blade thickness

T_d = rotor driving torque

T_h = rotor hub retarding torque due to fluid drag

T_o = reference temperature

T_{BT} = retarding torque due to blade tip clearance drag

T_{JB} = journal bearing retarding torque

T_p = retarding torque due to pickup drag

T_{BRL} = retarding torque due to ball bearing drag

U_1 = inlet velocity relative to blade

U_2 = exit velocity relative to blade

U_θ = circumferential component of relative velocity

U_∞ = free stream or mean flow velocity relative to blade

u^+ = non-dimensional fluid velocity

V_1 = absolute blade inlet velocity

V_z = axial component of absolute velocity

$\bar{V}$ = average fluid velocity

w = rotor width

y_i^+ = non-dimensional radius for inner portion of velocity profile

y_o^+ = non-dimensional radius for outer portion of velocity profile

α = angle of inclined portion of preswirler

α_{st} = transformed angle in potential flow solution

β_b = coefficient of thermal expansion for meter body

β_r = coefficient of thermal expansion for meter rotor

β_1 = angle made by the inlet velocity with the meter axis

β_2 = angle made by the exit velocity with the meter axis

β_{∞} = angle between the mean flow velocity direction and the meter axis

γ = blade stagger angle

Γ = fluid circulation

δ = blade effective angle of attack ($\delta = \gamma - \beta_{\infty}$)

ϵ = effective lift experimental factor

ζ = transformed plane in potential flow

η = non-dimensional distance defined for velocity profile

Θ = dimensionless momentum thickness

λ = blade airfoil efficiency

μ = absolute or dynamic fluid viscosity

ν = kinematic fluid viscosity

ζ_v = cascade loss coefficient

ρ = fluid density

τ_R = wall shear stress

ϕ = angle between the meter axis and the vertical

ω_i = ideal nonslip rotor speed

ω_a = actual rotor speed of a real meter

APPENDIX B

COMPUTER PROGRAM LISTING

APPENDIX B

Computer Program Listing

A technical description of the turbine flowmeter performance model was given in the main body of the report. The purpose of this appendix is to provide a listing of the computer program and to describe the preparation of the input data and the use of the program. The input variables used to describe the meter geometry are illustrated on the meter cross section shown at the end of this text.

The computer program listing given at the end of the appendix was written for the IBM 7094 computer using Fortran II. For those systems where Fortran IV is desirable, the deck can be easily transposed with the proper conversion routines for this purpose. Every effort has been made to make the program readily adaptable to most existing computer systems with a minimum of modifications.

The original listing contained a set of statements for obtaining punch card output to be used with a plotter to obtain the velocity profiles and variation of other parameters with radius. Because of the wide variation in punched card format for plotters, these statements have been removed or replaced by a

Hollerith statement which indicates the location at which data cards should be punched using the format of the particular user's system.

Most of the input concerns the meter geometry and the fluid properties plus some numerical codes to utilize the optional subroutines. The only input variable requiring any judgment is the initial guess for the rotor speed. The program will automatically converge on the proper speed, but it is necessary to estimate a rotor speed as a starting point for the iteration. The program will converge even with a poor guess, but this practice wastes machine time. The program computes one set of variables for the assumed speed and a second set at a speed a small increment removed from the ideal speed. Based on these differences it predicts a speed and computes a third set and finally, after comparing these residual torques with the initial guess, it computes a fourth set. If the fourth iteration is within the specified convergence torque tolerance, the next case is computed. If the convergence criterion has not been satisfied, the iteration is continued until this occurs. The output for the third and fourth iterations should be reviewed and the case with the smallest resultant torque selected.

The present program torque convergence criterion is 0.001 ft-lb, i.e., when the driving torques and retarding torques balance to within this tolerance, the program proceeds to the next case. In most cases the predicted rotor speed by the Newton-Raphson method results in residual torques less than this by as much as another order of magnitude. This convergence criterion was not made an input variable, since it directly affects the machine time per case. For those who would like to modify this tolerance for specialized cases, the card after Statement 95 can be altered.

The data cards for a typical test case are listed at the end of the program listing. The first 25 cards compose the bearing drag vs thrust load and speed table for ball bearings. Prior to making this entry, the user should prepare a table of bearing running torques vs shaft speed for several values of bearing thrust load. The first entry on Card 1 is the number of load points plus one. The second entry is the number of bearing table card sets to follow. These entries should be right hand justified with no decimal points. The first entry on Card 2 is a zero, and the remainder of the entries are the thrust load values in pounds. If more than three load values are used, the remaining values should be entered on Card 3. In this case Cards 2 and 3 are referred to as a set. The first entry in Card 4 is the shaft speed at which the bearing drag entries will be made. The remaining entries on the card are the bearing running torque values in ft-lbs for each of the respective loads specified in Cards 2 and 3. Cards 6 and 7 are similar to 4 and 5, containing the bearing running torque values for the respective loads at another shaft speed. Additional card sets are prepared covering the anticipated range of rotor speed. The total number of card sets in the bearing drag table should correspond with the entry on Card 1. The bearing drag table accounted for the first 25 cards of input, i.e., 12 sets of 2 cards each, plus the initial code card.

(For meters having journal bearings instead of ball bearings, the user should enter a 1 in columns 5 and 10 of Card 1; Card 2 should be blank, followed by an identification card and the meter geometry cards.)

Card 26 for the test case is an identification card for the run and must be included. Entries on Card 27 are the meter body radius R_B in; the rotor hub radius R_H in; the fluid absolute or dynamic viscosity $\mu \frac{lbm}{ft\text{-}sec}$ the volumetric flow rate q ft^3/sec, the fluid density ρ lbm/ft^3, and the blade airfoil efficiency λ .

(Test cases have shown that λ has little influence on the rotor speed and $\lambda = 1.0$ is commonly assumed.)

Entries on Card 28 are the rotor blade thickness t in.; the rotor width w in.; the rotor lead L in/rev; the number of rotor blades N (fixed point entry - right hand justified); the overall meter length L_m in. Only these entries are required for a helical bladed rotor. (For a flat bladed rotor with a fixed stagger angle γ in degrees, this entry is made in Columns 50 to 60 of Card 28, and the rotor lead is entered as 0.0.)

Entries on Card 29 include the rotor mass M_r lbs, the external acceleration (if any) a ft/sec^2; the estimate of the actual rotor speed ω_a rad/sec; the angle between the meter axis and the vertical, ϕ degrees (must be 90° for horizontal operation); and the radius to the rotor tip R_T in.

Entries on Card 30 define the flow straightener geometry. These include the straightener blade thickness t_s in.; the width of the inclined preswirler section W_s in.; the angle of the inclined portion of the preswirler α degrees; the number of straightener blades N_s (fixed point and right hand justified); the outer radius of the flow straightener R_{os}, in.; the inner radius of the flow straightener R_{is}, in.; and the length of the flow straightener L_s in. (For meters with a conventional straightener section without a pre-swirler set, $\alpha = 0$.)

Entries on Card 31 include the RF pickup drag in ft-lb (this quantity is a negative drag in this case, since it actually contributes a positive torque); the coefficient of thermal expansion for the meter body β_B in/in °F; the coefficient of thermal expansion for the rotor body β_R in/in °F; and the nominal reference temperature T_o at which the above geometry is entered. For meters having a magnetic pickup, the drag due to the magnetic unit was expressed in the form $a + b\,\omega_a^2$, where the coefficients a and b are the last entries on Card 31 and the RF pickup drag is set equal to zero.

Entries on Card 32 are non-zero only if a journal bearing is being simulated. In this case the first entry is 1.0 as an indicator code. The remaining entries are the journal bearing shaft radius r_s in., the journal bearing clearance c_{JB} in., and the journal bearing length L_{JB} in.

Card 33 is used to describe the polynomial coefficients when a velocity profile based on test data is substituted for the profile normally calculated by the program. The velocity data (ft/sec) should be fit with the polynomial $C_1 + C_2r + C_3r^2 + C_4r^3 + C_5r^4 + C_6r^5 + C_7r^6 + C_8r^7$. The first entry on Card 33 is a code punch in Column 1 which should be zero if velocity profile will be calculated by the subroutine in the program, and unity if the profile will be described by the 8 coefficients which are specified on the remainder of the card. (Note that the first field is only 9 columns wide, while the remainder are 10.)

Entries on Card 34 are the number of bearings per meter (right hand justified); the number of computation intervals across the flow annulus (right hand justified -- 200 has been found to be sufficiently accurate); and the increment away from the rotor hub at which the integration begins (usually 0.00001). The integration cannot begin exactly at the hub because the velocity vanishes and some expressions contain velocity terms in the denominator.

A typical set of data cards is listed at the end of the main program listing. To avoid disclosing meter geometry that may be proprietary, the data entered are fictitious but typical of the class of meter used in the study.

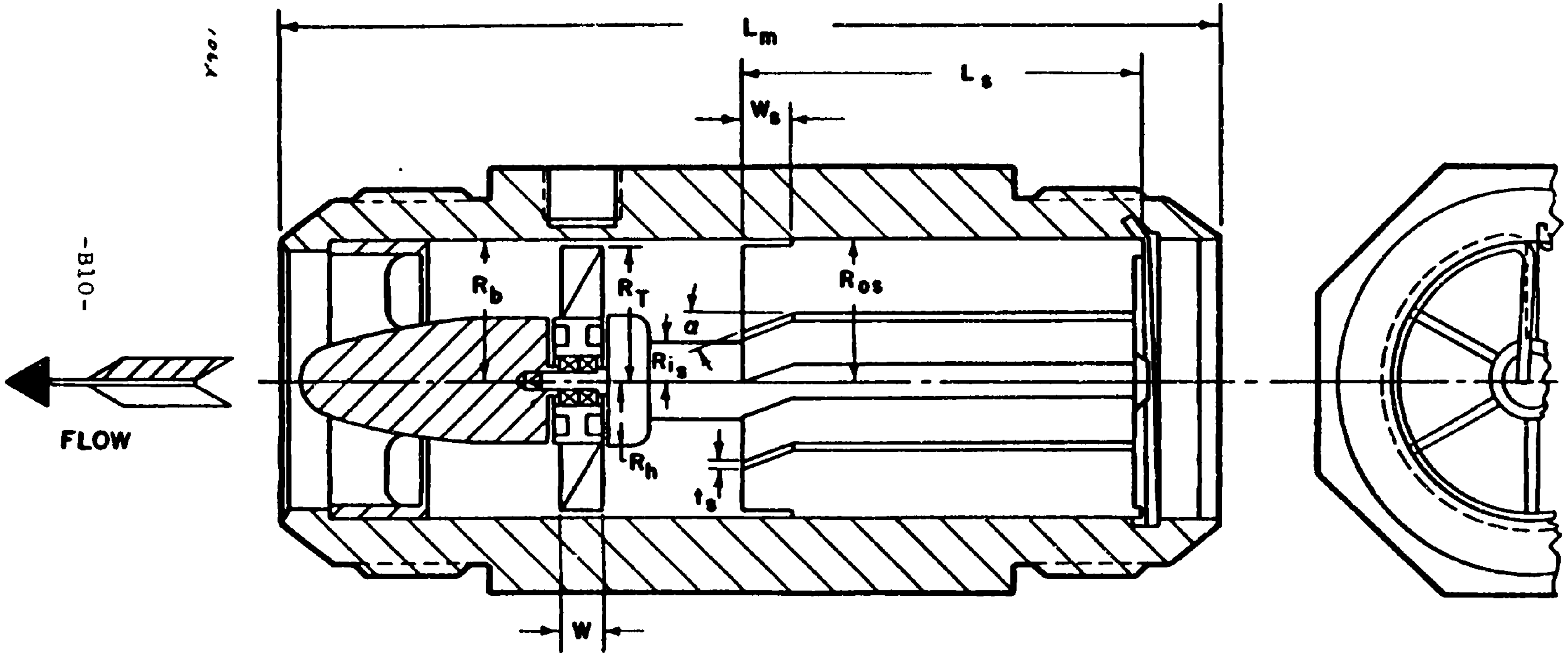

FISHER & PORTER MODEL 10C1510

TURBINE METER GEOMETRY

106A

CARD NO	STATEMENT NUMBER (1–5)	7–10	11–20	21–30	31–40	41–50	51–60	61–70	71–72	
1	① (xx)	② (yy)								
2	0.		THRUST LOAD 1 (lbs)		LOAD 2 (lbs)		LOAD 3 (lbs)			SET 1
3	LOAD 4 (lbs)			LOAD 5 (lbs)						
4	ω_1 (rad/sec)		BEARING DRAG FOR LOAD 1 (ft-lb)		BEARING DRAG FOR LOAD 2 (ft-lb)		BEARING DRAG FOR LOAD 3 (ft-lb)			SET 2
5	BEARING DRAG FOR LOAD 4 (ft-lb)			BEARING DRAG FOR LOAD 5 (ft-lb)						
6	ω_2 (rad/sec)		BEARING DRAGS FOR SPEED ω_2 AT LOADS SPECIFIED ON CARD 2 FOLLOWING SAME FORMAT AS CARD 4							
7										
			REPEAT CARD SETS FOR REQUIRED ROTOR SPEED RANGE							
25										
26			REQUIRED CASE TITLE CARD							
27	R_b	(in)	R_h (in)	μ (lbm/ft-sec)	Q (ft^3/sec)	ρ (lbm/ft^3)	λ			
28	t	(in)	w (in)	L (in/rev)	$N_{(x.x)}$	L_m (in)	γ (DEGREES)			
29	M_r	(lb)	A (ft/sec^2)	ω_0 (rad/sec)	ϕ (DEGREES)	R_1 (in)				
30	t_s	(in)	w_s (in)	α (DEGREES)	$N_{s(x.x)}$	R_{os} (in)	R_{is} (in)	L_s (in)		
31	RF	PICKUP DRAG (ft-lb)		β_b (in/in°F)	β_r (in/in°F)	T_0 (DEGREES)	a .x.x.x.x.x.E+x.x	b .x.x.x.x.x.E+x.x		
32	JB		r_s (in)	C_{jb} (in)	L_{jb} (in)					
33	1 0 C_1		C_2	C_3	C_4	C_5	C_6	C_7	C_8	
34	N_b (x)	N_{step}	INITIAL INTERUAL 0.0001							

① NUMBER OF BEARING THRUST LOAD POINTS

② NUMBER OF CARD SETS

```
C
C      SENSE SWITCH 1 MAY BE TURNED ON FOR AN EXPANDED OUTPUT.
C
C      SOME SYMBOLS USED IN THIS PROGRAM.
C          N = NUMBER OF BLADES
C          RH    = RADIUS TO ROTOR HUB
C          RT    = RADIUS TO ROTOR TIP
C          RB    = RADIUS TO INSIDE BORE OF METER BODY
C          W     = ROTOR WIDTH
C          C     = ROTOR BLADE CHORD LENGTH
C          S     = ROTOR BLADE SPACING
C          Q     = METER VOLUMETRIC FLOW RATE
C          RHO   = FLUID DENSITY
C          ZNU   = FLUID KINEMATIC VISCOSITY
C          BETA = COEFF. OF THERMAL EXPANSION
C          ZMR   = ROTOR MASS
C          A     = ACCELERATION OF METER
C          G     = ACCELERATION DUE TO GRAVITY
C          VBAR = FLUID AVERAGE VELOCITY
C          V     = FLUID LOCAL VELOCITY
C          WA    = ACTUAL ROTOR SPEED
C          CL    = LIFT COEFF.
C          ZKO   = RATIO OF ACTUAL TO IDEAL AIRFOIL LIFT
C          ALFST= ANGLE DEFINING BRANCH POINTS OF POTENTIAL SOL.
C          GAMMA= BLADE STAGGER ANGLE
C          CD    = DRAG COEFF.
C          PHI   = ANGLE BETWEEN GRAVITY VECTOR AND METER AXIS
C          ZL    = HELIX LEAD (IN/REV)
C          NB    = NO. OF BEARINGS.
C          DT    = TEMPERATURE DIFFERENTIAL.
C         ZLM     = METER LENGTH.
C       PICKUP   = MAGNETIC COOPER FORCES.
C
C      ALL TORQUES IN FT. LBS.
C      ALL FORCES IN LBS.
C
C      INPUT  RB, RH, ZNU, Q, RHO.
C
C            ****PROGRAM STEPS****
C
C               1)FIND VBAR=F(Q)
C               2)FIND REYNOLDS NO.
C               3)PREDICT FRICTION FACTOR
C               4)CHOOSE RM=MEAN RADIUS AND GET SHEAR (6A)
C               5)COMPUTE KO/KI
C               6)COMPUTE SHEAR FROM (6B)
C               7)FIND RATIO OF SHEARS FROM (2)
C               8)FIND SO, SI, AND ETAO, ETAI
C               9)COMPUTE A AND B
C              10)ITERATE UNTIL EQ(4) IS SATISFIED
C              11)USE (1) TO OBTAIN V= F(R) FOR TORQUE EQ.
C
C      WA IS THE ROTOR VEL. TO BE FOUND WHEN ALL TORQUES BALANCE.
```

```
C
C
      DIMENSION PLOT(5,400)
      DIMENSION BEAR(6,15),COEFT(8)
      COMMON BEAR,TTORQ,ZLM,NBTABI,NBTABJ
      COMMON IPOLY,COEFT
      COMMON VBAR,REYN,FRICT,ZKO,RB,RH,ZNU,Q,RHO,EO4,RATIO3
      COMMON A6,B6,STAURH,STAURB,RM,RMS,STAUSI,STAUSO,TANB1,TANB2
      COMMON T,W,ZL,ZN,GAMMA,AST,COSG,SING
      COMMON G,RMASS,A,WA,PHI,RT
      COMMON QQ,RHOH,DELTAP,CD,VH,DRIVF,FDRAG,BRLOAD,TTB,TANG
      COMMON RGUESS,COSGH,SH,GH,C,S,SGUESS
      COMMON TS,WS,AS,NS,ROS,RIS,NSTEP
      COMMON PICKUP,ZJBR,ZJBC,ZJBL,JB
      COMMON ETA,EPS,DT,NB
      COMMON EPSH,T1G,T2G,T1,T2,T3,GMB,ZLS
   96 CONTINUE
      WRITE OUTPUT TAPE 6,92
C        ALL IN INCHES.
      READ INPUT TAPE 5,4,NBTABI,NBTABJ
      DO 5 J=1,NBTABJ
      READ INPUT TAPE 5,3,(BEAR(I,J),I=1,NBTABI)
    3 FORMAT(F10.3,3F20.9/4F20.9)
    5 CONTINUE
   90 CONTINUE
      IJK=5
C     READ A LABEL CARD.
      READ INPUT TAPE 5,158
  158 FORMAT(80H
 1581                                                                          )
      READ INPUT TAPE 5,1,RB,RH,ZMU,Q,RHO,ETA
      IF(RB)96,96,97
   97 CONTINUE
      ZNU=ZMU/RHO
    1 FORMAT (7F10.4)
      READ INPUT TAPE 5,2,T,W,ZL,N,ZLM,GAMMA
    2 FORMAT(3F10.4,I5,5X,3F10.4)
      READ INPUT TAPE 5,1,RMASS,A,WA,PHI,RT
      READ INPUT TAPE 5,2,TS,WS,AS,NS,ROS,RIS,ZLS
      READ INPUT TAPE 5,6,PICKUP,BETAB,BETAR,TEMP,PICKA,PICKB
    6 FORMAT(F20.9,3F10.4,2E10.3)
      PICK=PICKUP
      READ INPUT TAPE 5,1,ZJB,ZJBR,ZJBC,ZJBL
C     IF THE ZJB ( OR JB ) IS NON ZERO, THEN USE JOURNAL BEARING.
      JB=ZJB
C     NOTE THAT COEFFICIENTS COME FROM A POLYNOMIAL FIT OF RADIUS IN
C        INCHES. THE COEFFICIENTS ARE CONVERTED TO FT. INTERNALLY.
      READ INPUT TAPE 5,7,IPOLY,COEFT
    7 FORMAT(I1,F9.0,7F10.0)
      READ INPUT TAPE 5,4,NB,NSTEP,EPSH
    4 FORMAT(2I5,F10.7)
      WRITE OUTPUT TAPE 6,158
      WRITE OUTPUT TAPE 6,4,NB,NSTEP,EPSH
```

```
      G=32.2
      WRITE OUTPUT TAPE 6,98,RB,RH,ZNU,Q,RHO,ETA
   98 FORMAT(20HORB,RH,ZNU,Q,RHO,ETA /6E15.7)
      WRITE OUTPUT TAPE 6,81,T,W,ZL,N,ZLM
   81 FORMAT(40HOT, W, L, N, LENGTH OF METER FOR TURBINE /
  811     3E15.7,I5,E15.7)
      WRITE OUTPUT TAPE 6,82,RMASS,A,WA,PHI,RT
   82 FORMAT(36HOMASS, A, OMEGA, PHI, RT FOR TURBINE  /5E15.7)
      WRITE OUTPUT TAPE 6,83,TS,WS,AS,NS,ROS,RIS
   83 FORMAT(31HOT, W, A, N, RO, RI FOR SWIRLER  /3E15.7,I5,2E15.7)
      WRITE OUTPUT TAPE 6,84,IPOLY,COEFT
   84 FORMAT(33HOVELOCITY POLYNOMIAL COEFFICIENTS /I2,8E10.3)
C     CONVERT POLYNOMIAL COEFFICIENTS TO FT.
      COEFT(1)=COEFT(1)/12.
      DENOM=12.
      DO 8 II=2,8
      COEFT(II)=COEFT(II)/DENOM
      DENOM=DENOM*12.
    8 CONTINUE
C     CONVERT TO FT.
      RB=RB/12.
      RH=RH/12.
      T=T/12.
      W=W/12.
      ZL=ZL/12.
      RT=RT/12.
      RIS=RIS/12.
      ROS=ROS/12.
      WS=WS/12.
      TS=TS/12.
      ZLS=ZLS/12.
      ZLM=ZLM/12.
      ZJBR=ZJBR/12.
      ZJBC=ZJBC/12.
      ZJBL=ZJBL/12.
C     CORRECT FOR TEMP. EXPANSION.
      CORRR=1.+BETAR*(TEMP-70.)
      CORRB=1.+BETAB*(TEMP-70.)
      RB=RB*CORRB
      RH=RH*CORRR
      T=T*CORRR
      W=W*CORRR
      RT=RT*CORRR
      RIS=RIS*CORRR
      ROS=ROS*CORRB
      WS=WS*CORRR
      TS=TS*CORRR
      ZLS=ZLS*CORRR
      ZLM=ZLM*CORRB
C     CONVERT RMASS TO SLUGS.
      RMASS=RMASS/G
C     CONVERT PHI TO RADIANS.
      PHI=PHI*3.14159/180.
```

```
      AS=AS*3.14159/180.
      GAMMA=GAMMA*3.14159/180.
C     CHECK THAT BODY RADIUS GREATER THAN TURBINE RADIUS.
      IF(RT-RB)564,565,565
  565 CONTINUE
      WRITE OUTPUT TAPE 6,566
  566 FORMAT(///59H THE TURBINE RADIUS IS GREATER OR EQUAL TO THE BODY R
 5661ADIUS. //45H CHECK INPUT DATA. WILL PROCEED TO NEXT CASE.)
      GO TO 90
  564 CONTINUE
C     USE RHO AT HUB AS FLUID RHO.
      RHOH=RHO
      ZN=N
      ZKD=.4
   93 CONTINUE
C     INTEGRATE FOR GIVEN WA.
      PICKUP=PICK
C     IF 'PICKUP' IS ZERO, THEN FIT FORM PICKUP=A*W*W+B
      IF(PICKUP)72,71,72
   71 CONTINUE
      PICKUP=PICKA*WA*WA+PICKB
   72 CONTINUE
      CALL ITERWA(PLOT)
C     CHECK REYNOLD'S NUMBER .GT. 10,000.
      IF(IPOLY)90,14,14
   14 CONTINUE
      WA1=WA
      TORQ1=TTORQ
      WA=WA*1.0001
      PICKUP=PICK
      IF(PICKUP)73,74,73
   74 CONTINUE
      PICKUP=PICKA*WA*WA+PICKB
   73 CONTINUE
      CALL ITERWA(PLOT)
C     CHECK REYNOLD'S NUMBER .GT. 10,000.
      IF(IPOLY)90,15,15
   15 CONTINUE
      WA2=WA
      TORQ2=TTORQ
C     CORRECT WA BY NEWTON-RAPHSON METHOD.
      DTORQ=(TORQ1-TORQ2)/(WA1-WA2)
      WA=WA1-TORQ1/DTORQ
      WRITE OUTPUT TAPE 6,91,WA,WA1,TORQ1,TORQ2
   91 FORMAT(19H ITERATION ON OMEGA ,2F10.3,2E15.7)
      WRITE OUTPUT TAPE 6,92
   92 FORMAT(1H1)
      IJK=IJK-1
      IF(IJK)90,90,95
   95 CONTINUE
C     CONVERGENCE CHECK IS HERE.
      IF(ABSF(TORQ1)-.001)94,94,93
   94 CONTINUE
```

```
C
C     THIS IS WHERE CARDS ( OR PLOTS ) WOULD BE PRODUCED. ARRAY 'PLOT'
C        CONTAINS 5 PARAMETERS - RADIUS, VELOCITY, ANGLE OF ATTACK,
C        INTERFERENCE COEFFICIENT, AND NET BLADE DRIVING TORQUE.
C
      GO TO 90
      END
```

```
      SUBROUTINE ITERWA(PLOT)
      DIMENSION PLOT(5,400)
      DIMENSION BEAR(6,15),COEFT(8)
      COMMON BEAR,TTORQ,ZLM,NBTABI,NBTABJ
      COMMON IPOLY,COEFT
      COMMON VBAR,REYN,FRICT,ZKO,RB,RH,ZNU,Q,RHO,EQ4,RATIO3
      COMMON A6,B6,STAURH,STAURB,RM,RMS,STAUSI,STAUSO,TANB1,TANB2
      COMMON T,W,ZL,ZN,GAMMA,AST,COSG,SING
      COMMON G,RMASS,A,WA,PHI,RT
      COMMON QQ,RHOH,DELTAP,CD,VH,DRIVE,FDRAG,BRLOAD,TT8,TANG
      COMMON RGUESS,COSGH,SH,GH,C,S,SGUESS
      COMMON TS,WS,AS,NS,ROS,RIS,NSTEP
      COMMON PICKUP,ZJBR,ZJBC,ZJBL,JB
      COMMON ETA,EPS,DT,NB
      COMMON EPSH,T1G,T2G,T1,T2,T3,GMB,ZLS
C     DO PART OF PRE-SWIRLER FIRST.
      ZNS=NS
      RBTURB=RB
      RHTURB=RH
      RB=ROS
      RH=RIS
      VBAR=Q/((3.1415927*(RB*RB-RH*RH)) -(ROS-RIS)*ZNS*TS)
      REYN=2.*VBAR*RB*(1.-RH/RB)/ZNU
      FRICT=.046/(REYN**.2)
C     CHECK REYNOLD'S NUMBER .GT. 10,000.
      IF(RENCHK(REYN))16,16,17
   16 RETURN
   17 CONTINUE
      IF(SENSE SWITCH 1)600,601
  600 CONTINUE
      WRITE OUTPUT TAPE 6,101,VBAR,REYN,FRICT,RB,RH
  101 FORMAT(80HOPRE-SWIRLER VBAR, REYN, FRICT, R-BODY, R-HUB  (FT.)
 1011                                              /5E15.7)
  601 CONTINUE
C     COMPUTE RM FOR PRE-SWIRLER.
      CALL SUBRM(RMS)
      IF(SENSE SWITCH 1)602,603
  602 CONTINUE
      WRITE OUTPUT TAPE 6,103,RMS
  103 FORMAT(20HO MEAN R (SWIRLER)   /E15.7)
  603 CONTINUE
C     STORE SHEARS FOR PRE-SWIRLER.
C     COMPUTE SQRT (TAURI/RHO) AND (TAURO/RHO)
      STAUSI=B6*ZNU/(RMS-RIS)
      STAUSO=A6*ZNU/(ROS-RMS)
C     CONVERT BACK TO TURBINE.
      RB=RBTURB
      RH=RHTURB
      VBAR=Q/ (3.1415927*(RB*RB-RH*RH))
      REYN=2.*VBAR*RB*(1.-RH/RB)/ZNU
      FRICT=.046/(REYN**.2)
C     CHECK REYNOLD'S NUMBER .GT. 10,000.
      IF(RENCHK(REYN))11,11,12
```

```
   11 CONTINUE
      RETURN
   12 CONTINUE
      IF(SENSE SWITCH 1)604,605
  604 CONTINUE
      WRITE OUTPUT TAPE 6,104,VBAR,REYN,FRICT,RB,RH
  104 FORMAT(80HO TURBINE    VBAR, REYN, FRICT, R-BODY, R-HUB  (FT.)
 1041                                /5E15.7)
  605 CONTINUE
      WRITE OUTPUT TAPE 6,97,VBAR,REYN,FRICT
   97 FORMAT(16HOVBAR,REYN,FRICT/3E15.7)
C     COMPUTE RM
      CALL SUBRM(RM)
      IF(SENSE SWITCH 1)606,607
  606 CONTINUE
      WRITE OUTPUT TAPE 6,106,RM
  106 FORMAT(20HO MEAN R TURBINE     /E15.7)
  607 CONTINUE
      RMT=RM
C     COMPUTE SQRT (TAURH/RHO) AND (TAURB/RHO)
      STAURH=B6*ZNU/(RM-RH)
      STAURB=A6*ZNU/(RB-RM)
C     INTEGRATE THE EQUATIONS IN A SUBROUTINE.
      CALL INTEG(PLOT)
      RETURN
      END
```

```
      SUBROUTINE INTEG(PLOT)
C     FORM INTEGRAL OF DRIVING TORQUE, FLUID DRAG AND BEARING DRAG.
      DIMENSION PLOT(5,400)
      DIMENSION BEAR(6,15),COEFT(8)
      DIMENSION Y(25)
      COMMON BEAR,TTORQ,ZLM,NBTABI,NBTABJ
      COMMON IPOLY,COEFT
      COMMON VBAR,REYN,FRICT,ZKO,RB,RH,ZNU,Q,RHO,EQ4,RATIO3
      COMMON A6,B6,STAURH,STAURB,RM,RMS,STAUSI,STAUSO,TANB1,TANB2
      COMMON T,W,ZL,ZN,GAMMA,AST,COSG,SING
      COMMON G,RMASS,A,WA,PHI,RT
      COMMON QQ,RHOH,DELTAP,CD,VH,DRIVE,FDRAG,BRLOAD,TT8,TANG
      COMMON RGUESS,COSGH,SH,GH,C,S,SGUESS
      COMMON TS,WS,AS,NS,ROS,RIS,NSTEP
      COMMON PICKUP,ZJBR,ZJBC,ZJBL,JB
      COMMON ETA,EPS,DT,NB
      COMMON EPSH,T1G,T2G,T1,T2,T3,GMB,ZLS
      LINE=0
C     COMPUTE IDEAL OMEGA FOR 4 POSSIBLE CASES.
      IF(AS)531,532,531
  531 CONTINUE
      IF(ZL)535,536,535
  535 CONTINUE
C     SWIRLER PRESENT. ALPHA S NOT ZERO AND L NOT ZERO.
      WIDEAL=VBAR*(6.2831854/ZL+1.5*SINF(AS)*(RT*RT-RH*RH)/
     1   (COSF(AS)*(RT*RT*RT-RH*RH*RH)))
      GO TO 533
  536 CONTINUE
      WIDEAL=1.5*VBAR*(SINF(GAMMA)/COSF(GAMMA)+SINF(AS)/COSF(AS))*
     1  (RT*RT-RH*RH)/(RT*RT*RT-RH*RH*RH)
      GO TO 533
  532 CONTINUE
      IF(ZL)537,538,537
  537 CONTINUE
C     STRAIGHT SWIRLER, L NOT ZERO.
      WIDEAL=VBAR*6.2831854/ZL
      GO TO 533
  538 CONTINUE
C     FLAT BLADE TURBINE, L=0 AS =0 NEED GAMMA FROM DATA.
      WIDEAL=1.5*SINF(GAMMA)*(RT*RT-RH*RH)*VBAR/
     1   (COSF(GAMMA)*(RT*RT*RT-RH*RH*RH))
  533 CONTINUE
      INDEX=1
C     GET ZKI FROM EQ. 4(OR3) OF RM CALC.
      ZNS=NS
      VBARS=Q/((3.1415927*(ROS*ROS-RIS*RIS))-(ROS-RIS)*ZNS*TS)
      ZKI=ZKO/EQ4
C     START INTEGRATION AT SOME SMALL DISTANCE AWAY FROM HUB.
C     INTEGRATE TO BLADE TIP.
      RHH=RH+EPSH
      ZNSTEP=NSTEP
      DR=(RT-RHH)/ZNSTEP
      R=RHH
```

```
C
C     THE FOLLOWING ARE INDEPENDENT OF R INTEGRAL.
C
      IF(SENSE SWITCH 1)608,609
  608 CONTINUE
      WRITE OUTPUT TAPE 6,101,R,RH,RB
  101 FORMAT(40HOINTEG NEAR HUB  R, R-HUB, R-BODY          /4E15.7)
  609 CONTINUE
C     INITIALIZE THE GUESS VALUE FOR SWIRLER.
      SGUESS=1.5
      RGUESS=1.5
      RBAR=.5*(RT+RH)
      RR=ROS-(ROS-RBAR)*(ROS-RIS)/(ROS-RH)
C     EVALUATE AT HUB.
      CALL QKS(RR,QQHS)
      CALL QK(RBAR,ZKH,QQH)
      Q1H=1./(1.+QQH)
      QQ1H=QQH*Q1H
      IF(ZL)651,652,651
  652 CONTINUE
      GH=SINF(GAMMA)/COSF(GAMMA)
      GO TO 653
  651 CONTINUE
      GH    =6.2831854*RH  /ZL
  653 CONTINUE
      GH=ATANF(GH)
      COSGH=COSF(GH)
      SINGH=SINF(GH)
      TANGH=SINGH/COSGH
      IF(SENSE SWITCH 1)610,611
  610 CONTINUE
      WRITE OUTPUT TAPE 6,102,  QQH,Q1H,QQ1H,GH,COSGH,SINGH,TANGH
  102 FORMAT(80HOQ(HUB),  1/(1+QH),  QH/(1+QH),  GAMMA(H), COS(GH), SIN(
 1021GH),  TAN(GH)                              /7E15.7)
  611 CONTINUE
C     NEW TAN BETA1 FOR SCALING OF FLOW PROFILES.
C     EVALUATE FLUID DRAG, ETC. AT RBAR.
      IF(RBAR-RM)121,121,122
  121 CONTINUE
      V=VEL(RBAR,RH,ZKI,STAURH)
      GO TO 193
  122 CONTINUE
      V=VEL(RBAR,RB,ZKO,STAURB)
  193 CONTINUE
      IF(RR-RMS)124,124,125
  124 CONTINUE
      V1=VEL(RR,RIS,ZKI,STAUSI)
      GO TO 126
  125 CONTINUE
      V1=VEL(RR,ROS,ZKO,STAUSO)
  126 CONTINUE
      TANB1H=RBAR*WA/V
     1           -(2.*QQHS*SINF(AS)/(1.+QQHS))*V1*((ROS*ROS-RIS*RIS)/
```

```
     2 ((RB* RB -RH*RH)*COSF(AS)))/V
       IF(SENSE SWITCH 1)612,613
  612 CONTINUE
       WRITE OUTPUT TAPE 6,103,V1,V,TANB1H
  103 FORMAT(50HOV(SWIRLER), V(TURBINE), TAN(BETA1(H))                    /
  1031  3E15.7)
  613 CONTINUE
C      COMPUTE DRAG COEFF.
       RBAR=.5*(RH+RT)
       SH=(6.2831854*RBAR           -ZN*T)/ZN
       CBAR=W/COSGH
       CD=.074/(VBAR*CBAR/ZNU)**.2
       IF(SENSE SWITCH 1)614,615
  614 CONTINUE
       WRITE OUTPUT TAPE 6,104,CD,SH,RBAR,CBAR
  104 FORMAT(50HODRAG COEFF. AT RBAR, S(RBAR), RBAR, C(RBAR)              /
  1041  4E15.7)
  615 CONTINUE
       SH=(6.2831854*RH             -ZN*T)/ZN
       CH=W/COSGH
       IF(SENSE SWITCH 1)616,617
  616 CONTINUE
       WRITE OUTPUT TAPE 6,105,SH,CH
  105 FORMAT(20HOS(RH), C(RH)        /2E15.7)
  617 CONTINUE
C      ROTOR HUB FLUID DRAG TERMS.
       IF(ZL)654,655,654
  655 CONTINUE
       TANGH=SINF(GAMMA)/COSF(GAMMA)
       GO TO 656
  654 CONTINUE
       TANGH=6.2831854*RBAR/ZL
  656 CONTINUE
       VBAR2=VBAR*VBAR
       T4=.5*RHOH*VBAR2*CD*CH*ZN*SH*COSGH
       TT5=QQ1H*TANGH+Q1H*TANB1H
       T5=TT5*SQRTF(1.+TT5*TT5)*RH
       FDRAG=T4*T5/G
C      MORE BEARING THRUST TERMS.
       T9=.5*RHOH*VBAR2*ZN*CD*CH*SH*COSGH/G
       TT8=1.+(QQ1H*TANGH+Q1H*TANB1H)**2
       T10=SQRTF(TT8)
       IF(SENSE SWITCH 1)618,619
  618 CONTINUE
       WRITE OUTPUT TAPE 6,108
  108 FORMAT(50HO***TERMS IN BEARING THRUST NOT DEP. ON RADIUS.           )
       WRITE OUTPUT TAPE 6,106,T9
  106 FORMAT(50HO.5*RHOH*VB*VB* N*CD*CH*SH*COS(GH)/G                      /
  1061  E15.7)
       WRITE OUTPUT TAPE 6,107,T10
  107 FORMAT(60HOSQRT(1+((QH/(1+QH)*TAN(GH)+1/(1+QH)*TAN(BETA1(H))**2)
  1071                /E15.7)
       T910=T9*T10
```

```
      WRITE OUTPUT TAPE 6,19,T910
   19 FORMAT(11HOHUB LOAD =,E15.7)
      WRITE OUTPUT TAPE 6,109
  109 FORMAT(30HO**** START INTEGRATION.         )
  619 CONTINUE
C     USE EFFICIENCY TERM IN DRIVING TORQUE.
C     NOTE USE OF 'CBAR' INSTEAD OF INTEGRATING OVER C.
      AR=(RT-RH)/CBAR
      EPS=ETA/(1.+2.*ETA/AR)
C     INITIALIZE INTEGRATION SUMS.
      DRIVER=0.
      BRINT=0.
      VV=0.
      VVS=0.
      ALPHIN=0.
      T1GG=0.
      T2GG=0.
C
      NSTEP1=NSTEP+1
      DO 26 I=1,NSTEP1
C     DO PRE-SWIRLER FIRST.
      RMT=RM
      RM=RMS
      RR=ROS-(ROS-R)*(ROS-RIS)/(ROS-RH)
      IF(RR-RMS)32,32,33
   32 CONTINUE
      V1=VEL(RR,RIS,ZKI,STAUSI)
      GO TO 34
   33 CONTINUE
      V1=VEL(RR,ROS,ZKO,STAUSO)
   34 CONTINUE
      RM=RMT
C     DETERMINE REGION ABOVE OR BELOW RM.
      IF(R-RM)22,22,23
C     HUB VELOCITY
   22 CONTINUE
      V=VEL(    R,RH,ZKI,STAURH)
      GO TO 24
   23 CONTINUE
      V=VEL(    R,RB,ZKO,STAURB)
   24 CONTINUE
      CALL QK(R,ZKC,QQ)
      IF(SENSE SWITCH 1)620,621
  620 CONTINUE
      WRITE OUTPUT TAPE 6,110,R,V1,V
  110 FORMAT(40HORADIUS, V(SWIRLER), V(TURBINE)           /3E15.7)
  621 CONTINUE
      CALL TORQUE(V,V1,R)
      RIN=R*12.
      TL=T1/G
      TBD=.5*CD*T2*T3/G
      IF(LINE)86,86,85
   86 CONTINUE
```

```
      LINE=50
      WOT 6,16
      WOT 6,87
      WOT 6,88
      WOT 6,89
      WOT 6,90
   87 FORMAT(103H0  RADIUS    TURBINE    ANGLE OF   INTERFENCE  DEFLECTI
  871ON  STRAIGHT  BLADE LIFT  BLADE DRAG  NET BLADE  )
   88 FORMAT(106H      (IN.)     VELOCITY    ATTACK    COEFFICIENT COEFFICI
  881ENT VELOCITY   TORQUE       TORQUE   DRIVING TORQUE  )
   89 FORMAT(102H                (FT/SEC)    (DEG)
  891    (FT/SEC)   (FT-LB)     (FT-LB)      (FT-LB)   )
   90 FORMAT( 99H       R            VT         DELTA           K           QT
  901        VS            TL           TBD           TD  )
   85 CONTINUE
      LINE=LINE-1
      WRITE OUTPUT TAPE 6,123,RIN,V,GMB,ZKC,QQ,V1,TL,TBD,DRIVE
  123 FORMAT(9F11.6)
      PLOT(1,INDEX)=RIN
      PLOT(2,INDEX)=V
      PLOT(3,INDEX)=GMB
      PLOT(4,INDEX)=ZKC
      PLOT(5,INDEX)=DRIVE
      INDEX=INDEX+1
C     CORRECT FOR END POINTS.
      IF(I-2)51,50,51
   50 DRIVER=((DRIVER/DR)+DRIVE)*.5*DR
      BRINT=((BRINT/DR)+BRLOAD)*.5*DR
      VV=((VV/DR)+V)*.5*DR
      VVS=((VVS/DR)+V1)*.5*DR
      ALPHIN=((ALPHIN/DR)+GMB)*.5*DR
      T1GG=.5*(T1GG+T1/G)*DR
      T2GG=.5*(T2GG+.5*CD*T2*T3/G)*DR
      GO TO 55
   51 CONTINUE
      IF(I+1-NSTEP1)52,53,54
   53 DR1=DRIVE
      BR1=BRLOAD
      VV1=V
      VVS1=V1
      ALPH1=GMB
      T1G1=T1G
      T2G1=T2G
      GO TO 52
   54 CONTINUE
      DRIVER=DRIVER+(DR1+DRIVE)*.5*DR
      BRINT=BRINT+(BR1+BRLOAD)*.5*DR
      VV=VV+.5*(VV1+V)*DR
      VVS=VVS+.5*(VVS1+V1)*DR
      ALPHIN=ALPHIN+.5*(ALPH1+GMB)*DR
      T1GG=T1GG+.5*(T1G1+T1/G) *DR
      T2GG=T2GG+.5*(T2G1+.5*CD*T2*T3/G) *DR
      GO TO 55
```

```
   52 CONTINUE
      DRIVER=DRIVER+DRIVE*DR
      BRINT=BRINT+BRLOAD*DR
      VV=VV+V*DR
      VVS=VVS+V1*DR
      ALPHIN=ALPHIN+GMB*DR
      T1GG=T1GG+T1G*DR
      T2GG=T2GG+T2G*DR
   55 CONTINUE
      R=R+DR
   26 CONTINUE
C     MOVE R BACK TO LAST INTEGRATION POINT.
      R=R-DR
C     AVERAGE VV
      VV1=VEL(RB-EPSH,RB,ZKO,STAURB)
      VLAST=.5*(V+VV1)*(RB-EPSH-RT)
      VV=VV+VLAST
      VV=VV/(RB-RH-2.*EPSH)
      VVS=VVS/(RT-RH)
C     BLADE TIP CLEARANCE DRAG.
C     NOTE THAT 'C' IS LEFT OVER FROM LAST INTEGRATION STEP.
      REN=WA*RT*(RB-RT)/ZNU
      F=.078/REN**.43
      BLADET=.5*F*RHO*WA*WA*RT*RT*RT*C*T*ZN/G
C     PRESSURE DROP CALCULATION.
C
C     FOR BLADES-----
      RBARS=.5*(ROS+RIS)
      CALL QKS(.5*(ROS+RIS),QQS)
      RBAR=.5*(RH+RB)
      CALL QK(RBAR,ZKC,QQ)
      ZNS=NS
      VBARS=Q/(3.14159*(ROS*ROS-RIS*RIS)) -ZNS*TS*(ROS-RIS)
C     REN. NO. AT CBAR OF TURBINE.
      REN=V*CBAR/ZNU
      IF(ZL)657,658,657
  658 CONTINUE
      GAM=GAMMA
      GO TO 659
  657 CONTINUE
      GAM=ATANF(6.2831854*RBAR/ZL)
  659 CONTINUE
      TANGS=SINF(GAM)/COSF(GAM)
      TANB1H=RBAR*WA/V
     1            -(2.*QQS *SINF(AS)/(1.+QQS ))*V1*((ROS*ROS-RIS*RIS)/
     2 ((RB*RB  -RH*RH)*COSF(AS)))/V
      TANB2=TANB1+ 2.*QQ*(TANGS-TANB1)/(1.+QQ)
      BETA2=ATANF(TANB2)
      DPH=.072*ZN*RHO*V*V*C/(S*COSF(BETA2)**3*REN**.2*G*144.)
C     DO PRESS. DROP FOR INCLINED PORTION OF SWIRLER.
      SS=(6.2831854*RBARS-ZNS*TS)/ZNS
      CS=WS/COSF(AS)
      REN=V1*CS/ZNU
```

```
      TANGS=SINF(AS)/COSF(AS)
      TANB2=TANGS*QQS/(1.+QQS)
      BETA2=ATANF(TANB2)
      DPHSW=.072*ZNS*RHO*V1*V1*CS/(SS*COSF(BETA2)**3*REN**.2*G*144.)
C     STRAIGHT SECTION.
      DPHS=.072*ZNS*RHO*V1*V1*ZLS/(SS*REN**.2*G*144.)
C     PIPE LOSS.
C     LENGTH OF METER.
C     CONVERT RAD. TO DIAM.
      ROS=2.*ROS
      RIS=2.*RIS
      ZMU=ZNU*RHO
      DPP=32.*VBARS*ZMU*ZLM/((ROS*ROS+RIS*RIS-(ROS*ROS-RIS*RIS)/
     1 LOGF(ROS/RIS))*G*144.)
C     CONVERT DIAM. TO RAD.
      ROS=.5*ROS
      RIS=.5*RIS
      DELTAP=DPH+DPP+DPHS+DPHSW
      IF(SENSE SWITCH 1)82,83
   82 CONTINUE
      WRITE OUTPUT TAPE 6,81,DELTAP,DPH,DPP
   81 FORMAT(22HOPRESSURE DROP (PSI) =,F8.3,18H , DUE TO BLADES =,F8.3,
     81124H  AND DUE TO PIPE LOSS =,F8.3)
   83 CONTINUE
C
      T11=RMASS*(A+G*COSF(PHI))+DPH   *(RT-RH)*T*ZN *144.
      BRIN=BRINT
      WRITE OUTPUT TAPE 6,12,BRIN,T11
   12 FORMAT(14HOBLADE LOAD =  ,E15.7,17H  PRESSURE LOAD =,E15.7)
      BRINT=BRINT+T9*T10+T11
C     THE RESULTANT TORQUE IS DRIVE-BEARING-FLUID -BLADE TIP- MAGNETIC.
C     FIND CORRECT THRUST LOAD FOR BEARING.
C     THRUST LOAD MAY BE NEGATIVE, BUT DRAG ALWAYS POS.
      BRI=ABSF(BRINT)
C     DIVIDE BEARING LOAD BEFORE CONVERSION TO TORQUE.
      ZNB=NB
C
C     SEE IF BALL BEARING OR JOURNAL BEARING TO BE USED.
C
      IF(JB)544,544,545
  545 CONTINUE
      REN=WA*ZJBR*ZJBC/ZNU
      CHECK=41.1*SQRTF(ZJBR/ZJBC)
      IF(REN-CHECK)540,540,541
  540 CONTINUE
       FRIC=2./REN
      GO TO 542
  541 FRIC=.078/REN**.43
  542 CONTINUE
      TJB=FRIC*RHO*3.14159*ZJBL*WA*WA*ZJBR**4/G
C     NOTE USE OF NUMBER OF BEARINGS.
      TJB=TJB*ZNB
      BEART=TJB
```

```
      GO TO 546
  544 CONTINUE
      BRI=BRI/ZNB
      DO 70 II=2,NBTABI
      IF(BRI-BEAR(II,1))71,71,70
   70 CONTINUE
      II=NBTABI
   71 CONTINUE
      I1=II-1
      I2=II
      X=BRI
      X1=BEAR(I1,1)
      X2=BEAR(I2,1)
C     SET UP AN ARRAY OF INTERPOLATED TORQUES.
      DO 73 I=2,NBTABJ
      Y(I)=BEAR(I1,I)+(X-X1)*(BEAR(I1,I)-BEAR(I2,I))/(X1-X2)
   73 CONTINUE
C     NOW FIND CORRECT TORQUES FOR GIVEN DRAG.
      DO 74 I=2,NBTABJ
      IF(BEAR(1,I)-WA)74,75,75
   74 CONTINUE
      I=NBTABJ
   75 CONTINUE
      BT=Y(I-1)+(WA-BEAR(1,I-1))*(Y(I-1)-Y(I))/(BEAR(1,I-1)-BEAR(1,I))
      BEART=BT*ZNB
  546 CONTINUE
      RESULT=DRIVER-BEART-FDRAG-BLADET-PICKUP
      TTORQ=RESULT
      ZMF=WA*ZN/(6.2831854*Q*7.4805)
      WRITE OUTPUT TAPE 6,501
      WRITE OUTPUT TAPE 6,511
      WRITE OUTPUT TAPE 6,521,VBAR,VV,ALPHIN,VBARS,VVS,T1GG,T2GG,DRIVER
      WRITE OUTPUT TAPE 6,502
      WRITE OUTPUT TAPE 6,512
      WRITE OUTPUT TAPE 6,522,BRINT,BEART,BLADET,FDRAG,PICKUP
      WRITE OUTPUT TAPE 6,503
      WRITE OUTPUT TAPE 6,513
      WRITE OUTPUT TAPE 6,523,WA,RESULT,ZMF,DELTAP,WIDEAL
  501 FORMAT(114H0V BAR TURB.  V-T INTEG.        ALPHA INTEG.  V BAR SWIR
 5011.    V SW. INTEG.   TL INTEG.       TBD INTEG.    TD INTEG.)
  511 FORMAT(114H  (FT/SEC)      (FT/SEC)             (DEG)          (FT/SEC)
 5111          (FT/SEC)        (FT-LB)          (FT-LB)        (FT-LB) )
  502 FORMAT( 96H0BEARING THRUST LOAD   BEARING TORQUE        BLADE TIP D
 5021RAG         ROTOR HUB DRAG        PICKUP DRAG)
  512 FORMAT(96H0            (LB)                (FT-LB)              (FT-LB)
 5121                  (FT-LB)            (FT-LB)     )
  503 FORMAT( 95H0  ROTOR SPEED WA     RESULTANT TORQUE       METER FACTOR
 5031         PRESSURE DROP           IDEAL SPEED  )
  513 FORMAT( 95H        (RAD/SEC)              (FT-LB)            (CYCLES/GA
 5131LLON)        (PSI)               (RAD/SEC)   )
  521 FORMAT(5F15.5,3F15.8)
  522 FORMAT(4F20.7,F20.9)
  523 FORMAT(F20.4,3F20.9,F20.4)

      WRITE OUTPUT TAPE 6,16
   16 FORMAT(1H1)
      RETURN
      END
```

```
      SUBROUTINE TORQUE(V,V1,R)
      DIMENSION BEAR(6,15),COEFT(8)
      COMMON BEAR,TTORQ,ZLM,NBTABI,NBTABJ
      COMMON IPOLY,COEFT
      COMMON VBAR,REYN,FRICT,ZKO,RB,RH,ZNU,O,RHO,EQ4,RATIO3
      COMMON A6,B6,STAURH,STAURB,RM,RMS,STAUSI,STAUSO,TANB1,TANB2
      COMMON T,W,ZL,ZN,GAMMA,AST,COSG,SING
      COMMON G,RMASS,A,WA,PHI,RT
      COMMON QQ,RHOH,DELTAP,CD,VH,DRIVE,FDRAG,BRLOAD,TT8,TANG
      COMMON RGUESS,COSGH,SH,GH,C,S,SGUESS
      COMMON TS,WS,AS,NS,ROS,RIS,NSTEP
      COMMON PICKUP,ZJBR,ZJBC,ZJBL,JB
      COMMON ETA,EPS,DT,NB
      COMMON EPSH,T1G,T2G,T1,T2,T3,GMB,ZLS
C     COMPUTE DRAG COEFF.
      C=ABSF(C)
      CD=.074/(V *C /ZNU)**.2
      Q1=1./(1.+QQ)
      QQ1=QQ*Q1
C     GET QQS FOR PRE-SWIRLER.
      RR=ROS-(ROS-R   )*(ROS-RIS)/(ROS-RH)
      CALL QKS(RR,QQS)
C     NEW TAN BETA1 FOR SCALING OF FLOW PROFILES.
      TANB1=(R*WA-(2.*QQS*SINF(AS)/(1.+QQS))*V1*(ROS*ROS-RIS*RIS)/
     1 ((RB*RB  -RH*RH)*COSF(AS)))/V
      TANB2=TANB1+ 2.*QQ*(TANG-TANB1)/(1.+QQ)
      TEMP1=R*WA/V
      TEMP2=TEMP1-TANB1
      IF(SENSE SWITCH 1)622,623
  622 CONTINUE
      WRITE OUTPUT TAPE 6,101,R,V1,V,QQ,QQS,CD
  101 FORMAT(80HOTORQUE SUB.  R, V(SWIRLER), V(TURBINE), Q(TURBINE),
  1011WIRLER), DRAG COEFF.                /6E15.7)
      WRITE OUTPUT TAPE 6,102,TANB1,TEMP1,TEMP2
  102 FORMAT(50HOTORQUESUB,  TAN(BETA1), R*W/V, CORRECTION
  1021  3E15.7)
  623 CONTINUE
C     DRIVING TORQUE TERMS.
      RV2N=RHO*V*V*ZN
      TT1=QQ1*TANG+Q1*TANB1
      T1=RV2N*S*2.*QQ1*(TANG-TANB1)*R*EPS
      T2=RV2N*C*TT1
      T3=SQRTF(1.+TT1*TT1)*R
C     BEARING THRUST LOAD TERMS.
      TT8=1.+(QQ1*TANG+Q1*TANB1)**2
      BRL=.5*RHO*V*V*C*ZN*(EPS* S*(TANB2*TANB2-TANB1*TANB1)/C+
     1   CD*SQRTF(1.+.25*(TANB2+TANB1)**2))
      BRL=BRL/G
      DRIVE=(T1-.5*CD*T2*T3)/G
C     BRLOAD=(T6*T7+.5*T8*CD)/G
      BRLOAD=BRL
      GMB=ATANF(.5*(TANB1+TANB2))
      GMB=GAMMA-GMB
```

```
C     CONVERT TO DEG.
      GMB=GMB*180./3.14159
      T1G=T1/G
      T23G=.5*CD*T2*T3/G
      T2G=T23G
      IF(SENSE SWITCH 1)626,627
  626 CONTINUE
      WRITE OUTPUT TAPE 6,153,BRL,BRLOAD
  153 FORMAT(23H0TANB2 LOAD, OLD LOAD          /2E15.7)
      WRITE OUTPUT TAPE 6,9,TANG,TANB1,GMB,QOS,T1G,T23G
    9 FORMAT(43H0TANG, TANB1, G-B, QOS, T1/G, .5 CD T2 T3/G/6E15.7
  627 CONTINUE
      RETURN
      END
```

```
      SUBROUTINE QK(RINT,ZK,QQ)
      DIMENSION BEAR(6,15),COEFT(8)
      COMMON BEAR,TTORQ,ZLM,NBTABI,NBTABJ
      COMMON IPOLY,COEFT
      COMMON VBAR,REYN,FRICT,ZKO,RB,RH,ZNU,Q,RHO,EQ4,RATIO3
      COMMON A6,B6,STAURH,STAURB,RM,RMS,STAUSI,STAUSO,TANB1,TANB2
      COMMON T,W,ZL,ZN,GAMMA,AST,COSG,SING
      COMMON G,RMASS,A,WA,PHI,RT
      COMMON QQ,RHOH,DELTAP,CD,VH,DRIVE,FDRAG,BRLOAD,TT8,TANG
      COMMON RGUESS,COSGH,SH,GH,C,S,SGUESS
      COMMON TS,WS,AS,NS,ROS,RIS,NSTEP
      COMMON PICKUP,ZJBR,ZJBC,ZJBL,JB
      COMMON ETA,EPS,DT,NB
      COMMON EPSH,T1G,T2G,T1,T2,T3,GMB,ZLS
C     EXPRESSION FOR (C/S) ON BASIS OF GUESSED R (RR).
      CCSSF(RR)=PIINV*(COSG*LOGF((RR*RR+2.*RR*COSAST+1.)/(RR*RR-2.*RR*
     1  COSAST+1.))+2.*SING*ATANF(2.*RR*SINAST/(RR*RR-1.)))
C
      PIINV=1./3.1415927
      IF(ZL)651,652,651
  651 CONTINUE
      GAMMA=6.2831854*RINT/ZL
      GAMMA=ATANF(GAMMA)
  652 CONTINUE
      COSG=COSF(GAMMA)
      SING=SINF(GAMMA)
      TANG=SING/COSG
C     FROM GEOMETRY
      S=(6.2831854*RINT-ZN*T)/ZN
      C=W/COSG
      CSGEOM=C/S
C     WOT6, 156,GAMMA,C,S,CSGEOM
  156 FORMAT(4H0156,5E15.7)
      R=RGUESS
   16 CONTINUE
      TANAST=TANG*(R*R-1.)/(R*R+1.)
      AST=ATANF(TANAST)
      COSAST=COSF(AST)
      SINAST=SINF(AST)
      CS1=CCSSF(R)
      CS2=CCSSF(R*1.001)
      DFDR=(CS1-CS2)/(R*.001)
      DR=(CSGEOM-CS1)/DFDR
      DIFF=CSGEOM-CS1
C     WOT6, 157,R,AST,CS1,CS2,DR,DIFF
  157 FORMAT(1H0,20X,4H 157,6E15.6)
C     KEEP R .GT. 1.0
   19 IF((R-DR)-1.)18,18,17
   18 DR=.5*DR
      GO TO 19
   17 CONTINUE
      R=R-DR
      IF(ABSF(DR)-.00001)15,15,16
```

```
   15 CONTINUE
      CLCLI=4.*R*COSAST*PIINV/(CS1*(R*R+1.)*COSG.
      CL=6.2831854*CLCLI*SING
C     QQ IS LITTLE Q USED IN INTEGRATION
      QQ=2.*R*COSAST/(R*R+1.)
      ZK =CLCLI
      RGUESS=R
      RETURN
      END
```

```
      SUBROUTINE QKS (RINT,QQS)
C     SUBROUTINE FOR INTEGRATION 'Q' FOR PRE-SWIRLER.
C     NOTE TRICKERY IN COMMON TO USE SAME NAMES BUT DIFFERENT VALUES.
      DIMENSION BEAR(6,15),COEFT(8)
      COMMON BEAR,TTORQ,ZLM,NBTABI,NBTABJ
      COMMON IPOLY,COEFT
      COMMON VBAR,REYN,FRICT,ZKO,RB,RH,ZNU,Q,RHO,E04,RATIO3
      COMMON A6,B6,STAURH,STAURB,RM,RMS,STAUSI,STAUSO,TANB1,TANB2
C     COMMON T,W,ZL,ZN,GAMMA,AST,COSG,SING
      COMMON TS,WS,ZL,ZNS,GAMMAS,ASTS,COSGS,SINGS
      COMMON G,RMASS,A,WA,PHI,RT
C     COMMON QQ,RHOH,DELTAP,CD,VH,DRIVE,FDRAG,BRLOAD,TT8,TANG
      COMMON ZQ,RHOH,DELTAP,CD,VH,DRIVE,FDRAG,BRLOAD,TT8,TANGS
C     COMMON RGUESS,COSGH,SH,GH,C,S,SGUESS
      COMMON SGUESS,COSGH,SH,GH,CSW,SSW,RGUESS
C     COMMON TS,WS,AS,NS,ROS,RIS
      COMMON T,W,AS,NS,ROS,RIS,NSTEP
      COMMON PICKUP,ZJBR,ZJBC,ZJBL,JB
      COMMON ETA,EPS,DT,NB
      COMMON EPSH,T1G,T2G,T1,T2,T3,GMB,ZLS
C     EXPRESSION FOR (C/S) ON BASIS OF GUESSED R (RR).
      CCSSF(RR)=PIINV*(COSG*LOGF((RR*RR+2.*RR*COSAST+1.)/(RR*RR-2.*RR*
     1  COSAST+1.))+2.*SING*ATANF(2.*RR*SINAST/(RR+RR-1.)))
C
      ZN=NS
      PIINV=1./3.1415927
C     FIXED ANGLE FOR PRE-SWIRLER.
      GAMMA=AS
      COSG=COSF(GAMMA)
      SING=SINF(GAMMA)
      TANG=SING/COSG
C     FROM GEOMETRY
      S=(6.2831854*RINT-ZN*T)/ZN
      C=W/COSG
      CSGEOM=C/S
      R=RGUESS
   16 CONTINUE
      TANAST=TANG*(R*R-1.)/(R*R+1.)
      AST=ATANF(TANAST)
      COSAST=COSF(AST)
      SINAST=SINF(AST)
      CS1=CCSSF(R)
      CS2=CCSSF(R*1.001)
      DFDR=(CS1-CS2)/(R*.001)
      DR=(CSGEOM-CS1)/DFDR
      DIFF=CSGEOM-CS1
   23 CONTINUE
C     WOT 6,157,R,AST,CS1,CS2,DR,DIFF
  157 FORMAT(1H0,20X,4H 157,6E15.6)
C     KEEP R .GT. 1.0
   19 IF((R-DR)-1.)18,18,17
   18 DR=.5*DR
      GO TO 19
```

```
   17 CONTINUE
C     KEEP DR IN BOUNDS.
      IF(ABSF(DR/R) -.25)21,21,22
   22 DR=.5*DR
      GO TO 23
   21 CONTINUE
      R=R-DR
      IF(ABSF(DR)-.00001)15,15,16
   15 CONTINUE
C     QQS IS LITTLE 'Q' USED IN TAN BETA 1.
      QQS=2.*R*COSAST/(R*R+1.)
      RGUESS=R
      RETURN
      END
```

```
      FUNCTION VEL(   R,RR,ZK,SQTAUR)
      DIMENSION BEAR(6,15),COEFT(8)
      COMMON BEAR,TTORQ,ZLM,NBTABI,NBTABJ
      COMMON IPOLY,COEFT
      COMMON VBAR,REYN,FRICT,ZKO,RB,RH,ZNU,Q,RHO,EQ4,RATIO3
      COMMON A6,B6,STAURH,STAURB,RM,RMS,STAUSI,STAUSO,TANB1,TANB2
      COMMON T,W,ZL,ZN,GAMMA,AST,COSG,SING
      COMMON G,RMASS,A,WA,PHI,RT
      COMMON QQ,RHOH,DELTAP,CD,VH,DRIVE,FDRAG,BRLOAD,T78,TANG
      COMMON RGUESS,COSGH,SH,GH,C,SS,SGUESS
      COMMON TS,WS,AS,NS,ROS,RIS,NSTEP
      COMMON PICKUP,ZJBR,ZJBC,ZJBL,JB
      COMMON DUMETA,DUMEPS,DT,NB
      COMMON EPSH,T1G,T2G,T1,T2,T3,GMB,ZLS
C     RR=RADIUS OF HUB OR BODY
C     R = RADIUS ALONG BLADE (FOR INTEGRATION)
C     CHECK FOR POLYNOMIAL VELOCITY SPECIFICATION.
      IF(IPOLY)5,5,6
    6 CONTINUE
      RP=R
      VEL=COEFT(1)
      DO 7 I=2,8
      VEL=VEL+COEFT(I)*RP
      RP=RP*R
    7 CONTINUE
      VEL=VEL
      RETURN
    5 CONTINUE
      ATSQ2=.95531659
      S=RM/RR
      SP1=S+1.
      SP1K=SP1*ZK
      SM1=1.-S
      ETA=(R-RM)/(RR-RM)
C     SQTAUR=SQRTF(TAUR/RHO)
      Y=ABSF(R-RR)*SQTAUR/ZNU
      IF(Y-5.)1,2,2
    1 CONTINUE
C     FROM GE REPORT, SET U+ = Y+ IF Y .LT. 5
      U=Y
      GO TO 3
    2 CONTINUE
      T1=LOGF(1.5*Y*(1.+ETA)/(1.+2.*ETA*ETA))/ZK
      T2=2.*SM1*S*LOGF(.5*(1.+ETA))/(SP1K*(2.*S-1.))
      T3=.5*S*SM1*(1.-3.*S)*LOGF((1.+2.*ETA*ETA)/3.)/(SP1K*(S*S+.5*
     1  SM1*SM1))
      T4=6.*LOGF(ETA*SM1+S)/(SP1K*((SM1/S)**2-1.)*((S/SM1 )**2+2.))
      T5=1.414214*S*SM1    *(ATSQ2-ATANF(1.414214*ETA))/( SP1K    *(S*S+
     1  .5*SM1*SM1))
      T6=14.84-3.73767/ZK
      U=T1+T2+T3+T4+T5+T6
    3 CONTINUE
      VEL=U*SQTAUR
      RETURN
      END
```

```
      SUBROUTINE SUBRM(RM)
      DIMENSION BEAR(6,15),COEFT(8)
      COMMON BEAR,TTORQ,ZLM,NBTABI,NBTABJ
      COMMON IPOLY,COEFT
      COMMON VBAR,REYN,FRICT,ZKO,RB,RH,ZNU,Q,RHO,EQ4,RATIO3
      COMMON A6,B6,STAURH,STAURB,RM,RMS,STAUSI,STAUSO,TANB1,TANB2
      COMMON T,W,ZL,ZN,GAMMA,AST,COSG,SING
      COMMON G,RMASS,A,WA,PHI,RT
      COMMON QQ,RHOH,DELTAP,CD,VH,DRIVE,FDRAG,BRLOAD,TTB,TANG
      COMMON RGUESS,COSGH,SH,GH,C,S,SGUESS
      COMMON TS,WS,AS,NS,ROS,RIS,NSTEP
      COMMON PICKUP,ZJBR,ZJBC,ZJBL,JB
      COMMON ETA,EPS,DT,NB
C     GUESS RM
      RM=.5*(RH+RB)
C     COMPUTE DERIVATIVE W.R. TO RM.
C     TRY TO OBTAIN RM BY NEWTON'S METHOD (X=X-F/DF)
    3 CONTINUE
      CALL RMCALC(RM)
      F1=RATIO3-EQ4
      CALL RMCALC(RM*1.001)
      F2=RATIO3-EQ4
      DF=(F1-F2)/(RM*.001)
      DRM=F1/DF
      IF(ABSF(DRM/RM)-.02)21,21,22
   22 CONTINUE
C     TAKE A SMALL STEP IF ITERATION STEP TOO LARGE.
      DRM=.010*RM*DRM/ABSF(DRM)
   21 CONTINUE
      RM=RM+DRM
C     CHECK ITERATION CONVERGENCE
      IF(ABSF(DRM)-.000001)2,2,3
    2 CONTINUE
      CALL RMCALC(RM)
      RETURN
      END
```

```
      SUBROUTINE RMCALC(RM)
      DIMENSION BEAR(6,15),COEFT(8)
      COMMON BEAR,TTORQ,ZLM,NBTABI,NBTABJ
      COMMON IPOLY,COEFT
      COMMON VBAR,REYN,FRICT,ZKO,RB,RH,ZNU,Q,RHO,EQ4,RATIO3
      COMMON A6,B6,STAURH,STAURB,RM,RMS,STAUSI,STAUSO,TANB1,TANB2
      COMMON T,W,ZL,ZN,GAMMA,AST,COSG,SING
      COMMON G,RMASS,AA,WA,PHI,RT
      COMMON QQ,RHOH,DELTAP,CD,VH,DRIVE,FDRAG,BRLOAD,TT8,TANG
      COMMON RGUESS,COSGH,SH,GH,C,S,SGUESS
      COMMON TS,WS,AS,NS,ROS,RIS,NSTEP
      COMMON PICKUP,ZJBR,ZJBC,ZJBL,JB
      COMMON ETA,EPS,DT,NB
      COMMON EPSH,T1G,T2G,T1,T2,T3,GMB,ZLS
      A6=.5*REYN*SQRTF(.5*FRICT)*((1.-RM/RB)/(1.-RH/RB))**1.5*SQRTF(
     1 1.+RM/RB)
      RATIO3=((RM-RH)/(RB-RM))**1.5*SQRTF(RB/RH)*SQRTF((RM+RH)/(RB+RM))
      B6= A6*RATIO3
      EQ2=RB*(RM*RM-RH*RH)/(RH*(RB*RB-RM*RM))
      SI=RM/RH
      SO= RM/RB
      C1=.4054651
      C2=.69314718
      C3=1.0986122
      C4=3.7376696
      C5=1.4142135
      C6=   .95531659
      TERM1=LOGF(ABSF(A6))
      TERM2=(2.*SO*(1.-SO)/((1.+SO)*(2.*SO-1.,))*C2
      TERM3=.5*C3*SO*(1.-SO)*(1.-3.*SO)/((1.+SO)*(SO*SO+.5*(1.-SO)**2))
      TERM4=6.*LOGF(SO)/((1.+SO)   *(((1.-SO)/SO)**2-1.)*((SO/(1.-SO)**2
     1 +2.)))
      TERM5=SO*(1.-SO)*C5*C6/((1.+SO)*(SO*SO+.5*(1.-SO)**2))
      A=C1+TERM1-TERM2-TERM3+TERM4+TERM5+14.84*ZKO-C4
      TERM1=LOGF(ABSF(B6))
      TERM2=(2.*SI*(1.-SI)/((1.+SI)*(2.*SI-1.)))*C2
      TERM3=.5*C3*SI*(1.-SI)*(1.-3.*SI)/((1.+SI)*(SI*SI+.5*(1.-SI)**2))
      TERM4=6.*LOGF(SI)/((1.+SI)   *(((1.-SI)/SI)**2-1.)*((SI/(1.-SI)**2
     1 +2.)))
      TERM5=SI*(1.-SI)*C5*C6/((1.+SI)*(SI*SI+.5*(1.-SI)**2))
      ZKI=ZKO/RATIO3
      B=C1+TERM1-TERM2-TERM3+TERM4+TERM5+14.84*ZKI-C4
      EQ4=(A/B)/SQRTF(EQ2)
C     PRINT 51,EQ2,RATIO3,A,B,EQ4
   51 FORMAT(31H0EQ2,RATIO3,A,B,EQ4 FROM RMCALC/5E15.7)
      RETURN
      END
```

```
      FUNCTION RENCHK(REYN)
      DIMENSION BEAR(6,15),COEFT(8)
      COMMON BEAR,TTORQ,ZLM,NBTABI,NBTABJ
      COMMON IPOLY,COEFT
      IF(REYN-10000.)11,11,12
   11 CONTINUE
      WRITE OUTPUT TAPE 6,13
   13 FORMAT(40HOREYNOLD'S NUMBER TOO LOW, CASE ABORTED. )
C     SET 'IPOLY' TO -1 FOR FILTERING BACK TO MAIN PROGRAM.
      IPOLY=-1
      RENCHK=-1.
      RETURN
   12 CONTINUE
      RENCHK=1.
      RETURN
      END
```

```
      6    12
0.          0.                         .5                          1.0
2.                        3.
104.72     .000003798                 .000009730                  .000018774
.000041418                .000068548         .
209.44     .000005209                 .000011141                  .000020185
.000042829                .000069959
314.16     .000006366                 .000012299                  .000021342
.000043986                .000071116
418.88     .000007524                 .000013456                  .000022500
.000045144                .000072274
523.6      .000008537                 .000014469                  .000023513
.000046157                .000073286
628.32     .000009405                 .000015337                  .000024381
.000047025                .000074155
733.04     .000010309                 .000016242                  .000025285
.000047929                .000075059
837.76     .000011214                 .000017146                  .000026190
.000048834                .000075964
942.48     .000011575                 .000017508                  .000026551
.000049195                .000076325
1047.2     .000012733                 .000018665                  .000027709
.000050353                .000077483
5236.0     .000034726                 .000040658                  .000049702
.000072345                .000099476
 WATER 100 PERCENT Q 70. DEG. BB NOM. G RF PRE-SW.    SAMPLE DATA SET.
.92        .40        .002        .5013033   62.3        1.
.070       .230       5.58          14       5.3
.256       0.         900.        90.         .900
.070       .400       30.           5        .9900       .30        2.597
-.0000010             .0000200    .00002000  70.
0.
1  -96.    336.       -240.
    2  200 .00001
```

APPENDIX C

SAMPLE COMPUTER OUTPUT TABULATION

VBAR,REYN.FRICT
0.3711517E 02 0.2744016E 06 0.3759071E-02

RADIUS (IN.) R	TURBINE VELOCITY (FT/SEC) VT	ANGLE OF ATTACK (DEG) ALPHA	INTERFERENCE COEFFICIENT K	DEFLECTION COEFFICIENT QT	SWIRLER VELOCITY (FT/SEC) VS	BLADE LIFT TORQUE (FT-LB) TL	BLADE DRAG TORQUE (FT-LB) TBD	NET BLADE DRIVING TORQUE (FT-LB) TD
0.417120	12.718510	-21.607359	0.353012	0.998271	13.138185	-1.010393	0.030279	-1.040672
0.419409	24.455108	-2.151192	0.355458	0.998210	24.350893	-0.293047	0.037056	-0.330103
0.421699	27.083783	0.487494	0.357899	0.998147	25.846265	0.080679	0.039376	0.041303
0.423988	28.653904	1.844413	0.360339	0.998084	28.328654	0.342589	0.041095	0.301494
0.426278	29.780586	2.721543	0.362780	0.998019	29.386807	0.549853	0.042573	0.507280
0.428567	30.661899	3.351749	0.365219	0.997953	30.210297	0.724347	0.043928	0.680419
0.430856	31.387147	3.833185	0.367657	0.997886	30.884595	0.876927	0.045211	0.831716
0.433146	32.004307	4.215964	0.370095	0.997818	31.455616	1.013813	0.046450	0.967363
0.435435	32.542153	4.528938	0.372533	0.997749	31.950895	1.138916	0.047661	1.091255
0.437725	33.019301	4.790138	0.374969	0.997678	32.388249	1.254857	0.048855	1.206001
0.440014	33.448499	5.011541	0.377404	0.997607	32.779871	1.363481	0.050040	1.313441
0.442303	33.838851	5.201480	0.379839	0.997534	33.134469	1.466137	0.051219	1.414918
0.444593	34.197091	5.365973	0.382273	0.997450	33.458484	1.563839	0.052397	1.511441
0.446882	34.528334	5.509498	0.384706	0.997385	33.756810	1.657369	0.053578	1.603791
0.449172	34.836564	5.635466	0.387138	0.997309	34.033251	1.747341	0.054762	1.692579
0.451461	35.124936	5.746534	0.389569	0.997232	34.290824	1.834247	0.055952	1.778295
0.453750	35.395994	5.844810	0.392000	0.997154	34.531960	1.918484	0.057150	1.861335
0.456040	35.651821	5.931988	0.394430	0.997074	34.758648	2.000379	0.058355	1.942023
0.458329	35.894140	6.009452	0.396859	0.996994	34.972533	2.080201	0.059571	2.020630
0.460619	36.124394	6.078341	0.399287	0.996913	35.174990	2.158176	0.060797	2.097380
0.462908	36.343802	6.139609	0.401714	0.996830	35.367183	2.234494	0.062034	2.172461
0.465197	36.553405	6.194057	0.404141	0.996747	35.550101	2.309315	0.063282	2.246033
0.467487	36.754094	6.242365	0.406566	0.996662	35.724597	2.382776	0.064543	2.318232
0.469776	36.946641	6.285115	0.408991	0.996577	35.891404	2.454991	0.065817	2.389174
0.472066	37.131721	6.322807	0.411416	0.996490	36.051161	2.526061	0.067105	2.458956
0.474355	37.309919	6.355872	0.413838	0.996402	36.204429	2.596070	0.068406	2.527664
0.476644	37.481754	6.384694	0.416261	0.996314	36.351697	2.665092	0.069721	2.595371
0.478934	37.647682	6.409600	0.418682	0.996225	36.493399	2.733188	0.071051	2.662137
0.481223	37.808110	6.430882	0.421103	0.996134	36.629917	2.800411	0.072396	2.728015
0.483513	37.963398	6.448798	0.423523	0.996043	36.761595	2.866808	0.073756	2.793051
0.485802	38.113867	6.463575	0.425942	0.995951	36.888736	2.932414	0.075132	2.857282
0.488091	38.259809	6.475418	0.428360	0.995857	37.011612	2.997263	0.076523	2.920740

RADIUS (IN.) R	TURBINE VELOCITY (FT/SEC) VT	ANGLE OF ATTACK (DEG) ALPHA	INTERFERENCE COEFFICIENT K	DEFLECTION COEFFICIENT QT	SWIRLER VELOCITY (FT/SEC) VS	BLADE LIFT TORQUE (FT-LB) TL	BLADE DRAG TORQUE (FT-LB) TBD	NET BLADE DRIVING TORQUE (FT-LB) TD
0.490381	38.401481	6.484508	0.430778	0.995763	37.130470	3.061381	0.077931	2.983450
0.492670	38.539118	6.491007	0.433194	0.995668	37.245527	3.124789	0.079355	3.045434
0.494960	38.672930	6.495060	0.435610	0.995573	37.356981	3.187504	0.080795	3.106708
0.497249	38.803109	6.496803	0.438024	0.995476	37.465011	3.249538	0.082253	3.167285
0.499538	38.929826	6.496350	0.440438	0.995378	37.569778	3.310901	0.083727	3.227173
0.501828	39.053238	6.493810	0.442851	0.995280	37.671426	3.371597	0.085219	3.286378
0.504117	39.173487	6.489280	0.445264	0.995181	37.770089	3.431630	0.086728	3.344901
0.506407	39.290701	6.482851	0.447675	0.995081	37.865884	3.490998	0.088255	3.402743
0.508696	39.404999	6.474603	0.450085	0.994980	37.958920	3.549699	0.089800	3.459898
0.510985	39.516485	6.464607	0.452495	0.994879	38.049295	3.607726	0.091369	3.516362
0.513275	39.625257	6.452934	0.454904	0.994776	38.137096	3.665070	0.092945	3.572125
0.515564	39.731400	6.439641	0.457312	0.994673	38.222404	3.721722	0.094545	3.627177
0.517854	39.834998	6.424786	0.459719	0.994570	38.305289	3.777667	0.096163	3.681504
0.520143	39.936120	6.408420	0.462125	0.994455	38.385818	3.832892	0.097800	3.735092
0.522432	40.034831	6.390589	0.464531	0.994360	38.464049	3.887378	0.099457	3.787921
0.524722	40.131190	6.371336	0.466935	0.994254	38.540033	3.941108	0.101132	3.839975
0.527011	40.225251	6.350702	0.469339	0.994147	38.613817	3.994058	0.102827	3.891231
0.529301	40.317060	6.328720	0.471742	0.994040	38.685443	4.046207	0.104541	3.941666
0.531590	40.406660	6.305421	0.474158	0.993932	38.754949	4.097529	0.106275	3.991255
0.533879	40.494091	6.280842	0.476559	0.993824	38.822366	4.148001	0.108028	4.039974
0.536169	40.579382	6.255006	0.478960	0.993715	38.887722	4.197593	0.109801	4.087792
0.538458	40.662567	6.227939	0.481360	0.993605	38.951045	4.246276	0.111594	4.134682
0.540748	40.743668	6.199666	0.483759	0.993495	39.012353	4.294019	0.113407	4.180612
0.543037	40.822709	6.170203	0.486157	0.993384	39.071664	4.340787	0.115240	4.225547
0.545326	40.899709	6.139576	0.488554	0.993272	39.128998	4.386549	0.117094	4.269456
0.547616	40.974683	6.107796	0.490950	0.993160	39.184361	4.431268	0.118967	4.312300
0.549905	41.047645	6.074884	0.493346	0.993048	39.237769	4.474907	0.120861	4.354045
0.552195	41.118604	6.040853	0.495741	0.992935	39.289226	4.517428	0.122776	4.394652
0.554484	41.187570	6.005714	0.498135	0.992821	39.338739	4.558790	0.124711	4.434079
0.556773	41.254547	5.969482	0.500528	0.992707	39.386314	4.598955	0.126666	4.472288
0.559063	41.319540	5.932170	0.502920	0.992592	39.431951	4.637879	0.128643	4.509236
0.561352	41.382548	5.893783	0.505312	0.992477	39.475652	4.675518	0.130640	4.544879
0.563642	41.443574	5.854332	0.507703	0.992362	39.517416	4.711831	0.132657	4.579174
0.565931	41.502614	5.813830	0.510093	0.992246	39.557243	4.746770	0.134695	4.612075
0.568220	41.559667	5.772279	0.512482	0.992130	39.595131	4.780291	0.136754	4.643537
0.570510	41.614727	5.729690	0.514871	0.992013	39.631076	4.812345	0.138834	4.673511
0.572799	41.667789	5.686068	0.517258	0.991896	39.665074	4.842886	0.140935	4.701951
0.575089	41.718846	5.641418	0.519645	0.991778	39.697123	4.871866	0.143056	4.728810

RADIUS (IN.) R	TURBINE VELOCITY (FT/SEC) VT	ANGLE OF ATTACK (DEG) ALPHA	INTERFERENCE COEFFICIENT K	DEFLECTION COEFFICIENT QT	SWIRLER VELOCITY (FT/SEC) VS	BLADE LIFT TORQUE (FT-LB) TL	BLADE DRAG TORQUE (FT-LB) TBD	NET BLADE DRIVING TORQUE (FT-LB) TD
0.577378	41.767892	5.595750	0.522031	0.991550	39.727217	4.899235	0.145198	4.754037
0.579667	41.814918	5.549066	0.524416	0.991542	39.755354	4.924945	0.147361	4.777585
0.581957	41.859912	5.501374	0.526801	0.991424	39.781528	4.948944	0.149544	4.799400
0.584246	41.902870	5.452677	0.529185	0.991305	39.805736	4.971185	0.151748	4.819438
0.586536	41.943779	5.402983	0.531568	0.991185	39.827974	4.991617	0.153972	4.837645
0.588825	41.982631	5.352294	0.533950	0.991066	39.848239	5.010189	0.156217	4.853972
0.591114	42.019415	5.300617	0.536332	0.990946	39.866529	5.026852	0.158483	4.868369
0.593404	42.054122	5.247957	0.538712	0.990826	39.882843	5.041555	0.160768	4.880787
0.595693	42.086742	5.194319	0.541092	0.990706	39.897180	5.054250	0.163074	4.891176
0.597983	42.117269	5.139711	0.543472	0.990585	39.909538	5.064887	0.165401	4.899487
0.600272	42.145689	5.084136	0.545850	0.990464	39.919920	5.073417	0.167747	4.905670
0.602561	42.171997	5.027600	0.548228	0.990343	39.928328	5.079793	0.170113	4.909680
0.604851	42.196185	4.970116	0.550605	0.990222	39.934767	5.083971	0.172499	4.911472
0.607140	42.218246	4.911679	0.552982	0.990100	39.939238	5.085898	0.174905	4.910993
0.609430	42.238174	4.852304	0.555357	0.989978	39.941750	5.085531	0.177330	4.908201
0.611719	42.255965	4.791997	0.557732	0.989856	39.942309	5.082827	0.179775	4.903052
0.614008	42.271614	4.730765	0.560106	0.989734	39.940924	5.077743	0.182239	4.895504
0.616298	42.285120	4.477285	0.562480	0.989612	39.299284	4.873115	0.186488	4.686627
0.618587	42.296479	4.414063	0.564853	0.989490	39.289602	4.860572	0.189015	4.671558
0.620877	42.305693	4.349999	0.567225	0.989357	39.278160	4.845573	0.191560	4.654013
0.623166	42.312760	4.285100	0.569597	0.989245	39.264972	4.828079	0.194124	4.633955
0.625455	42.317684	4.219374	0.571968	0.989122	39.250050	4.808056	0.196707	4.611350
0.627745	42.32046[illegible]	4.152831	0.574338	0.988999	39.233405	4.785470	0.199307	4.586162
0.630034	42.321120	4.085479	0.576708	0.988876	39.215051	4.760285	0.201926	4.558359
0.632324	42.330947	4.020307	0.579076	0.988753	39.195002	4.738346	0.204631	4.533715
0.634613	42.325967	3.951017	0.581445	0.988630	39.173271	4.707198	0.207278	4.499920
0.636902	42.318878	3.880943	0.583812	0.988507	39.149873	4.673354	0.209942	4.463412
0.639192	42.309692	3.810094	0.586179	0.988384	39.124823	4.636787	0.212624	4.424163
0.641481	42.298419	3.738479	0.588546	0.988251	39.098136	4.597474	0.215323	4.382151
0.643771	42.285069	3.666109	0.590912	0.988137	39.069828	4.555387	0.218040	4.337347
0.646060	42.269656	3.592992	0.593276	0.988014	39.039915	4.510501	0.220773	4.289728
0.648349	42.252190	3.519146	0.595641	0.987891	39.008413	4.462806	0.223523	4.239283
0.650639	42.232688	3.444571	0.598005	0.987768	38.975339	4.412268	0.226290	4.185978
0.652928	42.211161	3.369281	0.600368	0.987644	38.940711	4.358874	0.229074	4.129799
0.655218	42.187626	3.293288	0.602731	0.987521	38.904542	4.302604	0.231874	4.070729
0.657507	42.162098	3.216599	0.605093	0.987398	38.866854	4.243443	0.234691	4.008752
0.659796	42.134594	3.139228	0.607455	0.987275	38.827662	4.181376	0.237524	3.943852
0.662086	42.105132	3.061184	0.609816	0.987152	38.786983	4.116387	0.240373	3.876014

RADIUS (IN.) R	TURBINE VELOCITY (FT/SEC) VT	ANGLE OF ATTACK (DEG) ALPHA	INTERFENCE COEFFICIENT K	DEFLECTION COEFFICIENT QT	SWIRLER VELOCITY (FT/SEC) VS	BLADE LIFT TORQUE (FT-LB) TL	BLADE DRAG TORQUE (FT-LB) TBD	NET BLADE DRIVING TORQUE (FT-LB) TD
0.664375	42.073728	2.982478	0.612176	0.987029	38.744836	4.048465	0.243238	3.805227
0.666665	42.040399	2.903119	0.614536	0.986906	38.701238	3.977597	0.246119	3.731478
0.668954	42.005165	2.823119	0.616895	0.986783	38.656205	3.903774	0.249016	3.654758
0.671243	41.968044	2.742488	0.619254	0.986661	38.609755	3.826985	0.251929	3.575056
0.673533	41.929056	2.661236	0.621612	0.986538	38.561906	3.747223	0.254858	3.492365
0.675822	41.888218	2.579374	0.623970	0.986415	38.512675	3.664481	0.257802	3.406679
0.678112	41.845552	2.496911	0.626327	0.986293	38.462078	3.578750	0.260761	3.317989
0.680401	41.801075	2.413857	0.628684	0.986171	38.410131	3.490026	0.263736	3.226290
0.682690	41.754809	2.330222	0.631040	0.986049	38.356850	3.398304	0.266726	3.131578
0.684980	41.706772	2.246017	0.633396	0.985927	38.302253	3.303581	0.269731	3.033850
0.687269	41.656983	2.161249	0.635750	0.985805	38.246355	3.205855	0.272751	2.933103
0.689559	41.605463	2.075929	0.638105	0.985683	38.189170	3.105121	0.275786	2.829334
0.691848	41.552231	1.990065	0.640459	0.985562	38.130713	3.001377	0.278837	2.722540
0.694137	41.497303	1.903665	0.642813	0.985441	38.070997	2.894623	0.281902	2.612721
0.696427	41.440702	1.816740	0.645166	0.985320	38.010037	2.784859	0.284982	2.499877
0.698716	41.382441	1.729294	0.647519	0.985199	37.947845	2.672083	0.288076	2.384007
0.701006	41.322541	1.641337	0.649871	0.985078	37.884435	2.556295	0.291185	2.265111
0.703295	41.261018	1.552876	0.652223	0.984958	37.819817	2.437498	0.294308	2.143190
0.705584	41.197888	1.463917	0.654574	0.984838	37.754002	2.315690	0.297446	2.018244
0.707874	41.133168	1.374466	0.656925	0.984718	37.687000	2.190872	0.300598	1.890274
0.710163	41.066872	1.284528	0.659276	0.984598	37.618822	2.063046	0.303764	1.759283
0.712453	40.999015	1.194111	0.661626	0.984478	37.549473	1.932213	0.306944	1.625269
0.714742	40.929609	1.103218	0.663975	0.984359	37.478964	1.798372	0.310138	1.488234
0.717031	40.858667	1.011852	0.666325	0.984240	37.407380	1.661526	0.313346	1.348180
0.719321	40.786202	0.920017	0.668674	0.984121	37.334488	1.521673	0.316568	1.205105
0.721610	40.712222	0.827718	0.671022	0.984003	37.260531	1.378817	0.319803	1.059014
0.723900	40.636738	0.734954	0.673370	0.983885	37.185434	1.232956	0.323052	0.909904
0.726189	40.559757	0.641728	0.675717	0.983767	37.109200	1.084091	0.326314	0.757776
0.728478	40.481287	0.548040	0.678065	0.983650	37.031829	0.932220	0.329590	0.602630
0.730768	40.401333	0.453892	0.680412	0.983532	36.953322	0.777343	0.332878	0.444465
0.733057	40.319899	0.359280	0.682758	0.983415	36.873078	0.619458	0.336180	0.283278
0.735347	40.236987	0.264203	0.685104	0.983299	36.792894	0.458565	0.339494	0.119071
0.737636	40.152600	0.168656	0.687450	0.983183	36.710968	0.294654	0.342821	-0.048167
0.739925	40.066736	0.072641	0.689796	0.983067	36.627895	0.127732	0.346160	-0.218428
0.742215	39.979394	-0.023849	0.692141	0.982951	36.543665	-0.042209	0.349511	-0.391721
0.744504	39.890569	-0.120824	0.694486	0.982836	36.458274	-0.215177	0.352875	-0.568051
0.746794	39.800256	-0.218285	0.696830	0.982721	36.371711	-0.391174	0.356250	-0.747424
0.749083	39.708448	-0.316245	0.699175	0.982606	36.283964	-0.570211	0.359636	-0.929847

RADIUS (IN.) R	TURBINE VELOCITY (FT/SEC) VT	ANGLE OF ATTACK (DEG) ALPHA	INTERFERENCE COEFFICIENT K	DEFLECTION COEFFICIENT QT	SWIRLER VELOCITY (FT/SEC) VS	BLADE LIFT TORQUE (FT-LB) TL	BLADE DRAG TORQUE (FT-LB) TBD	NET BLADE DRIVING TORQUE (FT-LB) TD
0.751372	39.615135	-0.414710	0.701518	0.982492	35.195021	-0.752291	0.363034	-1.115324
0.753662	39.520304	-0.513693	0.703862	0.982378	36.104866	-0.937427	0.366443	-1.303870
0.755951	39.423943	-0.613204	0.706205	0.982265	36.013483	-1.125627	0.369862	-1.495489
0.758241	39.326032	-0.713259	0.708548	0.982152	35.920852	-1.316906	0.373292	-1.690197
0.760530	39.226556	-0.813872	0.710891	0.982039	35.826953	-1.511271	0.376731	-1.888003
0.762819	39.125491	-0.915060	0.713234	0.981927	35.731763	-1.708742	0.380181	-2.088923
0.765109	39.022814	-1.016842	0.715576	0.981815	35.635254	-1.909334	0.383639	-2.292973
0.767398	38.918498	-1.119238	0.717918	0.981704	35.537401	-2.113060	0.387106	-2.500166
0.769688	38.812510	-1.222270	0.720259	0.981593	35.438170	-2.319942	0.390582	-2.710525
0.771977	38.704819	-1.325963	0.722601	0.981482	35.337530	-2.530002	0.394066	-2.924067
0.774266	38.595387	-1.430346	0.724942	0.981372	35.235442	-2.743261	0.397557	-3.140818
0.776556	38.484172	-1.535446	0.727283	0.981262	35.131866	-2.959746	0.401054	-3.360800
0.778845	38.371130	-1.641295	0.729624	0.981153	35.026758	-3.179482	0.404558	-3.584040
0.781135	38.256211	-1.747927	0.731965	0.981044	34.920071	-3.402498	0.408067	-3.810566
0.783424	38.139361	-1.855382	0.734305	0.980936	34.811755	-3.628827	0.411582	-4.040408
0.785713	38.020522	-1.963700	0.736645	0.980828	34.701751	-3.858504	0.415100	-4.273604
0.788003	37.899629	-2.072928	0.738985	0.980720	34.590002	-4.091565	0.418622	-4.510186
0.790292	37.776611	-2.183111	0.741325	0.980613	34.476440	-4.328050	0.422146	-4.750196
0.792582	37.651393	-2.294306	0.743664	0.980507	34.360995	-4.568002	0.425672	-4.993674
0.794871	37.523891	-2.406567	0.746004	0.980401	34.243588	-4.811469	0.429198	-5.240667
0.797160	37.394014	-2.519959	0.748343	0.980295	34.124137	-5.058502	0.432724	-5.491226
0.799450	37.261665	-2.634548	0.750682	0.980190	34.002552	-5.309152	0.436248	-5.745400
0.801739	37.126734	-2.750409	0.753021	0.980085	33.878733	-5.563481	0.439769	-6.003250
0.804029	36.989106	-2.867624	0.755360	0.979981	33.752573	-5.821549	0.443286	-6.264836
0.806318	36.848651	-2.986282	0.757699	0.979877	33.623955	-6.083428	0.446798	-6.530225
0.808607	36.705228	-3.106478	0.760037	0.979774	33.492751	-6.349187	0.450302	-6.799489
0.810897	36.558687	-3.228318	0.762376	0.979671	33.358824	-6.618909	0.453797	-7.072706
0.813186	36.408658	-3.351920	0.764714	0.979559	33.222020	-6.892676	0.457281	-7.349957
0.815476	36.255557	-3.477413	0.767053	0.979457	33.082173	-7.170583	0.460752	-7.631335
0.817765	36.098581	-3.604933	0.769391	0.979356	32.939102	-7.452727	0.464208	-7.916935
0.820054	35.937708	-3.734640	0.771729	0.979256	32.792603	-7.739219	0.467646	-8.206865
0.822344	35.772690	-3.866705	0.774066	0.979165	32.642454	-8.030177	0.471065	-8.501242
0.824633	35.603255	-4.001320	0.776404	0.979056	32.488412	-8.325728	0.474459	-8.800188
0.826922	35.429098	-4.138699	0.778742	0.978967	32.330204	-8.626010	0.477828	-9.103838
0.829212	35.249883	-4.279079	0.781080	0.978858	32.167525	-8.931173	0.481166	-9.412339
0.831501	35.065232	-4.422729	0.783418	0.978770	32.000037	-9.241386	0.484470	-9.725856

RADIUS (IN.) R	TURBINE VELOCITY (FT/SEC) VT	ANGLE OF ATTACK (DEG) ALPHA	INTERFERENCE COEFFICIENT K	DEFLECTION COEFFICIENT QT	SWIRLER VELOCITY (FT/SEC) VS	BLADE LIFT TORQUE (FT-LB) TL	BLADE DRAG TORQUE (FT-LB) TBD	NET BLADE DRIVING TORQUE (FT-LB) TD
0.833791	34.874722	-4.569948	0.785755	0.978573	31.827362	-9.556826	0.487736	-10.044562
0.836080	34.677876	-4.721079	0.788093	0.978576	31.649073	-9.877692	0.490958	-10.368650
0.838369	34.474153	-4.876509	0.790431	0.978480	31.464687	-10.204204	0.494130	-10.698334
0.840659	34.262941	-5.036680	0.792768	0.978384	31.273653	-10.536600	0.497247	-11.033847
0.842948	34.043540	-5.202101	0.795106	0.978288	31.075346	-10.875144	0.500302	-11.375445
0.845238	33.815141	-5.373360	0.797443	0.978194	30.869046	-11.220133	0.503285	-11.723418
0.847527	33.576814	-5.551140	0.799780	0.978100	30.653919	-11.571891	0.506188	-12.078079
0.849816	33.327471	-5.736244	0.802118	0.978005	30.428994	-11.930782	0.509000	-12.439781
0.852106	33.065835	-5.929621	0.804455	0.977913	30.193130	-12.297217	0.511707	-12.808924
0.854395	32.790393	-6.132405	0.806793	0.977821	29.944975	-12.671653	0.514296	-13.185949
0.856685	32.499330	-6.345963	0.809130	0.977729	29.682911	-13.054606	0.516748	-13.571354
0.858974	32.190453	-6.571962	0.811468	0.977638	29.404977	-13.446657	0.519042	-13.965699
0.861263	31.861066	-6.812470	0.813806	0.977547	29.108770	-13.848471	0.521153	-14.369624
0.863553	31.507814	-7.070087	0.816143	0.977457	28.791293	-14.260801	0.523048	-14.783848
0.865842	31.126446	-7.348135	0.818481	0.977368	28.448754	-14.684496	0.524688	-15.209183
0.868132	30.711465	-7.650964	0.820805	0.977279	28.076244	-15.120527	0.526022	-15.646549
0.870421	30.255584	-7.984410	0.823144	0.977191	27.667264	-15.569956	0.526984	-16.096940
0.872710	29.748865	-8.356540	0.825481	0.977103	27.212946	-16.033950	0.527485	-16.561435
0.875000	29.177243	-8.778948	0.827820	0.977016	26.700737	-16.513668	0.527402	-17.041070

PRESSURE DROP (PSI) = 8.267 , DUE TO BLADES = 5.385 AND DUE TO PIPE LOSS = 0.009

TD INTEG. (FT-LB) 0.00194704

BLADE LOAD = -0.4516100E-00 PRESSURE LOAD = 0.2120252E 01

V BAR TURB. (FT/SEC)	V-T INTEG. (FT/SEC)	ALPHA INTEG. (DEG)	V BAR SWIR. (FT/SEC)	V SW. INTEG. (FT/SEC)	TL INTEG. (FT-LB)	TBD INTEG. (FT-LB)
37.11517	38.02013	0.07641	31.45443		0.01149084	0.00944454

BEARING THRUST LOAD (LB)	BEARING TORQUE (FT-LB)	BLADE TIP DRAG (FT-LB)	ROTOR HUB DRAG (FT-LB)	PICKUP DRAG (FT-LB)
1.7157747	0.0000476	0.0007453	0.0011543	-0.000000067

ROTOR SPEED WA (RAD/SEC)	RESULTANT TORQUE (FT-LB)	METER FACTOR (CYCLES/GALLON)	PRESSURE DROP (PSI)	IDEAL SPEED (RAD/SEC)
897.0193	-0.000000171	532.983654541	8.266733170	922.2835

APPENDIX D

RESULTS OF QUESTIONNAIRES

Part One. Turbine Meter Manufacturers' Survey

Part Two. Turbine Meter Users' Survey

APPENDIX D

RESULTS OF QUESTIONNAIRES

The Survey of Turbine Flowmeter Literature, Section III, attempted to outline all the major parameters or factors that have been considered by other investigators in the field and that were pertinent to the study. An attempt was made to include all the major effects, as well as those less important ones which may not have been explored in any detail in the literature.

The next phase of the study was the evaluation of the importance of these general factors as they relate to turbine performance and, more specifically, the meter size, type and operating fluids of typical aerospace applications, as opposed to the commercial petroleum industry, chemical processing, etc. As part of the literature search, however, it became apparent that many questions -- particularly pertaining to empirical flow effects -- remained unanswered and were not available in the published literature. Therefore, it was believed that several major turbine meter manufacturers should be consulted to aid in obtaining empirical correlations, test data, or general design practices that had been developed in recent years as part of company development programs, but had not been published in the open literature.

The commercial turbine meter manufacturers were also asked about the relative importance of various factors affecting performance, and the frequency with which users have been concerned about these effects in the common installation of turbine meters. Since the manufacturers are continually in contact with the users and their problems in application, it was believed that they would be in a far better position to judge the importance and the frequency with which many of these effects are encountered.

For the reasons given above, a questionnaire, consisting of the main questions raised during the literature survey, was prepared and distributed to Potter Aeronautical Corp., Fischer and Porter Co., Cox Instruments, and Foxboro Company. Each of the manufacturers responded, and their replies are included in this appendix.

It was hoped that these visits would result in a more objective approach to the preparation of the theoretical model and possibly some empirical expressions that could be incorporated in the model. Although the manufacturers answered all the questions, it became apparent that very little experimental work had been done in most areas, and what had been done was considered proprietary.

In addition to the manufacturers' questionnaire, a similar questionnaire was prepared for distribution to turbine flowmeter users in the rocket propulsion field. A companion questionnaire to determine the facilities requirements for the subject contract's follow-on test program was also distributed. Replies were received from ARO, Inc.; Aerojet-General Corp.; Air Force Rocket Propulsion Lab (Edwar s AFB); Army Missile Command; NASA (Lewis); NASA (MSFC); Pratt & Whitney Aircraft, and TRW Systems (received too late for inclusion.) Responses to these questionnaires are found at the end of this appendix.

Review of these three questionnaires illustrates the need for conducting experimental testing in the areas mentioned, since very little organized test data are available. This is particularly true with regard to upstream piping effects and velocity profiles, where empirical correlations are necessary. Because of the recognized sensitivity of meter registration to these effects, an experimental test program to explore these effects is essential to the complete understanding of turbine flowmeter operation and standard practice to obtain accurate flow measurement.

PART ONE. TURBINE METER MANUFACTURERS' SURVEY

A. Analytical

1. Have any blade interference tests been conducted or has any attempt been made to correlate with the effects predicted by Rubin, Miller and Fox?

   POTTER: No specific tests on blade interference have been conducted. An increase in blade number leads to increased blade drag effects and a greater variation in meter factor for high viscosity fluids.

   FISCHER & PORTER: No attempt has been made to correlate the effects predicted by Rubin, Miller and Fox, since F & P meters have small solidity ratios and blade interference effects are not a concern. F & P representatives feel that it is seldom necessary to design a rotor with a large number of blades where blade interference would be a factor.

   COX INSTRUMENTS: No.

   FOXBORO: Some tests varying number of blades have been conducted to correlate the effects predicted in Rubin, Miller and Fox. Results are proprietary.

2. Has any experimental testing been done that might reveal in any way the degree of secondary flows between blades of turbine flowmeters?

   POTTER: No experimental testing in this area. Potter representatives feel that an increase in blade number can be considered generally in terms of boundary layer displacement effects or as some factor related to the wetted area of the meter.

   FISCHER & PORTER: No flow visualization testing has been conducted in this area. No trouble has been noted with secondary flows or by blade interference effects, and therefore these areas have not been explored.

   COX INSTRUMENTS: No.

   FOXBORO: No testing has been done that reveals the degree of secondary flows between blades of turbine flow meters.

3. Have wall boundary layer effects been noted in the calibration of small meters as opposed to larger meter size?

POTTER: Boundary layer effects on all wetted surfaces in the plane of the turbine are a prime consideration in very small bore flowmeters. This effect is well demonstrated in a study of Figure 4 of Dr. Grey's paper entitled "Calibration of Flowmeters for Cryogenic Operation" (ARS Journal, February 1960), as it relates to viscosity effects.

FISCHER & PORTER: Yes, attempts are made to allow for boundary layer effects on the meter housing.

COX INSTRUMENTS: We do not have any analytical data to substantiate the effects of wall boundary layers on small turbine flowmeters. However, we know that we cannot produce a very small flowmeter which is linear. This phenomenon can be attributed to the wall boundary layer effect.

FOXBORO: Wall boundary layer effects have been noted to a greater degree in small meters.

4. Has blade trailing edge thickness appeared as a parameter in meter registration? If so, was it important in just low-Reynolds-number high-viscosity flows or was it an effect at higher Reynolds numbers?

POTTER: Present meter designs use thin blades and therefore blade thickness effects have not been important. Tapering of the trailing edge has influenced a meter characteristic which was linear at high Reynolds flow. Blades of extreme thickness can cause distortion in meter characteristics at high Reynolds number flow rates, particularly in fluids having high vapor pressure and low viscosities.

FISCHER & PORTER: The shape of the meter characteristic curve can be controlled for high Reynolds number flows by modifying the trailing edge thickness, but the maximum change that could be expected would be 1%. Wake effects are encountered more with the large turning angles appearing in the reaction turbine industry than in turbine flowmeters.

COX INSTRUMENTS: We do not have any analytical data to substantiate the effect of blade trailing edge thickness. However, we do know that we can effect the shape of the meter calibration curve by filing the blade trailing edges.

FOXBORO: Yes, blade trailing edge thickness has appeared as a parameter in meter registration; it seems to have an effect at both high and low Reynolds numbers.

5. Has any testing been conducted with rotors where a portion of the blades had stalled or where the blades ran in transition or different blade surfaces in different flow regimes?

POTTER: No, some experimentation has been done with tripping boundary layers and controlling the flow as it approaches the meter.

FISCHER & PORTER: No, helical blades are used and therefore significant angles of attack at the blade ends are not encountered. Also, the high flow end of the meter characteristic curve is always turbulent.

COX INSTRUMENTS: No.

FOXBORO: No tests have been conducted in the area indicated by this question.

6. What blade geometries other than helical rotors are presently employed in production flowmeters?

POTTER: Flat and helical blades have been produced. Experimentation with other blade shapes has always led to compromises.

FISCHER & PORTER: All rotors for turbine flowmeters are helical.

COX INSTRUMENTS: All turbine flowmeters manufactured by Cox Instruments use helical rotors.

FOXBORO: Straight blades with fixed angles, and shaped helical blades are used in production flow meters as well as helical bladed rotors.

7. What are typical blade thicknesses and trailing edge thicknesses in the 2-inch meter size range?

POTTER: 0.020" uniform across the blade.

FISCHER & PORTER: 0.030".

COX INSTRUMENTS: Unknown

FOXBORO: The typical blade thickness of a two inch meter is .042 inches.

8. At what maximum "effective angle of attack" does any portion of a typical blade operate?

POTTER: Since flow velocity profiles vary from minimum to maximum flow, it is fundamentally impossible to shape a blade to operate without an angle of attack. Accordingly, angle of attack in the linear operating range of a flowmeter has not been a deterring criterion to good flow measurement.

FISCHER & PORTER: Helical blades are employed to eliminate the variation in angle of attack with blade radius.

COX INSTRUMENTS: A nominal value for the "effective" angle of attack of a typical blade is 35 degrees.

FOXBORO: Have not calculated the maximum "effective" angle of attack of the blades. Helical blades operate at virtually zero angle of attack.

9. Any general comments on NASA TND-3770 or TND-3773 with regard to calibration techniques, flow simulation, meter dimensional effects, temperature correction, etc.?

POTTER: No.

FISCHER & PORTER: No.

COX INSTRUMENTS: No.

FOXBORO: No comments on NASA TND-3770 or 3773.

10. **Has blade tip clearance appeared as an important manufacturing tolerance in terms of meter linearity? For the 2-inch size range, what are the typical blade clearances and manufacturing tolerances, and what percentage of the total flow passes through this clearance area?**

POTTER: Blade tip clearance appears only in the form of non-linearity at the low end. Typical dimensions for one rotor are $1.700\pm^{0.000}_{0.001}$ and for the housing bore 1.750 ±0.001 inclusive.

FISCHER & PORTER: No, typical blade clearance is 0.015 ± 0.002 inches.

COX INSTRUMENTS: Blade tip clearance definitely is an important factor in determining meter linearity. We have noted that we can make a flowmeter linear for a slightly viscous fluid by producing a small clearance near the center of the blades and a wide clearance near the ends of the blades. However, we do not have any analytical data to establish an exact relationship between blade tip clearance and meter linearity, or an exact relationship between blade tip clearance tolera[illegible] and meter linearity.

FOXBORO: Blade tip clearance is an important manufacturing tolerance in terms of meter linearity in the smaller size meters. For a two inch meter the tip clearance is .012 and the tolerance is ± 0.0005. Total flow through this area depends on Reynolds number. No calculations are available.

11. What production tests are employed to detect defective or out-of-spec bearings?

POTTER: Poor meter characteristics or bearing ringing on calibration.

FISCHER & PORTER: On the basis of bearing torque during calibration tests. A series of different fluids with overlapping viscosities are used, and the meter must exhibit the same behavior for a given set of flow conditions.

COX INSTRUMENTS: Cox Instruments procures bearings directly from bearing manufacturers and assumes that these bearings are not defective. However, any defective bearing which is used in a turbine flowmeter will result in non-repeatability of that flowmeter and will be detected during meter calibration.

FOXBORO: Calibration tests are used to detect out-of-spec ball bearings -- sleeve bearings are dimensionally inspected.

12. What bearing designs are employed for small meter sizes to minimize bearing drag? Are glass-filled Teflon retainers employed in the large meters?

POTTER: Both sleeve and ball bearings are employed.

FISCHER & PORTER: Sleeve and ball bearings are used. Ball bearings are recommended above sleeve bearings when the fluid is suitable. Sleeve bearings are used where problems with lubricity, corrosion or dirt may be encountered. Teflon retainers are used with ball bearings for larger sizes in cryogenic service.

COX INSTRUMENTS: Cox Instruments uses ball bearings in all its flowmeters, including the small sizes. Glass-filled teflon retainers are available and will be installed if specified by our customers.

FOXBORO: No, special bearing designs are used in the small meters to prevent drag, except elimination of excessive pre-loading. Glass-filled teflon retainers are not used in the large meters.

13. Has any significant breakthrough been made in attempting to measure bearing drag and to minimize it? Can a typical bearing spec for small meter sizes be made available?

POTTER: Bearing drag effects are evident from a study of low end flow rate linearity. Specifications on ball bearings require:

(a) Running clearance be 0.0005 to 0.0009.

(b) Temperature stabilized alloys to eliminate bearing warpage under operating conditions.

(c) Passivation treatment for maximum corrosion resistance.

(d) Ball separators of nonmetallic materials for improved lubrication under cryogenic operating conditions, as well as elevated temperature conditions to 300°F.

(e) Bearing shields utilized for prelubricated bearings in gas measuring applications.

(f) Appropriate bearing run-in time.

FISCHER & PORTER: Some development testing has been done with the direct measurement of bearing drag. Test data on bearing drag has been obtained for use in meter designs. Lubricity is a big factor in bearing drag. A typical bearing is supplied by Miniature Precision with a spec MPB S2-1/2 CP 68. Bearings are used in unmatched sets.

COX INSTRUMENTS: No.

FOXBORO: No breakthrough has been made in measuring bearing drag. Yes, typical bearing spec #A2010ZW is enclosed.

B. Empirical

1. What testing has been done to determine meter installation effects such as the effect of upstream valves and elbows?

POTTER: Installation piping configuration effects and straightener properties were studied in Potter Pacific Report PP-2, "Evaluation--Fluid Flow Straightener," July 18, 1959.

FISCHER & PORTER: Some test data have been accumulated in this area and may be made available.

COX INSTRUMENTS: Definite testing has not been performed which would determine the effect of upstream piping installation on flowmeter operation. However, we have noted that this effect is quite significant for large meters, such as 3" and up, while it is almost negligible for smaller meters.

FOXBORO: Testing has been conducted on selected sizes of production series meters, using elbows and swirl inducers, to determine the effectiveness of straighteners.

2. How is swirl generated and measured in your testing and do you do you have any experimental test data to show its importance?

POTTER: Refer to Potter Pacific Report #PP-2 mentioned in reply to previous question.

FISCHER & PORTER: Swirl is generated by means of a double elbow. Data are not immediately available, but may be released.

COX INSTRUMENTS: We are unable to comment on this question.

FOXBORO: Swirl is generated for test by using machined helical blades installed in the line upstream of the turbine meter. Yes, we have data to show its importance; however, data is proprietary.

3. Are flow straighteners employed in the calibration equipment? If so, of what type and for what type of disturbances do they successfully straighten the flow?

POTTER: Straighteners are always employed on test stands when meters are calibrated. These straighteners are the tubular bundle type.

FISCHER & PORTER: Flow straighteners are used in calibration equipment but not in general installations. The most difficult problem is transition from a smaller pipe to a larger meter. Transition from large pipe to smaller meter is acceptable. Equal pipe and meter size are also acceptable, since meter blockage due to rotor hub and blades effectively produces a large-to-smaller flow area transition.

COX INSTRUMENTS: All Cox flowmeters are calibrated with both upstream and downstream flow straighteners installed. Cox upstream flow straighteners have six straight radial vanes. The downstream straighteners consist of simply a straight length of pipe.

FOXBORO: Yes, flow straighteners are used in calibration equipment. They generally are bladed straighteners. Straighteners effectively remove disturbance generated by pumps.

4. Has any testing been conducted to correlate meter error with swirl or asymmetric velocity distributions?

POTTER: Very little. Recommended practice to avoid upstream effects is 20 diameters upstream of meter and 10 downstream. Generally, the practices of the American Gas Association and American Petroleum Institute are followed with regard to meter installation. Some experiments with pipe roughness and settling length have been conducted.

FISCHER & PORTER: A few tests have been conducted with meter error related to pipe diameter. This data may be made available.

COX INSTRUMENTS: No.

FOXBORO: Yes, testing has been conducted to correlate meter error with swirl and asymmetric velocity distributions. Data is proprietary.

5. Are any empirical correlations available to predict the error in meter registration due to installation effects?

POTTER: No.

FISCHER & PORTER: See item 4. Also, NBS may have some data.

COX INSTRUMENTS: No.

FOXBORO: Empirical correlations for installation effects are not available.

6. What design techniques are employed to avoid meter vibration? What production tests are employed to detect rotor unbalance and meter concentricity? Are any empirical correlations available for meter error due to operation in flow systems subject to vibration?

POTTER: Clearance in bearing is controlled and mass unbalance in rotor is avoided. Rotors are statically and dynamically balanced. Meters are designed to avoid vibration coupling.

FISCHER & PORTER: Rotors are balanced on all meters. There have been no complaints in the field about meter error from external vibration except that caused by increased wear. No means of predicting error with environmental vibration.

COX INSTRUMENTS: None.

FOXBORO: No special techniques are employed to prevent meter vibration other than dynamic balancing of rotor, inspection of concentricities on shaft and rotors and blade thickness. Do not have empirical correlations for external vibration.

7. Are any test data or empirical correlations available describing the effects of meter orientation and acceleration effects?

POTTER: Vibration and acceleration testing of a Potter turbine flowmeter (Model 1-5851) is documented in NASA Marshall Space Flight Center Astrionics Laboratory Report R-ASTR-IM-65-1, Qualification testing of Potter Aeronautical Company Turbine Flowmeter Model 1-5851, R-ASTP-IM Type III, March 4, 1965.

FISCHER & PORTER: No. Testing has been done, and users may have test data.

COX INSTRUMENTS: No.

FOXBORO: Some tests and data are available describing the effects of meter orientation. No data on acceleration effects is available.

8. To what extent has meter transient testing been performed and in what fashion is the test conducted?

POTTER and FISCHER & PORTER: None; only analytical predictions using analysis of Dr. Grey.

COX INSTRUMENTS: None

FOXBORO: Some transient testing has been conducted; however, calculations have proved to give sufficiently accurate transient response data.

9. To what extent is pulsating flow encountered in the application of turbine flowmeters and what is the typical magnitude of the pulsation intensity when it is encountered? Is 0.1 a practical pulsation intensity below which meter error is negligible?

POTTER: Very little information is available in this area except several references which will be forwarded.

FISCHER & PORTER: Very little experience in this area. More severe in gas flows which have been the subject of past investigations. No additional references to offer.

COX INSTRUMENTS: Pulsating flow applications are quite commonly encountered during flowmeter use. However, we do not have any analytical data regarding the intensity of these pulsations.

FOXBORO: Do not have information about pulsating flow.

10. Miscellaneous Items

(a) Have you noted any change in meter registration due to oxide formation on blades with corrosive propellants?

POTTER: No effect with fluorides, which are the worst case. Some blades in hydrocarbon service build up mechanical deposits, but not in aerospace applications.

FISCHER & PORTER: Oxide effects not detected. Bearing failure would come first.

COX INSTRUMENTS: We regret that we are unable to provide positive answers to questions 10A through 10F.

FOXBORO: Have not observed the effect of oxide deposits.

(b) How closely is meter and bearing material controlled?

POTTER: Commercial grade materials; bearings made to specifications mentioned in reply to question A-13 above.

FISCHER & PORTER: Use commercially available materials, which are certified when required.

FOXBORO: Meter and bearing material is controlled by certification and inspection; control is dependent upon usage and customer requirements.

(c) Any comments on the importance of inlet surface finish and noncylindrical inlets? Any empirical correlations for these effects?

POTTER: Anything to induce or insure turbulence is a beneficial effect.

FISCHER & PORTER: No inlet effects except small to larger pipe transition. Flow area at rotor is smaller than pipe diameter so flow is accelerating.

FOXBORO: No comments on inlet surface finish or shape. No empirical correlation.

(d) Any important factors concerning the chemical reactivity of fluid affecting meter error with time?

POTTER: Meters have been run with LOX and LF_2 with no deleterious effects. If upstream coatings break away and contaminate bearings, there can be problems.

FISCHER & PORTER: No.

FOXBORO: No comments on chemical reactivity effect on meter factor with time, other than the obvious effect of material removal from blades on flow area.

(e) Have you ever noted any nonquantifiable calibration shifts between fluids?

POTTER: Yes, a mixture of fluids to obtain a given viscosity will often give a different effect than a homogeneous fluid at the same viscosity.

FISCHER & PORTER: Yes, with a non-Newtonian fluid where the viscosity is a function of the shear rate. This was encountered in a hydrocarbon fluid with an additive. Be very cautious about additives in a system.

FOXBORO: Yes, non-quantifiable shifts between fluids have been experienced, mainly calibration curves in viscous fluids have not always been characterizable with Reynolds number.

(f) Have you established any "experience" or empirical correlations that predict meter error or shift with breaking in or running time?

POTTER: Yes, sleeve bearings employing at least one element of a soft material such as Teflon or Graphitar have a run in time of 1/2-hour of maximum rate of flow rate for very small meters of 1/2" or under. A curve of calibrations vs. time over a 54-hour period have been obtained in a life test of Meter MF80-4196. Ball bearings and hard sleeve bearings do not require a break-in period.

FISCHER & PORTER: No break-in is required with ball bearings, but there is one with sleeves. Estimated break-in time is one hour. Break-in completion is determined by comparison of a number of successive calibrations until no shift is obtained.

FOXBORO: Some experience has been established with meter running time vs error, but no empirical correlations.

11. Are there any empirical effects that have not been mentioned that should be included in a study of turbine flowmeters?

POTTER: None. Recommend attempted derivation of an equivalent "coefficient of discharge" as it relates specifically to the orifice immediately upstream of the turbine and its correlation to the mean radius for the turbine meter.

FISCHER & PORTER: None that are immediately apparent.

COX INSTRUMENTS: Believe that your performance study can provide a better answer to this question than we can.

FOXBORO: Effects of "lubricity" on turbine meter performance require investigation.

PART TWO. TURBINE METER USERS' SURVEY

SUMMARY OF REPLIES TO USER Q

EXPERIMENTAL DATA REQUIREMENTS

TURBINE FLOWMETER PERFOR

USER QUESTIONNAIRE	AFRPL(RPPTR) EDWARDS AFB	NASA LEWIS RESEARCH CENTER	ARO,
1. Has your organization ever performed any experimental calibration test of turbine flowmeters?	Yes	Yes	Yes
2. Do you have any experimental data which illustrate installation effects on turbine flowmeters (e.g., effect on flowmeter registration of elbows, bends, valves, swirl inducers, pipe reducers or expanders, straighteners, couplings, pressure probes, thermocouples, etc.)? If so,	No	Yes	Yes
(a) What pipe (meter) sizes?		3/4" to 1-1/2" (1954), 1-1/2" (1965)	2-1/2"
(b) What fluids?		H_2O, LH_2	Water, N_2O_4
(c) What effects?		H_2O: valve, elbow LH_2: orientation (vertical up, vertical down, horizontal)	Bends downstre
(d) Any formal reports or papers? (Give report titles, numbers and dates.)		H_2O in-house data, private - 1954 LH_2 NASA TND-3770 - 1965	AEDC-TR-65-233 Testing of the Propulsion Syst Development Te and J. F. DeFo
3. Do you have any experimental data which indicate the effects of fluid properties (e.g., viscosity, density, lubricity, surface tension, etc.) on turbine flowmeter registration? If so,	No	Yes	Yes
(a) What pipe (meter) sizes?		1/2" to 2? D.	1-1/2" and 2-1/
(b) What fluids?		Glycol, H_2O	Water, N_2O_4
(c) What properties?		Viscosity	Temperature De fluids as list are dependent, varied indepen
(d) Any formal reports or papers? (Give report titles, numbers and dates.)		1954 in-house data, no publication	AEDC-TR-67-27 Calibration Sy cryogenic, Hig by D. L. Barto
4. Do you have any experimental data which might indicate the effect of meter construction on turbine flowmeter registration (e.g., blade angle, bearing type, output pickoff, meter size, blade clearance, hub diameter, blade thickness, blade shroud, etc.)?	NO	Yes	No
(a) What pipe (meter) sizes?		3", 4", 5"	
(b) What fluids?		LO_2 RP1, H_2O	
(c) Which construction features?		Blade angle, bearing types	
(d) Any formal reports or papers? (Give report titles, numbers and dates.)		Numerous internal memoranda	
5. Do you have any experimental data which might indicate the effect of environmental factors on turbine flowmeter registration (e.g., vibration, acceleration, fluid pressure, temperature, fluid chemistry, etc.)? If so,	Yes	Yes	No
(a) What pipe (meter) sizes?	1-1/2", 2", 2-1/2"	14", 8", 6", 2", 2-1/2"	
(b) What fluids?	N_2O_4, AZ-50	N_2O_4, (LO_2 - 6", 8" 14")	
(c) What environmental factors?	Fluid temperature effects +27°F to +120°F	Pressure, Temperature	
(d) Any formal reports or papers? (Give report titles, numbers and dates.)	No	TN-149 Numerous internal memoranda	
6. Do you have any other experimental data on turbine meters which you believe may be of assistance in the formulation of empirical coefficients in an analytical model of turbine flowmeter performance? If so, please identify.	No	No	No

A

...ES TO USER QUESTIONNAIRE ON REQUIREMENTS FOR FORMULATION OF ...METER PERFORMANCE MODEL

...	ARO, INCORPORATED	AEROJET-GENERAL CORPORATION	NAA, ROCKETDYNE	UNITED AIRCRAFT CORPORATION
	Yes	Yes	Yes	Yes
	Yes	Yes	Yes	Yes
(1965)	2-1/2"	8", 6", 5", 4", 2", 1-1/2"	1" OUT	2"
	Water, N_2O_4	N_2O, N_2O_4, A-50, RP_1, LO_2	H_2O	Hydrocarbon fuel
verti-	Bends downstream of flowmeter	Upstream valves, elbows, straighteners, temperature probes, flanges, reducers, expanders.	Influence of elbows - detected out to 60 diameters upstream of 1" Potter Flowmeters.	Effects of various configurations of 90° elbows upstream of the flowmeter were examined. The primary effect was reduced meter linearity. Plumbing effects were negated by installation of a standard swirl suppressor upstream of the meter
1954	ARDC-TR-65-233(U) "Simulated Altitude Testing of the Apollo Service Module Propulsion System (Report 1, Phase II Development Test): by G. H. Schultz and J. P. DeFord, Jan. 1966 (Unclas.)	Numerous internal memoranda.	Technical Report prior to 1960, available on special request.	None
	Yes	Yes	No	Yes
	1-1/2" and 2-1/2"	4", 1-1/2"		1/4" through 2"
	Water, N_2O_4	AeroZINE, N_2O, N_2O_4		Hydrocarbon Fuel
	Temperature Dependent Properties of fluids as listed in No. 3. Properties are dependent, and are, therefore, not varied independantly.	Viscosity		Normal calibration data exists for meters of 0.1 to 35 GPM range at 100°F, 200°F and 300°F fluid temperature and for meters of 5 to 215 GPM range at 100°F and 200°F fluid temperature.
...tion	ARDC-TR-67-27 "An In-place Flowmeter Calibration System for Use with Non-cryogenic, High-Vapor-Pressure Liquids" by D. L. Barton, ARO, Inc., Mar. 1967	Numerous internal memoranda	No	Some limited data exists for 2" and 2-1/2" cryogenic meters calibrated at various fluid temperatures on hydrocarbon fuel and at normal LOX conditions.
	No	Yes	No	No
		1-1/2" D.		
		LH_2		
		Blade clearance, blade twist		
		NASA TN D-3770 NASA TN D-3773		
	No	No	No	No
	No	The 1954 data shows the "Universal" dimensionless correlation action is not adequate to predict calibration to better than probable error of 2% (8% peak-to peak uncertainty band). No publications available.	No	No

S U M M A R Y   O F   R E P L I E S   T O   Q U

T E S T   F A C I L I T Y   A V A I L A B I L I T Y   P

T U R B I N E   F L O W M E T E R   P E R F O

A. GENERAL CAPABILITY	ARO, INCORPORATED	AEROJET-GENERAL CORPORATION	AFRPL(RPFTR) EDWARDS AFB
1. Does your organization possess any test facilities in operating condition which are suitable for turbine flowmeter calibration?	Yes	Yes	Yes
2. State the fluid capabilities of your turbine flowmeter calibration facilities.	Water, Hydrocarbon fuels, Hydrazine and mixtures, Nitrogen Textroxide, Alcohol, IRFNA, UDMH	Water, Hydrocarbon fuels, Hydrazine and mixtures, Nitrogen Textroxide, Liquid Air, Oxygen or Nitrogen, Liquid Hydrogen	Water
3. Give your fluid temperature limits (other than normal ambient or cryogenic conditions - fluid, high limit, low limit).	N_2O_4 - +140°F, +30°F AZ-50 - +140°F, +30°F Water - +150°F, +40°F JP-4 - +100°F, -50°F	N_2O_4 - +120°F, +26°F H_2O - +150°F, +40°F	
4. Flow rate capability	N_2O_4 2 test stands Range: 1 to 250 gpm Meter sizes: 1/2" to 3" AZ-50 1 test stand Range: 1 to 250 gpm Meter sizes: 1/2" to 3" Water 1 test stand Range: 0.01 to 300 gpm Meter sizes: 1/4" to 3" JP-4 - H_2O 1 test stand Range: 1 to 250 gpm Meter sizes: 1/4" to 2-1/2"	See Page D 2	Water 1 test stand Range: 5 to 350 gpm Meter sizes: 1/2 to 2-1/2"
5. Flow stand construction features (a) Calibration Standard	Weigh-scale and mercury (or other repeatable) switch Weigh scale, in-place calibrated load cell and diverter valve, N_2O_4 and AZ-50. Continuous weight measurement dead-weight calibrated load cell, N_2O_4 and JP-4 - H_2O.	Weigh-scale and mercury (or other repeatable) switch. Reference standard flowmeter (Turbine) Measured volume (D-6) Positive Displacement Piston J-1, H-2, C-5	Weigh-scale and mercury (or other repeatable) switch
(b) Principal readout method	Digital Timer (counters).	Digital Timer HP 2520	Digital timer (counters).
(c) Pressure source	GN_2 or Helium (4a, 4b, 4d)	GN_2; GHe; GH_2	
(1) Gas Pressure: Fluids		H_2O	Yes
(2) Circulating Pump: Fluids			
(d) Description of facility	AEDS-TP-67-27 (Complete Report Description) Water - Cox 311 AMT Flow calibration standard	Schematics H-2 J-1, T.Lab., E-5 Complete Report Description, D-6	
(e) Your best estimate of overall precision and absolute accuracy (break down by fluid, meter size, test stand type, etc., as applicable).	Fluid Meter Precis. Accur. N_2O_4 2-1/2" 0.24% 0.36% N_2O_4 2-1/2" 0.21% 0.25% AZ-50 2-1/2" 0.24% 0.42% Water 2-1/2" - 0.25% JP-4 NOT AVAILABLE Water 2-1/2" 0.09% 0.13%	See page D 27	

A

LIES TO QUESTIONNAIRE ...
ILABILITY FOR EVALUATION ...
ETER PERFORMANCE MODEL

(RPFYR) EDWARDS AFB	NASA LEWIS RESEARCH CENTER	NAA, [illegible]	UNITED AIRCRAFT CORPORATION	ARMY MISSILE COMMAND	NASA (MSFC)
	Yes	Yes	Yes	Yes	Yes
	Water, Liquid Hydrogen (water facility is conventional Cox-type weigh stand)	Water, Hydrazine & mixtures, Nitrogen Tetroxide, Liquid Air, Oxygen or Nitrogen, Freon TF	Hydrocarbon fuels, Liquid Air, Oxygen or Nitrogen, Liquid Hydrogen	Mil-H-5606 Hydraulic Oil	Water (Liquid Hydrogen, Hydrazine and mixtures, and Nitrogen Tetroxide pending)
			Hydrocarbon Fuel - (0.1 to 35 GPM) +300°F - +100°F (5 to 215 GPM) +200°F - +100°F	Mil-H-5606 - +120°F, +20°F (when planned heat system construction is completed)	
1 test stand Range: 5 to 350 gpm Meter sizes: 1/2 to 2-1/2"	LH_2 1 test stand Range: 1 to 20 liter/sec. Meter Sizes: 1-1/2"	See Page [illegible]	Hydrocarbon Fuel 2 test stands Range: 0.1 to 215 GPM Meter sizes: 1/8" to 2-1/2" LOX 1 test stand Range: 100 to 500 GPM Meter Sizes: 2" to 3" LH_2 1 test stand Range: 400 to 1200 GPM Meter sizes: 2" to 4"	Mil-H-5606 1 test stand Range: 0.01 to 300 GPM Meter sizes: 1/2" to 4"	Water Range: 0 to 40,000 GPM Meter sizes: 1/4" to 18"
Scale and mercury (or repeatable) switch	Mass displacement	Weigh-scale and mercury (or other repeatable) switch (6) Measured volume (11)	Weigh scale and mercury (or other repeatable) switch Standpipe and manometer	Weigh-scale and mercury (or other repeatable) switch.	Weigh-scale and mercury (or other repeatable) switch. Time Volume
timer (counters).	Digital timer (counters).	Digital timer - Berkeley, Anadex	Digital Timer - Totalizer (C.M.C. and Potter)	Digital timer - Cox Mod. 854A Analogue timer - Cox Mod. 884A	Digital timer
		LOX, H_2O, RP-1, Freon, Trichl., N_2H_4, MMH	LOX, LH_2		
	Helium				Yes
			Hydrocarbon fuel	Calibration fluid	Yes
	NASA TN [illegible] Adv. in Cryogenic Engrg. Vol. 7 NASA TN D-3770	Descriptions available at specific request		No spare schematic available, but may be obtained from Cox Instruments - Calibrator Model 311 AHT	
	Detailed in references listed above	Generally, overall uncertainty (accuracy) maintained between ± 0.20 and ± 0.25%, traceable to NBS	Fuel. Precis.* Accur.* Hydr. Fuel ±0.23% ±0.10% LOX ±0.27% ±0.15% LH_2 ±0.40% ±0.15% * 3 sigma, % of point It is assumed that, here, precision refers to purely random effects and that accuracy refers to the amount of unknown bias that may exist.	Estimated standard deviation of the mean for reported calibration values of a 3/4" turbinemeter on Mil-H-5606 fluid will be approximately 0.05%, and the overall uncertainty will be approximately ± 0.15%.	± 0.15%

	[illegible] INCORPORATED	AEROJET-GENERAL CORPORATION	AFRPL(RPPTR) EDWARDS AFB	N[illegible]
6. Other remarks or comments which may be of assistance in evaluating your facility capabilities.	With the exception of the water calibrator, these facilities are each a part of [illegible] meter test facilities and are designed for in-place calibration of the turbine meters being used during motor testing.	Copies of internal memoranda and reports are enclosed which may be of help in the flowmeter model definition.		
B. <u>SPECIFIC CAPABILITIES REQUIRED FOR SUBJECT PROGRAM</u>				
1. Do you have transparent piping connections to the meter, for observation and photography of both upstream cavitation and wake phenomena?	No	No		No
2. Do you have a [illegible] densimeter?	Yes	No		No
3. Can you measure surface tension?	Yes	No		No
4. Do you have in-line fluid temperature measurement capability (at the meter inlet)?	Yes	Yes		Ye
5. Can you measure <u>directly</u> the meter retarding torque as a function of speed in the test fluid? If so, describe method used	No	No		No
6. Can you install (and readily change or move) the following items at any reasonable distance (e.g., up to 30 pipe diameters) in a straight pipe upstream and downstream of the meter:				
(a) Flow straightener sections (e.g., 5-10 diameters long)?	Yes	Yes		Ye
(b) Valves (gate, globe, throttle, etc.)?	Yes	Yes		No
(c) One or more elbows?	Yes	Yes		No
(d) Flanges with instrumentation projections (e.g., orifices, thermocouples, pressure probes, etc.)?	Yes	Yes		No
(e) Pumps?	Yes	No		No
(f) Other flowmeters?	Yes	Yes		Ye
(g) Different upstream pipe diameters (with reducers)?	Yes	Yes		Ye
7. Can you vibrate the meter while in test? (a) How many axes? (b) Frequency range ________ to ______ Hz. (c) Amplitude range _______ to _______ gravities. (d) Up to what size meter (inches)? (e) Up to what flow rate (GPM)? (f) On what fluids?	No	No		No
8. Do you have a centrifuge to apply uniform acceleration to the meter while in test? (a) How many axes? (b) Amplitude: up to _______ gravities? (c) Up to what size meter (inches)? (d) Up to what flow rate (GPM)? (e) On what fluids?	No	No		No
9. Can you produce repeatable flow pulsations, and measure their frequency and amplitude, in the flow rate to a turbine flowmeter during a calibration test? (a) What frequency range? (b) What rms amplitude range? (c) Up to what mean flow rate (GPM)? (d) Up to what size meter (inches) (e) On what fluids?	No	No		No
10. Can you run long-term calibrations? Describe any limitations on these long-term tests.	Yes. This is applicable to the water loop only. The system may be plumbed for continuous circulation.	Yes. Limited to H_2O.		No

A

[illegible] EDWARDS AFB	NASA LEWIS RESEARCH CENTER	NAA - ROCKETDYNE	UNITED AIRCRAFT CORPORATION	ARMY MISSILE COMMAND	NASA (MSFC)
		Rocketdyne operates the stands described as support equipment for its own programs. [illegible] them can be made available for [illegible] purposes. Generally, all major performance measurements are backed by in-place volumetric calibrations, e.g., in LH_2. There are approximately [illegible] in-place [illegible] standards at Rocketdyne's facilities. Many propellants are involved.	a) "Calibration Systems and Turbine Type Flow Transducers for Cryogenic Flow Measurements," [illegible] Kroll, Paper F-5, Advances in Cryogenic Engineering, V. 8, Plenum Press, Inc., N.Y. 1963 b) "Cryogenic Flow Measurement," W.I. Bucknell, [illegible], and R.I. Street, ISA Paper No. 12 2-3-64	This organization is in the process of re-evaluating its flowmeter calibration program. It is a certainty that some changes in the facilities described here will occur in the near future. The extent of the changes is uncertain at the present, but it may involve expansion of calibration fluid capabilities	
	No	No	No	No	No
	No	No	Yes	Yes	Yes
	No	No	No	No	No
	Yes	Yes	Yes	Yes	Yes
	No	No	No	No	No
	Yes	Yes	Yes	Yes	Yes
	No	Yes	Yes	Yes	Yes
	No	Yes	Yes	Yes	Yes
	No	Yes	Yes	Yes	Yes
	No	No	No	No	Yes
	Yes	Yes	Yes	Yes	Yes
	Yes	Yes Above limited to small meters (less than 2")	Yes	Yes	Yes
	No	No	No	No	No
	No	No	No	No	No
	No	No	[illegible]	No	
	[illegible]	Yes	[illegible]	No	Yes - work load.

B

AEROJET-GENERAL CORPORATION

TEST FACILITY AVAILABILITY QUESTIONNAIRE

Questions 4 and 5(e)

Question 4 - Flow Rate Capability					Question 5(e	
Calib. Fluid	Type of System	Range (GPM)	Meter Size (inches)	No. of Test Stands	Precision (3)	A
H_2O	Time-Vol.	18-3960	1-1/4 to 10	1	0.10	
H_2O	Time-Wt.	1-230	3/8 to 2-1/2	2	0.3	
H_2O	Vol.-Vol.	1-238	3/8 to 2-1/2	2	0.24	
H_2O	Vol.-Vol.	250-2376	3 to 8	2	0.24	
AeroZINE 50	Time-Vol.	18-400	1-1/4 to 2-1/2	2	0.09	
N_2O_4	Time-Vol.	18-400	1-1/4 to 2-1/2	2	0.09	
H_2O	Time-Wt.	0.001-4.0	Mini-flow to 3/8	1	0.15	
N_2O_4	Vol.-Vol.	18-400	1-1/4 to 2-1/2	1	0.3	
LH2 LO_2 N_2O_4 AeroZINE 50	Time-Vol.	18-400	1-1/4 to 2-1/2	1	0.09	
H_2O and Freon	Time-Wt. Time-Vol.	4-288	1 to 2-1/2	1	0.18	
LH2	Time-Vol.	18-500	1-1/4 to 3	1	0.09	
LH_2	Time-Wt.	1000-10,000	3 to 12	1	0.3	

NAA, ROCKETDYNE

TEST FACILITY AVAILABILITY QUESTIONNAIRE

Question 4

FLOW RATE CAPABILITY

Calib. Fluid	Range (GPM)	Meter Size	Number of Test Stands
Water	0-30,000	1/8 to 24	1
N_2O_4	0-5	1/8 to 1/2	1
MMH	0-5	1/8 to 1/2	1
Freon TF, Trichlorethylene	0-5	1/8 to 1/2	1
LOX	1-200 300-5,000	1/2 to 18	4
RP-1	1-1400	1 to 6	1
Hydraulic Oil Lube Oil	0-15	1/8 to 1	1

APPENDIX E

RECOMMENDED TEST PROGRAM

APPENDIX E

RECOMMENDED TEST PROGRAM

The three major objectives of the test program, as stated in the body of the report, are as follows:

I. Evaluation of the analytical model.

II. Correlation of flowmeter inlet velocity profile with piping parameters.

III. Effects of parameters not included in the model or in Item II.

In each of these sections, as detailed below, the test objective is stated, the required experimental equipment is specified, and a suggested test series outlined. Because of the urgent necessity for establishment of inlet velocity profile correlations, it is strongly recommended that Item II be given priority in any test program.

I. Evaluation of Analytical Model

(1) Test Objective: To determine whether the analytical model properly accounts for the effects on meter registration of the meter and fluid parameters considered.

(2) Test Equipment:

(a) Flanged Turbine Flowmeter with replaceable bearings and rotors. Preferred size: 2" (optional 1" or 4" meter may be added to evaluate effect of scale on registration.)

(b) Piping configuration consisting of at least 30 diameters of straight pipe upstream of a commercial annular flow straightener with hub of same diameter as flowmeter inlet hanger, a commercial full-pipe flow straightener (no hub), a piece of replacement pipe without straightener vanes, an inlet profile instrumentation section(see below),and at least 20 diameters of straight pipe downstream. All internal piping must be smooth, with no appreciable steps in pipe ID at the flanged joints.

(c) Approximately 10 sets of typical production ball bearings for each of the flowmeters tested.

(d) At least three rotors with different blade-tip clearances.

(e) An instrumented inlet test section (smooth straight pipe) of the smallest possible length, with the following instrumentation:

(i) Static pressure taps (three taps manifolded).

(ii) Input pressure rake with probe tips at test section inlet (i.e., just downstream of the straightener section). Radial spacing of the probes (which may be staggered circumferentially) should be no more than 0.1 inch, with probe outer diameters not exceeding 1/16" and preferably smaller. The rake should be symmetrical radially (i.e., cover a full diameter), both to obtain symmetry data and to avoid creating an asymmetric disturbance.

(iii) Temperature probes (three recommended); penetration of no more than 0.1 radius is satisfactory.

(iv) Swirl measurement device. This is subject to development, but is recommended to be in the form of a very thin vane no more than, say 0.2 radii square, suspended by a freely rotating bearing from a radially movable strut. An orientation detector (e.g., magnetic or optical) is needed to determine the vane angular position to the order of ± 0.1°. Three such devices are recommended, equally spaced (120° apart), at any convenient axial location in the instrumentation section. Their purpose is to measure <u>local</u> swirl angles, rather than mean pipeline swirl, for use both in determining the radial distribution of blade incidence angle utilized in the analytical model and (in Part II) for determining the true effect on meter registration of upstream piping components.

(f) A pressurized mass or volumetric calibration facility (for 2" meter size) capable of approximating 0.1% accuracy on (i) water, (ii) oil up to

20 cs, and (iii) a typical storable liquid propellant suitable to ICRPG.

(g) Capability for temperature conditioning of the test fluid over a minimum range of 150°F.

(3) Test Program Outline

(a) Configuration.

All tests are to be conducted using water at rated flow and one reference temperature; e.g., 70°F, with the standard piping configuration as follows (unless otherwise noted):

(i) 30 diameters of straight 2" pipe upstream of meter.

(ii) 2" annular flow straightener just downstream of 30-diameter straight pipe section.

(iii) 2" instrumentation section downstream of straightener.

(iv) 20 diameters of straight 2" pipe downstream of meter

"Standard" input data for all runs are:

(i) Inlet impact pressure rake profile.

(ii) Inlet swirl profile.

(iii) Meter and pipeline configurational data.

(iv) Upstream fluid temperature (and all other usual fluid data).

(v) Meter registration per unit volume of fluid.

Note that the measured inlet velocity and swirl profiles for each test are to be used in the analytical computer program.

(b) Tests

(i) Effect of flow rate: run standard configuration at three different fluid temperatures in at least two different fluids of widely different viscosities (e.g., water and oil). There are three effects of these parameters which must be checked against the analytical model: inlet profile, blade tip and hub drag, and flowmeter material expansion. Each of these can be isolated by this test series, provided the specified instrumentation is used.

(iii) Effect of bearing tolerances: run standard configuration with 10 different sets of bearings in high-viscosity fluid (e.g., oil).

(iv) Effect of blade-tip clearance: run standard configuration with three rotors having different blade-tip clearances in two fluids of widely different viscosities, e.g., water and oil.

(v) Effect of inlet velocity profile: run standard configuration with three different flow straightener configurations: standard, full-pipe (no hub), and no straightener (straight-pipe section instead).

(vi) Effect of changing fluids: run standard configuration, and use results to predict, using the analytical model, flowmeter registration on a storable propellant. Then run the storable propellant and compare (a) predicted registration, and (b) computed registration using actual storable-propellant inlet profile.

Note: the above test outline does <u>not</u> include the following effects, which are accountable by the analytical model but are believed by this contractor (based on the analysis of the Fischer & Porter design example discussed in the body of this report) to be of negligible effect in the high Reynolds number regime:

(1) Journal bearings, including material tolerances.

(2) Surface finish and lubricity.

(3) Type of readout device.

II. Correlation of Flowmeter Inlet Velocity Profile with Piping Parameters.

(1) Test Objective: to determine the effects of all installation parameters on the inlet

velocity and inlet swirl profiles, so that these installation parameters may be used systematically, through the analytical model, to predict quantitative flowmeter registration variations.

(2) Test Equipment

(a) Piping configuration listed in Item (2b) of previous test series (I).

(b) Instrumented inlet test section as detailed in Item (2e) of previous test series (I).

(c) Three 2" standard pipe elbows (flanged).

(d) Two each standard 2 to 1 and 1-1/2 to 1 pipe reducers (flanged).

(e) Two each, standard 2" globe valves, gate valves, needle valves, and ball valves (flanged).

(f) Three each, straight 2" pipe sections (flanged), 10, 20 and 30 diameters long.

(g) One typical piston-type, vane-type or centrifugal hydraulic pump (2" size).

(h) Pressurized source of test fluid with temperature-conditioning capability.

(i) One impeller type swirl generator.

(j) Flowmeter to record level of flow rate (accuracy <u>not</u> important; $\pm$ 3% adequate).

Note: Turbine flowmeter and prover or calibration stand are not necessary for this phase of the test program.

(3) Test Program Outline

(a) Configuration

All tests are to be conducted using water from the pressurized source at approximately rated 2" turbine meter flow and one reference temperature; e.g., 70°F. The "standard" piping configuration and test data are identical with those listed in Item (3a) of the previous test series (I) (except for flowmeter configuration data, which are not necessary), unless otherwise noted.

(b) Tests

(i) Effect of valves: run each type of valve 0, 10, 20, 30 and 60 diameters upstream of flow straightener inlet, with annular flow straightener, full-pipe straightener, empty pipe section, and no straightener at all (valve at instrumentation section inlet).

(ii) Effect of single elbows: run one elbow 0, 10, 20, 30 and 60 diameters upstream of flow straightener inlet with each of the four straightener configurations designated in (i) above.

(iii) Effect of multiple elbows in the same plane: run 2 and 3 elbows in at least two of the above configurations (e.g., 0 and 30 diameters upstream of straightener) with annular straightener and with no straightener, with 0, 10, 20 and 30 diameters between elbows, and with elbows turning the flow in the same and in opposite directions.

(iv) Effect of multiple elbows in different planes: run at least four configurations of the same test as (iii) above, but with only two elbows, oriented at 6 different angles with respect to each other.

(v) Effects of pipe reducers upstream and downstream of the meter: run three configurations of two reducers equally spaced upstream and downstream of the meter at 0, 10 and 20 pipe diameters.

(vi) Effects of straight pipe length and fluid parameters: run different lengths of straight pipe at different fluid temperatures with two fluids of widely different viscosities.

(vii) Effect of pump: run at least one each of the above straight, valved and elbow configurations with pressurized and pump source.

(viii) Downstream effects of valves, elbows and pumps: run at least two configurations similar to tests (i), (ii) and (vi) above with these components located a distance 0, 10, 20 and 30 diameters downstream of the meter.

(ix) Effects of controlled swirl: run tests with swirl generator installed 0, 10, 20, 30 and 60 diameters upstream of the meter with and without flow straightener, to study simple swirl and to correlate effects of compound swirl from elbow.

(c) Data Analysis

To obtain meaningful experimental correlations that can be generally applied, complete specification of the fluid properties, velocity profiles, and system geometry is essential. Otherwise, the test data will be peculiar to a specific test configuration. Before organizing the test sequence, the key test parameters to be recorded must be established and a proper dimensional analysis conducted to avoid repetitious tests involving the same parameter groups in one instance or the omission of required tests in another instance. The use of computerized data processing systems should be considered if the quantity of data warrants this.

III. Effects of Parameters Not Included in the Model or in Item II.

(1) Test Objective: to evaluate effects which could not be included analytically in the theoretical model, and on which insufficient empirical data were available in the prior literature or from the questionnaires of Appendix D.

(2) Test Equipment: Same as in Item I, paragraph (2), plus the following:

(a) Static pressure tap just downstream of the flowmeter.

(b) Static pressure tap at the minimum cross-section flow area section of the flowmeter.

(c) Centrifuge with all necessary inlet, outlet and instrumentation connections needed to accelerate meter without or with, if possible, instrumentation section, up to 20 g in any of three principal planes.

(d) Vibration table capable of vibrating flowmeter with or without instrumentation section up to 50 g amplitude and variable frequencies up to 1000 Hz in any of the three principal planes.

(e) A source of particulate matter which can be injected into the pipe well upstream (e.g., 60 diameters) of the flow straightener.

(f) Elbow or other pipeline configurations which produced maximum asymmetries in inlet velocity and swirl in Item II.

(3) Test Program Outline

(a) Configuration

All tests are to be conducted with the "standard" configuration and data records of Item I, paragraph (3a) unless otherwise specified. Additional data pertaining to the specialized equipment detailed above should, of course, be taken when appropriate.

(b) Tests

(i) Effect of asymmetric velocity profile: for the standard configuration, determine change in meter registration due to different degrees of asymmetry in swirl and velocity. Results of this test will eventually be used to formulate a transformation capable of converting an asymmetric profile into an equivalent symmetric profile, as indicated in the "Recommendations" section of the main report. THIS TEST IS OF CRITICAL IMPORTANCE TO THE USEFULNESS OF ITEM II RESULTS.

(ii) Effect of particulate matter: for the standard and at least one severely asymmetric-profile configuration, determine the change in meter registration produced by different numbers, different sizes, and different material densities of particulate matter.

(iii) Effects of acceleration and vibration: standard tests to evaluate these effects quantitatively.

(iv) Effect of cavitation: operate standard-configuration flowmeter at several flow rates in excess of rated flow, using flowmeter pressure data to characterize cavitation, and determine meter registration change.

(v) Effect of meter position: operate standard-configuration meter in several positions (at least three principal planes) and determine meter registration change.

NOTE: Other effects not included in this program, which were indicated by the questionnaire results of Appendix D to be negligible, are as follows:

(i) Breaking in and/or running time.

(ii) Chemical reactivity of test fluid.

SUPPLEMENTARY

INFORMATION

√ AD-825 354 Greyrad Corp., Princeton, N. J. Final rept. 31 Oct 67 Contract DAAH01-67-C-1609	No Foreign without approval of Headquarters, Army Missile Command, Attn: AMSMI-RKL, Redstone Arsenal, Ala.	No limitation	OASD, DoD, 14 Mar 69